Packaging Photoreceptors for Cell Replacement Therapy: Optimizing Form for Function

By
Allison Lyn Ludwig

A dissertation submitted in partial fulfillment of
the requirements for the degree of

Doctor of Philosophy
(Comparative Biosciences)

at the
UNIVERSITY OF WISCONSIN – MADISON
2023

Date of final oral examination: 8/23/2021

The dissertation is approved by the following members of the Final Oral Committee:

David M. Gamm, Professor, Ophthalmology and Visual Sciences
Gillian McLellan, Professor, Surgical Sciences
Bikash Pattnaik, Associate Professor, Pediatrics
Masatoshi Suzuki, Professor, Comparative Biosciences
Xinyu Zhao, Professor, Neuroscience

Table of Contents

Dedication

This dissertation is dedicated to my maternal grandmother, Marilyn Modrell Corey, whose influence on my education, compassion for others, and love of learning lasted far beyond the time we were blessed to have with her on earth.

Acknowledgements

Completing this dissertation amid a pandemic has taught me that people, like photoreceptors, are generally happier together. I am especially thankful for the individuals mentioned below who were with me in presence or in spirit without whom this dissertation would not have been possible.

There are good scientists and good people in the world; I will be forever grateful that my scientific career has been shaped by the individuals listed here and many more unnamed who are both of these and then some. There are not enough words to express how thankful I am for the guidance and support of each and every one of you, and I hope that excuses my relative brevity where many know I would prefer to write volumes. In short: I am a better scientist and a better person because I spent the most formative years of my career with you. From the bottom of my heart, thank you all.

Thank you to the many collaborators on and off campus who helped make the ideas presented in this dissertation a reality. In particular, I would like to thank members of the Molecular and Genetic Sciences Group, the McPherson Eye Research Institute, and Department of Comparative Biosciences for providing excellent feedback and lively discussion of these findings throughout my PhD.

Thank you to my committee members: Dr. Gillian McLellan, Dr. Bikash Pattnaik, Dr. Masatoshi Suzuki, and Dr. Xinyu Zhao, for your unwavering support, professional guidance, and investment in my development as a scientist. I have been incredibly lucky to have had the pleasure of knowing and being trained by each of you.

To my mentor, Dr. David Gamm, and the entire Gamm Lab family: Kim Edwards, Dr. Steven Mayerl, Dr. Lindsey Jager, Dr. Divya Sinha, Dr. Joe Phillips, and Dr. Beth Capowski: you taught me everything I know and made this possible. I cannot put into words how much each of you has shaped my life, both as a scientist and as a person. You fed me and gave me plants and were there for so much life over the past several years, and I am endlessly grateful.

Thank you to the following current and former mentees, research interns, and transplant team technicians, who spent endless hours assisting with these experiments and more often than not made me laugh along the way: Patrick Barney, Katie Barlow, Kelsy Nilles, Sara Stuedemann, Maya Bhadkhamkar, Alondra Fernandez, Uche Nlebedum, Ashley Willes, Suzanne Litscher, Brandon Haughey, Karina Schmidt, Alex Pitts, Megan Piraino, Jamie Mustful, Nico Rubio.

To the following individuals who supported my dual degree training and occasionally fed me chocolate: Jenny Dahlberg, Susan Thideman, Dr. Suresh & Dr. Bjorling.

To the members of the Waisman Rodent Models Core, especially Megan Eastwood: thank you for being the kind of people who make me proud to work in animal research, and to the rats who made the entirety of this work possible.

To Dr. N. Matthew Ellinwood, without whom I would never have dreamed of pursuing a PhD: thank you for sending me on this crazy adventure. Your dedication to changing the world has always been and continues to be a source of inspiration

To my family, who kept my heart and freezer full even on the most difficult days: thank you for listening, encouraging, and patiently listening while I tried to figure out how to explain what I do.

To my husband, Kyle, who helped me to see this was possible on the days I doubted it the most. You have been my biggest fan and my best reviewer from the moment we met, and I am forever indebted to you for your support throughout this dissertation and all the life it encompassed. I love you endlessly.

Finally, thank you to the generous sources of funding who have supported this research and my career development, including the National Institutes of Health, National Eye Institute, the Foundation Fighting Blindness, and UW-Madison School of Veterinary Medicine Dual Degree Program.

Abstract

Retinal degenerative diseases (RDDs) affecting light-sensitive photoreceptors (PRs) are a leading source of incurable blindness worldwide. Due to a lack of endogenous repair mechanisms, functional cell replacement of PRs is among the most promising approaches for restoring vision in advanced RDD. Human pluripotent stem cell (hPSC)-derived retinal organoid (RO) technologies have accelerated development of cell replacement therapies, providing a virtually unlimited source of photoreceptor precursors (PRPs), the preferred type of donor cell. First-in-human hPSC neuroretinal replacement safety and efficacy trials have recently begun, but a number of questions regarding efficiency, reproducibility, and functional mechanisms remain. This dissertation addresses remaining challenges in PR replacement, exploring issues of donor cell survival, organization, and connectivity to advance retinal regenerative therapies.

Survival and maturation of hPSC-PRP using two different delivery forms—single cell suspension and cellular aggregates—were characterized via quantitative histologic assessment in a rat model of advanced retinal degeneration. Donor cell engraftment was markedly improved with aggregate transplantation, suggesting that survival of donor cells can be optimized by modulating the form of delivery. Transplanted hPSC-PRP aggregates survived for at least 6 months *in vivo,* maturing into rod and cone PRs with synaptic protein expression and formation of outer segment-like structures. However, aggregate transplants resulted in varying degrees of graft organization and did not restore reflexive or electrophysiologic light-evoked responses. Poor graft organization and lack of direct evidence for synapse formation were identified as possible contributing factors to suboptimal transplant outcomes. A novel micro-patterned polymeric scaffold was thus

developed to support a dense layer of hPSC-PRP, achieving organized expression of presynaptic and outer segment proteins *in vitro.* Finally, an *in vitro* monosynaptic retrograde tracing assay was optimized to determine whether hPSC-derived retinal neurons could form new synaptic connections after dissociation from retinal organoids. Synaptic tracing revealed remarkable plasticity of RO-derived retinal neuron synapse formation and identified hPSC-PRP among traced presynaptic cells, providing direct evidence of synapse re-formation by hPSC-PRP.

In conclusion, these studies outline complementary approaches to traditional preclinical animal model testing and provide strategies for directly studying survival, organization, and synaptic re-connectivity in further studies of hPSC-PRP replacement. Collectively, the results of this dissertation demonstrate strong potential for the advancement of next-generation retinal cell therapies and provide a clear path forward for future translational studies aimed at PR replacement and photoreceptive circuit restoration.

Chapter 1 -

From reaggregation to retinal organoids

Ludwig, A. L., Wright, L. S., Gamm, D. M., Layer, P. G.

Highlights

- Vertebrate cellular reaggregation studies provide insight into retinal histogenesis
- 3D retinal structures produced *in vitro* depend largely on environmental constraints
- Histogenetic mechanisms uncovered with in vitro reaggregation systems may prove useful for advancing human retinal organoid-based technologies and therapies

Author contributions: A. L. L., L. S. W.: figure preparation, data curation, and writing (editing and revision). D. M. G.: conception and design, writing (editing and revision), financial support and supervision. P. G. L.: conception and design, figure preparation, data curation, and writing (initial draft, editing, and revision).

Introduction

In the decades since human induced pluripotent stem cells (iPSCs) and embryonic stem cells (ESCs) (collectively, human pluripotent stem cells, or hPSCs) became widely available, the seemingly improbable quest for organ regeneration has been realized through ground-breaking biomedical research and technologies[1–3]. Organoids, the spherical products of suspension-based three-dimensional (3D) tissue engineering, have been successfully cultured through propagation of tissue-specific lineages of stem and precursor cells for all major body systems[4,5]. The envisaged applications of organoids in biomedicine are seemingly innumerable, with scientists worldwide advancing diverse organoid technologies for disease modeling, drug discovery, precision medicine, and cell replacement therapy. In ophthalmology these applications have progressed rapidly toward clinical use due to intrinsic features of the eye (surgical accessibility, low required dose, and relative immune privilege) and a wealth of foundational research on the basic biology of 3D cellular aggregates (or, *spheroids*, see Glossary).

With the recent initiation of several clinical trials using stem and/progenitor cell-based transplantation for retinal degenerative disease, the hope that these technologies will lead to treatments for blinding diseases finally appears to be within reach[6–8]. Despite increasingly sophisticated organoid techniques and substantial progress toward organoid-derived therapies, many basic developmental mechanisms these approaches rely upon—proliferation, differentiation, cell migration, lamination, and synaptogenesis—are incompletely understood in the context of human retinal development. Numerous questions as to how hPSC-derived organoids achieve a highly organized histological structure, why some organoids form laminar tissue while others do not, what leads to rosette formation among engrafted cells in retinal replacement, and which histogenic mechanisms are behind these observed phenomena remain.

Regenerative therapies and organoid technologies have fortunately been established on a bedrock of historic research examining tissue formation in retinal 3D spheroids from other vertebrate species. As the field moves forward, a revisiting of the developmental biology that it was built upon is prudent and perhaps necessary to unlocking the next phase of retinal regenerative medicine. To that end, this review provides a history of relevant lessons learned from avian and rodent studies of retinal cellular reaggregation predating stem cell technologies, with a strong focus on lamination and histogenesis related to issues of incomplete or disorganized histological structures in organoid-based technologies.

I. Cellular reaggregation: History, definitions, and mechanisms

Given rapidly advancing modern culture methods, it is somewhat surprising that the history of cell culture began before the 19th century. Reaggregate cultures are a method by which a singularized population of cells is re-associated—that is, reaggregated—in suspension or rotational cultures to generate 3D tissue structures. So-called "shaking cultures" represented the first reaggregation experiments and established some of the most basic tenets of cell biology. Before the turn of the 20th century, Hans Driesch discovered the phenomenon of totipotency by dissociating sea urchin embryos at the 4-cell stage[9], using a suspension culture approach in what may be regarded as the very beginnings of stem cell biology. A subsequent experiment by Henry van Peters Wilson using similar methods deserves mentioning here[10].

Wilson dissociated sponges by passing them through a mesh cloth, transferring the cell suspension into glass dishes and shaking them softly in salt water to follow their growth into cell clusters *("reaggregates"*). To his surprise, his *reaggregates* eventually developed into complete, viable sponges. Even more surprisingly, when he combined suspensions from two different sponge species (marked by distinct colors), cells of the same color were either found within separate, singly-colored reaggregates or amassed in distinct areas of the same reaggregate. Differently-colored cells that were initially intermixed would migrate to form species-specific

clusters (**Fig. 1**). Although Wilson himself largely disregarded the result at the time—noting that "it would be idle to discuss further the nature of the hypothetical dual organism"—what became known as the phenomenon of "sorting-out" amounted to the discovery of cell-cell recognition (distinction of self vs. non-self). Townes and Holtfreter later documented striking sorting effects of epidermal cells from neural plate cells of the amphibian embryo, whereby their relative position within reaggregates mimicked native embryonic structure[11]. Such recapitulation of embryonic development undoubtedly required sophisticated tissue-specific differentiation processes to occur *in vitro*.

In the years that followed, reaggregation studies painted a picture of a central theme in modern developmental biology—that maturing cells in each tissue are highly dependent on physicochemical conditions, which in turn influence a variety of forces (attraction, repulsion, expansion, rotation, etc.) contributing to organized tissue formation. Classical reaggregation analyses using the slime mold (*Dictyostelium d*), the frog embryo (*Xenopus*), and the chick embryo (*Gallus g. domesticus*) uncovered the roles of cell adhesion molecules (CAMs), cell migration, and tissue patterning in histogenesis[12–15]. It was during this period that retinal reaggregation from embryonic chicken eyes arose (**Fig. 2**) and became a preferred model for studying retinal histogenesis *in vitro*[14,16–18]. The successful transformation of *rosetted spheroids* (**Fig. 2b**) into fully laminar *stratified spheroids* (**Fig. 2c**) in 1984 marked a critical milestone for modern retinal regeneration, demonstrating for the first time that near-complete reconstruction of a neural tissue from progenitor cells was possible[19].

Conventional 2D and 3D cell cultures

As the study of immortalized and proliferative cells increased, less labor-intensive methods for maintaining such cells grew in popularity, and over decades reaggregation procedures were practiced in the laboratories of few researchers. Plated 2D cultures became the standard in most fields, including retinal development, for many years beginning in the early 1970s[20].

In traditional 2D culture, plastic dishes or flasks are coated with extracellular matrix-mimicking substrates (poly-lysine, laminin, etc.) to encourage cell adhesion to 2D surfaces. Under appropriate *in vitro* conditions, cells with proliferative capacity (e.g., pluripotent, malignant, or immortalized cells) divide and expand until they reach confluency. Relatively benign cells stop dividing at this point, while tumorigenic cells often continue to proliferate upward without restraint. In most cases, pluripotent cells also stop dividing and begin differentiating upon reaching confluence.

Thus, when kept at low densities, proliferative stem and progenitor cells in 2D cultures can and will migrate along flat surfaces to contact one another, assembling into clusters with rudimentary spatial organization and rosetted structures. Rudimentary instances of retinal cell sorting have historically been observed in 2D cultures. For example, when dissociated neonatal rabbit retinal cells were cultured on laminin-coated glass slides, two separate cell clusters quickly separated, containing cells of the inner and outer retina, respectively (Layer, unpublished observation). Nonetheless, 3D structures that closely mimic native tissue formation—particularly for a structure as complex as the vertebrate retina—are rarely achieved using 2D culture methods.

Reaggregates are a combination of cell sorting and development

In contrast to conventional 2D cultures, higher degrees of tissue formation are readily achievable with 3D reaggregate cultures. To successfully generate 3D spheroids, several critical features of cell isolation—the first step toward reaggregation—must be considered. The process begins with physical isolation of a developing tissue from its surroundings to produce a cell suspension. In the case of retinal reaggregation, it is essential to ensure that tissues are free of retinal pigment epithelium (RPE), mesenchyme, and/or neural crest. Enzymatic dissociation of the tissue (depending upon reagents, incubation times, and temperature) is followed by quite harsh

dispersal procedures, often stripping off surface receptors and other membrane-bound components of the extracellular matrix.

For reaggregation to occur, dishes containing singularized cells are kept in constant motion through rotation or shaking, employing an assortment of devices to introduce additional kinetic energy into the system. This movement keeps individual cells in suspension, preventing adherence to the base of the dish and increasing the likelihood for encounters with other cells. Adhesion can and often does result from such encounters, promoting aggregation and cell sorting. Cell clusters gradually become small spheres and grow larger. In this dynamic environment, *in vitro* proliferation arises, and differentiation can begin.

3D cultures often follow distinct mechanisms of differentiation relative to 2D cultures[21] and can thereby initiate tissue reconstruction. Notably, volume growth of spheroids is relatively limited. In fact, the size of spheroids is often surprisingly fixed—that is, they experience size regulation. The size of tumor spheroids is known to be self-regulated by the ratio of surface area to volume[22]. Tumorigenic cells in 2D culture with unlimited space and fresh culture medium will continue to grow, as the ratio of surface area to volume remains constant. In contrast, a tumor spheroid grown in unlimited space and fresh medium will eventually reach a dormant phase. At a certain size, there is insufficient surface area relative to its volume for the spheroid to absorb nutrients and remove catabolites, and the inner zone consequently undergoes necrosis. Transverse gradients of nutrients and growth factors appear to play a role in the spatial organization of cell types in non-tumorous reaggregates as well[23].

A change in terminologies: from retinal reaggregates to spheroids to organoids

Originally, pattern formation in reaggregate was thought to be exclusively a result of sorting-out processes. Malcolm Steinberg provided an explanation of the simple sorting-out phenomenon based solely on physicochemical properties of cells[17,24]. Citing relatively simple mathematical rules of morphogenesis, Steinberg explained pattern formation in reaggregates mainly in terms

of rheology and proposed that the cells comprising an aggregate behaved like a two-phase fluidic system. Accordingly, different cell types in a mixture were assumed to segregate primarily because of differential intercellular adhesion strength—the *differential adhesion hypothesis*.

In addition to simple sorting-out, retinal development is also initiated in the earliest days of retinal cell reaggregation. In this sense, the term "*reaggregate*" does not accurately express what it intends to convey. *Reaggregate* insinuates that aggregation and sorting-out are the only necessary processes required to generate these structures. The contributions of development, proliferation, and differentiation are discounted. To address these shortcomings, Layer and colleagues proposed a “rebranding” of sorts in the late 1990s. “Retinal reaggregates” were instead referred to as “retinal spheroids or “retinospheroids,” indicative of the smooth spherical structure not typically seen in simple reaggregates and the histological resemblance to the original retinal tissue. The term “spheroid” originally arose from research on “tumor spheroids”[22,23,25,26]. In the specific case of these tumor structures, "spheroid" was merely intended to indicate their smooth spherical shape. Major topics of research in this field were not focused on developmental processes, but rather on space restrictions within spheroids (oxygen supply, nutrient supplementation, etc.) and their relation to angiogenesis. For clarity, throughout this review "retinal spheroids" is intended to refer to all "retinal reaggregates" derived from primary embryonic or postnatal dispersed retinal cells, while all ESC/iPSC-derived structures are referred to as retinal organoids (ROs).

Reaggregation vs. retinal explant cultures

The uniqueness of retinal spheroids lies in the fact that this model begins with a fully dispersed cell population. These relatively simple structures reveal an individual cell’s autonomous tissue-forming capacity with greater clarity than what is typically achievable amid the complex milieu of normal retinal development. In this regard, both explant cultures and pluripotent stem cell (PSC) cultures are fundamentally distinct from spheroid cultures. In explants, a sample is extracted from

the primary tissue at a certain developmental stage and then placed in culture intact. Cell-cell contacts and spatial relationships are thus largely preserved, though retinal explants cultured in suspension often eventually roll into spherical morphologies. Spheroids represent a simpler, albeit more artificial system relative to explants for modeling development. Spheroids and explant cultures both fill an important niche in understanding retinal morphogenesis, but as with all model systems, conclusions about retinal developmental drawn from these approaches should be carefully interpreted in the context of their inherent limitations.

Reaggregate model systems

The wide availability of developing avian retinal and RPE tissue initially made chick retina the preferred model for reaggregation studies[27,28]. Due to the ease with which quail and chicken nuclei can be distinguished from one another, chimeric quail/chick retinal reaggregate models have been especially useful. Extensive effort has also been invested into the generation of retinal spheroids from rodents, largely from rats and (less frequently) gerbils or mice. While a plethora of available genetic models would make mice appear most preferable, a low yield of cones and comparatively small eye size have limited widespread use in reaggregation research; rats are thus one of the more common mammalian models utilized in reaggregation.

In the first described rat study, spatial sorting of glycine- and GABA-positive cells was detected in neonatal rat retinal spheroids[29,30]. In a subsequent study, many rosettes with photoreceptors (PRs) forming disc-containing outer segments and layers containing ribbon synapses were found. All neuronal types were present except retinal ganglion cells (RGCs), many of which were found in locations comparable to the retina *in vivo*[30]*.* A series of subsequent studies using mixed rat retinal spheroids by both the Raff and Cepko groups provided further insight to the degree of tissue formation possible with rat spheroids[31]. Watanabe and Raff characterized the morphology and histology of what they called *pellet cultures* (Watanabe et al., 1997). All cell types were identified, including PRs with inner and outer segments. Most were organized in so-called

pale and *dark* rosettes, mimicking the INL (inner nuclear layer) and ONL (outer nuclear layer), respectively. Moreover, areas resembling both an OPL (outer plexiform layer) and an IPL (inner plexiform layer) were noted. Cepko´s rat reaggregate studies documented determination and plasticity of various retinal cell types[32–34]. Collectively, these studies demonstrated that both intrinsic properties of neuroepithelial cells and cell-cell interactions determined cell fates in rat retina. Moreover, this work demonstrated that rat spheroids could attain an advanced stage of outer tissue formation comparable to that of chicken *rosetted spheroids*, though IPL sublamination had not yet been assessed in rat spheroids. To the best of our knowledge, there are no published reports on retinal spheroids from mice nor rabbits. However, retinal cells readily form spheroids from the Mongolian gerbil, a diurnal rodent with a cone-dominant retina[35,36], providing an excellent model for studying retinogenesis in the context of cone-rich development.

The zebrafish (*Brachydanio rerio*) has become one of the premier models of developmental biology. Several advantages for its use as a model include relatively short development, translucent embryos, and large numbers of transgenic lines available to label cell types. Laminar spheroids were generated from developing SoFa1 transgenic zebrafish eyes (stage 24 and 32 hours post-fertilization) using a specially designed 3D Petri dishes; revealing a remarkable reversal of retinal cell layers with arrangement of RGCs on the outer surface of spheres[37]. Zebrafish spheroids developed all major retinal cell types and differentiated on a time scale comparable to *in vivo*; though neuropil formation and stratification remained rudimentary. Reaggregation was inhibited by PACMA31, an inhibitor to the cell adhesion molecule R-cognin. Similar to chicken spheroids, patterning was severely affected by the ablation of Müller glial cells with application of Notch-inhibitory DAPT.

There are very few documented attempts at spheroid generation from amphibian retinae, which is somewhat surprising given the wide use of amphibia (Xenopus, newt, etc.) for regenerative and transplant-based studies[38]. Since newts and frogs are highly amenable to amenable to *in vivo* studies[39,40], it is likely that reaggregation approaches were deemed unnecessary.

II. Retinal architecture and development

In this section, a brief introduction to the general structure of the vertebrate retina and its embryonic development is provided, but only to the extent necessary for the unacquainted reader to become familiar with major topics of the present review. Readers are directed to more detailed reviews of parallel processing[41], photoreceptors[42], and circuit assembly in the developing retina[43,44] for further information.

Cell types that delineate the mature retinal architecture

All vertebrate retinae exhibit a highly laminar and evolutionarily conserved basic plan consisting of three distinct layers of cell bodies: the outer nuclear layer (ONL), the inner nuclear layer (INL), and the ganglion cell layer (GCL), which are separated from each other by two sequential synaptic layers, the outer plexiform layer (OPL) and the inner plexiform layer (IPL) (**Fig. 3**). The apical surface of the retina is bound by the outer limiting membrane (OLM) and interdigitation with the retinal pigmented epithelium (RPE), with which it is structurally and functionally interconnected (see below), while the innermost surface is bound by the inner limiting membrane (ILM).

A multitude of subtypes for each major retinal cell type

The cellular composition of the retina is also highly conserved and consists of six major neuronal cell types: rod and cone photoreceptors (PRs), horizontal cells (HCs), bipolar cells (BCs), amacrine cells (ACs), and ganglion cells (GCs). The retina also contains Müller glia (MG), the radial glial cells of the retina. PRs are sensory neurons residing in the outermost layer of the retina (the ONL) that receive incoming light and transform it into electrical signals. There are two types of PRs: rods, which mediate vision in dim light, and cones, which mediate high-acuity daylight and color vision. Signaling from PRs is transmitted to HCs and BCs through synaptic connections in the OPL. HCs are located at the outer border of the INL and integrate signals from several neighboring rod and cone PRs (*converging* signal transmission), thereby modulating signals between PRs and BCs.

HCs are distinguished by the presence or absence of an axon and the number of distinct subtypes varies by species [e.g. mouse (1), primate (2), Zebrafish (≤4)][45]. Cell bodies of ACs (whose name loosely translates to "axonless") are located in the inner half of the INL. They receive input from one or more BCs and relay signals via synaptic connections to a group of GCs (*diverging* signal transmission) at specific sublaminae of the IPL. ACs represent a vast group of large interneurons, with more than 60 distinct subtypes classified by morphological and physiological criteria in some vertebrate species. BCs can be separated into either rod BCs or cone BCs as defined by their inputs. Cone BCs are further categorized into diffuse, flat midget, and invaginating BCs, depending on the type of synapse formed with their respective cone PRs. Physiologically, BCs can be subdivided into so-called OFF bipolar cells, which project to the outer half of the IPL and hyperpolarize as light increases, and depolarizing ON bipolar cells which synapse in the inner ON-half of the IPL.

The GCL represents the innermost nuclear layer and is separated from the vitreous body by an inner limiting membrane (ILM). The GCL contains GC soma and displaced amacrine cells (dACs). GCs have large cell bodies and come in three morphologically distinct subtypes, α-, β- and γ-type GCs[46]. GCs are the final cell type in the retinal circuit, receiving highly integrated signals from BCs and ACs at the level of the IPL. GCs make exclusive use of classical action potentials for retinal output; all other synaptic activities within the retinal circuitry elicit only small potential changes.

Retinogenesis: Formation of a laminar, highly integrated retinal network

Formation of eye stalk and optic cup

Early eye development begins as part of the differentiation of the rostral neural tube, the latter becoming morphologically evident by emergence of brain vesicles (**Fig. 4A**). The optic stalk represents a lateral outgrowth of the second brain vesicle, the diencephalon. The optic stalk extends until it physically contacts the surface ectoderm, which immediately induces the production of a lens placode in the ectoderm and is followed by lens formation. Partially driven by physical/mechanical forces, the neuroepithelium at its outer tip turns inwardly (inversion of neuroepithelium; **Fig. 4B**). Due to its robust mitotic activity, the neuroepithelial tissue further expands (a process later called "lateral growth", see below), and the future optic cup, composed of an outer and an inner layer, begins to appear (**Fig. 4C**). These two tissue sheets will form the RPE and the retina, respectively. As both sheets enlarge, they come into close physical contact with each other at their apical surfaces, facilitating a unique histo-formative interaction representing the onset of complex interactions between the two mature structures. Differentiation advances under the control of both intrinsic and extrinsic mechanisms[47], with a network of eye field transcription factors (EFTFs: *Rx, Lhx2, Pax6, Six3,* and *Six6*) and distinct developmental programs guiding specification[48–55]. The two layers begin to follow distinct developmental pathways dictated by specific gene expression programs, regulated in part by MITF for RPE and

VSX2 (CHX10) for the neurosensory retina[56,57]. Morphological differences between the inner and outer layers soon become evident (**Fig. 4D**)—the RPE remains as a single cell layer-wide epithelium, while the retina widens to form three nuclear layers through a process termed "radial growth." As retinal spheroid studies have shown, tissue formation within the retina is not only driven by specific genetic-molecular actions; mechano-physical effects act in concert with gene regulatory networks to guide decisive formative steps.

Production periods of retinal cell types overlap

The inner layer of the optic cup is comprised of distinct neural retina progenitor cells (RPCs), which are capable of generating all six neuronal cells as well as Müller glia of the future retina (the *competence model* of retinal cell fate determination)[58]. Applying different experimental approaches, many studies have clearly established an evolutionarily conserved temporal sequence in which the different retinal cell types are "born" (these and other classical studies contributing to our current understanding of retinogenesis are highlighted in **Figure 5**). Large retinal neurons are generally born before smaller ones—GCs ACs, HCs and PRs complete their final mitoses far before BCs. Retinal development occurs in overlapping waves of waxing and waning cell type genesis. In the mouse, GCs are produced from E10/11until E18, HCs until E14, ACs and cones until P3; while BCs are generated only from E14 until P10, and MCs until P11[59,60]. In chick, the earliest GCs exit the cell cycle at late E2/early E3 (stage HH12-13)[61,62] and continue to be produced until E7 (with a small number as late as E12). The other three large cell types (ACs, HCs, PRs) follow in short order, and their genesis overlaps substantially with that of GCs[61]. BCs and MG are born far later in development, with no MG detected before E8[62]. Across all species, early-stage retinogenesis is traditionally characterized by the birth of RGCs, HCs, cone PRs and HCs, while late-phase retinogenesis is characterized by the birth of BCs and MG. A

small number of MG and/or their precursors are likely present much earlier and may also function during development. Notably, rod PRs are born across both periods[58].

Spatio-temporal gradients of retinal differentiation

The broad window for cell type production can be explained by the fact that distinct spatiotemporal gradients dictate the development of the retinal tissue. In all vertebrate retinas, cells in central positions near the fovea are older (e.g., are born earlier) than more peripheral ones (the *central-to-peripheral gradient*). In chick, the first postmitotic GCs will be found in a central position at the ILM (the future vitreal border) at E3.5, and the last ones will be produced 3-4 days later at the outer periphery[61,62]. Some species variations in this progression have been noted; for example, a temporal to nasal and ventral to dorsal developmental progression has been documented in the chick[63–65]. Hence, retinal differentiation and growth spreads continually from a central spot to the eye peripheries ("lateral growth"; **Fig. 4C**). In parallel, retinal cell types are sequentially produced and find their positions in the radial (*e.g.,* vertical and transversal) dimension of the growing retina (“radial growth”). The *ora serrata* marks the peripheral retinal position where both lateral and radial growth terminates. In the chick, the regulation of growth in this region is in part mediated by a unique type of retinal neuron termed the bullwhip cell, which can modulate RPC proliferation through the secretion of neuropeptides[66]. At the far periphery (containing future iris tissue), retinal stem cells capable of self-renewal reside in a single cell layer-wide neuroepithelium[39,67]. A few cells of this nature remain in the more mature (or even adult) ciliary margin and are capable of initiating retinal regeneration in multiple species (*e.g.* salamanders, frogs, fish, birds, etc.)[39,67]. For a time, such cells were also thought to reside in mammalian retinas, sparking interest in their use for regenerative therapies, but their existence in the human and mouse retina has since been refuted[68].

The cell cycle and mechanisms of retinal lamination

What we refer to as "radial growth" within the retina includes a variety of distinct and complex mechanisms for laminar network formation. A critical first question is how a particular cell finds its position within the radial dimension (e.g., a retinal laminar arrangement). Multipotent RPCs capable of forming all retinal cell types reside within the outermost aspect of the early retina (equivalent to mitotic/ventricular zone vs. mantle layer in brain)[69]. These mitotic RPCs engage in a degree of restricted interkinetic movement, but generally remain in this outer zone. Consequently, cells in G1 and S-phase are oriented near the innermost half of the retina, while cells in the outermost half (toward the RPE) are predominantly in G2 and M phase. There are ambiguities in the exact delineation of each zone, but generally speaking, each postmitotic cell derived from an RPC may migrate further inward (GCs, HCs, ACs) or outward (as is the case for rod and cone PRs). GCs and ACs migrate basally as they are born, forming a postmitotic inner half, while mitotic RPCs remain in the outer half of the tissue. Due to varying ONL architecture between species, different positioning mechanisms are required. In the chick and zebrafish, the ONL may be just one cell layer thick, while the mammalian ONL may contain 10 or more neatly stacked PR cell bodies[70]. To accommodate the large number of PR outer segments within one confluent lattice, processes from the PR cell nuclei extending toward the synaptic terminal are variable in length. After completing the last mitotic cycle, PRs remain in the outer half and take their position in the future ONL. Horizontal cells (HCs) may take an unusual route to their final destination. In the chick, HC progenitors become arrested in G2-phase and migrate inward to complete their terminal mitotic cycle, but only migrate back outward to their final position at the future INL/OPL border after their final division[71].

Thus, radial growth is the generation of sequential cell clones derived from RPCs which, in their simplest form, remain arranged in radial cell columns. This process was first demonstrated by viral labeling of chick retina[72], and also in rosetted spheroids *in vitro*[73,74] (**see Fig. 6** and below).

Lateral intermingling of cells appears to be much restricted in avians, but is more prominent in some mammals[75]. Transverse processes of neuroepithelium, MG precursors, and mature MG (see below) are hypothesized to serve as the stabilizing structure that keeps cell clones within columns.

Formation of plexiform layers and stratification

Individual cells thus find their relative position within stacked cell columns as a result of their sequential birthdates. A logical next question is how various retinal cell types become interconnected with one another to establish a retinal neuronal network. Although the onset of inner retinal neuron (GCs, ACs) and of outer retina neuron (HCs, PRs) genesis widely overlaps, formation of the IPL significantly precedes that of the OPL; for example, IPL genesis occurs approximately 2 days prior to OPL genesis in the chick[76].

Differentiation of photoreceptors and formation of OPL

Photoreceptors undergo a lengthy process to achieve their final morphology and functionality, the entirety of which is beyond the scope of this review (see Swaroop, *et al.* 2010 for further detail)[77]. In brief, all PRs arise from photoreceptor precursors (PRP) which have the potential to become short wavelength (S) cones (considered the "default" PR program), medium-long wavelength cones (ML) cones, and rod PRs. A series of six transcription factors (OTX2, CRX, NRL, NR2E3, RORB, and THRB2) regulate one another via a stepwise process of lineage restriction that guides RPCs from commitment throughout differentiation of mature rod and cone PRs (the *transcriptional dominance* model of PR fate determination)[77].

The OPL harbors glutamatergic synapses between PRs, BCs and HCs. Its formation is temporally delayed relative to the IPL. In the chick, segregation between the ONL and INL is detectable from E9 onwards[78,79]. Similar to ACs, differentiation of HCs displays an initial radial

outgrowth of processes that becomes laterally oriented[80]. This transition appears to be dependent upon the presence of rods, but not cones[81,82]. With their wide lateral plane of dendritic processes, HCs cover a huge circular field of rod and cone synaptic terminals. During development, the number of terminals is distributed relatively evenly over the entire field, but terminals become more concentrated near the HC cell body towards maturity. In the absence of cones, a transition of terminal branching does not occur[82].

IPL network formation

The IPL is a cell-free zone filled with complex synaptic interactions. A multitude of laterally arranged parallel sublaminae can be histologically documented in which synaptic connections between specific subpopulations of GCs, ACs, dACs and BCs are formed at discrete locations in the IPL (see **Fig. 3**). Major synaptic sublaminae are conventionally denoted by small letters (a-d) or numbers (1-5), although the definitive number of sublaminae is still debated[41]. The outermost and innermost sublaminae are most prominent, are likely the first to be established[44]. A given sublamina represents synaptic connections between specific cell subpopulations and contains synapses using the same neurotransmitter (glutamate, GABA, ACh, glycine, etc.). Individual sublamina may also facilitate distinct physiological functions, as observed in distinct OFF and ON channels.

How and when are these sublaminae established? Which cells are first to project their processes into a future IPL (e.g., RGCs, ACs, or BCs)? Some neurotransmitters are expressed long before synapses occur[83] and appear to play important roles for IPL stratification. The only cholinergic cell type in retina is the *starburst amacrine cell* (SAC), which is amongst the first cell types born in the inner retina and is therefore of particular developmental interest. Since RGCs are the very first retinal cells to be born, one might suppose that they would also be the first to extend dendrites

into the IPL, thereby initiating and dictating IPL stratification. Indeed, interference with RGC differentiation affects their branching pattern within the IPL. For instance, dendritic stratification patterns of α- and ß-RGCs in cat and ferret were disturbed after injection of 2-amino-4-phosphonobutyrate (ABP, an agonist of mGluR6 receptors)[84–86]. Blocking glutamatergic or cholinergic transmission in chick and turtles, respectively, also decreased the branching sizes of RGCs[87,88]. Surprisingly, however, the branching pattern of ACs was largely undisturbed after optic nerve crush in rodents (destroying all RGCs), or similarly, in mice and zebrafish mutants lacking RGCs[89–91]. Clearly, establishment of specific sublaminae and arborization of ACs do not depend on RGCs[92], and while neurotransmitter systems are important drivers of IPL stratification, RGCs do not play an essential role in its development.

III. Formation of outer retina *in vitro*

Retinal spheroid research has proven instrumental to revealing the interdependence of differentiation between outer and inner retinal laminae. These interactions include those between PRs and HCs or BCs, ACs with GCs, and MG that span the outer and inner retina (**Fig. 7**). The emergence of inner and outer retinal structures in retinal spheroids has revealed remarkable differences across several vertebrate models. Three questions are particularly instructive: 1) How is histological structure achieved in retinal spheroids? 2) How do cells find their final relative position within spheroids (radial laminar polarity)? 3) To what degree do outer retinal structures mature *in vitro*?

In this section, we briefly address what may be learned from retinal spheroids regarding these questions. Since most of these processes are highly dependent on specific culture conditions, the following section deals with "plasticity" (e.g., with *indeterminate aspects* of retinal spheroid formation).

The outer retina consists of PRs, an OPL and horizontal cells (HCs). In the chick, stratified and rosetted retinal spheroids can both yield these components (**Fig. 7a**), depending on culture conditions. Although HCs are seldom detected, both types of PRs (rods and cones) and an OPL are consistently formed. Both rod and cone PRs reside within a well-delineated ONL in stratified spheroids (**Fig. 7b**) and appear within organized cellular rosettes in rosetted spheroids (**Fig. 7a, right; 7c, 7e**). PR precursors are often more loosely distributed throughout the spheroid space (**Fig. 7c**), in areas called "non-organized zones" (*noz*); (**Fig. 7e**).

How is histological structure achieved in retinal spheroids?

Immediately after primary reaggregation of chick retinal cells, cells replenish their surface markers and a subset of RPCs begin to proliferate. RPCs form primary rosettes via sorting-out (scheme in **Fig. 6A**), though this effect is generally much less pronounced with rodent retinal cells than in the chick. These rosettes increase consistently in size and diameter via cell division to form a one cell-wide layer. From an early stage, these rosettes appear to provide an "anchor structure" upon which newly produced daughter cells emanate radially outwards (**Fig. 6B**).

How do cells find their final relative position within spheroids?

Newly born cells produced from rosettes remain arranged within stable radial cell columns, as demonstrated in chimeric spheroids produced from mixtures of dissociated chick and quail retinal cells (**Fig. 6B, C**). Nomarski optics in chick/quail chimeric rosetted spheroids and stratospheroids established the clonal cell production of cell columns[74,93]. Spherical building modules are consequently formed rather rapidly by an assembly of cell columns, each containing cells of a future ONL and INL (**Fig. 7**). A narrow cell-free space within building modules indicates the presumptive OPL prior to its emergence. After 2-3 days *in vitro*, each single rosetted spheroid contains several spherical building modules (**Fig. 7c, 7e, 7f**).

In chicken spheroids derived from E5/6 retina, many rod and cone PRs reside within one-cell-wide rosettes (**Fig. 7c, 7e**), while varying numbers of wayward PRs (predominantly rod precursors) are found within non-organized zones (**Fig. 7e**). Morphologic observations suggest that all PRs in rosettes are derived from mitotic cells within early rosettes (**Fig. 6**). However, it appears unlikely that all PRs in *noz* are derived from mitoses in rosettes; immunolabeling of *noz* revealed that the very first cones were actually detected outside of rosettes[94,95]. In fact, a large fraction of disorganized cells in two day-old spheroids (**Fig. 7e**) already expressed XAP-1 or visinin, both early markers of PR precursors[96]. In primary rosettes consisting of approximately 10 cells, roughly half expressed visinin. Notably, whenever *rosetted spheroids* of the chick had fully matured into laminar stratospheroids, all PRs became well integrated into a proper ONL (**Fig. 6B**).

To what degree do outer retinal structures mature in vitro?

There is evidence to suggest that both rod and cone photoreceptors develop to varying degrees in retinal spheroids, depending on species, embryonic age, and tissue organization. In chicken rosetted spheroids, putative outer segments with PR disc formation were detected by electron microscopy[97], but complete maturation of PRs including well-developed outer segments was never achieved in any of the reported models (chick, rat, gerbil, fish). These cells thus represent immature PRs at various stages of development and are best defined as PR precursors rather than PRs. In fully laminar stratospheroids outer segments were largely absent (though stumps reminiscent of their structure remained), likely lost as result of shearing due to constant rotation.

IV. Plasticity of retinal tissue formation in spheroids

The availability of different types of retinal spheroids provides a unique platform to analyze the basics of retinal tissue formation *in vitro*. In particular, the fact that four distinct morphologies can be produced from chicken embryonic retinae (e.g., non-organized zones, PR rosettes, IPL-like areas in *rosetted spheroids*, and laminar tissue in stratospheroids), shows that retinal tissue formation *in vitro* is regulated by non-autonomous environmental constraints. These structures have proved most instrumental when testing a wide spectrum of culture conditions affecting retinal histogenesis. Based on analyses of all four tissue types, we will briefly discuss the dependence of these formations on the species of original cells, embryonic age, relative origin of cells (central, peripheral, or ciliary margin), and the molecular and cellular tissue environment (e.g., growth factors, RPE cells or supernatants).

Age and location of original cells dictate spheroid morphology

The age and the retinal location of cells from which spheroids are generated is a decisive factor in the type of spheroid that will be preferentially formed *in vitro*. The percentage of proliferating cells contained in the original cellular dispersion decreases with age. More peripheral regions also appear to contain a higher percentage of proliferative cells. Since each retinal area holds cells of different developmental stages due to a central-to-peripheral gradient of retinal differentiation (**Fig. 4C**), a retinal cell population derived from a central retinal area at a younger stage (e.g., E5) will lead to spheroids that resemble spheroids from more peripheral parts from older tissue (e.g., E6). For instance, spheroids from chicken E5 retinae display a higher proportion of PR rosettes, while cells from E6 retinae present larger proportions of IPL areas. By 6 days *in vitro*, these IPL areas become assembled below the spheroid surface, where eventually protrude as distinct tissue bulges from the surface[96]. Thus, the ratio of cells from the outer to inner retina in chicken spheroids is dependent upon the age and/or location of the original cell population.

Photoreceptor plasticity in retinal spheroids

In spheroids from embryonic rat retina, rods differentiate along a similar developmental timeline as observed *in vivo*. When retinal cells from rat embryos were grown in mixed-age culture with an abundance of neonatal retinal cells, the relative ratio of rods increased among embryonic neuroepithelial cells. Neonatal cells were less proliferative and attained rod features at a much earlier time point, indicating some degree of plasticity for rod development[98]. As in normal rat retinas, two distinct phases of rod production were also detected in *in vitro* spheroids. The early phase appeared to be unaffected by *in vitro* exposure of spheroids to a postnatal retinal cell environment, indicative of intrinsic (cell-autonomous) determination of early rods[33]. When RPCs from embryonic rat retina were labeled and cultured as spheroids in mixed-age cultures with an excess of postnatal retinal cells, the postnatal cells appeared to inhibit AC production and affect cone production. ACs also inhibited production of additional ACs by feedback inhibition[32]. In a reverse experiment with RPCs from postnatal rat retina cultured with excess of embryonic retinal cells, a change in cell fates was documented with fewer rods produced[34]. More BCs were also detected, possibly due to LIFR-ß signaling by embryonic cells.

For avian spheroids, a comparative immunohistochemical study on the development of ML cones and of rods revealed notable differences between *noz,* rosetted spheroids, and stratospheroids[95] (**Fig. 7a-c**). In both rosetted and stratified spheres, the total ratio of ML-cones was similar to that observed *in vivo*, suggesting that cones genesis was autonomous in all tissue conditions. In contrast, a distinct rod differentiation appeared to be dependent on the presence of cones and the degree of tissue organization. In stratified spheres, rods appeared approximately one day after cones and were consistently located within clusters of existing cones. The ratio of rods to cones increased as tissue organization decreased; that is, in stratified spheres the rod-to-cone ratio was 0.5 (1 rod/2 cones); in rosetted spheroids it was 0.74 (3 rods/4 cones), and in *noz* it was 1.09 (1 rod/1 cone). It therefore seems that cones may foster rod development and appear

to dictate the number of rods produced in a given tissue environment, suggesting multiple potential pathways for rod cell lineages. Paradoxically, in many retinal dystrophies rods degenerate before cones, and it is now well-established that cone maintenance depends on the secretion of trophic factors by rods[99,100]. Thus, while rod development *in vivo* depends on preexistence of cones, long-term survival of cones relies on functional rods. The fixed rod-to-cone relations observed in spheroids with varying degrees of organization appear to hint at mutual regulatory effects between rods and cones.

Environmental organization of tissues: How does a rosetted structure become a laminar retinal tissue?

The retina develops continuously within a growing eyecup. As the eyecup increases in volume, the retina expands in the planar dimension (*i.e.,* as a sheet). In a reaggregate system arising from singularized cells, a tissue can only develop in 3D (*i.e.,* as a spheroid), since reaggregation of cells in suspension leads to clustering of cells. As outlined above, such retinal reaggregates can still achieve a high degree of tissue differentiation, including histotypic modules akin to the normal retina, though the polarity of layered structures is often inverted (as in PR rosettes). A fundamental question thus arises as to whether and how such spheroids might be transformed into planar retinal tissues.

Which conditions were most effective to induce *stratified spheroi*ds from chick retina? The RPE is closely opposed to the retina *in situ*, and both tissues mutually influence one another during development and upon maturation. In 1984, a landmark study demonstrated the reconstruction of a fully laminar spheroid when dispersed retinal cells were co-cultured with RPE cells from the chick embryo[19]. In subsequent experiments, individual cultures of central and peripheral retina, central and peripheral RPE, and all potential combinations of these four tissues were analysed to determine which types of retinal spheroids were produced[101]. The highest proportion of *stratified*

spheroids (up to 90%) was detected from ciliary marginal tissue, containing both RPE plus adhering neuroepithelial stem cells (cf. Fig 0/1d). In this case, transdifferentiation from RPE into retinal cells appeared to contribute to spheroid formation. Furthermore, co-culture with MG or supplementation with supernatants from RPE or from isolated Müller glia were highly effective in successful spheroid production[102].

The histological transformations from a rosetted into a stratospheroid could were analyzed in detail in chicken rosetted spheroids due to the early occurrence of PR rosettes, columnar cell organization, and IPL formation. These transformations included polarity inversions of large sections of laminar structure, initiated either by fusion of PR rosettes, or by fusion of IPL areas. When PR rosettes dominate the spheroid, the rosettes will enlarge and eventually combine with one another, resulting in concomitant fusion of corresponding INL/IPL sections. Eventually, voluminous PR rosettes will fuse with the surface of the sphere, and thereby induce a complete reversal of all cell layers. Under conditions where PR rosettes remain small, larger organized INL/IPL subunits act as building blocks which fuse with one another to form large laminar stretches. In these cases, fusion is initiated by long MG processes extending from one IPL area to an adjacent one, thus mediating contacts between individual building blocks. Dramatic fusion of IPL areas could be achieved through treatment with FGF2[96].

V. Reaggregates and retinal organoids

Spheroids are the product of a short primary period of sorting-out among dispersed cells, and a longer period of development including cell proliferation and differentiation. The emergent tissue properties depend on ever-changing physicochemical conditions further mediated by complex genetic and molecular cascades, which begs the question of whether findings gained from spheroids reliably explain *in vivo* development. Spheroids are in many aspects highly artificial models, and results must be interpreted with due caution. The use of extreme, non-physiologic

culture conditions (environment, chemical supplies, stress, etc.)—whether intentional or unintentional—may lead to results which bear no significance for any *in vivo* situation. Though spheroids are an artificial system, valuable information can also be garnered from them, and many classical studies of retinogenesis have used spheroids to uncover central themes of retinal differentiation[19,32–34]. It is thus clear that a variety of external forces and cell-autonomous factors direct primary steps of spheroid tissue formation in an artificial *in vitro* space. Comparing and contrasting observations between spheroids and retinal organoids provides an additional layer of rigor in distinguishing relevant histogenic mechanisms from oddities of 3D culture systems.

Are PSC-derived organoids reaggregates?

Retinal organoids as they are presently produced from mouse and human PSCs[103–106] share some similarities to the above-described retinal spheroids but are also fundamentally distinct, largely due to differences in the developmental stage of the original cell source and the specific experimental procedures required for development to occur. PSCs are cells that have—by definition—two capacities: 1) the ability to proliferate *in vitro* indefinitely, and 2) the ability to differentiate into all bodily cell types. PSC retinal organoid cultures thus begin with cells corresponding to the very earliest developmental stages. They are subsequently guided in a stepwise manner through distinct developmental stages[107,108] (e.g., neural tube, optic stalk, retina/RPE, etc.) to form 3D retinal structures. Almost immediately, PSCs establish appropriate cell-to-cell interactions within maturing cell formations (e.g., embryoid bodies, neurospheres, etc.). As they proliferate and begin to differentiate, PSCs can and do form a developmentally appropriate molecular-cellular environment[106], following relatively normal developmental pathways. While PSC-derived retinal organoids are grown in similar suspended culture conditions, they are not "reaggregates" in the above-described sense. Cells of a PSC-derived aggregate are rarely exposed to the harsh conditions used to make spheroid cultures. Given these

distinct differences in origin, it is often remarkable how similar spheroids and organoids can appear.

Human retinal organoid technology

Since the isolation of hESCs[2] and subsequent generation of hiPSCs[1,3], many protocols for differentiation of 3D retinal organoids (ROs) from hPSCs have been described[109]. The earliest and most recent variations on RO differentiation are alike in that both follow cues from classical retinal development studies in spheroids and other model systems (**Fig. 3**). PSC-derived retinal culture initially began with 2D approaches; exogenous expression of Wnt and BMP antagonists were used to direct ESCs toward an anterior neural cell fate for production for RPCs[110,111]. However, these first studies required co-culture with mature retina or transplantation into the subretinal space to reach a PR fate, suggesting that critical cell-to-cell interactions or signaling factors were missing. Subsequent methods were successful in generating PR precursors[112] from PSCs in the absence of retinal tissue, albeit with relatively low efficiency. Approaches which approximated the timeline of normal human retinogenesis in a stepwise manner were the first to successfully generate spherical cultures now known as retinal organoids containing early retinal cell types from two-dimensional neural rosettes[103,104,108].

The general approach to nearly all current protocols involves aggregating PSCs in suspension culture to form spherical embryoid bodies (EBs) with subsequent neuralization of EBs[109,113] toward an anterior neuroectodermal fate through inhibition of Wnt and BMP signaling pathways[109]. The introduction of BMP4 during neuralization drastically increases the yield of RPCs in such cultures[106,109,114]. Over time, phase-bright laminar optic vesicle-like structures arise and are isolated from non-retinal tissues for long-term 3D culture[103,105,106,115]. RO differentiation occurs across three distinct stages that mirror epochs of human fetal retinal development and follow developmentally conserved spatiotemporal retinogenesis[106,116]. Stage 1 is characterized by dominance of RPCs and genesis of early-born RGCs and ACs, with a classic phase-bright

neuroepithelial rim. Stage 2 is characterized by a peak in PRP production with rising numbers of BCs and other interneurons; a lobed appearance with or without tufts of RPE is relatively common. The final stage (Stage 3) extends indefinitely and is characterized by relative maturation of PRs and MG genesis[106] with a re-emergence of bright outer lamination and the appearance of hair-like outer segment projections.

Numerous studies in recent years have documented the authenticity of PSC-derived ROs. We now know that PSC-derived ROs pass through classic stages of retinogenesis[106], mature to form all classes of retinal neurons, form characteristic laminae[115], are capable of responding to light[105], and form functional synapses within organoids[117]. Moreover, PRs from ROs form characteristic histological and ultrastructural features of PRs, including synaptic ribbons[106,117,118] and stacked discs within outer segments[106,117,119]. These findings have led to their rapid deployment toward neuroretinal cell replacement, though there are limitations of this approach that remain to be addressed. A discussion of the similarities and differences between spheroids and retinal organoids provides a useful framework for exploring strengths and weaknesses of current organoid technologies.

Similarities and differences between retinal spheroids and retinal organoids

Striking similarities exist between spheroids and retinal organoids, particularly in the context of the outer retinal laminae and development of PRs. Both provide an excellent system for modeling PR-specific development, as production of many rod and cone PRP is a hallmark of spheroid and organoid approaches. Early 2D protocols and 3D protocols for RO generation that predate the introduction of BMP4 often resulted in rosetted organoids that were highly remniscent of the organization of rosetted spheroids[103,108,115]. Newer methods are characterized by an advanced degree of outer lamination over months in culture that bear a stronger resemblance to laminar spheroids, although inner regions of wayward displaced cones (akin to the *noz* in spheroids) are

also present. The nature and origin of such cells is of interest to many within the field, and a revisiting of mechanisms leading to the production of the *noz* in spheroids my provide further insight to the mysteries of displaces cones in RO cultures. Moreover, the appearance (and potential disappearance) of outer segment-like structures between both systems is quite similar. Though the appearance of hair-like projections at the outermost surface of ROs is common by stage 3, such structures may be sheared off as a result of being grown in suspension as has been observed in stratified spheroids. Immunohistochemical analyses of such structures in ROs are inconsistently successful, and strategies for preserving their structure is a priority of ongoing research.

Maturation of spheroid-derived PRs is particularly useful in understanding and accurately defining PSC-derived retinal neurons. While a surprisingly high degree of anatomic and functional similarity exists between PSC-derived neurons and mature human retinal neurons, PSC-derived neurons generally do not reach “maturity“ in the classical sense, as they are at most months old (rather than years). While PSC-derived RO cultures appear to recapitulate development in a less artificial manner relative to spheroids, caution regarding interpretation of developmental studies is still warranted. As RO technologies continue to evolve, is has become apparent that even seemingly small alterations to the physicochemical conditions of 3D cultures can profoundly affect the maturity, structure, and function of ROs[106,120].

In ROs, the GCL and “displaced” starburst amacrine cells are the first to arise from RPCs (RGCs are largely absent from retinal spheroids). Longer-term organoid cultures eventually lose RGCs, hypothesized to occur in response to poor oxygen and nutrient exchange in the centre of the RO over time (>100 days) rather than the immediate loss occurring in spheroids. Both approaches do suggest that high degrees of lamination in outer retinal structures may still be achieved in the absence of substantial RGC involvement. Formation of the OPL is prevalent in more mature spheroids and organoids[106], and while spheroids often develop some degree of IPL

structure, this layer is largely absent in most organoid cultures over time. At least one example of a fully laminated (i.e., three-layered) organoid with IPL formation has been reported, though it appears to be a phenomenon of cell line rather than protocol development.[117] Various labs have sought to address these issues by revisiting shaking cultures or employing higher-technology bioreactors[109], though the implications of such approaches for long-term reproducibility remain to be seen.

Developmental lessons from retinal spheroids

Many of the most critical developmental lessons to be learned from spheroids relate to applications in cell transplantation using PSC-derived retinal tissues. The formation of rosetted morphologies following PSC organoid sheet transplantation is an ongoing source of investigation. The development of rosettes in PSC-derived grafts seems to most closely mirror the histological transformations documented between rosetted and stratified spheroids. Indeed, sheets of tissue from PSC-derived retinas—whose PRP reside along the outermost rim—almost invariably produce “inverted” rosettes in the subretinal environment and display minimal interaction with host retinal tissue. These rosettes bear a striking resemblance to columnar formations arising from RPCs in rosetted spheroids and thus appear to be a result of residual RPCs within grafted PSC retinal tissues; whether this mechanism can effectively be harnessed to further guide graft organization remains to be seen.

Furthermore, spheroids have demonstrated the potential to capitalize on co-culture of retinal laminae with RPE and/or MG to further guide morphogenesis. While there is substantial interest in the application of RO technologies for co-delivery of retinal neurons and RPE[121], such methods are still in their infancy. While some organoids eventually develop their own “tufts” of attached RPE, this process is not yet easily regulated in cultures. Further efforts to facilitate apposition between PSC-derived ROs and RPE will likely benefit from the mechanisms outline in

classical spheroid studies of laminar and rosetted structures, which demonstrated remarkable responses to modulation by adjacent RPE and/or MG.

Finally, classical spheroid studies have highlighted a multitude of physicochemical, environmental, and cell-autonomous factors that can contribute to the *in vitro* development of highly organized retinal tissue. Retinal organoids have provided an avenue for expanding upon these studies, opening the door to studies of disease modelling, cell therapy, and human retinal development that were previously unavailable. As the field advances further into these arenas, spheroid studies serve as an excellent example of how to maximize translation of *in vitro* systems to better understand and guide the development of organized retinal structures.

Figures

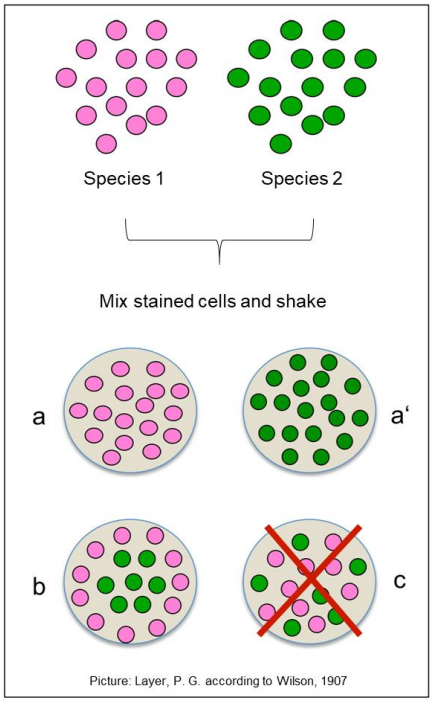

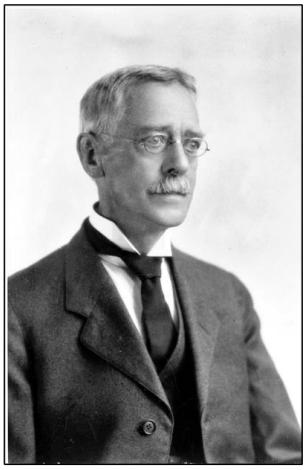

Figure 1. The sponge sorting experiments of Henry Van Peters Wilson. Following singularization of sponges, Wilson observed remarkable sorting effects when mixing sponges of distinctly colored species. Sponges formed single-color reaggregates (a, a’) or self-organized within a single reaggregate (b) but did not remain intermixed (c). Photograph of Henry Van Peters Wilson (credit: Johns Hopkins Sheridan Libraries; https://jscholarship.library.jhu.edu/handle/1774.2/52096).

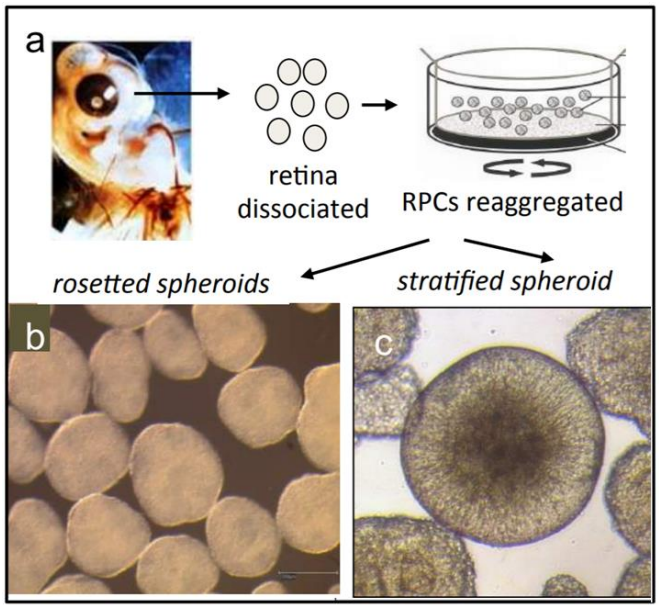

Figure 2. Generation of spheroids from the dissociated chick retina. (**a**) Chick retinas are isolated and singularized for reaggregation in shaking cultures. Spheroids were initially rosetted in morphology (**b**), but generation of stratified spheroids (**c**) was a critical milestone, as it demonstrated proof-of-concept for reformation of organized retinal tissues from stem/progenitor cells.

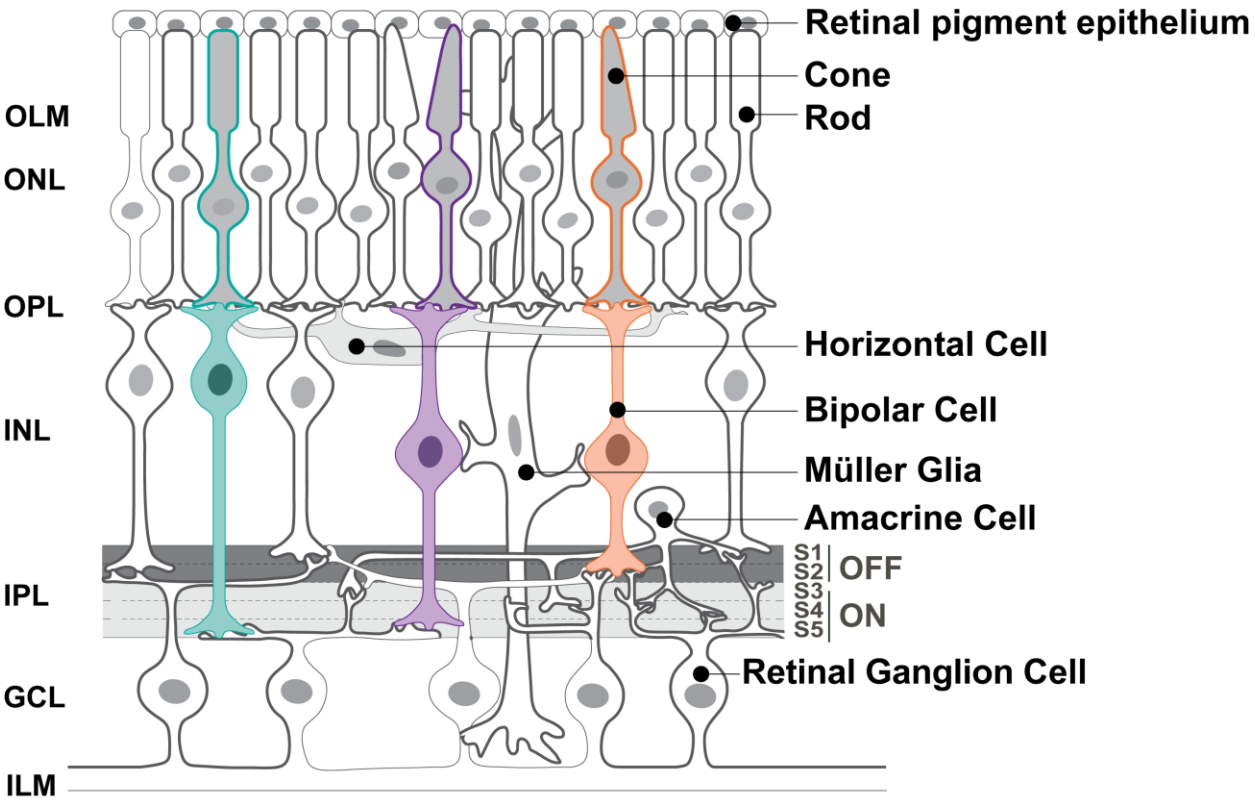

Figure 3. Anatomy and functional circuitry of the retina. Seven major cell types delineate the mature vertebrate retina: rod and cone photoreceptors (PRs), horizontal cells (HCs), bipolar cells (BCs), amacrine cells (ACs), and retinal ganglion cells (RGCs). A host of morphologic and physiologic features define subtypes for each major type of retinal cell. Müller glia (MG) span the entirety of the retina, forming the inner and outer limiting membrane (ILM and OLM). The retinal pigment epithelium (RPE) lies in close interdigitation with rod and cone PRs. Three layers of cell bodies—the outer nuclear layer (ONL), inner nuclear layer (INL), and ganglion cell layer (GCL)—are sequentially connected by the outer plexiform layer (OPL) and inner plexiform layer (IPL). The IPL contains several sublaminae with synapses of ON and OFF retinal circuits.

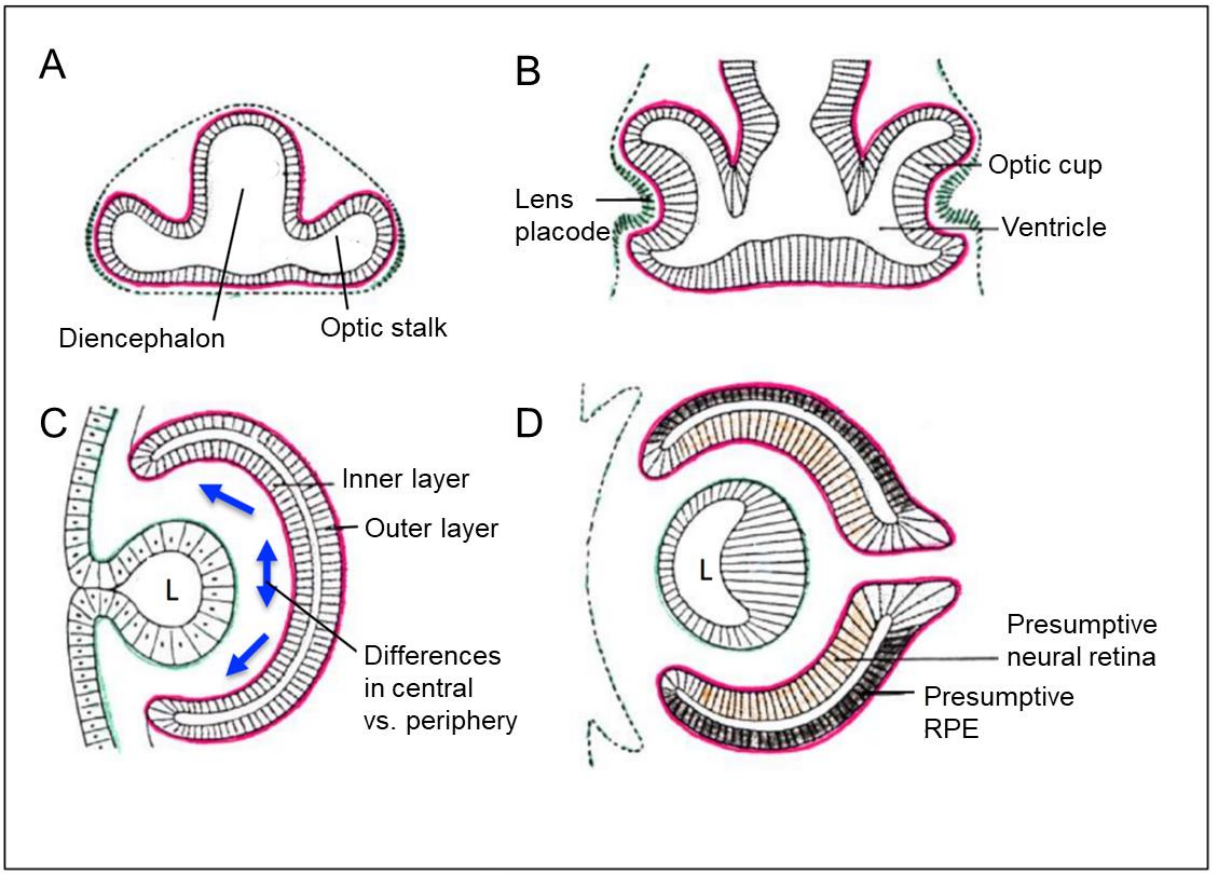

Figure 4. Vertebrate optic cup morphogenesis. (**A**) The optic stalk initially forms as an outpouching of the diencephalon, extending until it reaches the overlying surface ectoderm. (**B**) Induction at the site of contact between the optic stalk and surface ectoderm results in the formation of a lens placode and optic cup. As the optic cup invaginates, the basal aspect (highlighted in red) faces outward. (**C**) Inner and outer layers of the presumptive optic cup, which eventually form the presumptive neural retinal and RPE, respectively (**D**). As the presumptive neural retina and RPE develop, the apical aspect of both layers face one another, with the basal aspect of presumptive RPE facing outward and the basal aspect of presumptive neural retina facing inward (highlighted in red).

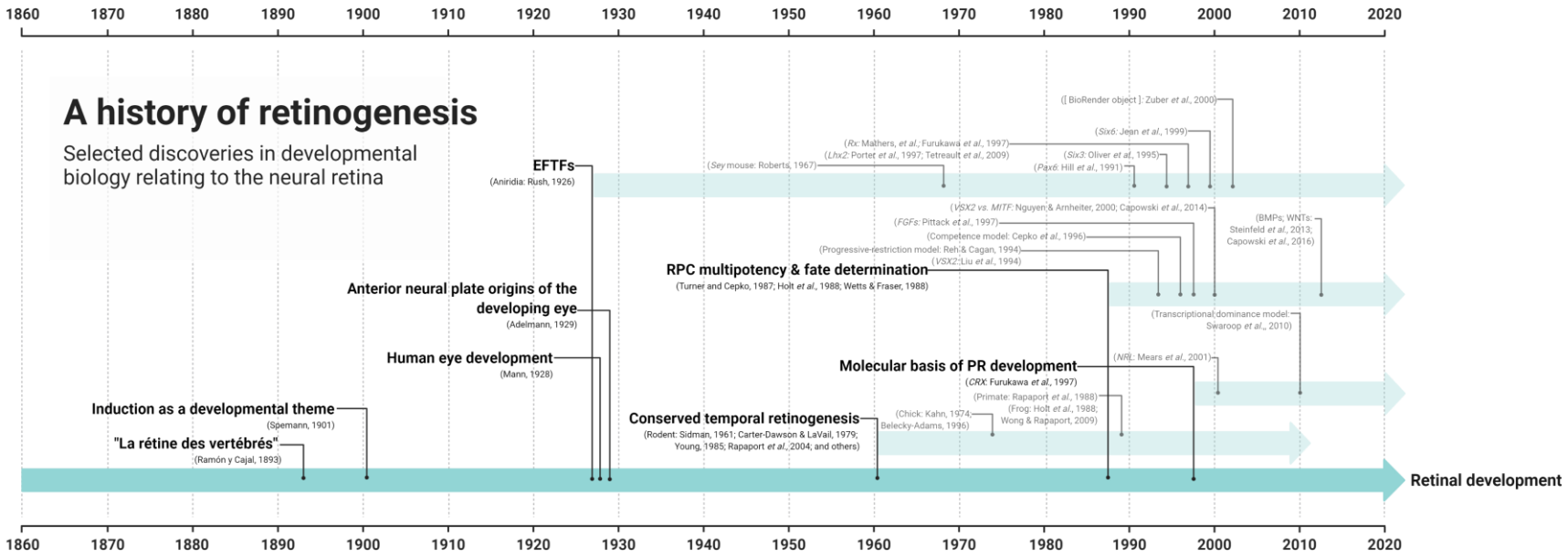

Figure 5. Historic studies of retinal development foundational to modern spheroid and organoid studies of retinogenesis.

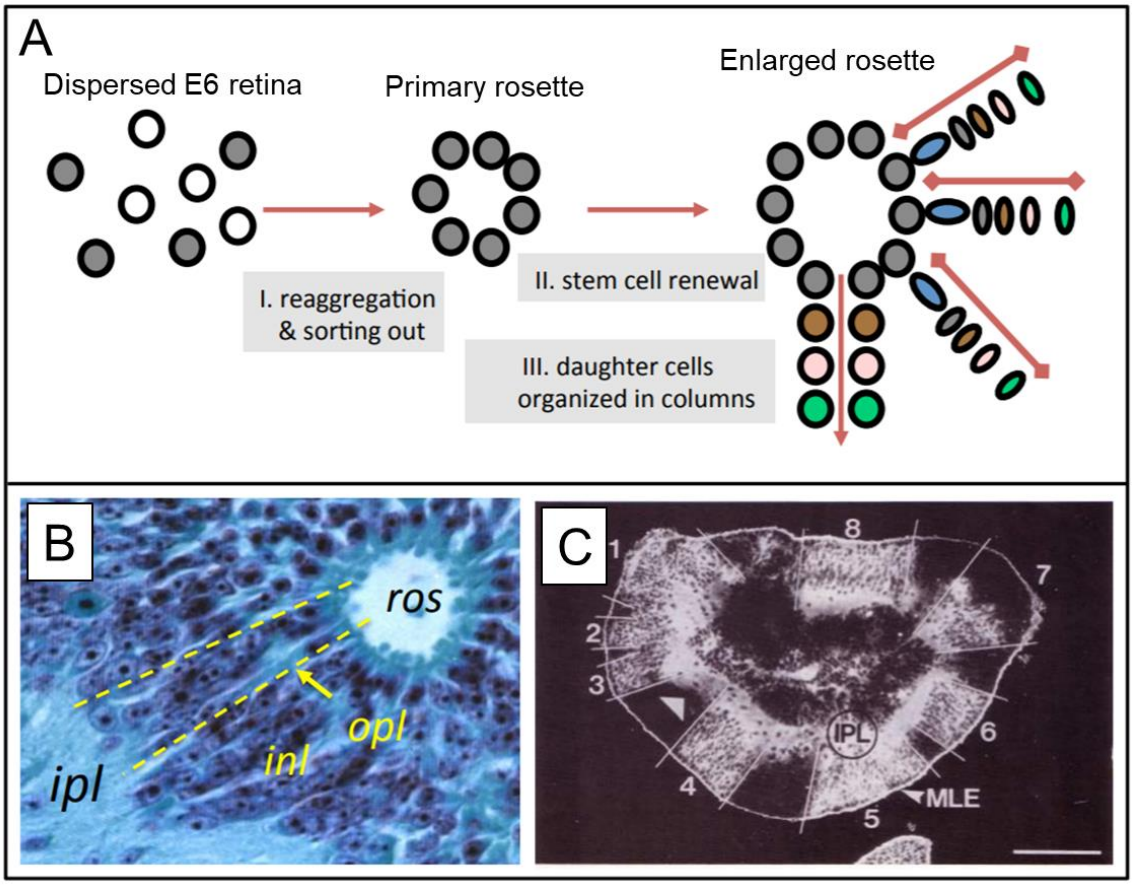

Figure 6. (**A**) Scheme of PR rosette and cell column formation in stratified spheroids. (**B**) A rosette with confluent cell columns in a chick/quail spheroid. (**C**) Sectors of stained quail cells in a chimeric stratospheroid, derived from a mixture of dispersed chick and quail cells.

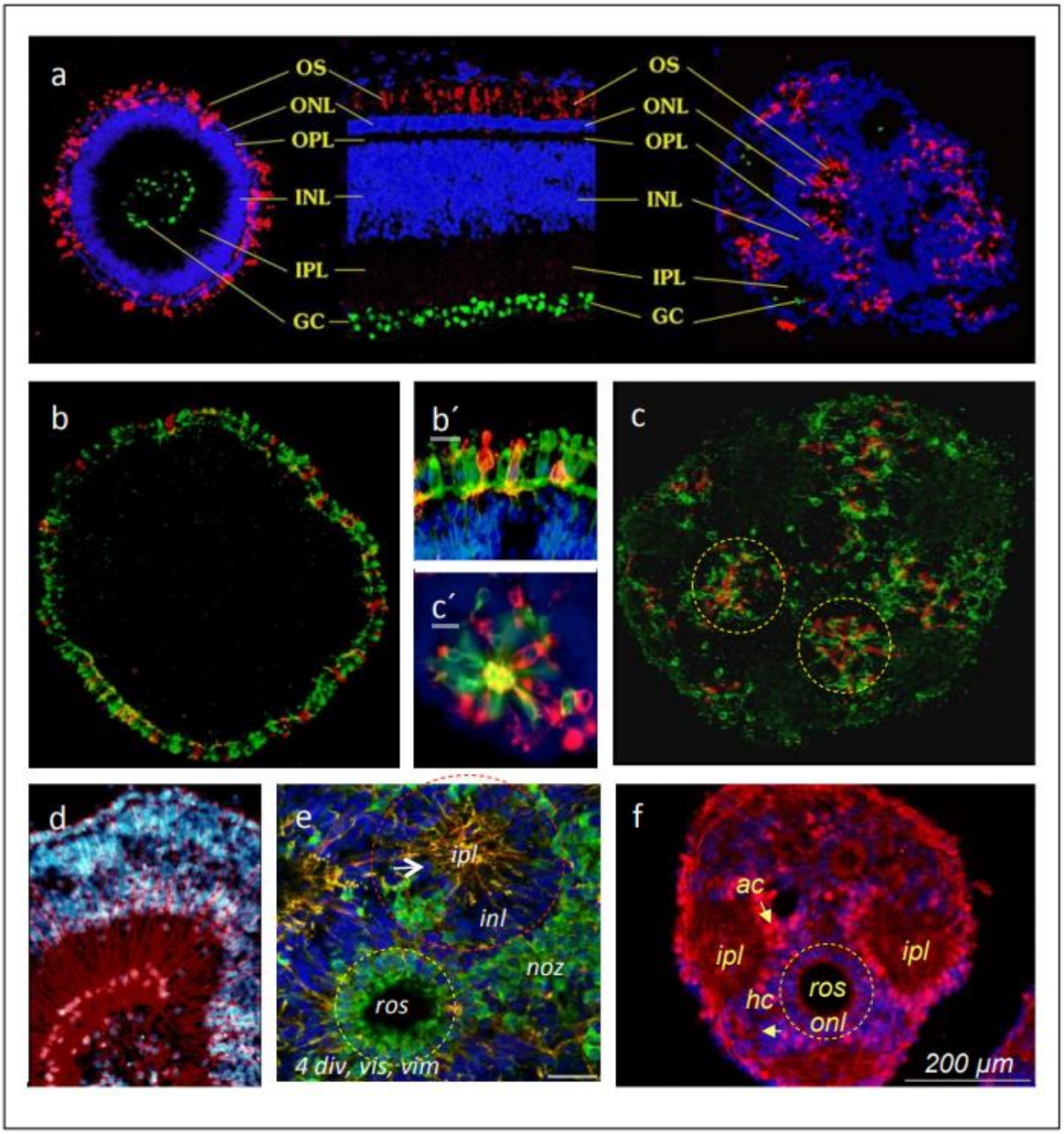

Figure 7. Retinal spheroids from EE5/6 chick embryo. (**a**) *Stratified* spheroids (left) and *rosetted* spheroids (right) contain distinct regions corresponding to various layers of the chick retina (middle). (**b, b', d**) Further examples of *stratified* spheroids. (**c, c', e, f**) Further examples of *rosetted* spheroids. Rising structures are encircled: PR rosettes (yellow circles, **c, e, f**), IPL (red circle, **e**). (**d**) Columnar organization by MG precursor processes.

References

1. Takahashi, K. *et al.* Induction of Pluripotent Stem Cells from Adult Human Fibroblasts by Defined Factors. *Cell* **131**, 861–872 (2007).
2. Thomson, J. A. *et al.* Embryonic stem cell lines derived from human blastocysts. *Science* **282**, 1145–1147 (1998).
3. Yu, J. *et al.* Induced pluripotent stem cell lines derived from human somatic cells. *Science* **318**, 1917–1920 (2007).
4. Corrò, C., Novellasdemunt, L. & Li, V. S. W. A brief history of organoids. *American Journal of Physiology-Cell Physiology* **319**, C151–C165 (2020).
5. Lancaster, M. A. & Knoblich, J. A. Organogenesis in a dish: Modeling development and disease using organoid technologies. *Science* **345**, (2014).
6. Singh, M. S. *et al.* Retinal stem cell transplantation: Balancing safety and potential. *Progress in Retinal and Eye Research* **75**, 100779 (2020).
7. Wang, Y., Tang, Z. & Gu, P. Stem/progenitor cell-based transplantation for retinal degeneration: a review of clinical trials. *Cell Death & Disease* **11**, 1–14 (2020).
8. Maeda, T., Sugita, S., Kurimoto, Y. & Takahashi, M. Trends of Stem Cell Therapies in Age-Related Macular Degeneration. *Journal of Clinical Medicine* **10**, 1785 (2021).
9. Khaner, O. The potency of the first two cleavage cells in echinoderm development: the experiments of Driesch revisited. *Rouxs Arch Dev Biol* **202**, 193–197 (1993).
10. Wilson, H. V. On some phenomena of coalescence and regeneration in sponges. *Journal of Experimental Zoology* **5**, 245–258 (1907).

11. Townes, P. L. & Holtfreter, J. Directed movements and selective adhesion of embryonic amphibian cells. *Journal of Experimental Zoology* **128**, 53–120 (1955).
12. Fujimori, T., Miyatani, S. & Takeichi, M. Ectopic expression of N-cadherin perturbs histogenesis in Xenopus embryos. 10.
13. Gerisch, G. Inter-Relation of Cell Adhesion and Differentiation in Dictyostelium Discoideum. *J Cell Sci* **1986**, 201–219 (1986).
14. Moscona, A. Rotation-mediated histogenetic aggregation of dissociated cells: A quantifiable approach to cell interactions in vitro. *Experimental Cell Research* **22**, 455–475 (1961).
15. Weiss, P. & Taylor, A. C. Reconstitution of Complete Organs from Single-Cell Suspensions of Chick Embryos in Advanced Stages of Differentiation. *PNAS* **46**, 1177–1185 (1960).
16. Mayerson, P. L. & Moscona, A. A. Malformation of Embryonic Neural Retina Elicited by BrdU. *Differentiation* **13**, 173–184 (1979).
17. Steinberg, M. S. Reconstruction of Tissues by Dissociated Cells. *Science* **141**, 401–408 (1963).
18. Steinberg, M. S. Mechanism of Tissue Reconstruction by Dissociated Cells, II: Time-Course of Events. *Science* **137**, 762–763 (1962).
19. Vollmer, G., Layer, P. G. & Gierer, A. Reaggregation of embryonic chick retina cells: Pigment epithelial cells induce a high order of stratification. *Neuroscience Letters* **48**, 191–196 (1984).
20. Jensen, C. & Teng, Y. Is It Time to Start Transitioning From 2D to 3D Cell Culture? *Front. Mol. Biosci.* **0**, (2020).

21. Antoni, D., Burckel, H., Josset, E. & Noel, G. Three-Dimensional Cell Culture: A Breakthrough in Vivo. *International Journal of Molecular Sciences* **16**, 5517–5527 (2015).
22. Folkman, J. & Hochberg, M. Self-regulation of growth in three dimensions. *J Exp Med* **138**, 745–753 (1973).
23. Mueller-Klieser, W. Three-dimensional cell cultures: from molecular mechanisms to clinical applications. *Am J Physiol* **273**, C1109-1123 (1997).
24. Steinberg, M. S. Differential adhesion in morphogenesis: a modern view. *Curr Opin Genet Dev* **17**, 281–286 (2007).
25. Gimbrone, M. A., Leapman, S. B., Cotran, R. S. & Folkman, J. Tumor dormancy in vivo by prevention of neovascularization. *J Exp Med* **136**, 261–276 (1972).
26. Sutherland, R. M. & Durand, R. E. Growth and cellular characteristics of multicell spheroids. *Recent Results Cancer Res* **95**, 24–49 (1984).
27. Layer, P. G. & Willbold, E. Regeneration of the avian retina by retinospheroid technology. *Progress in Retinal and Eye Research* **13**, 197–230 (1994).
28. Layer, P. G. & Willbold, E. Histogenesis of the avian retina in reaggregation culture: from dissociated cells to laminar neuronal networks. *Int Rev Cytol* **146**, 1–47 (1993).
29. Akagawa, K. & Barnstable, C. J. Identification and characterisation of cell types accumulating GABA in rat retinal cultures using cell type specific monoclonal antibodies. *Brain Res* **408**, 154–162 (1987).
30. Akagawa, K. & Barnstable, C. J. Selective localization of glycine-accumulating cells in reaggregate culture of rat retina. *Brain Res* **428**, 124–128 (1987).

31. Watanabe, T. *et al.* Differentiation and morphogenesis in pellet cultures of developing rat retinal cells. *J Comp Neurol* **377**, 341–350 (1997).
32. Belliveau, M. J. & Cepko, C. L. Extrinsic and intrinsic factors control the genesis of amacrine and cone cells in the rat retina. *Development* **126**, 555–566 (1999).
33. Morrow, E. M., Belliveau, M. J. & Cepko, C. L. Two phases of rod photoreceptor differentiation during rat retinal development. *J Neurosci* **18**, 3738–3748 (1998).
34. Belliveau, M. J., Young, T. L. & Cepko, C. L. Late retinal progenitor cells show intrinsic limitations in the production of cell types and the kinetics of opsin synthesis. *J Neurosci* **20**, 2247–2254 (2000).
35. Bytyqi, A. H., Bachmann, G., Rieke, M., Paraoanu, L. E. & Layer, P. G. Cell-by-cell reconstruction in reaggregates from neonatal gerbil retina begins from the inner retina and is promoted by retinal pigmented epithelium. *Eur J Neurosci* **26**, 1560–1574 (2007).
36. Rieke, M., Gottwald, E., Weibezahn, K.-F. & Layer, P. G. Tissue reconstruction in 3D-spheroids from rodent retina in a motion-free, bioreactor-based microstructure. *Lab Chip* **8**, 2206–2213 (2008).
37. Eldred, M. K., Charlton-Perkins, M., Muresan, L. & Harris, W. A. Self-organising aggregates of zebrafish retinal cells for investigating mechanisms of neural lamination. *Development* **144**, 1097–1106 (2017).
38. Ail, D. & Perron, M. Retinal Degeneration and Regeneration-Lessons From Fishes and Amphibians. *Curr Pathobiol Rep* **5**, 67–78 (2017).
39. Araki, M. A Model for Retinal Regeneration in Xenopus. in *Xenopus Development* 346–367 (John Wiley & Sons, Ltd, 2014). doi:10.1002/9781118492833.ch18.

40. Araki, M. Regeneration of the amphibian retina: Role of tissue interaction and related signaling molecules on RPE transdifferentiation. *Development, Growth & Differentiation* **49**, 109–120 (2007).
41. Wässle, H. Parallel processing in the mammalian retina. *Nat Rev Neurosci* **5**, 747–757 (2004).
42. Kolb, H. Photoreceptors. in *Webvision: The Organization of the Retina and Visual System* (eds. Kolb, H., Fernandez, E. & Nelson, R.) (University of Utah Health Sciences Center, 1995).
43. Morgan, J. & Wong, R. Development of Cell Types and Synaptic Connections in the Retina. in *Webvision: The Organization of the Retina and Visual System* (eds. Kolb, H., Fernandez, E. & Nelson, R.) (University of Utah Health Sciences Center, 1995).
44. Hoon, M., Okawa, H., Della Santina, L. & Wong, R. O. L. Functional architecture of the retina: development and disease. *Prog Retin Eye Res* **42**, 44–84 (2014).
45. Boije, H., Shirazi Fard, S., Edqvist, P.-H. & Hallböök, F. Horizontal Cells, the Odd Ones Out in the Retina, Give Insights into Development and Disease. *Front Neuroanat* **10**, 77 (2016).
46. Wässle, H., Peichl, L. & Boycott, B. B. Dendritic territories of cat retinal ganglion cells. *Nature* **292**, 344–345 (1981).
47. Casey, M. A., Lusk, S. & Kwan, K. M. Build me up optic cup: Intrinsic and extrinsic mechanisms of vertebrate eye morphogenesis. *Developmental Biology* **476**, 128–136 (2021).

48. Zuber, M. E., Gestri, G., Viczian, A. S., Barsacchi, G. & Harris, W. A. Specification of the vertebrate eye by a network of eye field transcription factors. *Development* **130**, 5155–5167 (2003).

49. Jean, D., Bernier, G. & Gruss, P. Six6 (Optx2) is a novel murine Six3-related homeobox gene that demarcates the presumptive pituitary/hypothalamic axis and the ventral optic stalk. *Mech Dev* **84**, 31–40 (1999).

50. Mathers, P. H., Grinberg, A., Mahon, K. A. & Jamrich, M. The Rx homeobox gene is essential for vertebrate eye development. *Nature* **387**, 603–607 (1997).

51. Furukawa, T., Kozak, C. A. & Cepko, C. L. rax, a novel paired-type homeobox gene, shows expression in the anterior neural fold and developing retina. *Proc Natl Acad Sci U S A* **94**, 3088–3093 (1997).

52. Porter, F. D. *et al.* Lhx2, a LIM homeobox gene, is required for eye, forebrain, and definitive erythrocyte development. *Development* **124**, 2935–2944 (1997).

53. Tétreault, N., Champagne, M.-P. & Bernier, G. The LIM homeobox transcription factor Lhx2 is required to specify the retina field and synergistically cooperates with Pax6 for Six6 trans-activation. *Dev Biol* **327**, 541–550 (2009).

54. Oliver, G. *et al.* Six3, a murine homologue of the sine oculis gene, demarcates the most anterior border of the developing neural plate and is expressed during eye development. *Development* **121**, 4045–4055 (1995).

55. Hill, R. E. *et al.* Mouse small eye results from mutations in a paired-like homeobox-containing gene. *Nature* **354**, 522–525 (1991).

56. Nguyen, M. & Arnheiter, H. Signaling and transcriptional regulation in early mammalian eye development: a link between FGF and MITF. *Development* **127**, 3581–3591 (2000).
57. Capowski, E. E. *et al.* Loss of MITF expression during human embryonic stem cell differentiation disrupts retinal pigment epithelium development and optic vesicle cell proliferation. *Hum Mol Genet* **23**, 6332–6344 (2014).
58. Cepko, C. L., Austin, C. P., Yang, X., Alexiades, M. & Ezzeddine, D. Cell fate determination in the vertebrate retina. *Proc. Natl. Acad. Sci. USA* 7 (1996).
59. Carter-Dawson, L. D. & LaVail, M. M. Rods and cones in the mouse retina. II. Autoradiographic analysis of cell generation using tritiated thymidine. *J Comp Neurol* **188**, 263–272 (1979).
60. Young, R. W. Cell differentiation in the retina of the mouse. *Anat Rec* **212**, 199–205 (1985).
61. Kahn, A. J. An autoradiographic analysis of the time of appearance of neurons in the developing chick neural retina. *Dev Biol* **38**, 30–40 (1974).
62. Prada, C., Puga, J., Pérez-Méndez, L., López And, R. & Ramírez, G. Spatial and Temporal Patterns of Neurogenesis in the Chick Retina. *Eur J Neurosci* **3**, 1187 (1991).
63. Layer, P. G. & Kotz, S. Asymmetrical developmental pattern of uptake of Lucifer Yellow into amacrine cells in the embryonic chick retina. *Neuroscience* **9**, 931–941 (1983).

64. Liu, L., Layer, P. G. & Gierer, A. Binding of FITC-coupled peanut-agglutinin (FITC-PNA) to embryonic chicken retinas reveals developmental spatio-temporal patterns. *Brain Res* **284**, 223–229 (1983).
65. Prada, F. *et al.* Spatiotemporal gradients of differentiation of chick retina types I and II cholinergic cells: identification of a common postmitotic cell population. *J Comp Neurol* **410**, 457–466 (1999).
66. Fischer, A. J., Ritchey, E. R., Scott, M. A. & Wynne, A. Bullwhip neurons in the retina regulate the size and shape of the eye. *Dev Biol* **317**, 196–212 (2008).
67. Reh, T. A. & Fischer, A. J. Retinal stem cells. *Methods Enzymol* **419**, 52–73 (2006).
68. Cicero, S. A. *et al.* Cells previously identified as retinal stem cells are pigmented ciliary epithelial cells. *Proc Natl Acad Sci U S A* **106**, 6685–6690 (2009).
69. Davis, D. M. & Dyer, M. A. Retinal progenitor cells, differentiation, and barriers to cell cycle reentry. *Curr Top Dev Biol* **93**, 175–188 (2010).
70. Baden, T. & Osorio, D. The Retinal Basis of Vertebrate Color Vision. *Annu. Rev. Vis. Sci.* **5**, 177–200 (2019).
71. Boije, H., Edqvist, P.-H. D. & Hallböök, F. Horizontal cell progenitors arrest in G2-phase and undergo terminal mitosis on the vitreal side of the chick retina. *Dev Biol* **330**, 105–113 (2009).
72. Turner, D. L. & Cepko, C. L. A common progenitor for neurons and glia persists in rat retina late in development. *Nature* **328**, 131–136 (1987).
73. Layer, P. G., Alber, R., Mansky, P., Vollmer, G. & Willbold, E. Regeneration of a chimeric retina from single cells in vitro: cell-lineage-dependent formation of radial

cell columns by segregated chick and quail cells. *Cell Tissue Res* **259**, 187–198 (1990).

74. Willbold, E., Mansky, P. & Layer, P. G. Lateral and radial growth uncoupled in reaggregated retinospheroids of embryonic avian retina. *Int J Dev Biol* **40**, 1151–1159 (1996).
75. Reese, B. E. & Tan, S. S. Clonal boundary analysis in the developing retina using X-inactivation transgenic mosaic mice. *Semin Cell Dev Biol* **9**, 285–292 (1998).
76. Drenhaus, U., Morino, P. & Veh, R. W. On the development of the stratification of the inner plexiform layer in the chick retina. *J Comp Neurol* **460**, 1–12 (2003).
77. Swaroop, A., Kim, D. & Forrest, D. Transcriptional regulation of photoreceptor development and homeostasis in the mammalian retina. *Nature Reviews Neuroscience* **11**, 563–576 (2010).
78. Zeevalk, G. D. & Hyndman, A. G. Transferrin in chick retina: distribution and location during development. *Brain Res* **465**, 231–241 (1987).
79. Bird, M. M. An ultrastructural study of embryonic chick retinal neurons in culture. *Cell Tissue Res* **245**, 563–577 (1986).
80. Schnitzer, J. & Rusoff, A. C. Horizontal cells of the mouse retina contain glutamic acid decarboxylase-like immunoreactivity during early developmental stages. *J Neurosci* **4**, 2948–2955 (1984).
81. Donovan, S. L. & Dyer, M. A. Developmental defects in Rb-deficient retinae. *Vision Res* **44**, 3323–3333 (2004).

82. Raven, M. A. & Reese, B. E. Mosaic Regularity of Horizontal Cells in the Mouse Retina Is Independent of Cone Photoreceptor Innervation. *Invest. Ophthalmol. Vis. Sci.* **44**, 965–973 (2003).
83. Andreae, L. C. & Burrone, J. The role of neuronal activity and transmitter release on synapse formation. *Curr Opin Neurobiol* **27**, 47–52 (2014).
84. Bodnarenko, S. R. & Chalupa, L. M. Stratification of ON and OFF ganglion cell dendrites depends on glutamate-mediated afferent activity in the developing retina. *Nature* **364**, 144–146 (1993).
85. Bodnarenko, S. R., Jeyarasasingam, G. & Chalupa, L. M. Development and regulation of dendritic stratification in retinal ganglion cells by glutamate-mediated afferent activity. *J Neurosci* **15**, 7037–7045 (1995).
86. Bodnarenko, S. R., Yeung, G., Thomas, L. & McCarthy, M. The development of retinal ganglion cell dendritic stratification in ferrets. *Neuroreport* **10**, 2955–2959 (1999).
87. Sernagor, E. & Mehta, V. The role of early neural activity in the maturation of turtle retinal function. *J Anat* **199**, 375–383 (2001).
88. Wong, W. T., Faulkner-Jones, B. E., Sanes, J. R. & Wong, R. O. Rapid dendritic remodeling in the developing retina: dependence on neurotransmission and reciprocal regulation by Rac and Rho. *J Neurosci* **20**, 5024–5036 (2000).
89. Kay, J. N. *et al.* Transient requirement for ganglion cells during assembly of retinal synaptic layers. *Development* **131**, 1331–1342 (2004).
90. Brown, N. L., Patel, S., Brzezinski, J. & Glaser, T. Math5 is required for retinal ganglion cell and optic nerve formation. *Development* **128**, 2497–2508 (2001).

91. Wang, S. W. *et al.* Requirement for math5 in the development of retinal ganglion cells. *Genes Dev* **15**, 24–29 (2001).

92. Chalupa, L. M. & Günhan, E. Development of On and Off retinal pathways and retinogeniculate projections. *Progress in Retinal and Eye Research* **23**, 31–51 (2004).

93. Willbold, E. *et al.* Müller glia stabilizes cell columns during retinal development: lateral cell migration but not neuropil growth is inhibited in mixed chick-quail retinospheroids. *Eur J Neurosci* **7**, 2277–2284 (1995).

94. Layer, P. G. *et al.* Pigmented epithelium sustains cell proliferation and decreases expression of opsins and acetylcholinesterase in reaggregated chicken retinospheroids. *Eur J Neurosci* **9**, 1795–1803 (1997).

95. Rothermel, A. & Layer, P. G. Photoreceptor plasticity in reaggregates of embryonic chick retina: rods depend on proximal cones and on tissue organization. *Eur J Neurosci* **13**, 949–958 (2001).

96. Frohns, F., Mager, M. & Layer, P. G. Basic fibroblast growth factor increases the precursor pool of photoreceptors, but inhibits their differentiation and apoptosis in chicken retinal reaggregates. *Eur J Neurosci* **29**, 1931–1942 (2009).

97. Wolburg, H., Willbold, E. & Layer, P. G. Müller glia endfeet, a basal lamina and the polarity of retinal layers form properly in vitro only in the presence of marginal pigmented epithelium. *Cell Tissue Res* **264**, 437–451 (1991).

98. Watanabe, T. & Raff, M. C. Rod photoreceptor development in vitro: intrinsic properties of proliferating neuroepithelial cells change as development proceeds in the rat retina. *Neuron* **4**, 461–467 (1990).

99. Léveillard, T. *et al.* Identification and characterization of rod-derived cone viability factor. *Nat Genet* **36**, 755–759 (2004).

100. Mohand-Said, S., Hicks, D., Dreyfus, H. & Sahel, J. A. Selective transplantation of rods delays cone loss in a retinitis pigmentosa model. *Arch Ophthalmol* **118**, 807–811 (2000).

101. Layer, P. G. & Willbold, E. Embryonic chicken retinal cells can regenerate all cell layers in vitro, but ciliary pigmented cells induce their correct polarity. *Cell Tissue Res* **258**, 233–242 (1989).

102. Willbold, E., Rothermel, A., Tomlinson, S. & Layer, P. G. Müller glia cells reorganize reaggregating chicken retinal cells into correctly laminated in vitro retinae. *Glia* **29**, 45–57 (2000).

103. Meyer, J. S. *et al.* Optic vesicle-like structures derived from human pluripotent stem cells facilitate a customized approach to retinal disease treatment. *Stem Cells* **29**, 1206–1218 (2011).

104. Nakano, T. *et al.* Self-Formation of Optic Cups and Storable Stratified Neural Retina from Human ESCs. *Cell Stem Cell* **10**, 771–785 (2012).

105. Zhong, X. *et al.* Generation of three-dimensional retinal tissue with functional photoreceptors from human iPSCs. *Nat Commun* **5**, 4047 (2014).

106. Capowski, E. E. *et al.* Reproducibility and staging of 3D human retinal organoids across multiple pluripotent stem cell lines. *Development* **146**, dev171686 (2019).

107. Pankratz, M. T. *et al.* Directed Neural Differentiation of Human Embryonic Stem Cells via an Obligated Primitive Anterior Stage. *STEM CELLS* **25**, 1511–1520 (2007).

108. Meyer, J. S. *et al.* Modeling early retinal development with human embryonic and induced pluripotent stem cells. *Proceedings of the National Academy of Sciences of the United States of America* **106**, 16698–703 (2009).

109. Bell, C. M., Zack, D. J. & Berlinicke, C. A. Human Organoids for the Study of Retinal Development and Disease. *Annu Rev Vis Sci* **6**, 91–114 (2020).

110. Banin, E. *et al.* Retinal Incorporation and Differentiation of Neural Precursors Derived from Human Embryonic Stem Cells. *STEM CELLS* **24**, 246–257 (2006).

111. Lamba, D. A., Karl, M. O., Ware, C. B. & Reh, T. A. Efficient generation of retinal progenitor cells from human embryonic stem cells. *PNAS* **103**, 12769–12774 (2006).

112. Osakada, F. *et al.* Toward the generation of rod and cone photoreceptors from mouse, monkey and human embryonic stem cells. *Nat. Biotechnol.* **26**, 215–224 (2008).

113. O'Hara-Wright, M. & Gonzalez-Cordero, A. Retinal organoids: a window into human retinal development. *Development* **147**, dev189746 (2020).

114. Kuwahara, A. *et al.* Generation of a ciliary margin-like stem cell niche from self-organizing human retinal tissue. *Nature Communications* **6**, 6286 (2015).

115. Phillips, M. J. *et al.* Blood-Derived Human iPS Cells Generate Optic Vesicle–Like Structures with the Capacity to Form Retinal Laminae and Develop SynapsesProduction of Retina from Human Blood iPS Cells. *Investigative Ophthalmology & Visual Science* **53**, 2007–2019 (2012).

116. Kruczek, K. & Swaroop, A. Pluripotent stem cell-derived retinal organoids for disease modeling and development of therapies. *STEM CELLS* **n/a**,.

117. Cowan, C. S. *et al.* Cell Types of the Human Retina and Its Organoids at Single-Cell Resolution. *Cell* **182**, 1623-1640.e34 (2020).

118. Cora, V. *et al.* A Cleared View on Retinal Organoids. *Cells* **8**, 391 (2019).

119. Wahlin, K. J. *et al.* Photoreceptor Outer Segment-like Structures in Long-Term 3D Retinas from Human Pluripotent Stem Cells. *Scientific Reports* **7**, 766 (2017).

120. Collin, J. *et al.* CRX Expression in Pluripotent Stem Cell-Derived Photoreceptors Marks a Transplantable Subpopulation of Early Cones. *Stem Cells* **37**, 609–622 (2019).

121. Zarbin, M., Sugino, I. & Townes-Anderson, E. Concise Review: Update on Retinal Pigment Epithelium Transplantation for Age-Related Macular Degeneration. *STEM CELLS Translational Medicine* **8**, 466–477 (2019).

Chapter 2 -

Outer Retinal Cell Replacement: Putting the Pieces Together

Ludwig, A.L., Gamm, D.M. (2021). *Transl Vis Sci Technol.* PMID: 34724034

Author contributions: A. L. L.: conception and design, manuscript and figure preparation. D. M. G.: conception and design, manuscript editing, financial support and supervision, final approval of manuscript.

Acknowledgements: The authors thank Kimberly Edwards, Steven Mayerl, Lindsey Jager, Praveen J. Susai Manickam, Divya Sinha, Beth Capowski, and Joe Phillips, and other members of the Gamm laboratory for providing critical feedback and helpful discussion of the contents of this review. All figures were prepared in BioRender; Figure 3 was adapted from the “Timeline of Adjuvant Used in Human Vaccines” template by BioRender.com (https://app.biorender.com/biorender-templates).

Introduction

The retina is a complex tissue whose anatomy and circuitry (**Fig. 1A**) is predicated on the function of rod and cone photoreceptors (PRs), specialized neurons (**Fig. 1B**) that have evolved over millions of years to optimally harness light for navigating diverse environments[1,2]. In healthy retinas, PRs are the initiators of visual activity; they are defined by their ability to capture light entering the eye and generate an electrical signal through a cascade of biochemical activity known as phototransduction[2]. Sparking this signal is not solely enough to confer vision—PRs must also successfully relay light sensory information via synapses with interneurons to begin a stepwise process of conveying visual stimuli to the brain along retinal ganglion cell (RGC) axons. The biochemical processes within PRs require extensive metabolic activity, largely mediated by their interactions with the retinal pigment epithelium (RPE)[3]. Together with Müller glia (MG), the RPE plays a crucial role in supporting PRs to maintain outer retinal structure, function, and homeostasis[3–5].

Like all retinal cells, both PRs and RPE arise from a common retinal progenitor cell (RPC) (**Fig. 2**); intrinsic[6] and extrinsic factors work in concert to guide cells through distinct developmental stages[7,8] to reach functional maturity. In outer retinal degenerative diseases (RDDs) the interdependent nature of PRs and RPE becomes a weakness; primary dysfunction in either population often causes secondary damage in the other[9-12]. Regardless of the inciting cause, PR damage instigates a predictable cascade of degenerative changes within the retina[12], progressing from widespread PR malfunction to cell death, retinal remodeling, and—in the absence of successful intervention—inner retinal neurodegeneration[13]. Like most neurons, human PRs are non-regenerative, and these processes ultimately lead to irreversible vision loss. Retinitis pigmentosa (RP) and age-related macular degeneration (AMD) are the most common inherited and acquired RDDs, respectively, and collectively affect millions of individuals worldwide. Blinding outer RDDs affect an increasing proportion of the global population,[14-16] and

beyond being a source of visual morbidity, can cause severe emotional distress in some individuals.[17,18] The estimated global economic impact of potential productivity lost due to moderate and severe visual impairment is a staggering $411 billion USD annually[17]. In response, the National Eye Institute launched the Audacious Goals Initiative (AGI) in 2015 to accelerate development and deployment of ocular stem cell-based therapies for incurable RDDs[20,21]. Specifically, the AGI aims to restore "usable vision in humans through the regeneration of neurons and neural connections" through endogenous or exogenous replacement[20].

Gene therapies developed for individuals across the RDD spectrum have made remarkable progress in recent years[22]; however, with more than 200 distinct causative genes[16], curative interventions remain out of reach for most patients. Cell therapies—the delivery of live cells to treat or cure disease—have emerged as a promising alternative (or adjunct[23]) to gene therapy, offering a broad-spectrum and gene-independent strategy for restoring vision. There are currently no U.S. Food and Drug Administration (FDA)-approved cell therapy applications for retinal disease, although several approaches have reached early phases of translational research (**Box 1**). Cell therapies come in many varieties, but are fundamentally characterized in the context of their source (patient-derived or donor-derived), their capacity to become other types of cells[22], and their purity (**Table 1**). Of the many varieties proposed for use in RDDs, several autologous (patient-derived) and allogeneic (donor-derived) cell therapies have reached clinical trials[23,24]. Human pluripotent stem cells (hPSCs) have proven to be an indispensable source of cells for such therapies as they can, by definition, self-replicate almost indefinitely and form virtually any type of cell. hPSC-based therapies advancing most rapidly toward clinical translation are aimed at supporting surviving host PRs, either through neuroprotective approaches (e.g., delivery of trophic factor-secreting stem/progenitor cells) or replacement of defective underlying RPE[23,24]. Exogenous replacement of photoreceptors has progressed comparatively slowly, as it relies upon

survival of a sufficient number of properly polarized, light-sensitive cells and establishment of functional synaptic connections with host interneurons.

Exogenous PR replacement currently appears best poised to reach the National Eye Institute's (NEI's) audacious goal first, although several key hurdles remain as the field advances into clinical trials. With the initiation of a first-in-human safety study of hiPSC-derived neuroretinal sheets in advanced RP (RIKEN, JRCT ID jRCTa050200027)[27], a critical appraisal of where the field currently stands with respect to PR replacement is warranted. This review summarizes relevant historic literature and highlights recent developments in exogenous hPSC-derived PR replacement therapies, identifying remaining challenges and emerging strategies. Therapies aimed at rescue of remaining PRs have recently been reviewed extensively elsewhere and, for the purposes of this review, are largely discussed in the context of principles relevant to PR replacement. Readers interested in PR rescue are directed to several excellent reviews of RPE replacement[27,28] and other approaches including stem/progenitor trophic cell therapies[29]. In addition, recent reviews of biomaterial transfer[30], outer retinal scaffolds[31,32], immune responses in subretinal cell therapies[33], PR replacement in rodents[34], and clinical trials of cell transplantation in RDDs[25,26] may also aid the reader in gaining a comprehensive understanding of the field.

The Rise of Photoreceptor Replacement Therapy

1950s to 1990s: Early Studies in Primary Cell Transplantation

The number of published studies aimed at retinal cell replacement has increased in recent years, but the field itself is far from new. Retinal regeneration stands on the shoulders of giants in many regards, building upon more than a century of research in regenerative medicine and retinal development (**Fig. 3**). While intraocular delivery of retinal tissue began in the late 1950s[35,36], proof-of-principle for neuroretinal cell replacement (i.e., retina-into-retina transplantation) was established by a series of landmark studies by del Cerro, Turner, and Blair in the late 1980s[37–41].

Turner and Blair were the first to transplant primary retinal tissue from neonatal rats into the subretinal space (SRS) of adult rats with outer retinal lesions[37], reporting survival and differentiation of neonatal grafts at 4 weeks post-transplant. These experiments documented some of the earliest evidence of "integration" between donor cells and host retinal tissue, a phenomenon that would eventually grow to become a source of significant debate in retinal regenerative therapies (**Box 2**).

Retinal developmental biology saw unprecedented progress throughout the 1980s and 1990s; the introduction of cell birth dating and advanced molecular biology techniques uncovered uncovered mechanisms of cell specification, organization, and neuronal maturation within the retina[6–8,42]. As the developmental trajectory of PRs was defined (see **Fig. 2**), investigators continued to experiment with primary cell isolation to determine the optimal donor stage for cell replacement [43–45]. Those studies led to the observation that donor cell suitability for transplantation decreased with age. That is, in both allografts (i.e., same-species transplants) and xenografts (i.e., cross-species transplants), embryonic and early postnatal retinal grafts incorporated into lesioned retinas far more readily than their older counterparts[45,46]. Given these findings, dissociated suspensions of multipotent neural[47–52] or retinal progenitor cells[53–56]—were initially preferred by many. However, limited survival due to reflux and cell death (often less than 0.01% of the starting dose[53,57]) in addition to unpredictable differentiation led to low rates of PR engraftment, making translation to human therapies difficult[51].

1990s to Early 2000s: Improving on Dissociated RPC Delivery

Two main approaches emerged to address the issue of poor engraftment. Studies building on the findings of del Cerro, Turner, and Blair suggested that human fetal RPC (fRPC) microaggregates (i.e., clusters of cells) and retinal sheets offered improved survival relative to dissociated cell transplants[58], likely due to enhanced structural support and maintenance of cell-cell contacts

(reviewed by Seiler and Aramant, 2012). Anoikis, the anchorage-dependent death of cells following loss of extracellular matrix (ECM) contacts, was thought to play a role in the poor survival of subretinally transplanted dissociated cells[59]. Tissue-engineered scaffolds were introduced as a customizable approach for mimicking the native structure of retinal tissue to improve survival in RPC transplants[57,60–66]. A variety of naturally-occurring gelatinous matrices, hydrogels, and decellularized tissues were initially used; however, graft organization was limited and concerns regarding batch-to-batch variability restricted future clinical use[31,67–69]. Among others, the Young laboratory developed criteria for an ideal neuroretinal scaffold: biodegradable and/or biocompatible, optically clear, porous, flexible yet strong, and thin enough for relatively easy subretinal delivery (<50μm)[57,60–66]. Synthetic biomaterials optimally met these criteria, and a variety of polymers including poly(e-caprolactone) (PCL), poly(L-lactic acid) (PLLA), poly(lactic-*co*-glycolic acid) (PLGA), poly(methyl methacrylate) (PMMA), polydimethylsiloxane (PDMS), and poly(glycerol sebacate) (PGS) were found to be well-tolerated in the SRS and supportive of improved RPC delivery in pigs and rodents [60,62–65,70,71]. However, RPCs were not limited to producing PRs (see **Fig. 2**), and despite enhanced survival the efficiency of PR engraftment following RPC scaffold delivery remained relatively low[57,64].

The second approach—enrichment of committed PR precursors (PRPs)—was introduced by MacLaren *et al.* in 2006 with transplantation of green fluorescent protein (GFP)-labeled rod precursors (*Nrl-gfp*$^{+/+}$ cells) in mice[72]. Characterized by a defined cell fate, PRPs offered substantial improvement in apparent PR engraftment in the retinas of wild type and rhodopsin-null mice. MacLaren and colleagues observed recovery of light sensitivity in rhodopsin-null mice, providing some of the earliest evidence of functional rescue following cell replacement and sparking broad interest within scientific and lay communities alike. Though the study (and at least one subsequent report[73]) referenced fusion between donor and host cells as a potential alternative explanation for their results[72], it was not believed to occur to a significant degree in the

retina at the time. Indeed, as a control, *Nrl-gfp*$^{+/+}$ cells were transplanted into transgenic cyan fluorescent protein (CFP) reporter mice, and on the basis of qualitative data showing a lack of multinucleate or double-labeled GFP+/CFP+ cells, MacLaren *et al.* argued that cell fusion—at least in the classical sense—was unlikely.

Studies within the Ali, Wallace, and Ader laboratories (among others) replicated the findings of MacLaren *et al.* in the years that followed, primarily in rodent models with an intact or partially degenerating outer nuclear layer (ONL). Manipulation of the degenerative retinal environment by disrupting potential barriers to integration—including the outer limiting membrane (OLM)[74,75], glial scarring[76,77], and chondroitin sulfate proteoglycan deposition[78–80]—was proposed to further enhance PRP incorporation. Fluorescence-activated cell sorting (FACS)[72,81–83] and magnetic-activated cell sorting (MACS)[84–86] were optimized to obtain relatively uniform batches of transplantable cells. The developmental window paradigm, which proposed that effective PRP cell replacement could only be achieved through delivery of postmitotic cells at the precise peak of PRP genesis (E15 to P4 in mice), was introduced during this time[87]. With mounting evidence of their success in cell replacement—including improvements in light-mediated activity[76,82,88] even in advanced degeneration[89]—PRP became the preferred developmental stage for primary cell transplantation among most investigators[73,81–86,88–91]. As in MacLaren *et al.*[72], integration was assumed to be the predominant mechanism in these studies; however, the MacLaren lab first raised concerns regarding PRs double-labeled with donor and host fluorescent reporters in 2014[92], suggesting that fusion between donor and host cells was indeed possible.

Limitations of Primary Cells

Both strategies—scaffolds and PRP enrichment—offered apparent improvements relative to dissociated RPC delivery, but primary cells presented major challenges to translation beyond

animal studies. Phase I and II clinical trials of human fetal-derived retinal cells[93], microaggregates[94], and retinal sheets with RPE[95–97] in advanced RP and AMD began in the late 1990s, but ultimately reported mixed effects on visual outcomes in humans. A phase 2 study led by Radtke and colleagues reported transient visual acuity improvement in 7 of 10 subjects with long-term stabilization in a single subject[95], but the study did not distinguish trophic effects from functional integration, and interpretations of the underlying mechanism varied[26,58,98,99]. These early studies (conducted without immunosuppression) provided evidence of safety for future cell therapies, demonstrating a clear path to clinical trials through careful preclinical study planning, but the primary cell approach to replacing PRs faced a difficult road to widespread application.

Procurement of human fetal retinal tissue for transplantation proved controversial from its introduction in the early 1980s[100], and debate around its use in biomedical research continues[101]. The developmental window paradigm for PRP (E15-P4 in mice) coincided with the second trimester of pregnancy in humans, presenting an ethical minefield for translation to clinical use. Attempts to expand[102,103] and immortalize[104] human fetal retinal cells were largely unable to circumvent the issue as RPCs were, by definition, not restricted to the PR lineage (see **Fig. 2**) and generated few PRs. In most cases, human fRPCs lost neurogenic potential over time in culture[105,106] and demonstrated poor long-term survival following transplantation[104]. Improvement under low-oxygen culture conditions was reported in some cases[53,107–110], eventually resulting in the recent initiation of a phase 1/2a clinical trial of subretinal fRPC delivery in late-stage RP (Reneuron, clinicaltrials.gov identifier NCT02464436, recruitment ongoing). Although this trial is expected to yield valuable safety and efficacy data[24], results have not yet been published[26], and difficulty in distinguishing trophic support from functional PR replacement remains[24]. Ethical constraints and ambiguous mechanisms aside, primary cells and their derivatives continued to present a yield dilemma: with millions of potential patients[14,16], reproducible manufacturing was expected to be a bottleneck for larger phase 3 clinical trials and beyond[26,58].

Early 2000s-late 2010s: Expanding Potential With Human Pluripotent Stem Cells

The isolation of human embryonic stem cells (hESCs) in 1998[111] ushered in a new era for retinal cell replacement. The first completely *in vitro* differentiation of RPE was achieved in relatively short order[112], but PR differentiation proved more challenging. Building on existing mouse ESC protocols[113,114], studies by the Reubinoff and Reh laboratories showed hESCs could be guided toward a PR fate, but only when transplanted into the SRS[115] or co-cultured with retinal tissue[116]. Osakada *et al.* were the first to achieve *in vitro* generation of hPSC-derived PRP in the absence of mature retinal tissue[117] in 2008. The earliest neuroretinal differentiation protocols yielded few PRP, however (just 12-20% of all cells[116,117]) and accordingly, generated even fewer maturing PRs (<0.01-10% of all cells[116,117]). Induced pluripotent stem cells (iPSCs) were introduced shortly thereafter[118,119], and expanding on earlier approaches[106,113,117,120,121], our laboratory and the Takahashi laboratory soon reported successful differentiation of RPE, RPCs, and putative PRPs from both ESCs and iPSCs[121,122]. Lamba and colleagues demonstrated that transplantation of retinal cells derived from both classes of hPSCs was feasible,[123,124] reporting results strikingly similar to that of MacLaren *et al*., though donor cell survival and light responses were comparatively low[123,124].

Protocols introduced by our laboratory and the Sasai laboratory in the early 2010s[125,126] enabled hPSC-derived 3D retinal organoid production, overcoming the yield barriers of fetal-derived primary tissues and earlier differentiation protocols. Organoid cultures produced PRP far more efficiently—40 to 80% of all cells[122,125]—and proved to be a breakthrough technology for the field. For the first time, bulk production of PRs from a single donor source was achievable. Methods to further bias organoids toward robust PR production were refined in the years that followed[127–129], demonstrating a surprising degree of anatomic and functional authenticity in cells along the PR lineage[127,129–135] (see Bell *et al.*, 2020[133] for further discussion). With growing evidence of PSC-derived retinal cells as a reliable and reproducible source of donor cells, the

field shifted toward rodent[136–143] and human[90,144,145] PSC-derived cells and tissues for PR replacement. The preference to use PRP-rich donor cells and retinal sheets[146–149] over RPC donor material largely persisted, given the greater degree of proliferation, disorganization, and uncontrolled migration observed in transplants using the latter[150,151].

Late 2010s: The Paradigm-Shifting Discovery of Material Transfer

The field effectively experienced a reset with the revelation of widespread fluorescent material transfer between conspecific donor and host PRs, independently reported by several groups between 2016 and 2017[152–156]. In a subsequent transplant study by Waldron *et al*., nearly all GFP+ cells (99%) found in wildtype host retinas and most GFP+ cells (>75%) in degenerative *Nrl*$^{-/-}$ *and* *Prph2*$^{rd2/rd2}$ retinas were estimated to result from material transfer[157], calling the results of several previous rodent studies into question[72,76,82,88,123,145,158]. Although the exact mechanism and longevity of this phenomenon remains to be determined, at present, several points are clear. First, material transfer is more likely to occur in degenerating retinas with remaining host PRs[152–156] than in models of end-stage retinal degeneration[89,141,146,147,149,159–163]. Second, a variety of PR-specific proteins (cone arrestin, opsins, and peripherin-2 [PRPH2], see **Fig. 2**) as well as cytoplasmic reporters can be passed via material transfer in mice[34], leading to a re-evaluation of how the field identifies and defines integration (see **Box 2** for further discussion). Third, PSC-derived PRP do not appear to be exempt from this phenomenon[34,137,140,157]; however, at least one study has suggested that the capacity for material transfer is lower within human-into-rodent xenografts than in allogeneic transplantation[144]. Finally, many of the central tenets of successful cell replacement—including the developmental window paradigm, estimated donor cell survival rates, evidence of a dose response, integration, and synaptogenesis—are currently being re-examined in the context of material transfer.

Lessons Learned From Historic Studies of PR Replacement

Collectively, early studies in retinal cell replacement identified several guiding principles for carrying PR cell therapies closer to the clinic. Multiple strategies, including the use of enriched donor cell populations and biomaterial-based scaffolds, have been shown to enhance cell survival in the face of low PR engraftment[34,70,72]. The PRP stage of differentiation remains preferred for replacing PRs, although the window of transplant competence is likely not so narrow as previously estimated[34]. Three-dimensional retinal organoids are the most often used source of authentic donor cells and tissue sheets, and have in some cases been associated with modestly improvements in host retinal light sensitivity following transplantation[26,34]. Finally, rodent PSC allografts and human-into-rodent PSC xenografts have established unequivocal proof-of-concept for PR survival and anatomic engraftment following transplantation. They have also identified remaining hurdles for the field to overcome. Surviving donor cells often remain disorganized within the subretinal space, and the mechanisms by which they affect vision remain unclear. With many prior studies now known to result from material transfer rather than functional integration, there is substantial interest in the development of quantitative methods for assessing integration, organization, and synaptogenesis.

Current Status and Remaining Questions for Retinal Cell Therapies

As outlined above, cell replacement therapies in the retina have been studied for decades (see **Fig. 3**), and hPSC-RPE and hPSC-PRP cell products are now in the T1 translational research phase (which spans preclinical studies through phase II clinical trials). Thus far, the majority of clinical trials have used hESC or hiPSC-RPE, inserted into the SRS either as dissociated cell suspensions or as monolayer sheets with or without scaffolds (see Uyama *et al.,* 2021 for further discussion[98]). Early reports suggest that these therapies are feasible, safe, and well-tolerated in individuals with advanced retinal degenerative disease[26,98]. However, functional outer retinal cell replacement—and more particularly PR replacement—remains a complex puzzle of cell manufacturing and preclinical testing challenges, some of which may not be fully surmountable

ahead of human trials (**Fig. 4**). Even so, efforts to address each piece of this puzzle in a deliberate, stepwise manner would help build confidence in the potential for success. This section discusses these pieces in detail, comparing and contrasting major strategies and identifying areas where additional research is necessary to advance outer retinal cell therapeutics.

Clinical-Grade Production

Clinical hPSC-derived cell therapies must be sterile and free from infectious agents, impurities, residual pluripotent cells, unidentified cell types, and genomic instabilities[28]. Such criteria can only be met under strict Good Manufacturing Practice (GMP)-compliant conditions[28,164–166] and must also be scalable far beyond the capacity of the average laboratory setting to be feasible for clinical trials and commercialization. Although detailed discussions of stem cell source (ES or iPS) and culture technique are beyond the scope of this review, proper induction and/or maintenance of PSCs is fundamental to any successful retinal differentiation program. Advantages and disadvantages of autologous and allogeneic cell replacement should be weighed early in product development to avoid the need for correction mid-program. Preclinical safety studies for autologous products emphasize the safety of the manufacturing process in addition to the final clinical product, whereas safety studies for allogeneic products focus on the latter. Thus, programs are effectively "locked in" very early to an autologous or allogeneic approach[25]. Autologous therapies are subject to fewer infectious disease testing requirements and are theoretically less likely to result in immune rejection[28], though cost (an estimated $800,00/cell line for clinical-grade iPSC production[167]) and reproducibility across patient-specific iPSC lines are often limiting factors. "Off-the-shelf" human leukocyte antigen (HLA)-matched[168] or HLA knockout[169] allogeneic products offer a scalable, more cost-effective production pipeline; however, immune rejection and long-term safety become a greater concern, and many dozens of HLA "super donor" cell lines would still be needed depending on the genetic diversity of the target population[167].

Lessons learned from existing Investigational New Drug (IND)-enabling studies, particularly those from investigators with experience in cell therapies and Biologics License Applications with the FDA[26], should be considered early in product development to mitigate additional "known unknown" risks for scaling regenerative therapies[170] (for further discussion of quality control for clinical-grade hPSC retinal cell production, see Wright *et al.,* 2014[171] and Sharma *et al.,* 2020[28]). Current methods for generating hPSC retinal organoids are both time and labor-intensive, limiting their utility in clinical production pipelines. The use of bioreactors[172], microfluidics[166,173], and automated culture systems[27] are all promising approaches currently under investigation for scaling clinical-grade organoid-based technologies.

Donor Cell Enrichment

Reproducible methods for purifying or enriching PRP from stem cell-derived retinal organoids are a critical bottleneck in the regenerative medicine pipeline for PR degenerative diseases[34]. MACS and FACS-based enrichment strategies originally developed in mouse models[174] have not yet translated into consistent success for enrichment of hPSC-PRP for transplantation[161], possibly due to species- or maturation stage-specific differences in PR cell surface markers. Although some groups have reported successful development of hPSC-PRP enrichment protocols, most have not been widely adopted outside individual labs, possibly due to low yield (<1 million cells)[175–177] and/or suboptimal purity (40-70%) across various differentiation protocols[135]. A fully homogenous cell product is not necessarily a prerequisite for clinical trial initiation[26] because the FDA allows study sponsors to set their own release criteria for product purity, but a highly enriched PRP product (>80%) would be desirable. Some groups have proceeded with unsorted cell populations or retinal sheets in the absence of reproducible sorting methods[145,149], but residual proliferating cells (e.g., immature RPE, RPCs, etc.) often remain. Unsorted populations thus contain cells that may continue to divide, leading to PRs being outnumbered by off-target cell

types[178] or to the development of disorganized, rosetted grafts following tissue sheet transplants[136,146–149,179].

Human PSC reporter lines[135,177,180–183] and viral labeling constructs[144] have been generated as an alternative approach to enable rapid PRP enrichment via FACS. Although precedent exists for FDA allowance of biologics expressing fluorescent proteins in clinical trials[184] (GenSight Biologics' optogenetic GS030 [clinicaltrials.gov identifier NCT03326336] encodes a tdTomato-linked fusion protein), nontherapeutic inclusions add safety and regulatory hurdles to an already complex approval process. Sorting via cell surface markers[162,176] (e.g., MACS) or label-free microfluidics[175] offer a more favorable approach to obtaining enriched PRP for cell replacement. Given the current lack of consensus on optimal PRP sorting strategies, particularly for cones[34], further investigations of human PRP-specific cell surface markers and enrichment approaches are warranted.

Functional Validation of Donor Cells

The advancement of hPSC-RPE therapies has been accelerated in part by the relative ease with which RPE donor cell identity and function can be validated[28]. A battery of biomarkers and assays including cobblestone morphology, pigmentation, transepithelial resistance (TER), photoreceptor outer segment (POS) phagocytosis, electrophysiology, apical-basal polarization, tight junction marker expression and microvilli formation, are all indicative of healthy, maturing hPSC-RPE[28,31,98,185,186]. Standardized methods for PRP validation have proven less straightforward, partly due to cell heterogeneity (rods; short-, medium-, and long-wavelength sensitive cones) and complexity, and partly due to the range in donor cell maturation used across studies. Neuronal age is a simple and widely used metric for estimating maturation in hPSC culture systems[187], and functional maturation is associated with age in hPSC-derived retinal neurons[114,117,122] regardless of the differentiation protocol used. However, the rate of maturation is often asynchronous across

protocols, cell lines, and even differentiation batches[129]. Age can serve as a rough surrogate marker of maturation, but this metric provides a somewhat false sense of assurance for consistency between lines or differentiations[129,188]. A recent study by Capowski et al. demonstrated the utility of morphology for assessing maturation, introducing a light microscopic staging system for classifying ROs[129]. Stage 1 ROs contain RPCs, early-born inner retinal neurons, and an outer neuroblastic layer, whereas stage 2 ROs are characterized by differentiation of an abundance of PRs and inner retinal neurons. The hallmarks of stage 3 ROs are the development of PR outer segments and increased outer neuroretinal organization along with production and maturation of Müller glia and ongoing deterioration of the innermost retinal layers[129].

Because the characteristic light-sensitive components of PRs, outer segments, often appear months past the peak of PRP genesis in ROs (stage 2, approximately day 80-D120 of differentiation), development of *in vitro* potency assays for validating hPSC-PRP remains a high priority. One intriguing approach to this conundrum is the use of optogenetically engineered hiPSC-PRP, which have recently been shown to generate modest responses to bright light *in vitro* and *in vivo*[163,189]*.* However, such a genetic modification presumes that hPSC-derived PRs cannot innately respond to light and also introduces aforementioned regulatory hurdles. In the absence of genetic modification of hPSC-PRP, other potency assays may prove useful for authenticating batches of transplantable hPSC-PRP, including examinations of cell polarity, synaptic marker expression[190], PR marker expression, axon outgrowth, and membrane electrophysiology[135].

Cell Preparation, Delivery, and Organization

A number of recent xenograft studies have demonstrated proof-of-concept for PR survival and anatomic engraftment (see **Box 2**) following transplantation of dissociated hPSC-derived cell suspensions or retinal sheets in rodents[146,149,161–163,179,189] and non-human primates (NHPs)[147,160]

using controls for biomaterial transfer. Dissociated cell injections have the advantage of being relatively simple, cost-effective, rapid, and minimally invasive, although graft organization and cell survival is often suboptimal[34]. Retinal sheet delivery can afford a striking degree of self-organization relative to dissociated cells[34,98,146,147,149,179], but the surgical technique requires specialized instrumentation and is more complex and invasive than simple subretinal injections. Furthermore, rosetted PRs, formation of ectopic inner retinal laminae, and lack of apposition to host RPE remain limitations to this approach[26].

PRs and RPE are both highly specialized cells for which apical-basal polarity plays a crucial role in function; there is thus substantial interest in cell delivery strategies supportive of donor cell organization. Polymeric retinal patches or scaffolds are among the most promising solutions for improving cell retention[191] and maintaining 3D distribution[192–194]. Added benefits also include a defined dose, targeted delivery to a discrete region, and potential for customization of scaffold size, shape, and material. Scaffold-based hPSC-RPE delivery has thus far been well-tolerated in clinical trials, and despite more complex surgical procedures, there is evidence to suggest that scaffold delivery may be achievable in an outpatient setting[195]. Neuroretinal scaffold approaches are still in their infancy but appear to be similarly advantageous for PR replacement. Current hPSC approaches include two-photon polymerized PCL scaffolds seeded with clinical-grade RPCs[191,196] and micromolded PGS scaffolds seeded with hPSC-PRPs[192,193]. Both scaffolds are sterilizable, biodegradable, and have a desirable elastic and/or compressive modulus, which play a critical role in ease of surgical handling[193,196,197]. Extensive *in vivo* safety testing has been performed for the former, though the use of RPCs rather than PRPs was a limiting factor in determining capacity for PR delivery. Micromolded scaffolds are capable of pre-organizing polarized PRPs even at high cell densities, although it remains to be seen whether such organization can be retained *in vivo*. Optimization of scaffold delivery requires the use of clinically relevant large animal models to simulate targeted subretinal scaffold implantation in the human

macula. In addition to delivery of PRP-only scaffolds, envisaged applications include co-delivery of hPSC-RPE and PRPs, as replacement of both cell types will likely be necessary for individuals suffering from late-stage AMD[198] or inherited maculopathies, such as Stargardt and Best disease.

Assessment of Donor Cell Survival

Dissociated cell survival in RPC[199] or allogeneic PSC-PRP transplants in rodents[143] is extremely low (1-4%), and because these studies predate the discovery of material transfer, may be overestimated. Given the widespread use of percentages rather than discrete cell counts in published datasets, it is often difficult to obtain an approximation of cell survival relative to the starting dose. Standardized methods for counting cells or regions of interest, like the QUANTOS workflow developed for synapse identification[190], will be critical for studying such outcomes. Where possible (and with appropriate controls), unbiased stereology and automated image analysis can also provide a less subjective approach to histologic analyses. Several studies have highlighted the importance of standardized cell quantification in biological research to increase reproducibility and aid comparisons between studies or across research groups[200–202]. Greater adoption of such methods for assessing donor cell survival in PR replacement would serve the field well.

Functional Integration and Synaptogenesis

The presence of new synaptic connections following transplantation is often inferred by pre- and postsynaptic protein co-immunolabeling or electron microscopic evidence of synaptic ribbons near donor cells[136,147–149,160,161,179]. However, immunocytochemical evidence of synaptic marker expression does not establish a definitive causal link to observed changes in retinal function or visual behavior. Further evidence in favor of functional synaptogenesis includes electrophysiologic, reflexive, and behavioral assessments of light responsivity, although most of these readouts measure processes several synapses downstream from presumptive donor-host

contacts[23,146,147,149,159,161,163,179]. High levels of donor cell disorganization[26,34,136,141,146] and relatively mild degrees of light-induced response recovery observed in most hPSC-PRP transplants[23,141,146,159,161,163,203] also suggest that synapse formation likely occurs at lower rates than previously predicted[34].

It is currently difficult to fully distinguish bona fide synaptic connections from existing ones—however rare they may be—in the absence of direct and effective methods for studying synaptic contacts of donor cells[34,204]. A recent study by Cowan *et al.* suggests that PRP are capable of forming synapses within retinal organoids as evidenced by calcium imaging[134]. However, no study to date has definitively shown that hPSC-PRPs can form new functional synapses after being isolated from retinal organoids. Evidence of functional post-transplant synaptogenesis currently includes modest light responses recorded with multi-electrode array (MEA) and micro-electroretinography (mERG)[146,147,161,189,205], and often does not conclusively distinguish light-induced donor cell responses from possible neuroprotective effects on residual host retinal circuitry. Reproducible, well-controlled approaches for assessing de novo synaptogenesis at the level of individual donor hPSC-PRPs (via calcium imaging or viral monosynaptic circuit tracing), particularly in the context of xenogeneic transplantation[206], will be necessary to further clarify mechanisms of functional recovery. The efficiency of synaptogenesis in xenografts is currently unknown[206]; however, by increasing PRP survival, alignment, and organization, it may be possible to increase the likelihood of synapse formation between donor and host cells. Strategies to directly measure hPSC-PRP synaptic contacts via trans-synaptic tracing or patch-clamp recordings have been highlighted as crucial[34], but have not yet come to fruition.

Animal Model Selection for Safety and Efficacy Studies

Rodents have historically been the preferred model system for retinal cell replacement studies due to cost, ease of genetic manipulation, and widespread availability. Several reports have shown that transplanted hPSC-PRP can survive and be associated with varying degrees of visual and/or electrophysiologic activity in degenerating rodent retinas[146,149,161–163,179,189] but there is not yet direct evidence of causation. The well-documented neuroprotection caused by virtually any subretinally transplanted material (including control vehicles[110,207]) in the Royal College of Surgeons (RCS) rat makes it highly difficult to fully control for alternate mechanisms in this model. To address the confounding variables of neuroprotection and biomaterial transfer, many investigators have instead opted for models with near-complete PR loss. Models with severe PR loss[89,150,159,208] are currently considered most appropriate for studying functional integration, although even these models are not free of confounding variables, because residual cones remain in severely atrophic models like the *rd1* mouse and *S334ter-3* rat[26,206].

To date, most available data regarding cell survival and effects on vision are skewed toward rod-dominant rodent models, although there is some evidence to suggest similar responses are possible in non-human primates[147]. Given notable species-specific differences in photoreceptor development and synaptic architecture[206], the degree to which these observations will directly translate to human allogeneic or autologous transplants remains to be seen. The introduction of scaffolds and more complex tissue constructs, which necessarily includes more complicated surgeries, will require a shift toward larger animal models with ocular anatomy more akin to that of humans to provide meaningful assessments of such approaches. Development of translation-enabling models that faithfully recapitulate aspects of human RDDs is an explicit aim of the NEI AGI[21], and these models will be a valuable resource for advancing retinal cell therapies. There is substantial interest in allogeneic transplantation of same-species PSC-derived retinal cells in parallel with xenogeneic studies, as this approach can potentially provide extrapolatable insight into the degree of functional restoration that may be reasonably expected in human clinical

trials. Continued observance of field standards for defining integration (see **Box 2**) and development of protocols to generate retinal organoids from additional laboratory model species will be essential to such activities.

Although a variety of reflexive and behavioral assays are available for assessing visual function, even electrophysiologic methods ultimately may not be sensitive enough to directly assay PR-transplant driven responses[161,205]. Several such studies have documented light-evoked electrophysiologic responses[209] and visual behavior[210] in degenerating retinas even when surviving donor PRs are nearly absent. Adequately powered studies controlling for alternate explanations of restored function—including material transfer to host interneurons[206], aberrant firing of intrinsically photosensitive RGCs (ipRGCs), and neuroprotection of remaining host retinal circuits—will be challenging, but necessary, for definitively establishing a causal link between anatomic integration and vision rescue[26,206].

There is no single animal model that is perfect for each cell replacement application. Rather, a variety of factors including ocular anatomy, nocturnal versus diurnal activity (*i.e.,* rod versus cone-dominance), and genetic causation should be taken into consideration when designing preclinical IND-enabling studies for cell therapies (summarized in **Table 2**, also see Winkler *et al.,* 2020[211] for a discussion of RDD animal models). A recent study by Laver and Matsubara also suggests that the lack of robust responses observed in human-to-rodent xenografts[147,161,163] may be due in part to synapse incompatibilities between donor and host retinal interneurons[206]. The degree of divergence in synaptic proteins between humans and non-human model organisms is just one of many factors to consider when selecting preclinical models for testing functional effects of hPSC-PRP therapeutics.

Noninvasive Imaging to Assess Therapeutic Efficacy

The healthy retina is a highly organized, laminated structure that has evolved to maximally harness light entering the eye[212]. Recent advances in noninvasive retinal imaging have capitalized on these features to provide increasingly detailed pictures of *in vivo* retinal architecture[213–216]. Both the NEI AGI and the Monaciano Corsortium have highlighted a relative lack of rigorous, reproducible ocular imaging as a potential bottleneck in advancing clinical trials[20,21,217]. Several recent studies have demonstrated the utility of noninvasive imaging for comprehensively studying integration and therapeutic efficacy in hPSC-PRP cell therapies[160,218]. The Singh laboratory at Johns Hopkins has identified quantifiable biomarkers for tracking fluorescent mouse cells after transplantation, developing a scoring system for multimodal confocal scanning laser ophthalmoscopy (cSLO) imaging[218]. Several properties, including fluorescence size and intensity, graft placement, lamination, and peri-retinal proliferation were scored longitudinally, facilitating long-term tracking of individual grafts over time. Similarly, Aboualizadeh *et al*. recently used fluorescence adaptive optics scanning light ophthalmoscopy (FAOSLO) to follow individual photoreceptors *in vivo* in a laser-damage NHP model of photoreceptor loss[160]. These types of correlative studies augment histologic assessment of efficacy, although further research is necessary to determine how to translate these imaging techniques to clinical trials and commercial products. As mentioned earlier, fluorescent reporters are not necessarily prohibited in clinical trials, but development of high-resolution, label-free noninvasive imaging for tracking migration and integration is preferable.

Modulating Retinal Microenvironment and Immune Response

The ideal cell replacement toolbox will almost certainly include approaches for priming the degenerative host retina for enhanced integration. Although there is evidence of some efficacy following hPSC-PRP delivery even in end-stage retinal degeneration—suggesting that host inner retinal circuitry remains viable for a time—the exact window of opportunity for effective replacement is currently unknown[34,219]. Treatments being studied seek to modulate a variety of

naturally occurring processes that may act as barriers to donor PR integration in the degenerate outer reinta, including glial scarring[220], interneuron plasticity[221], and neurite outgrowth[222], which may in turn help create a more donor cell-receptive environment. Basic discovery research to better understand the molecular mechanisms involved in retinal circuit assembly, disassembly, and re-assembly will also be essential to addressing host-specific barriers to neuronal replacement[20,223].

While the eye is historically considered to be immune-privileged, current evidence suggests that this privilege is relative rather than absolute, and is perhaps lost in the course of disease[33]. Preclinical xenografts require immunodeficient hosts[46,146,150,224] or immunosuppressive regimens[147,160,225], but allograft studies and clinical trials to date report conflicting evidence regarding the degree of immune suppression necessary for long-term donor cell survival. Recent studies suggest that the immunogenicity of hPSC-derived retinal tissues may actually be relatively low, and hPSC-derived retinal cells might even confer a degree of local immune suppression[226]. As methods for assessing graft survival improve, further research regarding the role of the immune system in xenografts, allografts, and autografts will be necessary to predict best practices. Reports from hPSC-RPE clinical trials, which use a variety of immune suppressive regimens, will be highly informative for designing future clinical trials aimed at outer retinal cell replacement[26,33].

Conclusions: A Shared Responsibility

Exogenous RPE and PR transplantation efforts—bolstered by decades of research in regenerative medicine and retina developmental biology—have overcome significant hurdles in recent years and are now being tested in clinical trials. Although hPSC-RPE therapies are further along, remaining challenges to clinical translation for hPSC-PRP include scaling clinical-grade

cell production, creating organized grafts, addressing synapse function, and optimizing safety and efficacy outcomes in relevant model systems.

Singh *et al.* recently observed that, as these challenges are met and retinal cell therapies reach early-phase clinical trials, peer-reviewed interim reports may have unintended ripple effects on patients and lay audiences[26]. Eye-catching headlines rarely reflect the nuance of underlying research findings and further fuel public enthusiasm for stem cell-based therapies. Preclinical research can often elicit similar responses when reports of vision restoration in animal models are picked up by the media. The current landscape of milestone-oriented funding and open-source science necessitates timely publication of results, but Singh *et al.* stress the importance of appropriately powered, long-term follow-up to mitigate "scientifically unfounded over-optimism" within the non-scientific community. Recent case reports have underscored the grave impacts[227–229] of clinics prematurely capitalizing on this enthusiasm and preying on patient hope[230] with unregulated stem cell treatments.

A recent *Lancet* commission on regenerative medicine argues that the shift from "small-scale bespoke experimental interventions" to *bona fide* clinical application of hPSC-based therapies will require "substantial rethinking of the social contract that supports such research and clinical practice in the public arena." The commission contends that improving four areas—science, funding models, governance, and public/patient engagement—can prevent erosion of public trust and bridge the gap between patient expectations and currently available therapies[231]. While it is clear that tremendous scientific progress has been made toward retinal cell replacement, transitioning from bench to bedside will require substantial engagement from a variety of stakeholders regarding economic burden[21], international governance[27], and public/patient interaction[26].

The challenges that lie ahead for outer retinal cell therapies can be overcome, and the recent advances highlighted in this review suggest that the future for retinal regenerative medicine is bright. However, the transition from bench to bedside will require considerable investment of time and scientific effort from public and private entities alike. Moreover, the necessary focus on safety in early phase research means that preliminary efficacy in human subjects, who will necessarily be at the severe end of the disease spectrum, will likely be modest at first. In short, the reality we collectively face is that translating cell therapies to effective clinical practice will take time, and for families currently battling vision loss, it will rarely feel like progress comes fast enough. In the interim, scientists and clinicians will continue to play a crucial role in right-sizing public expectations for when hPSC-RPE and PRP cell therapies may realistically be available and encouraging patients to make informed decisions regarding unproven stem cell treatments. To this end, materials from the International Society for Stem Cell Research, including the *Patient Handbook on Stem Cell Therapies*[232] (available in 12 languages) and disease-specific fact sheets[233], as well as the McPherson Eye Research Institute's similarly themed "10 Things to Know Before You Fall Victim to a Retinal Stem Cell Scam" (see **Box 3**) can help patients navigate stem cell claims while researchers around the world continue to work toward solving the complex puzzle of outer retinal cell replacement.

Abbreviations, Definitions, & Glossary

Allograft, allogeneic: same-species (but genetically distinct) cell or tissue transplant

AMD: age-related macular degeneration

Anoikis: anchorage-dependent apoptosis (Greek, literally referring to cells “without a home”)

Anatomic integration: histologic or ultrastructural evidence of synaptogenesis by donor cells

Autograft, autologous: transplant in which cells or tissues are derived directly from the host

Crepuscular: animals active at dusk and dawn, often linked to evolution of both cone-rich and rod-dominant retinal regions to accommodate a variety of lighting conditions

Differentiation: the process through which a cell transitions into another, typically more specialized, cell type

Diurnal: animals active primarily during the day, often resulting in evolution of high acuity cone-dominant retinal regions

ERG: electroretinogram; a functional test measuring retinal electrical activity in response to a light stimulus; the various components (a-wave, b-wave, c-wave, etc.) indicate the health of specific retinal cell types

FACS: fluorescence activated cell sorting

Fate: cellular identity or cell type; defined by specific gene expression programs, downstream proteins, and functional effects

FDA: United States Food and Drug Administration

FISH: fluorescent *in situ* hybridization

Functional integration: in the context of PRP replacement, functional synaptic connectivity between donor and host neurons

GMP: Good Manufacturing Practice

HLA: human leukocyte antigen

HSC: hematopoietic stem cell

INL: inner nuclear layer

IPL: inner plexiform layer

ipRGCs: intrinsically photosensitive retinal ganglion cells

IRD: inherited retinal disease

MACS: magnetic activated cell sorting

Material transfer: exchange of proteins and/or RNA between donor and host cells

MEA: multi-electrode array; an electrophysiologic technique used to record electrical activity within tissues or populations of neurons

MG: Müller glia

Multipotency: a feature of lineage-restricted proliferative cells, which may give rise to multiple classes of tissue-specific cells (e.g., neural progenitor or retinal progenitor cells)

NHP: non-human primate

ONL: outer nuclear layer

OPL: outer plexiform layer

OS: outer segment; a specialized structure in rod and cone photoreceptors containing stacked discs with light-sensitive opsins

Pluripotency: a hallmark of stem cells (ES or iPS); the ability to give rise to any cell type within the body

PR: photoreceptor; generally refers to mature or maturing rods and cones

Primary cell: a cell directly isolated from its source tissue (e.g., flow-sorted rods from mouse retina)

PRP: photoreceptor precursor; a postmitotic neuron with the potential to become a rod, M/L cone, or S cone

PSCs: pluripotent stem cells; includes embryonic stem cells (ESCs) and induced pluripotent stem cells (iPSCs)

RD: retinal degeneration

RDDs: retinal degenerative disease

RGC: retinal ganglion cell

RPC: retinal progenitor cell; a proliferative, mitotic cell from which all retinal cells are derived

RP: retinitis pigmentosa

RPE: retinal pigment epithelium; a layer of cells underlying the neural retina that provides metabolic support to photoreceptors

SCNT: somatic cell nuclear transfer

Specification: the process of acquiring a particular cell fate

TER: transepithelial resistance

TRS: triad ribbon synapse

Xenograft: cross-species cell or tissue transplant (e.g., human-into-rat cell replacement)

Boxes, Figures, and Tables

Box 1. The translational research continuum.

Translational research aims to maximize basic science discoveries for direct application in advancing human health (also referred to as “bench-to-bedside” research). The process of bringing a new discovery to clinical practice often takes decades, and retinal cell therapies are still in the earliest stages of this process. Translational research is typically classified in four phases—T1 through T4 (see Zarbin, 2020[234] for further details):

- **T1 –** scientific discovery and development from preclinical studies to phase I and II clinical trials
- **T2** – determination of in humans through phase III & IV clinical trials
- **T3** – dissemination and implementation of therapies beyond clinical trials
- **T4** – public health and policy-level assessment of established therapies

Each phase also represents a continuum of research activities. Retinal cell therapies—including RPE and PR replacement—are both currently in phase T1. RPE replacement is nearing phase T2 with several clinical trials underway, while PR replacement is largely still in preclinical development.

Box 2. Defining integration in retinal cell replacement.

Although the term has appeared in the retinal regeneration literature across its entire history[37,161], the exact definition of integration is a present topic of debate within the field. A non-integrated donor cell—generally found in a self-contained mass in the subretinal space (SRS), floating in the vitreous or walled off by glial scarring[34]—is more easily defined than the integrated cell. Since many have historically relied on fluorescent reporters to identify donor cells, most studies prior to the mid-2010s referred to any fluorescent donor cells found within the SRS as “incorporated” or “integrated”. The discovery of donor-to-host cytoplasmic transfer of fluorophores has highlighted the need for stringent, universal criteria to distinguish true integration from material exchange events (see Nickerson et al., 2018[30] for further discussion). The field has since adopted a two-layered approach to identify and define integration[30]

Apparent donor PRP within the SRS should ideally: 1) express cytoplasmic markers specific to the donor cell population (e.g. *CRX-TdTomato*, *L/Mopsin-GFP*, Recoverin, etc.) and 2) co-label with at least one nuclear donor-specific marker (e.g., human nuclear antigen [HNA], Y-chromosome fluorescent in situ hybridization [FISH], BrdU, etc.). Nuclear diameter[30,162] and cellular morphology[160] are also useful adjunct approaches for distinguishing donor PRP from host cells.

Distinguishing between *anatomic integration* (i.e., histologic or ultrastructural evidence of synapse formation) and *functional integration* (i.e., direct evidence of donor cell-initiated synaptic transmission) is also critical. Recent computational modeling suggests that anatomic integration may not directly correlate with functional integration or visual behavior in xenotransplants due to evolutionarily divergent features in triad ribbon synapses[206] and visual function[250] in mammals. Many studies referenced in the present review have assessed anatomic integration and its association with light-evoked behavior. However, current studies aimed at exploring *functional integration*—often with electrophysiologic and/or behavioral assessments—often assay several synapses downstream of the donor-to-host PR synapse, making it difficult to control for alternate mechanisms of functional recovery. Methods to directly assay *functional integration* at the level of PR donor-to-host synapses are currently lacking, and development of such strategies are expected to aid clinical translation.

Box 3. 10 Things to Know Before You Fall Victim to a Retinal Stem Cell Scam

1. **The Hope is real:** Stem cell technology has created exciting new possibilities for understanding and treating diseases that have perpetually plagued humankind. But these remain early days in the technology and we have an overarching obligation to be honest and transparent and to “first do no harm."

2. **The difference between Hope and Hype is a single letter and a compelling website.** Private stem cell clinics touting miracle cures can cause you to lose whatever vision you have left – or your entire eye – due to infection, tumor, or another catastrophic event. And even if the treatment causes no physical harm, it can result in significant financial damage, with costs often reaching into the tens of thousands of U.S. dollars.

3. **Confused? It’s NOT the fault of you or your family.** Stem cell technology is complicated and still relatively new, and there are a growing number of private clinics that are attempting to financially capitalize on patients’ desperation and confusion. You should know that in many cases, the “stem cells” that are now being transplanted in these for-profit clinics are from fat, bone marrow, peripheral blood, or another source that has no proven ability to replace missing retinal cells.

4. **Be highly skeptical of any stem cell therapy that requires you to pay a fee or that claims to be a cure-all.** Almost all valid stem cell therapies are still in the clinical trial stage, or even earlier. Ethical scientists will enroll patients in these trials without asking for, or accepting, payment (often, they pay YOU). If you have doubts, ask questions – and not just of the people trying to sell you the stem cell procedure or the folks they refer you to, since they have an inherent conflict of interest.

5. **In order to avoid scams, it is important to understand what the retina is…** The retina is actually a complex “layer cake,” with each layer containing specific types of cells that perform a precise job and connect to other cells to form a neural circuit. Deepest within the retina lies a layer of photoreceptors – rods and cones – that detect light and initiate a cascade of events that ultimately lead to our perception of vision, which occurs in the brain. Retinal pigmented epithelial cells, or RPE cells, do not detect light but rather help photoreceptors do their job. If you lose RPE cells, the photoreceptors they serve will eventually lose their ability to function and die as well.

6. **…and also to understand what happens when retinal cells die.** Some of the most devastating and incurable causes of blindness are rooted in the death of retinal cells, including photoreceptors and RPE cells (the layer which nourishes photoreceptors). These diseases include age-related macular degeneration (AMD), retinitis pigmentosa (RP), Stargardt disease, Best disease, Usher syndrome, and others. For the vast majority of those affected, there are no cures

or successful treatments available.

7. **We are born with all the retinal "parts" we are ever going to have.** The human retina has no innate ability to replace these cells once they are lost. This is one reason why stem cells have drawn so much attention, since some types of stem cells (namely pluripotent stem cells, or PSCs) have the potential to provide replacement parts for the retina.

8. **Stem cell therapies may provide an option to replace the lost cells** by introducing new cells obtained from an outside source (retinal cell replacement through transplantation). Pluripotent stem cells (PSCs) – which are grown in the laboratory – can theoretically make any cell in the entire body. Many highly differentiated and specialized cell types, including photoreceptors and RPE cells, can now be produced from human PSCs in a reliable manner. There is another approach to replacing lost retinal cells, and that is to trick the retina into fixing itself (retinal regeneration), but that is a separate topic.

9. **The "installation challenge" is formidable for all cell types**, and scientists are working hard to develop effective methods of installing the new cells and getting them to connect properly and function within the retina itself. Of note, for-cost stem cell "clinics" will often just randomly inject their product into the middle of the eye, far away from the area where they would need to go if they truly could replace lost photoreceptors or RPE cells. Also, any such procedure has to be done by a skilled clinician, not a nurse or assistant.

10. **There is no magic to stem cells,** but there is a great deal of excellent, well-designed, and well-intentioned research being performed in the stem cell field. Stem cells have unique but variable properties that, if thoughtfully tested and applied, may be of considerable help to some patients in the foreseeable future. We're optimistic about this future…and you should be, too.

For a more detailed version of this article, please contact the McPherson Eye Research Institute at (608) 265-0690, vision.wisc.edu.

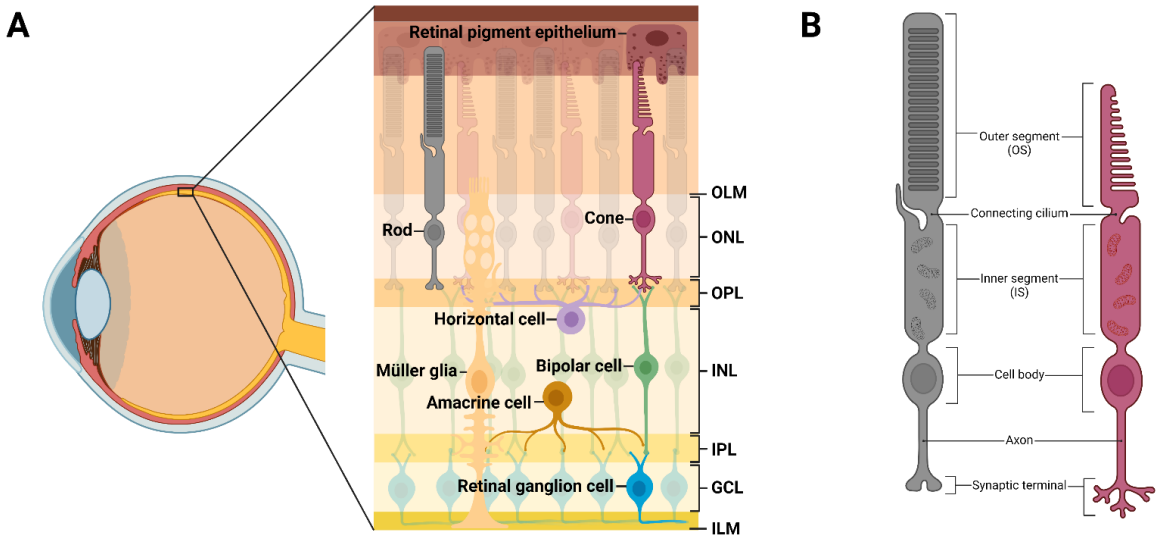

Figure 1. Organization and circuitry of the retina. (A) The retina contains three layers of cell bodies: the outer nuclear layer (ONL), in which rod and cone cell bodies reside; the inner nuclear layer (INL), containing horizontal cell (HC), bipolar cell (BC), amacrine cell (AC) and Müller glial (MG) cell bodies; and the ganglion cell layer (GCL) where retinal ganglion cell (RGC) somata and displaced ACs are found. PRs are supported by close apposition to the retinal pigment epithelium (RPE). The neural retina is bound apically by the outer limiting membrane (OLM) and basally by the inner limiting membrane (ILM), both formed by end-feet of the MG. PRs connect with BCs and HCs via synapses in the outer plexiform layer (OPL). The inner plexiform layer (IPL) contains signal-carrying synapses between BCs, ACs, and RGCs. (B) Rod and cone PRs display several distinct morphologic features. The outer segment (OS) contains stacked discs of photosensitive opsins for light detection. The connecting cilium facilitates trafficking between outer and inner segments (IS), the latter of which are rich in mitochondria. Extending from the cell body are axons with synaptic terminals, which interact with inner retinal neurons at triad ribbon synapses.

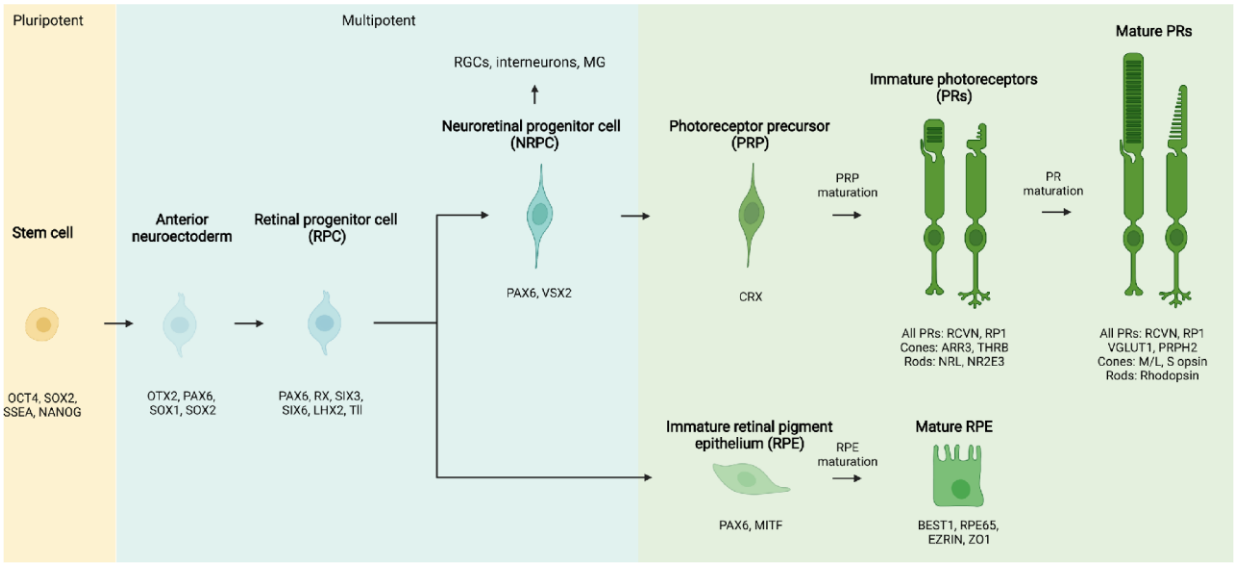

Figure 2. Phases of RPE and PR differentiation. Pluripotent stem cells pass through an anterior neuroectodermal stage to become multipotent retinal progenitor cells (RPCs), which are capable of producing all types of neuroretinal cells in addition to RPE. Neuroretinal progenitor cells (NRPCs) become further fate restricted over time and have the capacity to generate all neural retina cell types, including photoreceptor precursors (PRP). Over time, PRP and RPE mature to express several characteristic morphologic features. Examples of key transcription factors and defining cell markers for each stage are listed below each stage. Human PSC technologies follow these developmental pathways to reproducibly generate a variety of donor cells for replacement therapies.

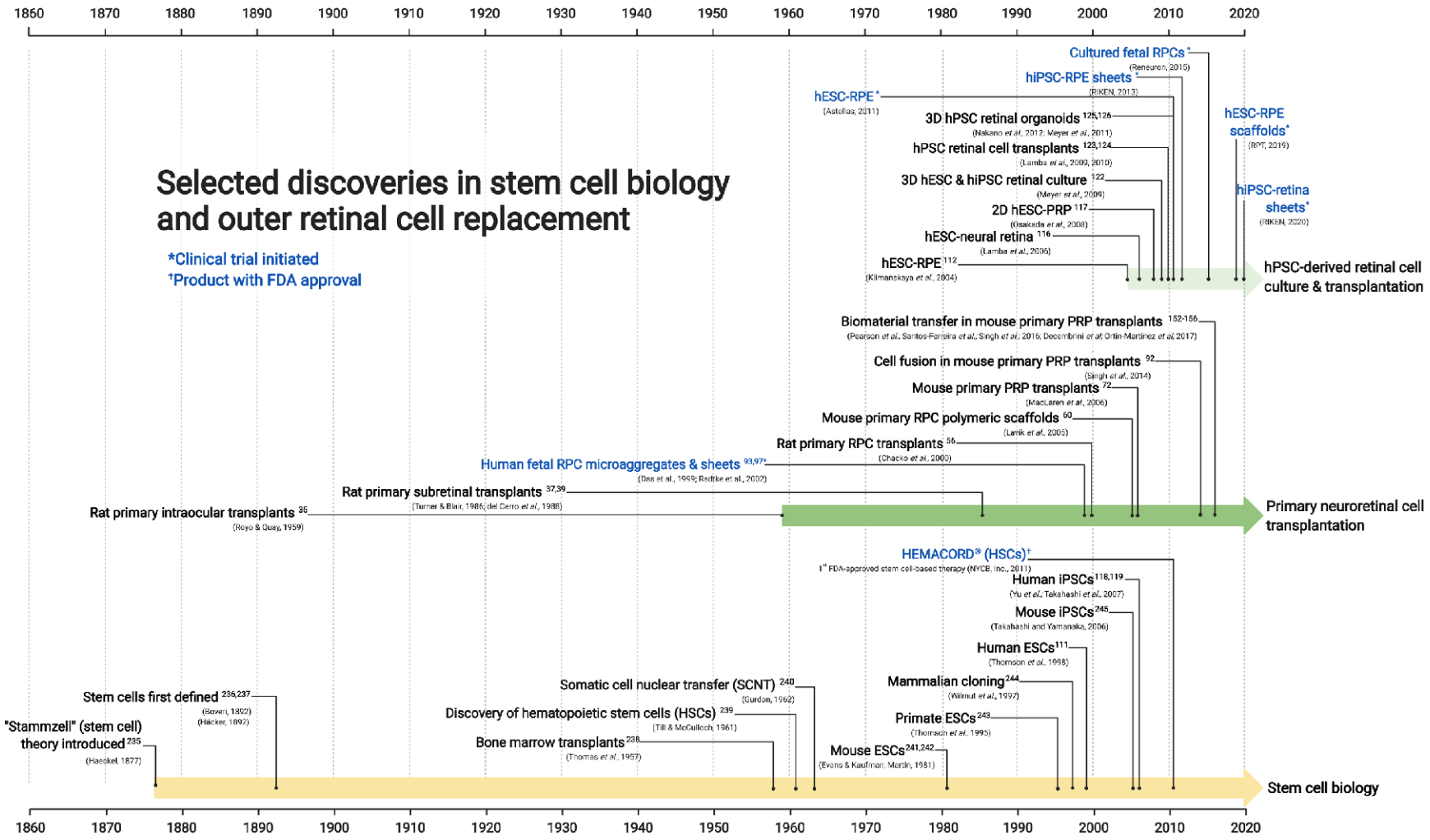

Figure 3. An abbreviated history of regenerative medicine and retinal cell replacement. An abbreviated history of stem cell biology and its applications to retinal cell replacement. Selected discoveries in stem cell biology and retinal cell transplantation that have contributed to the advancement of outer retinal cell replacement therapies.

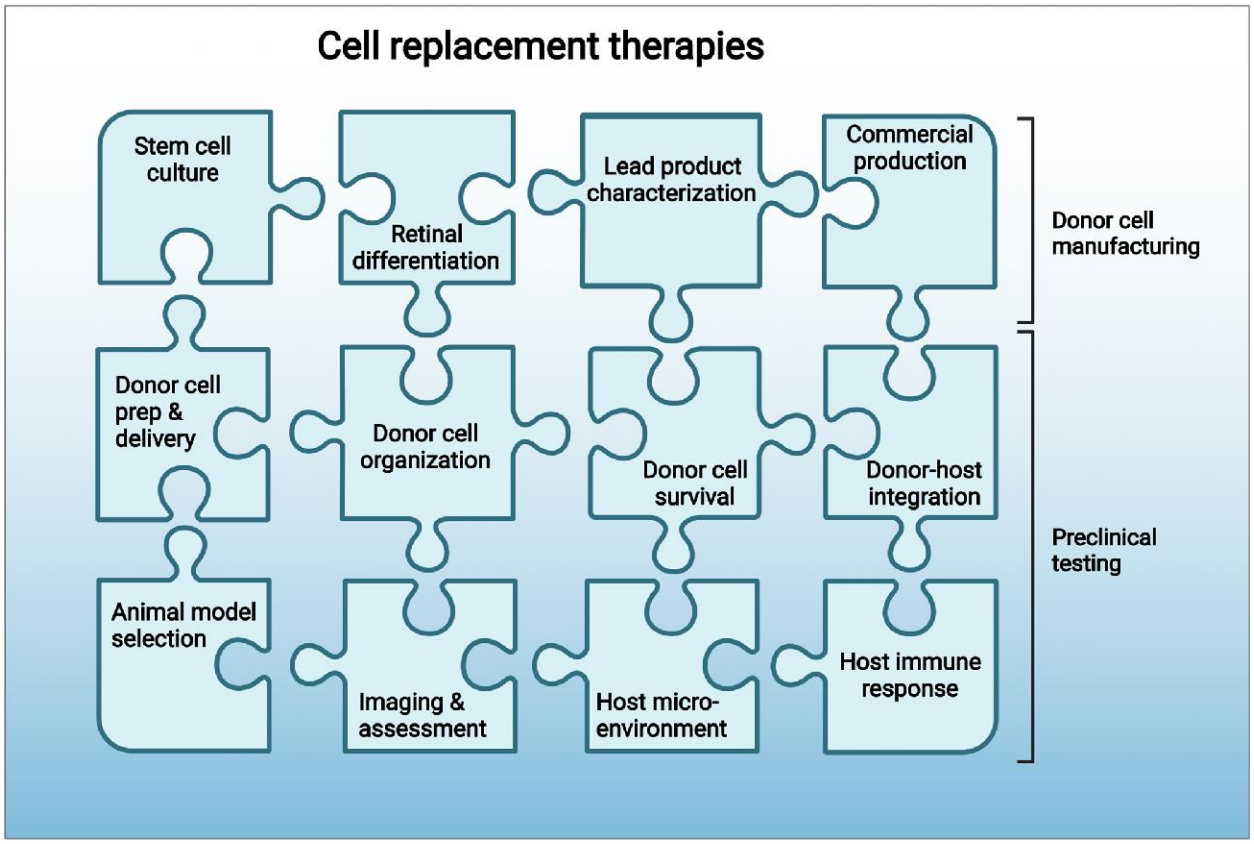

Figure 4. The complex puzzle of therapeutic development for outer retinal cell therapies. As cell therapies transition from phase T1 to phase T2 studies and beyond, several interconnected factors related to donor cell manufacturing and preclinical testing must be addressed.

Table 1. Defining characteristics of cell therapies.

Source	• Autologous: patient-derived • Allogeneic: donor-derived (potentially HLA-matched and/or genetically engineered)
Potential	• Pluripotent: capable of forming cells from all three germ layers (e.g. human ES or iPS cell) • Multipotent: capable of forming a limited range of cell types from a common lineage (e.g. retinal progenitor cell) • Unipotent: capable of forming one cell type or class (e.g. photoreceptor precursor)
Purity	• Heterogenous: the cell product consists of the target cell type intermixed with multiple off-target cell types • Enriched: the cell product is predominantly comprised of the target cell type • Purified: the cell product is exclusively comprised of the target cell type

Table 2. Animal RDD models and factors affecting suitability for preclinical retinal cell replacement†.

Species	Ocular Anatomy: Similarity to Human	Features	Predicted TRS* Compatibility with Human**	Options for Immune Suppression	Selected RDD models
Mouse	+	- Small globe with large lens - Rod-dominant retina	89%	Genetically modified Pharmacologic	*Rd1*, *Rd10*, many others
Rat	+	- Small globe with large lens - Rod-dominant retina	88%	Genetically modified Pharmacologic	*RCS, S334ter, P23H*
Ground squirrel	++	- Small globe with small lens - Cone-dominant retina	44%***	Pharmacologic	Retinal detachment
Rabbit	++	- Medium-sized globe with small lens - Visual streak	86%	Pharmacologic	*RHO* (P347L)[246]
Cat	+++	- Medium-sized globe with small lens - Area centralis	92%	Pharmacologic	Laser damage[247] *RDH5, CEP290, AIPL1*
Dog	+++	- Moderately large globe with small lens - Area centralis	81%	Pharmacologic	*RHO, RPE65, PDE6A, PDE6B, SAG, ABCA4*
Pig	++++	- Large globe with small lens - Visual streak	85%	Genetic models[248] Surgically-induced[224]	*RHO (P23H)* Laser damage
Macaque	+++++	- Large globe with small lens - Macula	98%	Pharmacologic	*PDE6C, BBS7* Laser damage

†A summary of findings from Stanzel *et al.*, 2019[249] (ocular anatomy, RDD models), Laver and Matsubara, 2017[206] (xenograft compatibility), and Winkler *et al.*, 2020[211] (RDD models)
*Photoreceptor triad ribbon synapse
**Based on the Pikachurin sequence similarity (percentage) between humans and the listed species.
***Laver and Matsubara broadly refer to squirrels; this may not directly reflect TRS compatibility of specific models (*e.g.* 13-lined ground squirrels)

References

1. Baden, T. & Osorio, D. The Retinal Basis of Vertebrate Color Vision. *Annu. Rev. Vis. Sci.* **5**, 177–200 (2019).
2. Lamb, T. D. Evolution of the genes mediating phototransduction in rod and cone photoreceptors. *Progress in Retinal and Eye Research* 100823 (2019) doi:10.1016/j.preteyeres.2019.100823.
3. George, S. M., Lu, F., Rao, M., Leach, L. L. & Gross, J. M. The retinal pigment epithelium: Development, injury responses, and regenerative potential in mammalian and non-mammalian systems. *Progress in Retinal and Eye Research* 100969 (2021) doi:10.1016/j.preteyeres.2021.100969.
4. Bringmann, A. *et al.* Cellular signaling and factors involved in Müller cell gliosis: neuroprotective and detrimental effects. *Prog Retin Eye Res* **28**, 423–451 (2009).
5. Reichenbach, A. & Bringmann, A. New functions of Müller cells. *Glia* **61**, 651–678 (2013).
6. Cepko, C. Intrinsically different retinal progenitor cells produce specific types of progeny. *Nature Reviews Neuroscience* **15**, 615–627 (2014).
7. Swaroop, A., Kim, D. & Forrest, D. Transcriptional regulation of photoreceptor development and homeostasis in the mammalian retina. *Nature Reviews Neuroscience* **11**, 563–576 (2010).
8. Brzezinski, J. A. & Reh, T. A. Photoreceptor cell fate specification in vertebrates. *Development* **142**, 3263–3273 (2015).
9. Sparrow, J. R., Hicks, D. & Hamel, C. P. The Retinal Pigment Epithelium in Health and Disease. *Curr Mol Med* **10**, 802–823 (2010).
10. Jones B. W., Pfeiffer R. L., Ferrell W. D., Watt C. B., Marmor M., Marc R. E.. Retinal remodeling in human retinitis pigmentosa. *Exp Eye Res* **150**, 149–165 (2016).

11. Jones BW, Marc RE, Pfeiffer RL.. Retinal Degeneration, Remodeling and Plasticity. In: Kolb H, Fernandez E, Nelson R, eds. Webvision: The Organization of the Retina and Visual System. Salt Lake City, UT: University of Utah Health Sciences Center (1995). Accessed August 26, 2021, http://www.ncbi.nlm.nih.gov/books/NBK482309/.
12. Jones, B. W. & Marc, R. E. Retinal remodeling during retinal degeneration. *Exp Eye Res* **81**, 123–137 (2005).
13. Pfeiffer, R. L., Marc, R. E. & Jones, B. W. Persistent remodeling and neurodegeneration in late-stage retinal degeneration. *Prog Retin Eye Res* **74**, 100771 (2020).
14. Wong W. L., Su X., Li X., et al. Global prevalence of age-related macular degeneration and disease burden projection for 2020 and 2040: a systematic review and meta-analysis. *Lancet Glob Health* **2**, e106–e116 (2014).
15. Flaxman S. R. , Bourne R. R. A., Resnikoff S., et al... Global causes of blindness and distance vision impairment 1990-2020: a systematic review and meta-analysis. The Lancet Glob Health. 2017; 5(12): e1221–e1234.13.
16. Verbakel S. K., van Huet R. A. C, Boon C. J. F, et al. Non-syndromic retinitis pigmentosa. Prog Retin Eye Res. **66,** 157–186 (2018).
17. van der Aa, H. P. A., Comijs, H. C., Penninx, B. W. J. H., Rens, G. H. M. B. van & Nispen, R. M. A. van. Major Depressive and Anxiety Disorders in Visually Impaired Older Adults. *Invest. Ophthalmol. Vis. Sci.* **56**, 849–854 (2015).
18. Taylor, D. J., Jones, L., Binns, A. M. & Crabb, D. P. 'You've got dry macular degeneration, end of story': a qualitative study into the experience of living with non-neovascular age-related macular degeneration. *Eye* **34**, 461–473 (2020).
19. Marques, A. P. *et al.* Global economic productivity losses from vision impairment and blindness. *EClinicalMedicine* **35**, 100852 (2021).

20. Gamm, D. M., Wong, R. & Panelists, and the A. W. Report on the National Eye Institute Audacious Goals Initiative: Photoreceptor Regeneration and Integration Workshop. *Trans. Vis. Sci. Tech.* **4**, 2–2 (2015).
21. Becker, S. M. & Wright, C. B. Update on the Status and Impact of the National Eye Institute Audacious Goals Initiative for Regenerative Medicine. *Journal of Ocular Pharmacology and Therapeutics* **37**, 144–146 (2021).
22. Botto, C. *et al.* Early and late stage gene therapy interventions for inherited retinal degenerations. *Progress in Retinal and Eye Research* 100975 (2021) doi:10.1016/j.preteyeres.2021.100975.
23. Barnea-Cramer, A. O. *et al.* Repair of Retinal Degeneration following Ex Vivo Minicircle DNA Gene Therapy and Transplantation of Corrected Photoreceptor Progenitors. *Molecular Therapy* **28**, 830–844 (2020).
24. Gene & Cell Therapy FAQs | ASGCT - American Society of Gene & Cell Therapy | ASGCT - American Society of Gene & Cell Therapy. https://asgct.org/education/more-resources/gene-and-cell-therapy-faqs.
25. Wang, Y., Tang, Z. & Gu, P. Stem/progenitor cell-based transplantation for retinal degeneration: a review of clinical trials. *Cell Death & Disease* **11**, 1–14 (2020).
26. Singh, M. S. *et al.* Retinal stem cell transplantation: Balancing safety and potential. *Progress in Retinal and Eye Research* **75**, 100779 (2020).
27. Maeda T., Sugita S., Kurimoto Y., Takahashi M. Trends of Stem Cell Therapies in Age-Related Macular Degeneration. *J Clin Med* **10**, 1785 (2021).
28. Sharma, R., Bose, D., Maminishkis, A. & Bharti, K. Retinal Pigment Epithelium Replacement Therapy for Age-Related Macular Degeneration: Are We There Yet? *Annual Review of Pharmacology and Toxicology* **60**, 553–572 (2020).

29. Canto-Soler, V., Flores-Bellver, M. & Vergara, M. N. Stem Cell Sources and Their Potential for the Treatment of Retinal Degenerations. *Invest. Ophthalmol. Vis. Sci.* **57**, ORSFd1-9 (2016).

30. Nickerson, P. E. B., Ortin-Martinez, A. & Wallace, V. A. Material Exchange in Photoreceptor Transplantation: Updating Our Understanding of Donor/Host Communication and the Future of Cell Engraftment Science. *Front Neural Circuits* **12**, 17 (2018).

31. Hunt, N. C., Hallam, D., Chichagova, V., Steel, D. H. & Lako, M. The Application of Biomaterials to Tissue Engineering Neural Retina and Retinal Pigment Epithelium. *Advanced Healthcare Materials* **7**, 1800226 (2018).

32. Jemni-Damer, N. *et al.* Biotechnology and Biomaterial-Based Therapeutic Strategies for Age-Related Macular Degeneration. Part II: Cell and Tissue Engineering Therapies. *Front. Bioeng. Biotechnol.* **8**, (2020).

33. Petrash, C. C., Palestine, A. G. & Canto-Soler, M. V. Immunologic Rejection of Transplanted Retinal Pigmented Epithelium: Mechanisms and Strategies for Prevention. *Front. Immunol.* **12**, (2021).

34. Gasparini, S. J., Llonch, S., Borsch, O. & Ader, M. Transplantation of photoreceptors into the degenerative retina: Current state and future perspectives. *Progress in retinal and eye research* (2018) doi:10.1016/j.preteyeres.2018.11.001.

35. Royo, P. E. & Quay, W. B. Retinal transplantation from fetal to maternal mammalian eye. *Growth* **23**, 313–336 (1959).

36. del Cerro, M. *et al.* Intraocular retinal transplants. *Invest. Ophthalmol. Vis. Sci.* **26**, 1182–1185 (1985).

37. Turner, J. E. & Blair, J. R. Newborn rat retinal cells transplanted into a retinal lesion site in adult host eyes. *Brain Res* **391**, 91–104 (1986).

38. Blair, J. R. & Turner, J. E. Optimum conditions for successful transplantation of immature rat retina to the lesioned adult retina. *Developmental Brain Research* **36**, 257–270 (1987).
39. del Cerro, M. *et al.* Chapter 16 Retinal transplants into adult eyes affected by phototoxic retinopathy. in *Progress in Brain Research* (eds. Gash, D. M. & Sladek, J. R.) vol. 78 125–130 (Elsevier, 1988).
40. del Cerro, M., Notter, M., Wiegand, S., Jiang, L. & del Cerro, C. Replacement of rod cells into adult eyes affected by late-state phototoxic retinopathy by transplanation of developing retinal cells. *J. Neur. Transpl.* **1**, 1–10 (1989).
41. Turner, J. E., Seiler, M., Aramant, R. & Blair, J. R. Chapter 17 Embryonic retinal grafts transplanted into the lesioned adult rat retina. in *Progress in Brain Research* (eds. Gash, D. M. & Sladek, J. R.) vol. 78 131–139 (Elsevier, 1988).
42. Cepko, C. L., Austin, C. P., Yang, X., Alexiades, M. & Ezzeddine, D. Cell fate deternination in the vertebrate retina. *Proc. Natl. Acad. Sci. USA* 7 (1996).
43. Gouras, P. *et al.* Survival and Synapse Formation of Transplanted Rat Rods. *Journal of Neural Transplantation and Plasticity* **2**, 91–100 (1991).
44. Gust, J. & Reh, T. A. Adult Donor Rod Photoreceptors Integrate into the Mature Mouse Retina. *Invest. Ophthalmol. Vis. Sci.* **52**, 5266–5272 (2011).
45. Aramant, R., Seiler, M. & Turner, J. E. Donor age influences on the success of retinal grafts to adult rat retina. *Invest Ophthalmol Vis Sci* **29**, 498–503 (1988).
46. Aramant, R. B. & Seiler, M. J. Human Embryonic Retinal Cell Transplants in Athymic Immunodeficient Rat Hosts. *Cell Transplant* **3**, 461–474 (1994).
47. Francis, P. J. *et al.* Subretinal transplantation of forebrain progenitor cells in nonhuman primates: survival and intact retinal function. *Invest Ophthalmol Vis Sci* **50**, 3425–3431 (2009).

48. Wang, S. *et al.* Long-term vision rescue by human neural progenitors in a rat model of photoreceptor degeneration. *Invest Ophthalmol Vis Sci* **49**, 3201–3206 (2008).

49. Gamm, D. M. *et al.* Protection of visual functions by human neural progenitors in a rat model of retinal disease. *PLoS One* **2**, e338 (2007).

50. Van Hoffelen, S. J., Young, M. J., Shatos, M. A. & Sakaguchi, D. S. Incorporation of murine brain progenitor cells into the developing mammalian retina. *Invest Ophthalmol Vis Sci* **44**, 426–434 (2003).

51. Young, M. J., Ray, J., Whiteley, S. J., Klassen, H. & Gage, F. H. Neuronal differentiation and morphological integration of hippocampal progenitor cells transplanted to the retina of immature and mature dystrophic rats. *Mol Cell Neurosci* **16**, 197–205 (2000).

52. Takahashi, M., Palmer, T. D., Takahashi, J. & Gage, F. H. Widespread Integration and Survival of Adult-Derived Neural Progenitor Cells in the Developing Optic Retina. *Molecular and Cellular Neuroscience* **12**, 340–348 (1998).

53. Klassen, H. J. *et al.* Multipotent retinal progenitors express developmental markers, differentiate into retinal neurons, and preserve light-mediated behavior. *Invest Ophthalmol Vis Sci* **45**, 4167–4173 (2004).

54. Qiu, G. *et al.* Photoreceptor differentiation and integration of retinal progenitor cells transplanted into transgenic rats. *Exp. Eye Res.* **80**, 515–525 (2005).

55. Akagi, T. *et al.* Different characteristics of rat retinal progenitor cells from different culture periods. *Neuroscience Letters* **341**, 213–216 (2003).

56. Chacko, D. M., Rogers, J. A., Turner, J. E. & Ahmad, I. Survival and Differentiation of Cultured Retinal Progenitors Transplanted in the Subretinal Space of the Rat. *Biochemical and Biophysical Research Communications* **268**, 842–846 (2000).

57. Tucker, B. A. *et al.* The use of progenitor cell/biodegradable MMP2-PLGA polymer constructs to enhance cellular integration and retinal repopulation. *Biomaterials* **31**, 9–19 (2010).

58. Seiler, M. J. & Aramant, R. B. Cell replacement and visual restoration by retinal sheet transplants. *Prog Retin Eye Res* **31**, 661–687 (2012).

59. Lund, R. D., Ono, S. J., Keegan, D. J. & Lawrence, J. M. Retinal transplantation: progress and problems in clinical application. *Journal of Leukocyte Biology* **74**, 151–160 (2003).

60. Lavik, E. B., Klassen, H., Warfvinge, K., Langer, R. & Young, M. J. Fabrication of degradable polymer scaffolds to direct the integration and differentiation of retinal progenitors. *Biomaterials* **26**, 3187–3196 (2005).

61. Pritchard, C. D., Arnér, K. M., Langer, R. S. & Ghosh, F. K. Retinal transplantation using surface modified poly(glycerol-co-sebacic acid) membranes. *Biomaterials* **31**, 7978–7984 (2010).

62. Neeley, W. L. *et al.* A microfabricated scaffold for retinal progenitor cell grafting. *Biomaterials* **29**, 418–26 (2008).

63. Redenti, S. *et al.* Engineering retinal progenitor cell and scrollable poly(glycerol-sebacate) composites for expansion and subretinal transplantation. *Biomaterials* **30**, 3405–3414 (2009).

64. Yao, J. *et al.* Enhanced differentiation and delivery of mouse retinal progenitor cells using a micropatterned biodegradable thin-film polycaprolactone scaffold. *Tissue Eng Part A* **21**, 1247–1260 (2015).

65. Yao, J. *et al.* Robust cell integration from co-transplantation of biodegradable MMP2-PLGA microspheres with retinal progenitor cells. *Biomaterials* **32**, 1041–1050 (2011).

66. Steedman, M. R., Tao, S. L., Klassen, H. & Desai, T. A. Enhanced differentiation of retinal progenitor cells using microfabricated topographical cues. *Biomedical Microdevices* **12**, 363–369 (2010).

67. Ballios, B. G. *et al.* A Hyaluronan-Based Injectable Hydrogel Improves the Survival and Integration of Stem Cell Progeny following Transplantation. *Stem Cell Reports* **4**, 1031–1045 (2015).

68. Ballios, B. G., Cooke, M. J., van der Kooy, D. & Shoichet, M. S. A hydrogel-based stem cell delivery system to treat retinal degenerative diseases. *Biomaterials* **31**, 2555–2564 (2010).

69. Silverman, M. S. & Hughes, S. E. Transplantation of photoreceptors to light-damaged retina. *Invest. Ophthalmol. Vis. Sci.* **30**, 1684–1690 (1989).

70. Tomita, M. *et al.* Biodegradable polymer composite grafts promote the survival and differentiation of retinal progenitor cells. *Stem cells (Dayton, Ohio)* **23**, 1579–88 (2009).

71. Tao, S. *et al.* Survival, migration and differentiation of retinal progenitor cells transplanted on micro-machined poly(methyl methacrylate) scaffolds to the subretinal space. *Lab Chip* **7**, 695–701 (2007).

72. MacLaren, R. E. *et al.* Retinal repair by transplantation of photoreceptor precursors. *Nature* **444**, 203–207 (2006).

73. Bartsch, U. *et al.* Retinal cells integrate into the outer nuclear layer and differentiate into mature photoreceptors after subretinal transplantation into adult mice. *Exp. Eye Res.* **86**, 691–700 (2008).

74. West, E. L. *et al.* Pharmacological disruption of the outer limiting membrane leads to increased retinal integration of transplanted photoreceptor precursors. *Exp. Eye Res.* **86**, 601–611 (2008).

75. Pearson, R. A. *et al.* Targeted disruption of outer limiting membrane junctional proteins (Crb1 and ZO-1) increases integration of transplanted photoreceptor precursors into the adult wild-type and degenerating retina. *Cell Transplant* **19**, 487–503 (2010).

76. Barber, A. C. *et al.* Repair of the degenerate retina by photoreceptor transplantation. *Proc. Natl. Acad. Sci. U.S.A.* **110**, 354–359 (2013).

77. Kinouchi, R. *et al.* Robust neural integration from retinal transplants in mice deficient in GFAP and vimentin. *Nat Neurosci* **6**, 863–868 (2003).

78. Suzuki, T. *et al.* Chondroitinase ABC treatment enhances synaptogenesis between transplant and host neurons in model of retinal degeneration. *Cell Transplant* **16**, 493–503 (2007).

79. Mandai, M. *et al.* Adequate Time Window and Environmental Factors Supporting Retinal Graft Cell Survival in rd Mice. *Cell Med* **4**, 45–54 (2012).

80. Ma, J., Kabiel, M., Tucker, B. A., Ge, J. & Young, M. J. Combining chondroitinase ABC and growth factors promotes the integration of murine retinal progenitor cells transplanted into Rho(-/-) mice. *Mol Vis* **17**, 1759–1770 (2011).

81. Lakowski, J. *et al.* Cone and rod photoreceptor transplantation in models of the childhood retinopathy Leber congenital amaurosis using flow-sorted Crx-positive donor cells. *Human Molecular Genetics* **19**, 4545–4559 (2010).

82. Pearson, R. A. *et al.* Restoration of vision after transplantation of photoreceptors. *Nature* **485**, 99–103 (2012).

83. Smiley, S. *et al.* Establishment of a cone photoreceptor transplantation platform based on a novel cone-GFP reporter mouse line. *Scientific Reports* **6**, (2016).

84. Eberle, D., Schubert, S., Postel, K., Corbeil, D. & Ader, M. Increased integration of transplanted CD73-positive photoreceptor precursors into adult mouse retina. *Investigative Ophthalmology and Visual Science* **52**, 6462–6471 (2011).

85. Eberle, D., Santos-Ferreira, T., Grahl, S. & Ader, M. Subretinal transplantation of MACS purified photoreceptor precursor cells into the adult mouse retina. *Journal of Visualized Experiments* (2014) doi:10.3791/50932.

86. Lakowski, J. *et al.* Effective transplantation of photoreceptor precursor cells selected via cell surface antigen expression. *Stem Cells* **29**, 1391–1404 (2011).

87. Jayakody, S. A., Gonzalez-Cordero, A., Ali, R. R. & Pearson, R. A. Cellular strategies for retinal repair by photoreceptor replacement. *Prog Retin Eye Res* **46**, 31–66 (2015).

88. Santos-Ferreira, T. *et al.* Daylight vision repair by cell transplantation. *Stem Cells* **33**, 79–90 (2015).

89. Singh, M. S. *et al.* Reversal of end-stage retinal degeneration and restoration of visual function by photoreceptor transplantation. *Proc. Natl. Acad. Sci. U.S.A.* **110**, 1101–1106 (2013).

90. Neves, J. *et al.* Immune modulation by MANF promotes tissue repair and regenerative success in the retina. *Science* **353**, (2016).

91. West, E. L. *et al.* Long-Term Survival of Photoreceptors Transplanted into the Adult Murine Neural Retina Requires Immune Modulation. *Stem Cells* **28**, 1997–2007 (2010).

92. Singh, M. S. *et al.* Cell fusion following photoreceptor transplantation into the non-degenerate retina. *Invest. Ophthalmol. Vis. Sci.* **55**, 3989–3989 (2014).

93. Das, T. *et al.* The transplantation of human fetal neuroretinal cells in advanced retinitis pigmentosa patients: results of a long-term safety study. *Exp Neurol* **157**, 58–68 (1999).

94. Humayun, M. S. *et al.* Human neural retinal transplantation. *Invest Ophthalmol Vis Sci* **41**, 3100–3106 (2000).

95. Radtke, N. D. *et al.* Vision improvement in retinal degeneration patients by implantation of retina together with retinal pigment epithelium. *Am J Ophthalmol* **146**, 172–182 (2008).

96. Radtke, N. D., Aramant, R. B., Seiler, M. J., Petry, H. M. & Pidwell, D. Vision change after sheet transplant of fetal retina with retinal pigment epithelium to a patient with retinitis pigmentosa. *Arch Ophthalmol* **122**, 1159–1165 (2004).

97. Radtke, N. D., Seiler, M. J., Aramant, R. B., Petry, H. M. & Pidwell, D. J. Transplantation of intact sheets of fetal neural retina with its retinal pigment epithelium in retinitis pigmentosa patients. *American Journal of Ophthalmology* **133**, 544–550 (2002).

98. Uyama, H., Mandai, M. & Takahashi, M. Stem-cell-based therapies for retinal degenerative diseases: Current challenges in the establishment of new treatment strategies. *Development, Growth & Differentiation* **63**, 59–71 (2021).

99. Stern, J. H. & Temple, S. Stem Cells for Retinal Replacement Therapy. *Neurotherapeutics* **8**, 736–743 (2011).

100. Applications, I. of M. (US) C. C. on F. R. and. *Setting the Stage: Fetal Research, Fetal Tissue Research, and Historical Timeline of Regulation and Legislation*. *Fetal Research and Applications: A Conference Summary* (National Academies Press (US), 1994).

101. Stem Cell Scientists Answer the Question, “Why Is It Important to You to Support Fetal Tissue Research?” *Stem Cell Reports* **12**, 186–190 (2019).

102. Schmitt, S. *et al.* Molecular characterization of human retinal progenitor cells. *Invest Ophthalmol Vis Sci* **50**, 5901–5908 (2009).

103. Yang, P., Seiler, M. J., Aramant, R. B. & Whittemore, S. R. In vitro isolation and expansion of human retinal progenitor cells. *Exp Neurol* **177**, 326–331 (2002).

104. Hasan, S. M. *et al.* Immortalized human fetal retinal cells retain progenitor characteristics and represent a potential source for the treatment of retinal degenerative disease. *Cell Transplant* **19**, 1291–1306 (2010).

105. Wright, L. S. *et al.* VSX2 and ASCL1 Are Indicators of Neurogenic Competence in Human Retinal Progenitor Cultures. *PLoS One* **10**, (2015).

106. Gamm, D. M. *et al.* Regulation of prenatal human retinal neurosphere growth and cell fate potential by retinal pigment epithelium and Mash1. *Stem Cells* **26**, 3182–3193 (2008).

107. Klassen, H. Stem cells in clinical trials for treatment of retinal degeneration. *Expert Opin Biol Ther* **16**, 7–14 (2016).

108. Klassen, H. *et al.* Progenitor Cells from the Porcine Neural Retina Express Photoreceptor Markers After Transplantation to the Subretinal Space of Allorecipients. *STEM CELLS* **25**, 1222–1230 (2007).

109. Semo, M. *et al.* Efficacy and Safety of Human Retinal Progenitor Cells. *Transl Vis Sci Technol* **5**, 6 (2016).

110. Luo, J. *et al.* Human retinal progenitor cell transplantation preserves vision. *J Biol Chem* **289**, 6362–6371 (2014).

111. Thomson, J. A. *et al.* Embryonic stem cell lines derived from human blastocysts. *Science* **282**, 1145–1147 (1998).

112. Klimanskaya, I. *et al.* Derivation and Comparative Assessment of Retinal Pigment Epithelium from Human Embryonic Stem Cells Using Transcriptomics. *Cloning and Stem Cells* **6**, 217–245 (2004).

113. Ikeda, H. *et al.* Generation of Rx+/Pax6+ neural retinal precursors from embryonic stem cells. *PNAS* **102**, 11331–11336 (2005).

114. Zhao, X., Liu, J. & Ahmad, I. Differentiation of embryonic stem cells into retinal neurons. *Biochemical and biophysical research communications* **297**, 177–84 (2002).

115. Banin, E. *et al.* Retinal Incorporation and Differentiation of Neural Precursors Derived from Human Embryonic Stem Cells. *STEM CELLS* **24**, 246–257 (2006).

116. Lamba, D. A., Karl, M. O., Ware, C. B. & Reh, T. A. Efficient generation of retinal progenitor cells from human embryonic stem cells. *PNAS* **103**, 12769–12774 (2006).

117. Osakada, F. *et al.* Toward the generation of rod and cone photoreceptors from mouse, monkey and human embryonic stem cells. *Nature biotechnology* **26**, 215–24 (2008).

118. Yu, J. *et al.* Induced pluripotent stem cell lines derived from human somatic cells. *Science* **318**, 1917–1920 (2007).

119. Takahashi, K. *et al.* Induction of Pluripotent Stem Cells from Adult Human Fibroblasts by Defined Factors. *Cell* **131**, 861–872 (2007).

120. Pankratz, M. T. *et al.* Directed Neural Differentiation of Human Embryonic Stem Cells via an Obligated Primitive Anterior Stage. *STEM CELLS* **25**, 1511–1520 (2007).

121. Hirami, Y. *et al.* Generation of retinal cells from mouse and human induced pluripotent stem cells. *Neuroscience Letters* **458**, 126–131 (2009).

122. Meyer, J. S. *et al.* Modeling early retinal development with human embryonic and induced pluripotent stem cells. *Proceedings of the National Academy of Sciences of the United States of America* **106**, 16698–703 (2009).

123. Lamba, D. A., Gust, J. & Reh, T. A. Transplantation of human embryonic stem cell-derived photoreceptors restores some visual function in Crx-deficient mice. *Cell stem cell* **4**, 73–9 (2009).

124. Lamba, D. A. *et al.* Generation, purification and transplantation of photoreceptors derived from human induced pluripotent stem cells. *PloS one* **5**, e8763 (2010).

125. Meyer, J. S. *et al.* Optic vesicle-like structures derived from human pluripotent stem cells facilitate a customized approach to retinal disease treatment. *Stem Cells* **29**, 1206–1218 (2011).

126. Nakano, T. *et al.* Self-Formation of Optic Cups and Storable Stratified Neural Retina from Human ESCs. *Cell Stem Cell* **10**, 771–785 (2012).

127. Zhong, X. *et al.* Generation of three-dimensional retinal tissue with functional photoreceptors from human iPSCs. *Nat Commun* **5**, 4047 (2014).

128. Kuwahara, A. *et al.* Generation of a ciliary margin-like stem cell niche from self-organizing human retinal tissue. *Nature Communications* **6**, 6286 (2015).

129. Capowski, E. E. *et al.* Reproducibility and staging of 3D human retinal organoids across multiple pluripotent stem cell lines. *Development* **146**, dev171686 (2019).

130. Phillips, M. J. *et al.* Blood-Derived Human iPS Cells Generate Optic Vesicle–Like Structures with the Capacity to Form Retinal Laminae and Develop SynapsesProduction of Retina from Human Blood iPS Cells. *Investigative Ophthalmology & Visual Science* **53**, 2007–2019 (2012).

131. Hallam, D. *et al.* Human-Induced Pluripotent Stem Cells Generate Light Responsive Retinal Organoids with Variable and Nutrient-Dependent Efficiency. *Stem cells (Dayton, Ohio)* **36**, 1535–1551 (2018).

132. Kim, S. *et al.* Generation, transcriptome profiling, and functional validation of cone-rich human retinal organoids. *Proceedings of the National Academy of Sciences of the United States of America* **116**, 10824–10833 (2019).

133. Bell, C. M., Zack, D. J. & Berlinicke, C. A. Human Organoids for the Study of Retinal Development and Disease. *Annu Rev Vis Sci* **6**, 91–114 (2020).

134. Cowan, C. S. *et al.* Cell Types of the Human Retina and Its Organoids at Single-Cell Resolution. *Cell* **182**, 1623-1640.e34 (2020).

135. Phillips, M. J. *et al.* A Novel Approach to Single Cell RNA-Sequence Analysis Facilitates In Silico Gene Reporting of Human Pluripotent Stem Cell-Derived Retinal Cell Types. *Stem Cells* **36**, 313–324 (2018).

136. Assawachananont, J. *et al.* Transplantation of embryonic and induced pluripotent stem cell-derived 3D retinal sheets into retinal degenerative mice. *Stem Cell Reports* **2**, 662–674 (2014).

137. Decembrini, S., Koch, U., Radtke, F., Moulin, A. & Arsenijevic, Y. Derivation of Traceable and Transplantable Photoreceptors from Mouse Embryonic Stem Cells. *Stem Cell Reports* **2**, 853–865 (2014).

138. Gonzalez-Cordero, A. *et al.* Photoreceptor precursors derived from three-dimensional embryonic stem cell cultures integrate and mature within adult degenerate retina. *Nat Biotechnol* **31**, 741–747 (2013).

139. Kruczek, K. *et al.* Differentiation and Transplantation of Embryonic Stem Cell-Derived Cone Photoreceptors into a Mouse Model of End-Stage Retinal Degeneration. *Stem Cell Reports* **8**, 1659–1674 (2017).

140. Santos-Ferreira, T. *et al.* Stem Cell–Derived Photoreceptor Transplants Differentially Integrate Into Mouse Models of Cone-Rod Dystrophy. *Invest. Ophthalmol. Vis. Sci.* **57**, 3509–3520 (2016).

141. Mandai, M. *et al.* iPSC-Derived Retina Transplants Improve Vision in rd1 End-Stage Retinal-Degeneration Mice. *Stem Cell Reports* **8**, 69–83 (2017).

142. Tucker, B. A. *et al.* Transplantation of Adult Mouse iPS Cell-Derived Photoreceptor Precursors Restores Retinal Structure and Function in Degenerative Mice. *PLOS ONE* **6**, e18992 (2011).

143. West, E. L. *et al.* Defining the integration capacity of embryonic stem cell-derived photoreceptor precursors. *Stem Cells* **30**, 1424–1435 (2012).

144. Gonzalez-Cordero, A. *et al.* Recapitulation of Human Retinal Development from Human Pluripotent Stem Cells Generates Transplantable Populations of Cone Photoreceptors. *Stem Cell Reports* **9**, 820–837 (2017).

145. Zhu, J., Cifuentes, H., Reynolds, J. & Lamba, D. A. Immunosuppression via Loss of IL2rγ Enhances Long-Term Functional Integration of hESC-Derived Photoreceptors in the Mouse Retina. *Cell Stem Cell* **20**, 374-384.e5 (2017).

146. Iraha, S. *et al.* Establishment of Immunodeficient Retinal Degeneration Model Mice and Functional Maturation of Human ESC-Derived Retinal Sheets after Transplantation. *Stem Cell Reports* **10**, 1059–1074 (2018).

147. Tu, H.-Y. *et al.* Medium- to long-term survival and functional examination of human iPSC-derived retinas in rat and primate models of retinal degeneration. *EBioMedicine* **39**, 562–574 (2019).

148. Shirai, H. *et al.* Transplantation of human embryonic stem cell-derived retinal tissue in two primate models of retinal degeneration. *Proceedings of the National Academy of Sciences of the United States of America* **113**, E81-90 (2016).

149. McLelland, B. T. *et al.* Transplanted hESC-Derived Retina Organoid Sheets Differentiate, Integrate, and Improve Visual Function in Retinal Degenerate Rats. *Invest. Ophthalmol. Vis. Sci.* **59**, 2586–2603 (2018).

150. Seiler, M. J. *et al.* A new immunodeficient pigmented retinal degenerate rat strain to study transplantation of human cells without immunosuppression. *Graefes Arch. Clin. Exp. Ophthalmol.* **252**, 1079–1092 (2014).

151. Hambright, D. *et al.* Long-term survival and differentiation of retinal neurons derived from human embryonic stem cell lines in un-immunosuppressed mouse retina. *Molecular Vision* **18**, 920–936 (2012).

152. Singh, M. S. *et al.* Transplanted photoreceptor precursors transfer proteins to host photoreceptors by a mechanism of cytoplasmic fusion. *Nat Commun* **7**, 13537 (2016).

153. Pearson, R. A. *et al.* Donor and host photoreceptors engage in material transfer following transplantation of post-mitotic photoreceptor precursors. *Nat Commun* **7**, 13029 (2016).

154. Santos-Ferreira, T. *et al.* Retinal transplantation of photoreceptors results in donor-host cytoplasmic exchange. *Nat Commun* **7**, 13028 (2016).

155. Ortin-Martinez, A. *et al.* A Reinterpretation of Cell Transplantation: GFP Transfer From Donor to Host Photoreceptors. *Stem Cells* **35**, 932–939 (2017).

156. Decembrini S., Martin C., Sennlaub F., et al. Cone Genesis Tracing by the Chrnb4-EGFP Mouse Line: Evidences of Cellular Material Fusion after Cone Precursor Transplantation. *Mol Ther* **25**, 634–653 (2017).

157. Waldron, P. V. *et al.* Transplanted Donor- or Stem Cell-Derived Cone Photoreceptors Can Both Integrate and Undergo Material Transfer in an Environment-Dependent Manner. *Stem Cell Reports* **10**, 406–421 (2018).

158. MacLaren, R. E. Cone fusion confusion in photoreceptor transplantation. *Stem Cell Investig* **4**, 71 (2017).

159. Barnea-Cramer, A. O. *et al.* Function of human pluripotent stem cell-derived photoreceptor progenitors in blind mice. *Sci Rep* **6**, 29784 (2016).

160. Aboualizadeh, E. *et al.* Imaging Transplanted Photoreceptors in Living Nonhuman Primates with Single-Cell Resolution. *Stem Cell Reports* **15**, 482–497 (2020).

161. Ribeiro, J. *et al.* Restoration of visual function in advanced disease after transplantation of purified human pluripotent stem cell-derived cone photoreceptors. *Cell Reports* **35**, (2021).

162. Gagliardi, G. *et al.* Characterization and Transplantation of CD73-Positive Photoreceptors Isolated from Human iPSC-Derived Retinal Organoids. *Stem cell reports* **11**, 665–680 (2018).

163. Garita-Hernandez, M. *et al.* Restoration of visual function by transplantation of optogenetically engineered photoreceptors. *Nature Communications* **10**, 4524 (2019).

164. Wiley, L. A. *et al.* cGMP production of patient-specific iPSCs and photoreceptor precursor cells to treat retinal degenerative blindness. *Sci Rep* **6**, 30742 (2016).

165. Reichman, S. *et al.* Generation of Storable Retinal Organoids and Retinal Pigmented Epithelium from Adherent Human iPS Cells in Xeno-Free and Feeder-Free Conditions. *Stem cells (Dayton, Ohio)* **35**, 1176–1188 (2017).

166. Stone, N. E., Voigt, A. P., Mullins, R. F., Sulchek, T. & Tucker, B. A. Microfluidic processing of stem cells for autologous cell replacement. *Stem Cells Transl Med* (2021) doi:10.1002/sctm.21-0080.

167. Huang, C.-Y. *et al.* Human iPSC banking: barriers and opportunities. *J Biomed Sci* **26**, 87 (2019).

168. Kramer, J., Chirco, K. R. & Lamba, D. A. Immunological Considerations for Retinal Stem Cell Therapy. in *Pluripotent Stem Cells in Eye Disease Therapy* (ed. Bharti, K.) 99–119 (Springer International Publishing, 2019). doi:10.1007/978-3-030-28471-8_4.

169. Petrus-Reurer, S. *et al.* Generation of Retinal Pigment Epithelial Cells Derived from Human Embryonic Stem Cells Lacking Human Leukocyte Antigen Class I and II. *Stem Cell Reports* **14**, 648–662 (2020).

170. Creasey, A. A., Stacey, G., Bharti, K., Sato, Y. & Lubiniecki, A. A strategic road map to filing a Biologics License Application for a pluripotent stem cell derived therapeutic product. *Biologicals* **59**, 68–71 (2019).

171. Wright L. S., Phillips M. J., Pinilla I., Hei D., Gamm D. M. Induced pluripotent stem cells as custom therapeutics for retinal repair: Progress and rationale. *Exp Eye Res* **123**, 161–172 (2014).

172. Ovando-Roche, P. *et al.* Use of bioreactors for culturing human retinal organoids improves photoreceptor yields. *Stem Cell Res Ther* **9**, 156 (2018).

173. Xue, Y. *et al.* Retinal organoids on-a-chip: a micro-millifluidic bioreactor for long-term organoid maintenance. *Lab Chip* (2021) doi:10.1039/d1lc00011j.

174. Koso, H. *et al.* CD73, a novel cell surface antigen that characterizes retinal photoreceptor precursor cells. *Invest Ophthalmol Vis Sci* **50**, 5411–5418 (2009).

175. Stone, N. E. *et al.* Label-free microfluidic enrichment of photoreceptor cells. *Exp Eye Res* **199**, 108166 (2020).

176. Lakowski, J. *et al.* Isolation of Human Photoreceptor Precursors via a Cell Surface Marker Panel from Stem Cell-Derived Retinal Organoids and Fetal Retinae. *Stem Cells* **36**, 709–722 (2018).

177. Collin, J. *et al.* CRX Expression in Pluripotent Stem Cell-Derived Photoreceptors Marks a Transplantable Subpopulation of Early Cones. *Stem Cells* **37**, 609–622 (2019).

178. Ludwig, A. *et al.* Transplantation of human pluripotent stem cell-derived photoreceptors on a biocompatible scaffold in the S334ter rat. *Invest. Ophthalmol. Vis. Sci.* **60**, 2886–2886 (2019).

179. Lin, B. *et al.* Retina Organoid Transplants Develop Photoreceptors and Improve Visual Function in RCS Rats With RPE Dysfunction. *Invest. Ophthalmol. Vis. Sci.* **61**, 34–34 (2020).

180. Phillips, M. J. *et al.* Generation of a rod-specific NRL reporter line in human pluripotent stem cells. *Scientific Reports* **8**, 2370 (2018).

181. Kaewkhaw, R. *et al.* Treatment Paradigms for Retinal and Macular Diseases Using 3-D Retina Cultures Derived From Human Reporter Pluripotent Stem Cell Lines. *Invest Ophthalmol Vis Sci* **57**, ORSFl1–ORSFl11 (2016).

182. Kaewkhaw, R. *et al.* Transcriptome Dynamics of Developing Photoreceptors in Three-Dimensional Retina Cultures Recapitulates Temporal Sequence of Human Cone and Rod Differentiation Revealing Cell Surface Markers and Gene Networks. *Stem cells (Dayton, Ohio)* **33**, 3504–18 (2015).

183. Vergara, M. N. *et al.* Three-dimensional automated reporter quantification (3D-ARQ) technology enables quantitative screening in retinal organoids. *Development* **144**, 3698–3705 (2017).

184. McClements, M. E., Staurenghi, F., MacLaren, R. E. & Cehajic-Kapetanovic, J. Optogenetic Gene Therapy for the Degenerate Retina: Recent Advances. *Front Neurosci* **14**, (2020).

185. Singh, R. *et al.* Functional analysis of serially expanded human iPS cell-derived RPE cultures. *Invest. Ophthalmol. Vis. Sci.* **54**, 6767–6778 (2013).

186. Sinha, D. *et al.* Human iPSC Modeling Reveals Mutation-Specific Responses to Gene Therapy in a Genotypically Diverse Dominant Maculopathy. *Am. J. Hum. Genet.* **107**, 278–292 (2020).

187. Engle, S. J., Blaha, L. & Kleiman, R. J. Best Practices for Translational Disease Modeling Using Human iPSC-Derived Neurons. *Neuron* **100**, 783–797 (2018).

188. Garita-Hernandez, M. *et al.* Control of Microbial Opsin Expression in Stem Cell Derived Cones for Improved Outcomes in Cell Therapy. *Front Cell Neurosci* **15**, 648210 (2021).

189. Akiba, R. *et al.* Quantitative and Qualitative Evaluation of Photoreceptor Synapses in Developing, Degenerating and Regenerating Retinas. *Frontiers in cellular neuroscience* **13**, 16 (2019).

191. Worthington, K. S. *et al.* Two-photon polymerization for production of human iPSC-derived retinal cell grafts. *Acta Biomater* **55**, 385–395 (2017).

192. Jung, Y. H. *et al.* 3D Microstructured Scaffolds to Support Photoreceptor Polarization and Maturation. *Advanced materials (Deerfield Beach, Fla.)* **30**, e1803550 (2018).

193. Lee, I.-K. *et al.* Ultrathin micromolded 3D scaffolds for high-density photoreceptor layer reconstruction. *Science Advances* **7**, eabf0344 (2021).

194. Sharma, R. *et al.* Clinical-grade stem cell-derived retinal pigment epithelium patch rescues retinal degeneration in rodents and pigs. *Sci Transl Med* **11**, (2019).

195. Kashani, A. H. *et al.* Surgical Method for Implantation of a Biosynthetic Retinal Pigment Epithelium Monolayer for Geographic Atrophy: Experience from a Phase 1/2a Study. *Ophthalmol Retina* (2019) doi:10.1016/j.oret.2019.09.017.

196. Thompson, J. R. *et al.* Two-photon polymerized poly(caprolactone) retinal cell delivery scaffolds and their systemic and retinal biocompatibility. *Acta biomaterialia* (2019) doi:10.1016/j.actbio.2019.04.057.

197. Wendland, R. J. *et al.* The effect of retinal scaffold modulus on performance during surgical handling. *Exp Eye Res* **207**, 108566 (2021).

198. Singh, M. S. & MacLaren, R. E. Stem Cell Treatment for Age-Related Macular Degeneration: the Challenges. *Invest. Ophthalmol. Vis. Sci.* **59**, AMD78–AMD82 (2018).

199. Klassen, H. *et al.* Photoreceptor Differentiation following Transplantation of Allogeneic Retinal Progenitor Cells to the Dystrophic Rhodopsin Pro347Leu Transgenic Pig. *Stem Cells International* **2012**, e939801 (2012).

200. Zhao, X. & van Praag, H. Steps towards standardized quantification of adult neurogenesis. *Nature Communications* **11**, 4275 (2020).

201. Schmitz, C. & Hof, P. R. Design-based stereology in neuroscience. *Neuroscience* **130**, 813–831 (2005).

202. Schmitz, C. *et al.* Current automated 3D cell detection methods are not a suitable replacement for manual stereologic cell counting. *Front Neuroanat* **8**, (2014).

203. Zerti, D. *et al.* Transplanted pluripotent stem cell-derived photoreceptor precursors elicit conventional and unusual light responses in mice with advanced retinal degeneration. *Stem Cells* (2021) doi:10.1002/stem.3365.

204. Zhang, K. Y., Aguzzi, E. A. & Johnson, T. V. Retinal Ganglion Cell Transplantation: Approaches for Overcoming Challenges to Functional Integration. *Cells* **10**, 1426 (2021).

205. Zerti, D. *et al.* Transplanted pluripotent stem cell-derived photoreceptor precursors elicit conventional and unusual light responses in mice with advanced retinal degeneration. *Stem Cells* (2021) doi:10.1002/stem.3365.

206. Laver, C. R. J. & Matsubara, J. A. Structural divergence of essential triad ribbon synapse proteins among placental mammals – Implications for preclinical trials in photoreceptor transplantation therapy. *Experimental Eye Research* **159**, 156–167 (2017).

207. Pardue, M. T. *et al.* Neuroprotective Effect of Subretinal Implants in the RCS Rat. *Invest. Ophthalmol. Vis. Sci.* **46**, 674–682 (2005).

208. Bryda, E. C. & LaVail, M. M. Letter to the editor announcing the availability of RCS and transgenic rats with P23H and S334ter rhodopsin mutations with inherited retinal degenerations. *Exp. Eye Res.* **178**, 176 (2019).

209. Fujii, M., Sunagawa, G. A., Kondo, M., Takahashi, M. & Mandai, M. Evaluation of micro Electroretinograms Recorded with Multiple Electrode Array to Assess Focal Retinal Function. *Sci Rep* **6**, 30719 (2016).

210. Lyubarsky, A. & Bennett, J. Light Avoidance in Mice May Be not Related to Photoreceptor-Driven Input. *Invest. Ophthalmol. Vis. Sci.* **57**, 2768–2768 (2016).

211. Winkler, P. A., Occelli, L. M. & Petersen-Jones, S. M. Large Animal Models of Inherited Retinal Degenerations: A Review. *Cells* **9**, 882 (2020).

212. Lamb, T. D. Evolution of vertebrate retinal photoreception. *Philosophical Transactions of the Royal Society B: Biological Sciences* **364**, 2911–2924 (2009).

213. Zarbin, M. Cell-Based Therapy for Degenerative Retinal Disease. *Trends in Molecular Medicine* **22**, 115–134 (2016).

214. Zarbin, M. Cell-Based Therapy for Retinal Disease: The New Frontier. *Methods Mol. Biol.* **1834**, 367–381 (2019).

215. Wynne, N., Carroll, J. & Duncan, J. L. Promises and pitfalls of evaluating photoreceptor-based retinal disease with adaptive optics scanning light ophthalmoscopy (AOSLO). *Progress in Retinal and Eye Research* **83**, 100920 (2021).

216. McGregor, J. E., Williams, D. R. & Merigan, W. H. Functional Assessment of Vision Restoration. *Adv Exp Med Biol* **1185**, 145–149 (2019).

217. Thompson, D. A. *et al.* Advancing Clinical Trials for Inherited Retinal Diseases: Recommendations from the Second Monaciano Symposium. *Transl Vis Sci Technol* **9**, (2020).

218. Liu, Y. V. *et al.* Quantifiable In Vivo Imaging Biomarkers of Retinal Regeneration by Photoreceptor Cell Transplantation. *Trans. Vis. Sci. Tech.* **9**, 5–5 (2020).

219. Reh, T. A. Photoreceptor Transplantation in Late Stage Retinal Degeneration. *Invest. Ophthalmol. Vis. Sci.* **57**, ORSFg1-7 (2016).

220. Hippert, C. *et al.* RNAi-mediated suppression of vimentin or glial fibrillary acidic protein prevents the establishment of Müller glial cell hypertrophy in progressive retinal degeneration. *Glia* (2021) doi:10.1002/glia.24034.

221. Chan, K. *et al.* Vigabatrin-Induced Retinal Functional Alterations and Second-Order Neuron Plasticity in C57BL/6J Mice. *Invest Ophthalmol Vis Sci* **61**, 17 (2020).

222. Tsai, E. L. S. *et al.* Modeling of Photoreceptor Donor-Host Interaction Following Transplantation Reveals a Role for Crx, Müller Glia, and Rho/ROCK Signaling in Neurite Outgrowth. *STEM CELLS* **37**, 529–541 (2019).

223. Hoon, M., Okawa, H., Della Santina, L. & Wong, R. O. L. Functional architecture of the retina: development and disease. *Prog Retin Eye Res* **42**, 44–84 (2014).

224. Itoh, M. *et al.* Development of an immunodeficient pig model allowing long-term accommodation of artificial human vascular tubes. *Nature Communications* **10**, 2244 (2019).

225. Singh, R. K., Occelli, L. M., Binette, F., Petersen-Jones, S. M. & Nasonkin, I. O. Transplantation of Human Embryonic Stem Cell-Derived Retinal Tissue in the Subretinal Space of the Cat Eye. *Stem Cells and Development* **28**, 1151–1166 (2019).

226. Yamasaki, S. *et al.* Low Immunogenicity and Immunosuppressive Properties of Human ESC- and iPSC-Derived Retinas. *Stem Cell Reports* **16**, 851–867 (2021).

227. Saraf Steven S. *et al.* Bilateral Retinal Detachments After Intravitreal Injection of Adipose-Derived 'Stem Cells' in a Patient With Exudative Macular Degeneration. *Ophthalmic Surgery, Lasers and Imaging Retina* **48**, 772–775 (2017).

228. Leung Ella H., Flynn Harry W., Albini Thomas A., & Medina Carlos A. Retinal Detachment After Subretinal Stem Cell Transplantation. *Ophthalmic Surgery, Lasers and Imaging Retina* **47**, 600–601 (2016).

229. Kuriyan, A. E. *et al.* Vision Loss after Intravitreal Injection of Autologous "Stem Cells" for AMD. *http://dx.doi.org/10.1056/NEJMoa1609583* https://www.nejm.org/doi/10.1056/NEJMoa1609583 (2017) doi:10.1056/NEJMoa1609583.

230. Knoepfler, P. S. The Stem Cell Hard Sell: Report from a Clinic's Patient Recruitment Seminar. *STEM CELLS Translational Medicine* **6**, 14–16 (2017).

231. Cossu, G. *et al.* Lancet Commission: Stem cells and regenerative medicine. *The Lancet* **391**, 883–910 (2018).

232. Patient Resources. *A Closer Look at Stem Cells* https://www.closerlookatstemcells.org/patient-resources/.

233. Age-Related Macular Degeneration. *A Closer Look at Stem Cells* https://www.closerlookatstemcells.org/stem-cells-medicine/age-related-macular-degeneration/.

234. Zarbin M. What Constitutes Translational Research? Implications for the Scope of Translational Vision Science and Technology. *Transl Vis Sci Technol* **9**, 22 (2020).

235. Haeckel E. H. P. A. *Anthropogenie.* Germany: W. Engelmann (1877).

236. Boveri. Ueber die Befruchtung der Eier von Ascaris (1887).

237. Häcker V. Die Kerntheilungsvorgänge bei der Mesodermund Entodermbildung von Cyclops. *Archiv f mikrosk Anatomie* **39**, 556–581 (1892).

238. Thomas E. D., Lochte H. L., Lu W. C., Ferrebee J. W. Intravenous Infusion of Bone Marrow in Patients Receiving Radiation and Chemotherapy. *N Engl J Med* **257**, 491–496 (1957).

239. Till J. E., McCulloch E. A. A Direct Measurement of the Radiation Sensitivity of Normal Mouse Bone Marrow Cells. *Radiation Research* **14,** 213–222 (1961).

240. Gurdon J. B. The developmental capacity of nuclei taken from intestinal epithelium cells of feeding tadpoles. *J Embryol Exp Morphol* **10***,* 622–640 (1962).

241. Evans M. J., Kaufman M. H. Establishment in culture of pluripotential cells from mouse embryos. *Nature* **292**, 154–156 (1981).

242. Martin G. R. Isolation of a pluripotent cell line from early mouse embryos cultured in medium conditioned by teratocarcinoma stem cells. *Proc Natl Acad Sci USA* **78**, 7634–7638 (1981).

243. Thomson J. A., Kalishman J., Golos T. G., et al. Isolation of a primate embryonic stem cell line. *Proc Natl Acad Sci USA* **92**, 7844–7848 (1995).

244. Wilmut I., Schnieke A. E., McWhir J., Kind A. J., Campbell K. H. Viable offspring derived From fetal and adult mammalian cells. *Nature* **385**, 810–813 (1997).

245. Takahashi K., Yamanaka S. Induction of pluripotent stem cells from mouse embryonic and

adult fibroblast cultures by defined factors. *Cell* **126**, 663–676 (2006).

246. Kondo M., Sakai T., Komeima K., et al. Generation of a transgenic rabbit model of retinal degeneration. *Invest Ophthalmol Vis Sci* **50**, 1371–1377 (2009).

247. Wang Z., Feng C., Yang R., et al. Large-Area Photoreceptor Degeneration Model in Rabbits by Photocoagulation and Oxidative Stress in the Retina. *Frontiers in Neuroscience* **15***,* 640 (2021).

248. Waide EH, Dekkers JCM, Ross JW, et al... Not All SCID Pigs Are Created Equally: Two Independent Mutations in the Artemis Gene Cause SCID in Pigs. *J Immunol* **195**, 3171 3179 (2015).

249. Stanzel B, Ader M, Liu Z, et al... Surgical Approaches for Cell Therapeutics Delivery to the Retinal Pigment Epithelium and Retina. In: Bharti K, ed. Pluripotent Stem Cells in Eye Disease Therapy. *Advances in Experimental Medicine and Biology*, 141–170 *(*2019)

250. Carvalho, L. S., Pessoa, D. M. A., Mountford, J. K., Davies, W. I. L. & Hunt, D. M. The Genetic and Evolutionary Drives behind Primate Color Vision. *Front. Ecol. Evol.* **5**, (2017).

Chapter 3 -

Better together: aggregate-based photoreceptor delivery

Phillips M. J. †, Ludwig, A.L. †, Barney, P., Jager, L. D., Lee, C., Barlow, K., Min, J., Jain, S., Gamm, D.M.

†These authors contributed equally to this work.

Author contributions: M. J. P.: conceptualization, experimental design, methodology, project supervision, subretinal transplantation, data collection and formal analysis, writing and data curation (original draft). A. L. L.: data collection and formal analysis, statistical analysis, subretinal surgical assistance, writing and data curation (original draft, review & editing). P. B., J. M.: data collection, subretinal surgical assistance. L. D. J.: data collection, project administration. C. L.: conceptualization, methodology, subretinal transplantation. K. B., S. J.: data collection and validation. D. M. G.: conceptualization, funding acquisition, methodology, project administration, project supervision, writing and data curation.

Introduction

Photoreceptor (PR) dysfunction and subsequent cell death are an inevitable outcome in blinding inherited diseases of the outer retina like Retinitis Pigmentosa (RP). Several therapeutic strategies—including retinal prosthetics, optogenetics, gene therapy, and cell replacement—are currently being studied alone or in combination[9–11] to restore vision in outer retinal disease. While all of these therapies have shown promise, cell replacement therapy is the only strategy which directly replenishes native cells lost to disease[12,13]. Human pluripotent stem cell (hPSC) technology[2,3,14] and subsequent protocols to develop individual retinal cell types[15,16], including PRs, have made the seemingly impossible task of *bona fide* PR replacement a reality.

One of the biggest breakthroughs toward PR replacement has been the production of organized retinal tissues from hPSCs, now most commonly known as retinal organoids[17,18] (ROs). ROs undergo distinct stages of differentiation that correspond to well-defined epochs of human retinal development[19–24]. Over time, neural retinal progenitor cells (RPCs) within ROs differentiate into all major cell types of the retina and can self-assemble to form distinct layers reminiscent of the retina in vivo[20,21,25]. Beyond the earliest stage of development (stage 1, occurring at ~30 days of differentiation [D30]) the predominant cell type within ROs is the photoreceptor, with both rods and cones differentiating and residing along the outer rim of the organoid. The development and maturation of PRs within ROs has been well characterized; it is now well-established that hPSC-PRs can polarize and produce inner and outer segments[20,26–28], express opsins[20,29], form axon terminals with synaptic protein and ultrastructure[20,26,27,30–35], and generate characteristic electrophysiological signatures and responses to light[21,23,31,33,36–38].

There are several approaches for delivering cells—either RPCs or, preferably, committed photoreceptor precursors (PRP)[12,13]—to the subretinal space (SRS) for PR replacement. Historic approaches include a bolus of fully dissociated cells[9,36,39], pre-seeded hydrogels[40–43] or scaffolds[44–47], cellular aggregates[48,49], and tissue sheets[50–54]. For hPSC-derived retinal cell

delivery, dissociated cells[9,36,39,55,56], scaffolds[45,57], and organoid sheets[51–54] are the most commonly used strategies, with benefits and drawbacks to each approach. Dissociated cell injections are the easiest and most straightforward method; however, disruption of cell-cell contacts negatively impacts cell survival[58], and survival rates of dissociated cell transplants are often low (<2%)[55]. Singularized cell injections also have an inherent propensity for reflux into the vitreous cavity, which can lead to post-surgical complications like epiretinal membrane formation and retinal detachment[13,59,60]. Delivery of cells on scaffolds can reduce reflux[61], although the seeding process also requires dissociating PRP from their native laminar structure and is more complex to produce. Retinal organoid transplantation—either as cellular aggregates or sheets—can theoretically provide a relatively simple approach for limiting reflux and improving cell survival.

To this end, several studies have recently investigated delivery of organoid sheets in rodent and non-human primate models[51–54]. These studies highlight the benefits of this approach, including excellent donor cell retention in the subretinal space[12,13], and pronounced long-term PR survival (months to years after transplantation)[52]. However, retinal sheet transplantation requires time-consuming mechanical dissection and custom instrumentation for subretinal delivery[51]. Furthermore, retinal sheet transplants often result in disorganized, rosetted grafts rather than properly laminated architecture. While dissociated cell and retinal sheet transplants have both been associated with mild increases in light-evoked responses[9,39,52,55], few studies to date have directly compared survival and differentiation of donor cells between delivery approaches. Moreover, since vision “rescue” is known to occur in the absence of substantial anatomic integration[12,13,62] and is virtually indistinguishable from neuroprotection of host cells[52] or aberrant firing of remaining neurons in the degenerating retinal environment[63], it is difficult to directly attribute these responses to donor cells.

The discovery of biomaterial transfer, whereby fluorescent proteins are transferred between donor and host PRs, has recently led the field to revisit definitions of anatomic and

functional integration of donor cells. Several recent studies have unequivocally demonstrated hPSC-PRP survival and anatomic integration after dissociated cell or retinal sheet delivery[9,36,52,53] while controlling for material transfer, but evidence to date is largely qualitative in nature and does not directly compare delivery approaches. Necessary differences in surgical procedure have the potential to confound such examinations, as retinal sheet transplantation requires different tools and more invasive surgeries than dissociated cell injections. Cellular aggregates—partially dissociated retinal organoids—offer many of the benefits to retinal sheet transplants and can be delivered via simple subretinal injection, but to date have not been extensively studied for hPSC-PRP delivery[64].

Comprehensive assessment of anatomic integration is a necessary first step toward directly linking PR replacement and vision restoration, but to date the evidence in this area is limited. In the present report, we expand upon previous studies by directly comparing hPSC-PRP survival in dissociated and aggregate organoid transplants—both delivered via simple subretinal injections—to examine the utility of clustered cell delivery. We extensively characterize hPSC-PRP survival, differentiation, and anatomic integration in hPSC-PRP aggregate transplants over time. Given the dynamic nature of RO development (i.e., a variety of cell types are born and differentiate over time), we also determine the proportion of specified PRs present at multiple timepoints following transplantation and assess maturation of PRP into rod and cone PRs. We explore the potential for rescue of reflexive and electrophysiologic functional recovery following hPSC-PRP aggregate transplantation, demonstrating that hPSC-PRP aggregate transplants are safe, but do not result in substantial functional improvement. Finally, we discuss factors potentially contributing to a lack of functional recovery in the present report, outlining strategies to enhance engraftment in future preclinical studies.

Materials and Methods

Retinal differentiation of WA09-CRX$^{+/tdTomato}$ hPSCs

Previously described retinal differentiation protocols[18,23,38] were optimized for bulk production of stage 2 ROs (D70 of differentiation) from WA09-CRX$^{+/tdTomato}$ hESCs[23] for transplantation. Briefly, pluripotent colonies were lifted to form embryoid bodies (EBs) and directed toward a neuroretinal cell fate to generate ROs. Phase-bright, laminar ROs were mechanically isolated at approximately d20 of differentiation and maintained at 37°C, 5% CO_2 in poly-2-hydroxyethyl methacrylate (polyHEMA)-treated flasks with twice weekly media changes. PRP genesis, evident by expression of the fluorescent tdTomato reporter[23], was monitored with epifluorescence microscopy.

Animals

The retinal degenerative SD-Foxn1 Tg(S334ter)3LavRrrc rat line[65] (Foxn1-S334ter-3) was obtained from the Rat Resource and Research Center (Columbia, MO, USA). This line is a cross between the athymic nude NIH-Foxn1^{rnu} rat (preventing T-cell-mediated xenograft rejection) and the S334ter line 3 transgenic rhodopsin mutant rat (a model of severe RP). Foxn1-S334ter-3 rats undergo rapid and near-complete loss of rods by P30, with subsequent cone dysfunction and cell death[65–67]. Rat housing followed a standard 12:12 hour light/dark cycle, with ad libitum access to water and food. Breeding schema, genotyping protocols, and husbandry of nude rats were as previously described by Seiler *et al.,* 2014[65]. All rats were transplanted between 1 and 4 months of age, when all but a single discontinuous layer of host cone PRs have fully degenerated[66]. Animal procedures were pre-approved by the University of Wisconsin-Madison Institutional Animal Care and Use Committee and were conducted in accordance with the Association for Research in Vision and Ophthalmology Statement for the Use of Animals in Ophthalmic and Vision Research, the National Institutes of Health (NIH) Guide for the Care and Use of Laboratory Animals, and the laws and regulations of the United States Department of Agriculture.

RO dissociation for transplantation

Stage 2 (D79-127) CRX$^{+/tdTomato}$ ROs were dissociated to single cells with papain (Worthington Biochemical). Following enzymatic deactivation with ovomucoid, cells were passed through a 40 µm filter and resuspended in sterile Hanks' Balanced Salt Solution (HBSS) without calcium and magnesium at a concentration of 100,000 cells/µL. Cell viability of 90-99% was routinely obtained following papain dissociation. Cell suspension was maintained on ice until transplantation.

Subretinal dissociated cell transplantation

Rats were anesthetized via intraperitoneal injection of ketamine (80 mg/kg) and xylazine (10 mg/kg). Eyes were dilated with tropicamide (1%) and phenylephrine (2.5%) ophthalmic solution; tetracaine hydrochloride (0.5%) drops were applied for topical anesthesia. Eyes were proptosed and an entry tunnel was made ~1mm distal to the limbus with a 30 gauge (30G) needle. Gonivisc (HUB Pharmaceuticals) and a coverslip were placed on the cornea to facilitate visualization of the microsyringe needle in the vitreous chamber throughout the procedure. A 33G needle and Hamilton microsyringe were used to deliver 3 µL total volume containing approximately 300,000 dissociated cells to the SRS. Post-surgery, rats were subcutaneously injected with a non-steroidal anti-inflammatory (NSAID; carprofen, 5mg/kg) and intramuscularly with the reversal agent yohimbine (1.5mg/kg) or atipamazole (1mg/kg). Triple antibiotic ointment was applied to the eye, and rats were recovered from anesthesia on a warm water circulating blanket. Full details for animal transplantation experiments are summarized in **Table S1**.

Preparation of cellular aggregates

Stage 2 (D70) CRX$^{+/tdTomato}$ ROs were counted, washed in HBSS, and resuspended in sterile 1X HBSS without calcium and magnesium (Thermo Fisher). To allow passage through a 29 gauge (29G) microneedle, ROs were gently triturated five times with a P20 micropipette to break up ROs into aggregates. Aggregates in suspension contained approximately 150,000 cells per 5 µL dose (146,000 ± 3,000 cells/dose, or 29,000 ± 600 cells/µL; n = 3 replicates) and had excellent viability

(99-100%). 5-16% of all cells were CRX$^{+/tdTomato}$-positive near this stage of development, as assessed via Countess automated fluorescence quantification (Thermo Fisher Scientific), consistent with the onset of PR genesis[20]. Aggregates were maintained on ice in HBSS until transplantation.

Subretinal aggregate transplantation

Rats were anesthetized and prepared for surgery as for dissociated cell injections with slight modifications. A 26G needle was used for initial entry to the SRS; a 29G needle and Hamilton microsyringe were used to deliver 5 µL total volume of aggregates in suspension with approximately 150,000 cells. A lower cell concentration (~30,000 cells/µL) was initially selected to test aggregate delivery under stringent conditions, with the potential to scale dosing up to the cell concentration of dissociated cell injections (100,000 cells/µL) if necessary.

Optokinetic threshold testing (OKT)

The virtual Optomotry system (Cerebral Mechanics, Inc.) was used to assess the visual acuity threshold (i.e., the maximum spatial frequency of high-contrast grating capable of eliciting an optokinetic tracking response) in awake and freely moving rats as described in previous studies[68,69]. Briefly, sine wave gratings at 100% contrast were randomly displayed at varying spatial frequencies and drifted in the clockwise or counterclockwise direction; rats capable of seeing this stimulus will involuntarily make a tracking head movement in the direction of the stimulus known as the optomotor response (OMR) and scored in a stepwise manner for tracking behavior to determine the spatial frequency threshold. Optokinetic tracking responses were scored in real-time by a lab member masked to treatment condition. Rats were assessed at baseline, 1 month, and 3 months following subretinal transplantation of CRX$^{+/tdTomato}$-PRP aggregates.

Full-field electroretinography (ERG)

At 6 months post-transplant, rats were dark adapted overnight and prepared for electroretinography under dim red light (>650 nm). Dark-adapted rats were anesthetized with ketamine (80 mg/kg) and xylazine (10 mg/kg) and eyes were dilated with tropicamide (1%) and phenylephrine (2.5%) ophthalmic solution. ERG was performed with the HMsERG system (Ocuscience) according to methods previously described by Thomas *et al.*[70] Briefly, silver thread electrodes were placed on the cornea with 2.5% methylcellulose gel (Akorn) and held in place with a 4-mm contact lens. Reference and ground needle electrodes were placed subcutaneously. Scotopic responses were tested with flash intensities ranging from 1 to 25,000 millicandela (mcd). Photopic responses were tested following a 10-minute light adaptation period with flash intensities ranging from 10-25,000 mcd.

Histology and immunofluorescence

Animals were humanely euthanized at 2 weeks, 1 month, 3 months, or 6 months post-transplant for histology. Transplanted rat eyes and free floating ROs were processed for immunofluorescence (IF) staining as previously described[20,23,56]. Rat eyes were labeled for orientation, enucleated, and fixed in 4% paraformaldehyde (PFA) for one hour. A small amount (≤0.1 mL) of PFA was injected into the vitreous chamber to augment retinal fixation. Following fixation and a round of washes in 1X PBS, the cornea, lens, and iris were removed from the posterior eyecup for cryosectioning. ROs were fixed for 30 minutes. Both ROs and rat eyes were cryoprotected overnight in PBS + 30% sucrose. Posterior eyecups were cryosectioned at 25 µm and OVs were cryo-sectioned at 15-20 µm. ROs and rat eyes were immunostained as previously described[20,56]. In brief, tissues were incubated at in blocking solution (10% NDS, 5% BSA, 1% fish gelatin, and 0.5% Triton-X in PBS) for one hour at room temperature, overnight in primaries (summarized in **Table S2**; primaries diluted in blocker) at 4°C, and 30 minutes in corresponding secondary antibodies (Millipore) with 3-4 rounds of 1X PBS washes between each step. Slides

were mounted in Prolong Gold with 4',6-Diamidino-2-Phenylindole, Dihydrochloride (DAPI) (Invitrogen) and imaged on a confocal microscope (Nikon A1R).

High content image analysis

Single optical plane images were captured with a confocal microscope (Nikon A1R) for quantification. Images for each marker were taken at the same magnification, gain, and laser power across samples for consistency. The thickest area of the transplant was captured at 10X magnification for each section imaged. For each sample, 3 different sections spaced 200-500 µm apart for each marker of interest were imaged to sample the entire length of the subretinal graft. Unprocessed images were segmented and counted with Columbus high content image analysis software (Perkin Elmer). Cells positive for each marker were defined by scatter plot gating of fluorescence intensity, and identical parameters for positive cell identification were used across samples for consistency in donor cell quantification.

Statistics

Cell counts were analyzed and graphed with GraphPad Prism version 9.1.2. (GraphPad Software). Due to small sample sizes (<50), the Shapiro-Wilk test was used to test for normality. An F-test was applied to compare variance between pairwise comparisons. A standard unpaired t-test was applied for pairwise comparisons when variances were equal. Welch's correction was applied for pairwise comparisons when variances were unequal. Brown-Forsythe and Bartlett's tests were applied to assess homogeneity of variance for multiple comparisons. For normally distributed data with unequal variance, an ordinary one-way analysis of variance (ANOVA) with Tukey's multiple comparisons test was applied. For non-normally distributed data, the Kruskal-Wallis analysis of variance by rank test was applied with Dunn's post-hoc analysis for multiple comparisons. Multiple comparisons for OKT analysis were performed using a mixed-effects model with Šídák's multiple comparisons test. Results were considered significant at a p value < 0.05.

Descriptive measurements for which means were not directly compared to another group in statistical analyses (cell dose, viability, aggregate diameter, etc.) are reported as the mean ± standard error of the mean (SEM). For cell engraftment and maturation counts, the precision of the mean was considered highly valuable to comparing means between or among groups. Averages for these measurements are thus reported with an upper and lower 95% confidence interval (CI) to demonstrate how precisely data defined the mean (presented in the text as the mean, CI [lower limit, upper limit]). Error bars in all graphs depict upper and lower limits of the 95% CI; bar graphs are overlaid with scatter plots of each value to convey the degree of variation among measurements.

Results

Generation and transplantation of hPSC-RO-derived PRP as dissociated cells

Validated protocols for retinal differentiation[18,23,38] were used to generate hPSC-ROs, which are readily distinguishable from non-retinal tissues in the earliest stage of differentiation by the presence of characteristic phase-bright lamination (**Fig. 1A**). In this phase of development, organoids contain many RPCs with few if any committed PRP[20,71]. For efficient tracking of PRP genesis and maturation, we used a recently characterized Cone Rod Homeobox (CRX) human embryonic stem cell (hESC) reporter line (WA09-CRX$^{+/tdTomato}$) which expresses tdTomato throughout the cytoplasm from specification through all stages of PR development[23,56,71,72]. Stage 2 organoids (D70-D130) were used for all transplants, as they have been previously shown to be a plentiful source of transplantable donor cells[56] and are predominantly comprised of the preferred donor cell stage for PR replacement (up to 60-80% CRX$^{+/tdTomato}$ PRP)[23,72]. By stage 2, CRX$^{+/tdTomato}$ expression was evident throughout organoids (**Fig. 1B-D**), confirming and coinciding with the period of peak PRP genesis in ROs[20].

We first transplanted PRP in single cell suspension, as several studies have recently described anatomic integration and modest recovery of light sensitivity following delivery of

dissociated hPSC-PRP[9,39,55]. Stage 2 WA09-CRX$^{+/tdTomato}$ retinal organoids were dissociated to single cells with papain to generate a PRP-rich suspension (historically, 40-80% CRX$^{+/tdTomato}$-positive[23,72]). Approximately 300,000 dissociated cells were delivered into the SRS of both eyes of twelve retinal degenerative Foxn1-S334ter-3 rats in 3 µL total volume (100,000 cells/µL). Animals were humanely euthanized at two weeks post-transplant and eyes were cryosectioned for immunolabeling to screen for donor cell survival and anatomic integration.

Survival of hPSC-RO-derived PRP dissociated cell transplants

Among rats transplanted with dissociated cell suspension, the cell recovery rate (i.e., the proportion of eyes in which donor cells were successfully located on histology post-transplant) in dissociated PRP delivery was 8.7% (2 of 23 eyes). Consistent with previous studies using dissociated cells[9,39,55] the number of engrafted CRX$^{+/tdTomato}$-positive donor cells was relatively low (**Fig. 1E**). Between the two animals with CRX$^{+/tdTomato}$-positive donor cells, just 5 cryosections with sparse, disorganized CRX$^{+/tdTomato}$-positive donor cells were identified. Despite low rates of engraftment, we did not observe evidence of material transfer between human hPSC-PRP and remaining donor cells—all detected CRX$^{+/tdTomato}$-positive donor cells also co-labeled with human nuclear antigen (HNA) (**Fig. 1F, S1**). An average of approximately 25 CRX$^{+/tdTomato}$-positive cells (24.6 ± 8.4, n = 5 cryosections from two separate eyes) were detected per section in dissociated cell transplants. In the eye with the greatest number of engrafted cells (**Fig. S1**), the total number of HNA-positive cells detected was 148 (0.05% of the starting dose). 68% of HNA+ cells were also CRX$^{+/tdTomato}$-positive, demonstrating a high proportion of PRP in the donor cell population even in the face of poor survival. Cell reflux was apparent in one of two eyes, with a clump of HNA-positive CRX$^{+/tdTomato}$-PRP present in the vitreous chamber (**Fig. S1**).

hPSC-PRP aggregate transplantation improves cell survival relative to dissociated cells

To determine whether delivery as cellular aggregates could enhance survival and engraftment of donor hPSC-PRP, we transplanted WA09-CRX$^{+/tdTomato}$ aggregates from stage 2 (D70) retinal organoids into both eyes of three Foxn1-S334ter-3 rats. Cells were prepared for transplantation by resuspending ROs in HBSS without calcium and magnesium, gently triturating the suspension to partially dissociate ROs into cellular aggregates (**Fig. 2A-2B**). Aggregates varied in size but were approximately 17 µm in diameter (16.8 ± 7.4 µm, *n* = 60 total aggregates from 3 independent preparations)—small enough to easily pass through a 29G microneedle (internal diameter = 184 µm)—and had excellent viability (>99%). Cell aggregate suspension contained approximately 150,000 viable cells per 5 µL dose (146,000 ± 3,000 cells/dose, or 29,000 ± 600 cells/µL; *n* = 3 replicates from two differentiations), which was delivered to the SRS using the same approach as for dissociated cell transplants. At two weeks post-transplant animals were humanely euthanized and eyes were screened for the presence of donor cells (**Fig. 2C**).

The cell recovery rate improved with aggregate delivery—donor cells were found in all eyes (*n* = 5) transplanted with hPSC-PRP aggregates. At two weeks post-transplant, we observed survival of transplanted CRX$^{+/tdTomato}$-PRP within the SRS of Foxn1-S334ter-3 rats relative to dissociated cell transplants (**Fig. 2D, 2E**). Engrafted CRX$^{+/tdTomato}$-positive donor cells were quantified in three aggregate-transplanted eyes (one from each animal) to directly compare donor cell engraftment between dissociated cell and aggregate-based delivery. As in dissociated transplants, all CRX$^{+/tdTomato}$-positive cells were labeled with HNA. HNA+ cells were predominantly CRX$^{+/tdTomato}$-positive (47-60%), comparable to the proportion of CRX$^{+/tdTomato}$ PRP found within stage 2 organoids[23,72] and that observed in dissociated CRX$^{+/tdTomato}$-PRP transplants. Anatomic engraftment was significantly greater ($p = 0.0215$, unpaired t-test with Welch's correction) in aggregate-transplanted eyes relative to dissociated cell transplants (**Fig. 2F**). We observed an 8-fold increase in the average number of CRX$^{+/tdTomato}$-positive cells per section in aggregate transplants (mean = 207 CRX$^{+/tdTomato}$-positive cells/section, 95% CI: [61, 354]), demonstrating

substantial improvement in donor cell engraftment compared to dissociated cell transplants (mean = 25 $CRX^{+/tdTomato}$-positive cells/section, 95% CI: [1, 48]). As in dissociated transplants, all $CRX^{+/tdTomato}$-positive cells were labeled with HNA (**Fig. 2G**). The diameter of host nuclei was also significantly smaller ($p < 0.0001$, unpaired t-test, $n = 18$ nuclei for donor and host) than that of HNA+ donor cells detected, providing further evidence of that the $CRX^{+/tdTomato}$-PRP detected were of donor cell origin.

Interactions between donor and host cells were examined via immunolabeling (**Fig 3**). Bipolar cell (BPC) marker PKCα revealed extension of neurites from host second-order neurons toward engrafted $CRX^{+/tdTomato}$ PRP (**Fig. 3A, 3B**), with close apposition between host BPCs and donor PRP. Punctate expression of presynaptic protein Vesicular glutamate transporter 1 (VGLUT1) was also observed in $CRX^{+/tdTomato}$-PRP adjacent to host second-order neurons (**Fig. 3C**). These results show striking improvement in hPSC-PRP engraftment following aggregate transplantation, with early evidence of anatomic integration and putative donor-host interactions.

Functional assessment, long-term survival, and maturation of hPSC-PRP aggregate grafts

Finally, we sought to determine functional effects and long-term maturation of hPSC-PRP aggregate grafts. Seventeen additional Foxn1-S334ter-3 rats were transplanted with $CRX^{+/tdTomato}$-PRP aggregates for scheduled tissue collection at 1, 3 or 6 months post-transplant (n = 5-6 per timepoint). Rats received a single monocular subretinal injection of 150,000 cells as aggregates in 5 µl total volume; untreated fellow eyes served as a control for functional testing. Animals in all three groups were assessed for optokinetic tracking (OKT) at 1 and 3 months post-transplant; animals in the 6 month post-transplant collection group were also tested with full field electroretinography (ERG) prior to scheduled tissue collection (**Fig 4A**). No significant differences in spatial frequency visual acuity were observed across at any timepoint, suggesting that hPSC-PRP aggregates were well-tolerated but did not generate meaningful improvements in retinal

degenerative rats relative to untreated control eyes (**Fig 4B**) (not significant [n.s.], adjusted p values at baseline, 1 month, and 3 months = 0.7674, 0.9646, 0.5928; *n* = 16 eyes per condition at baseline and 1 month; *n* = 9 eyes per condition at 3 months; mixed-effects analysis with Šídák's multiple comparisons test). Consistent with several recent reports[53,73,74], full field ERG responses were not detected under scotopic or photopic conditions in treated or control eyes (*n* = 5 animals).

On immunohistochemical analysis, a thick layer of $CRX^{+/tdTomato}$-PRP was evident at 1, 3, and 6 months post-transplant (**Fig. 4C-4E**). Rosetted structures similar to those occurring in retinal sheet transplantation were often observed at later time points (**Fig. S2 and S3**), particularly in the 6 month post-transplant group (**Fig 4E, S3**). Photoreceptor and proliferation-specific markers were quantified across all three timepoints with high content image analysis to assess maturation of $CRX^{+/tdTomato}$-PRP aggregate grafts (**Fig. 4, S2, S3**). As in previous transplants, $CRX^{+/tdTomato}$-PRP co-labeled with HNA and were thus not a result of material transfer (**Fig 4F**). $CRX^{+/tdTomato}$-PRP predominated among HNA+ cells at 1 month (62.9% of HNA+ cells, 95% CI: 59.6, 66.2), and the proportion of $CRX^{+/tdTomato}$-PRP remained stable at all timepoints examined (n.s. between groups, adjusted p values >0.5, ordinary one-way ANOVA with Tukey's multiple comparisons test, *n* = 3 sections/eye and *n* = 4 eyes/timepoint) (**Fig. 4G**). Cell proliferation (quantified with Ki-67) was relatively high at 1 month post-transplant (48.6% of HNA+ cells, 95% CI: 44.6, 52.6) (**Fig. 4H**), but decreased over time (**Fig. S2A**). The mean proportion of Ki-67 positive cells—most likely representing RPCs at this stage[20]—was significantly lower by 3 months post-transplant, and Ki-67-positive cells were virtually absent by 6 months ($p < 0.0021$ at 1 vs. 3 months, $p < 0.0001$ at 1 vs. 6 months; Kruskal-Wallis test with Dunn's post-hoc analysis; *n* = 3 sections/eye, *n* = 4 eyes/timepoint) (**Fig 4I**).

Immunolabeling of $CRX^{+/tdTomato}$-PRP aggregate to assess maturation and anatomic integration are shown in **Fig. 5**. At 6 months post-transplant, photoreceptor precursors in close proximity to the host INL expressed ribbon synapse protein CtBP2 (**Fig. 5A**). At all points

examined, approximately two-thirds of CRX$^{+/tdTomato}$-PRP aggregates were neural retina leucine zipper (NRL)-positive rods (**Fig. S2B, S2C, S3**) (67.8% of CRX$^{+/tdTomato}$-positive cells at 1 month, 95% CI: 58.4, 77.3; n. s. between timepoints, ordinary one-way ANOVA with Tukey's post-hoc). Over time, the percentage of rhodopsin-expressing NRL-positive rods increased significantly (**Fig. 5C**) ($p < 0.0001$ for all comparisons, one-way ANOVA with Tukey's multiple comparisons). Cones were also present and matured over time to express M/L opsin, forming putative outer segments by 6 months post-transplant (**Fig. 5D-5E**). Cone maturation peaked near three months post-transplant (21.0% of all CRX$^{+/tdTomato}$-positive cells, 95% CI: 14.5, 27.3), with a significant increase in M/L opsin expression between 1 and 3 months ($p <0.0001$, Kruskal-Wallis test with Dunn's multiple comparisons) and stable levels thereafter.

Discussion

In the present report, we demonstrate improved survival and maturation of PRs following delivery of CRX$^{+/tdTomato}$-PRP as cellular aggregates. Prior to this study, direct comparison of PRP survival and/or engraftment between methods had not been investigated. Moreover, assessment of donor cell maturation has historically been qualitative in nature and does not typically include investigation of off-target populations such as proliferative RPCs. Aggregate-based delivery resulted in an 8-fold increase in the number of detected CRX$^{+/tdTomato}$-PRP relative to dissociated cell injections, with long-term survival, maturation, and anatomic integration in the degenerative retinal environment and no evidence of untoward effects on remaining vision.

Evidence for anatomic integration of hPSC-PRP aggregates

While GFP material transfer has led to re-interpretation of previous PR replacement studies, many of these were allografts into mouse retinas with an abundance of remaining, structurally sound host PRs[56]. However, no study to date has demonstrated this phenomenon in xenografts delivered into animal models with complete or near-complete loss of host photoreceptors. Results

presented in this manuscript and many other recent studies[1-3,30,45-48 58] argue against the likelihood of material transfer in the severely degenerative rodent retina following xenotransplantation of hPSC-PRP as dissociated cells, sheets, and now aggregates. First, human nuclear specific staining is possible with xenografts, enabling clear delineation of donor and host cells. Consistent with prior reports[1,30], we observed significant differences ($p<0.0001$, unpaired t-test) in the diameter of donor and host nuclei, providing further evidence that detected $CRX^{+/tdTomato}$-PRP were of human origin. Studies describing material transfer from donor mouse PRs to host PRs did not find evidence of nuclear transfer; it is thus unlikely that HNA-positive nuclei were transferred to host cells in this study. Second, PRs were nearly absent in this model at all time-points examined, and to date, material transfer has only been demonstrated in mouse models with PRs present at the time of analysis[56]. Third, in previous studies later shown to likely be the result of material transfer, transplanted GFP+ PRs demonstrated pristine morphology, including a polarized axon terminal, appropriately positioned cell body, and inner/outer segments that were indistinguishable in morphology from host PRs. In this study, while we show the maturation of hPSC-derived rods and cones in *vivo*, including examples of polarized synaptic protein and outer segment formation, such structures were not fully organized and did not morphologically resemble rat PRs. Finally, evidence of anatomic integration was present in the earliest and latest timepoints examined—expression of synaptic protein VGLUT1 and ribbon synapse marker CtBP2 was observed in INL-adjacent PRP at 2 weeks and 6 months post-transplant, respectively.

Maturation of hPSC-PRP aggregates

$CRX^{+/tdTomato}$-PRP aggregates survived long-term in the SRS, and detection of donor cells was consistent with anatomic engraftment rather than material transfer. Proliferation within grafts decreased markedly over time, with few if any proliferating cells remaining by 6 months post-transplant. No significant differences in the percentages of $CRX^{+/tdTomato}$-positive cells out of the total population of HNA+ cells were noted over time. The large percentage of NRL+ rods found at

1 month did not significantly change with time, and although no NRL+ rods co-expressed rhodopsin at 1 month, a significant increase was noted over time. Stable populations of maturing rod and cone CRX$^{+/tdTomato}$-positive PRs with opsin expression were present within the SRS at the latest timepoint studied (6 months post-transplant), and polarized expression of ML opsin was observed in putative outer segments.

Safety and functional assessment of hPSC-PRP transplantation

CRX$^{+/tdTomato}$-PRP aggregates were well-tolerated in the SRS of nude retinal degenerative Foxn1-S334ter-3 rats, with no untoward effects on vision or teratoma formation noted. However, we did not observe any improvements in visual acuity (assessed via OKT) or electroretinographic function. There are several possible explanations for this observation, although it is again important to note that PRP delivery did not reduce the remaining cone-driven OKT responses in transplanted rats, indicating that this approach is relatively safe for visual outcomes even when some degree of function remains. While we observed a degree of synaptic protein expression at various points post-transplant, it is likely that these synapses are insufficient in number for generating a full-field ERG response or meaningful improvement in OKT. Previous studies have suggested that up to 150,000 functional PRs are required to elicit PR-driven responses with full-field ERG[59], and the number of engrafted cells in all animals in the present study was likely far below this threshold. While no such threshold has been reported for an OKT response, this test may have been insufficiently sensitive to detect relatively small changes to visual function. We often observed rosetted morphologies at later timepoints, and while no study to date has directly shown that such PRs are non-functional in the host retina, the likelihood of such cells forming functional synaptic connections with host neurons seems extremely low[57]. Finally, recent computational modeling suggests that the likelihood of functional synaptogenesis between human PRP and donor inner retinal neurons is low due to evolutionary divergence in the synaptic proteins involved in these connections.

Conclusions

In summary, we report substantial improvement in PRP survival following clustered delivery of $CRX^{+/tdTomato}$-PRP as cellular aggregates. PRP matured over time to express presynaptic proteins and opsins, and anatomic evidence of host connectivity was apparent as early as two weeks post-transplant. However, despite marked improvement in cell survival, we did not observe rescue of visual function, opening the door to several additional lines of research. The propensity of hPSC-PRs to form rosettes *in vivo* may be overcome in future studies by testing the transplantation of enriched PRP or more mature donor cells, as rosettes seem to develop over time with immature PR transplants. The development of scaffolds that support clustered delivery of hPSC-PRP may provide a means of retaining the benefits of aggregate delivery while addressing remaining issues of graft disorganization and variable graft size noted in the present study. Finally, despite evidence of synaptic protein expression in hPSC-PRP replacement, it remains unclear whether these represent *bona fide* synapses. Further investigation of the hPSC-PRP synapse is warranted to address ongoing questions of functionality in PR replacement.

Figures

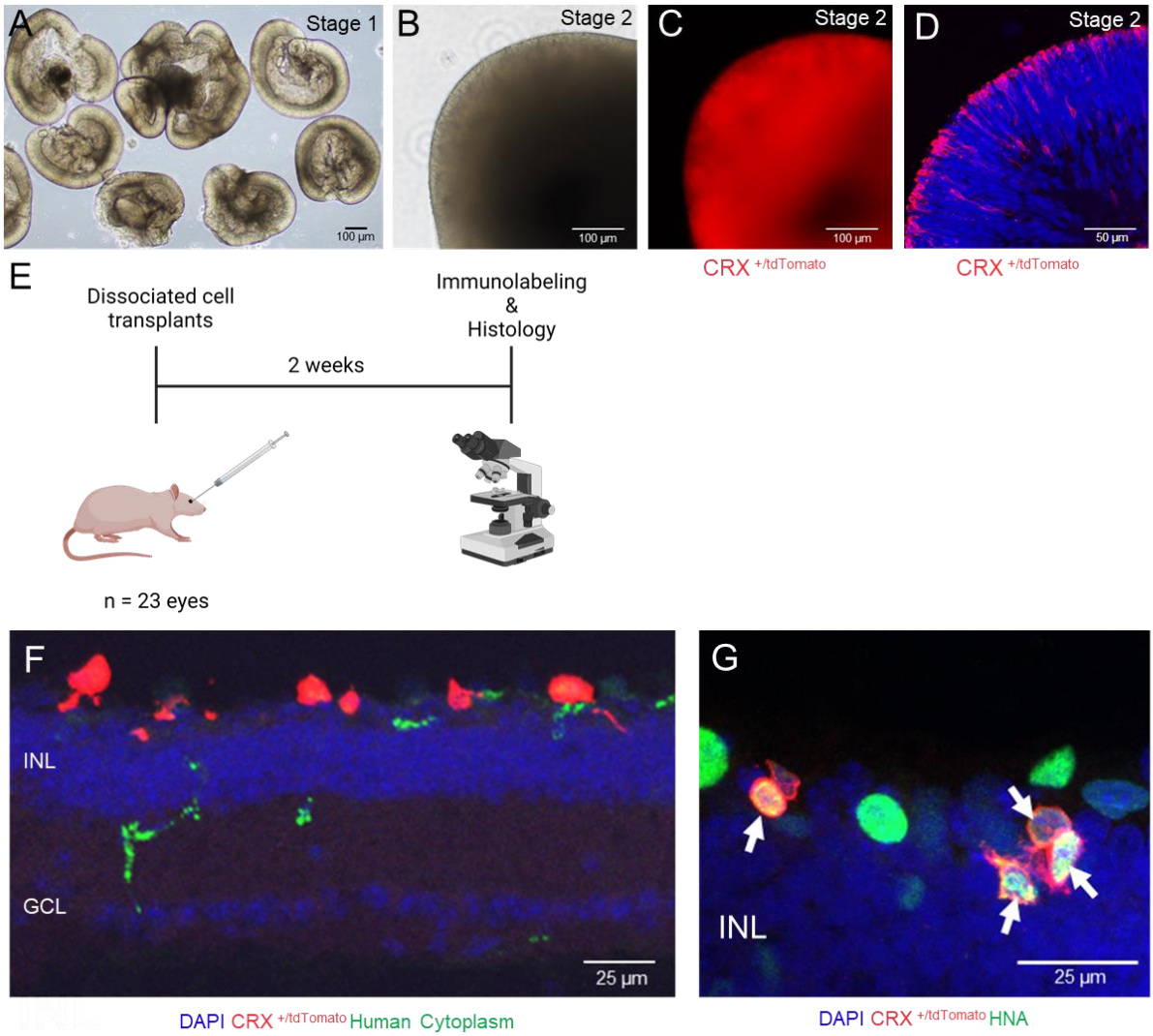

Fig. 1. Generation and transplantation of dissociated CRX$^{+/tdTomato}$-PRP in retinal degenerative Foxn1-S334ter-3 rats. (**A**) WA09-CRX$^{+/tdTomato}$ hPSCs were differentiated to produce ROs, which were isolated at stage 1 (D30) with characteristic phase-bright lamination. (**B, C**) PRP genesis and maturation occurs in stage 2 (D120) organoids, as demonstrated by CRXtdTomato fluorescence (brightfield image shown in B, corresponding epifluorescence image in C. (**D**) An abundance of CRX$^{+/tdTomato}$-PRP line the outer rim of a stage 2 (D70) organoid. (**E**) Experimental overview for dissociated cell transplants and histology. (**F**) Sparse CRX$^{+/tdTomato}$-PRP within the SRS of a 3-month-old Foxn1-S334ter-3 rat 2 weeks after subretinal transplantation of dissociated cell suspension from stage 2 ROs. PRP reside above the host inner nuclear layer (INL) and ganglion cell layer (GCL). (**G**) All CRX$^{+/tdTomato}$-PRP found in the SRS at two weeks post-transplant co-labeled with human nuclear antigen (HNA) (arrows, *n* = 2 rats, 5 cryosections); representative image from 2-month-old Foxn1-S334ter-3 rat.

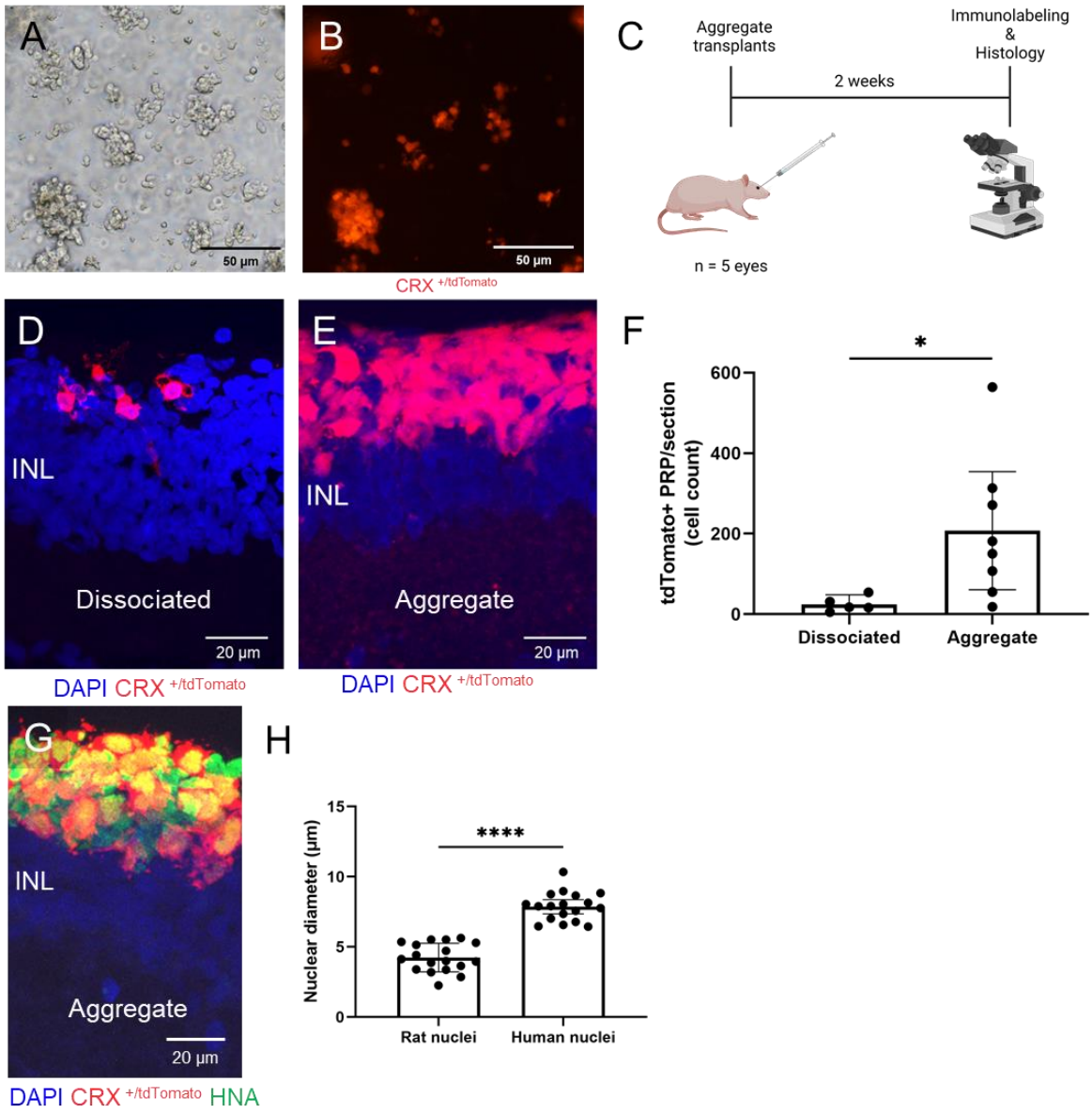

Fig. 2. Improved survival of CRX$^{+/tdTomato}$-PRP with aggregate transplants in degenerating rat retinas. (**A**) CRX$^{+/tdTomato}$-PRP aggregates generated from stage 2 (D70) ROs. Organoids were manually dissociated with a pipette to form clustered aggregates with robust tdTomato expression (brightfield image shown in A, corresponding epifluorescence image in B). (**C**) Experimental overview for 2 week aggregate cell transplants. (**D, E**) Representative images of cell survival in the SRS of Foxn1-S334ter-3 rats at 2 weeks post-transplant with dissociated (D) and aggregate (E) delivery. (**F**) Dissociated and aggregate transplants displayed a significant difference in the mean number of engrafted tdTomato-positive cells (dissociated—24.6 cells/section, 95% CI: [1, 48], *n* = 5 sections from 2 eyes; aggregate—207 cells/section, 95% CI: [61, 354], *n* = 8 sections from 3 eyes; *p = 0.0215, unpaired t-test with Welch's correction). (**G**) As in dissociated transplants, all CRX$^{+/tdTomato}$-PRP co-labeled with HNA. (**H**) Nuclei of donor cells (HNA-positive cells) were significantly larger in diameter than endogenous host nuclei (HNA-negative), providing further evidence against biomaterial transfer (mean ± 95% CI, *n* = 18 donor and host nuclei from grafted retinas, ****p < 0.0001, unpaired t-test).

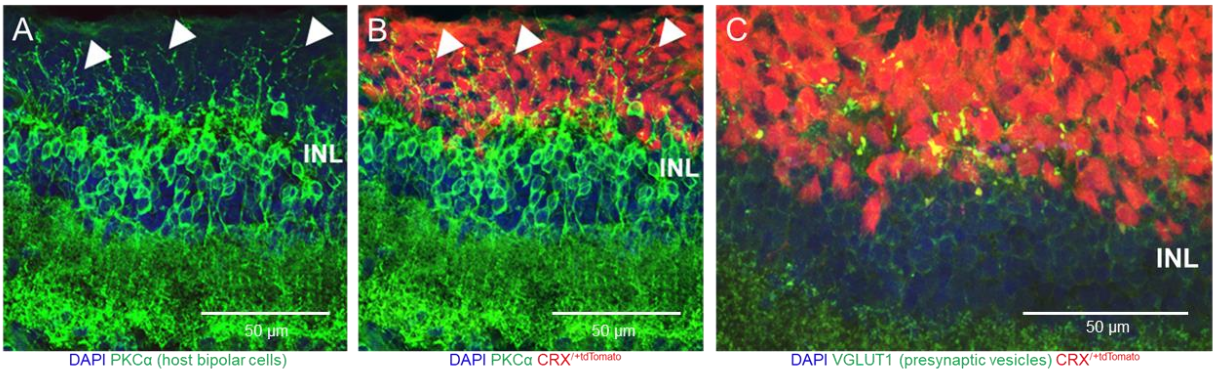

Fig. 3. Immunolabeling of anatomic CRX$^{+/tdTomato}$-PRP aggregate integration at two weeks post-transplant. (**A, B**) PKCα-positive rat host bipolar cells (BPCs) with dendritic projections extending into closely-apposed CRX$^{+/tdTomato}$-PRP grafts. (**C**) CRX$^{+/tdTomato}$-PRP aggregates express presynaptic protein VGLUT1 in regions adjacent to the host inner nuclear layer (INL).

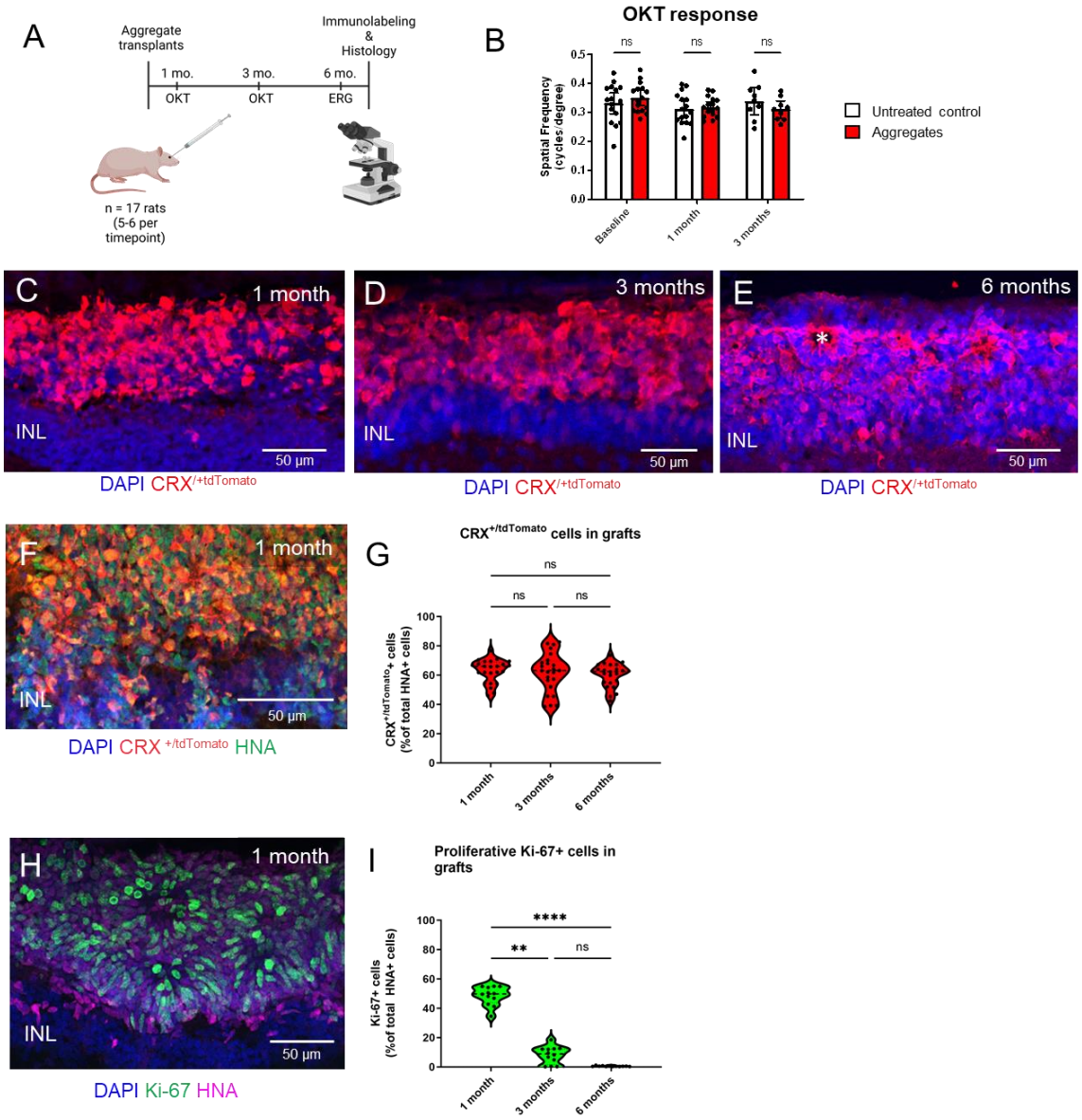

Fig. 4. Safety and long-term survival of CRX$^{+/tdTomato}$-PRP aggregates. (**A**) Experimental overview for 1, 3, and 6 month aggregate cell transplants. (**B**) No significant differences in visual acuity were observed between eyes treated with aggregates and untreated controls, indicating that aggregate delivery did not negatively affect remaining vision (n.s., mixed-effects analysis with Šídák's multiple comparisons test). (**C-E**) Survival of CRX$^{+/tdTomato}$-PRP aggregates was observed at all three timepoints examined. Rosetted morphology was observed at later timepoints (asterisk). (**F**) CRX$^{+/tdTomato}$-PRP aggregates co-labeled with HNA. (**G**) No significant differences in the percentage of CRX$^{+/tdTomato}$-PRP out of the total transplanted HNA+ population were noted over time (one-way ANOVA with Tukey's multiple comparisons). (**H, I**) Presumptive retinal progenitor cell (RPC) proliferation (Ki67) was initially high at 1 month post-transplant but decreased significantly between 1 and 3 months post-transplant (**** $p < 0.0001$, ** $p = 0.0021$, Kruskal-Wallis test with Dunn's multiple comparisons). Virtually no Ki-67-positive cells remained by 6 months post-transplant.

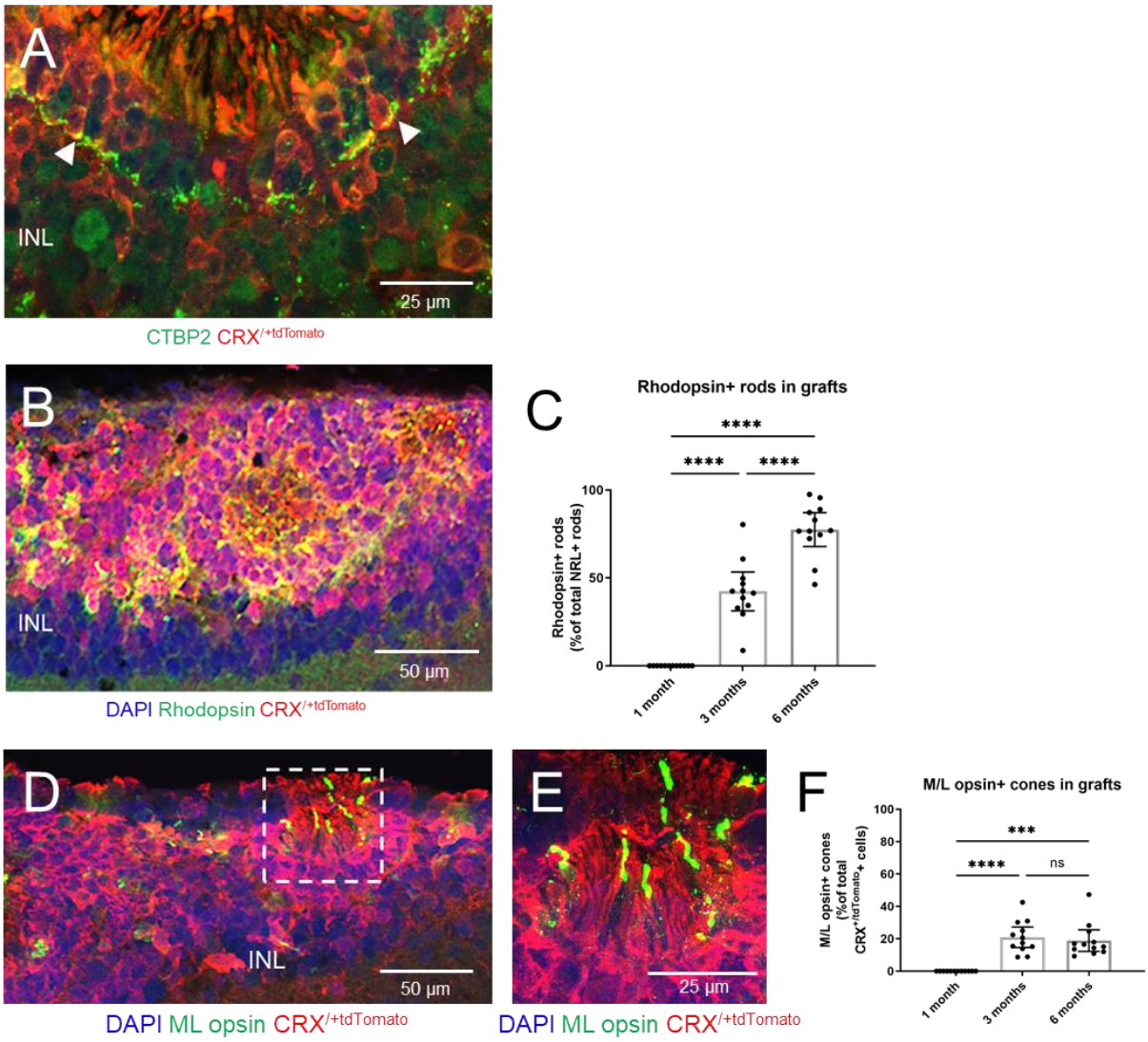

Fig. 5. CRX$^{+/tdTomato}$-PRP aggregate maturation at 6 months post-transplant. (**A**) Ribbon synapse marker CtBP2 (arrowheads) is found in transplanted PRs, with polarized expression noted adjacent to the host INL. (**B**) Rhodopsin expression in CRX$^{+/tdTomato}$-positive rods. (**C**) No NRL-positive rods co-expressed rhodopsin at 1 month; a significant increase in rhodopsin expression was noted at each time point (****p < 0.0001, ordinary one-way ANOVA with Tukey's multiple comparisons). (**D, E**) CRX$^{+/tdTomato}$-positive cones matured to express ML opsin, with polarized expression in putative outer segment-like structures. (**F**) M/L opsin expression in CRX$^{+/tdTomato}$-positive cones increased significantly from 1 to 3 months and remained stable at 6 months post-transplant (***p = 0.0002, ****p < 0.0001; Kruskal-Wallis test with Dunn's multiple comparisons).

Supplemental Information

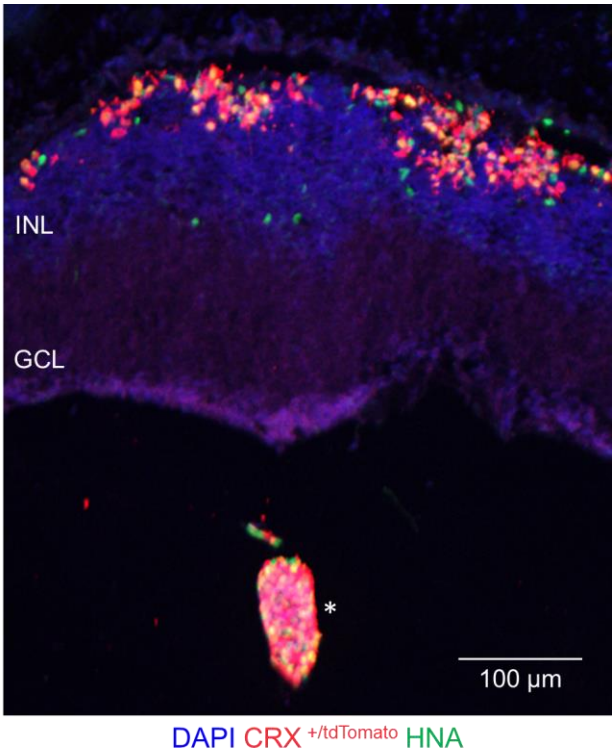

Fig. S1. Reflux into the vitreous chamber following dissociated cell delivery in the Foxn1-S334ter-3 rat. A clump of refluxed HNA-positive cells (asterisk) CRX$^{+/tdTomato}$-PRP within the vitreous chamber of a 3-month-old rat at two weeks post-transplant.

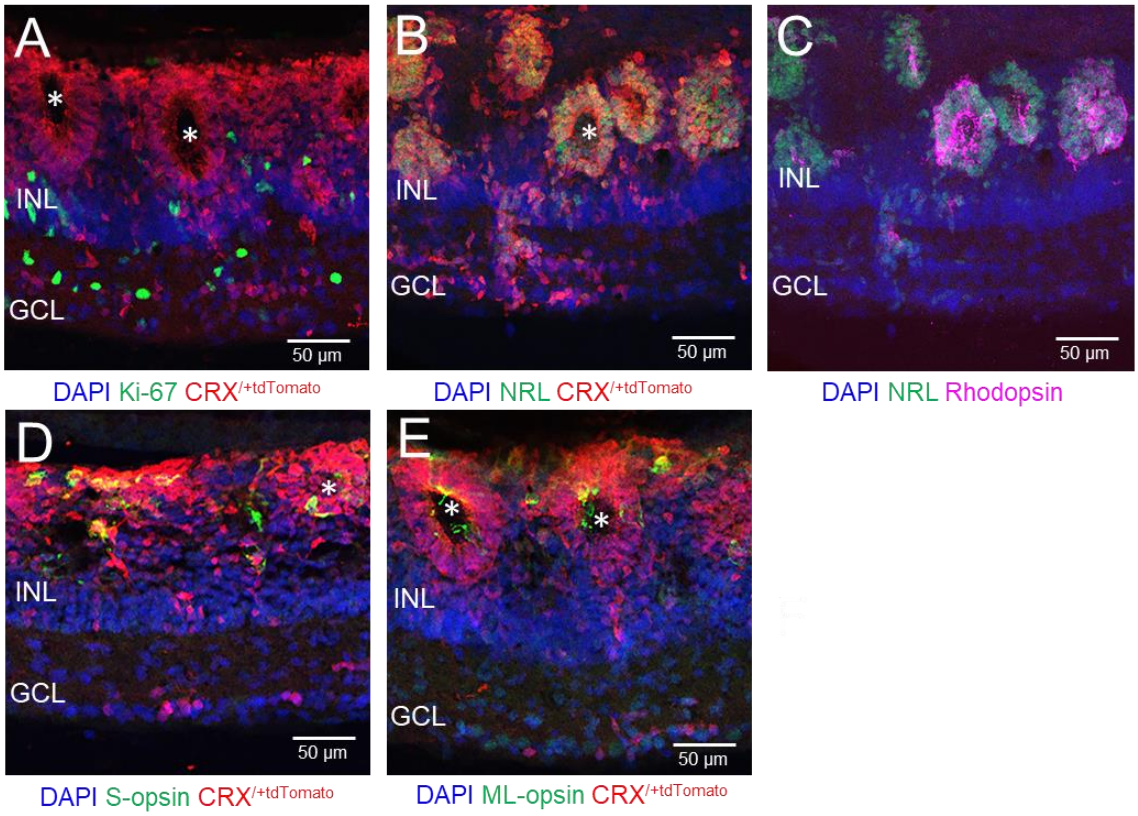

Fig. S2. CRX$^{+/tdTomato}$-PRP aggregate maturation at 3 months post-transplant. (**A**) Proliferative RPCs are present but reduced in number relative to 1 month post-transplant. (**B, C**) By 3 months, some NRL+ rods also express rhodopsin. (**D, E**) Cones also express opsins at this time. Rosetted morphology was apparent in several grafts at this timepoint and beyond (asterisks).

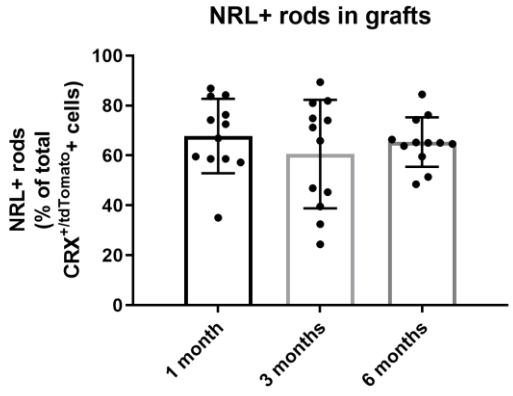

Fig. S3. CRX$^{+/tdTomato}$-PRP are predominantly rods. The large percentage of NRL+ rods found at 1 month did not significantly change with time.

Table S1. Animal details for transplants included in figures.

Figure(s)	ID	Genotype	Sex	Age	Delivery method	Dose	Time *in vivo*	Cell age at transplant / collection
1G, 2D	66315	Foxn1-S334ter-3	F	2 mo	Dissociated	300,000 cells/3 µL	2 weeks	D115 / 133
1F, S1	61834	Foxn1-S334ter-3	F	3 mo	Dissociated	300,000 cells/3 µL	2 weeks	D127 / 141
2E	79428	Foxn1-S334ter-3	F	7 mo	Aggregates	150,000 cells/5 µL	2 weeks	D70 / 84
2G	79427	Foxn1-S334ter-3	F	7 mo	Aggregates	150,000 cells/5 µL	2 weeks	D70 / 84
3A-C	79429	Foxn1-S334ter-3	F	7 mo	Aggregates	150,000 cells/5 µL	2 weeks	D70 / 84
4C	112310	Foxn1-S334ter-3	M	2 mo	Aggregates	150,000 cells/5 µL	1 month	D73 / 107
4D	97559	Foxn1-S334ter-3	M	3 mo	Aggregates	150,000 cells/5 µL	3 months	D114 / 224
4E, 5A, 5B, 5D, 5E	108348	Foxn1-S334ter-3	F	2 mo	Aggregates	150,000 cells/5 µL	6 months	D75 / 256
4F, 4H	112309	Foxn1-S334ter-3	M	2 mo	Aggregates	150,000 cells/5 µL	1 month	D73 / 107
S2	109026	Foxn1-S334ter-3	F	2 mo	Aggregates	150,000 cells/5 µL	3 months	D78 / 170

Table S2. Primary antibodies used for immunolabeling.

Antibody	Source	Catalog number	Host	Dilution
CtBP2	BD Pharmagen	612044	Mouse	1:300
Human cytoplasm	Cellartis	Y40410	Mouse	1:100
Ku80 (Human Nuclear Antigen)	Takara	Y40400	Mouse	1:100
Ki-67	Santa Cruz	SC-15402	Rabbit	1:100
M/L Opsin	Millipore Sigma	AB5405	Rabbit	1:500
NRL	R&D	AF2945	Goat	1:300
PKCα	Santa Cruz	SC-10800	Rabbit	1:50
RFP	Rockland	600-401-379	Rabbit	1:300
Rhodopsin	Millipore	MABN15	Mouse	1:100
S opsin	Millipore SIgma	AB5407	Rabbit	1:500
Tdtomato	SICGEN	AB8181-200	Goat	1:200
VGLUT1	Millipore Sigma	AB5905	Guinea Pig	1:1000

References

1. Garita-Hernandez, M. *et al.* Control of Microbial Opsin Expression in Stem Cell Derived Cones for Improved Outcomes in Cell Therapy. *Front Cell Neurosci* **15**, 648210 (2021).

2. Garita-Hernandez, M. *et al.* Restoration of visual function by transplantation of optogenetically engineered photoreceptors. *Nature Communications* **10**, 4524 (2019).

3. Barnea-Cramer, A. O. *et al.* Repair of Retinal Degeneration following Ex Vivo Minicircle DNA Gene Therapy and Transplantation of Corrected Photoreceptor Progenitors. *Molecular Therapy* **28**, 830–844 (2020).

4. Gasparini, S. J., Llonch, S., Borsch, O. & Ader, M. Transplantation of photoreceptors into the degenerative retina: Current state and future perspectives. *Progress in retinal and eye research* (2018) doi:10.1016/j.preteyeres.2018.11.001.

5. Singh, M. S. *et al.* Retinal stem cell transplantation: Balancing safety and potential. *Progress in Retinal and Eye Research* 100779 (2019) doi:10.1016/j.preteyeres.2019.100779.

6. Thomson, J. A. *et al.* Embryonic stem cell lines derived from human blastocysts. *Science* **282**, 1145–1147 (1998).

7. Yu, J. *et al.* Induced pluripotent stem cell lines derived from human somatic cells. *Science* **318**, 1917–1920 (2007).

8. Takahashi, K. & Yamanaka, S. Induction of pluripotent stem cells from mouse embryonic and adult fibroblast cultures by defined factors. *Cell* **126**, 663–676 (2006).

9. Meyer, J. S. *et al.* Modeling early retinal development with human embryonic and induced pluripotent stem cells. *Proceedings of the National Academy of Sciences of the United States of America* **106**, 16698–703 (2009).

10. Hirami, Y. *et al.* Generation of retinal cells from mouse and human induced pluripotent stem cells. *Neuroscience Letters* **458**, 126–131 (2009).

11. Nakano, T. *et al.* Self-Formation of Optic Cups and Storable Stratified Neural Retina from Human ESCs. *Cell Stem Cell* **10**, 771–785 (2012).

12. Meyer, J. S. *et al.* Optic vesicle-like structures derived from human pluripotent stem cells facilitate a customized approach to retinal disease treatment. *Stem Cells* **29**, 1206–1218 (2011).

13. Kruczek, K. & Swaroop, A. Pluripotent stem cell-derived retinal organoids for disease modeling and development of therapies. *STEM CELLS* **n/a**,.

14. Capowski, E. E. *et al.* Reproducibility and staging of 3D human retinal organoids across multiple pluripotent stem cell lines. *Development* **146**, dev171686 (2019).

15. Cowan, C. S. *et al.* Cell Types of the Human Retina and Its Organoids at Single-Cell Resolution. *Cell* **182**, 1623-1640.e34 (2020).

16. Kaewkhaw, R. *et al.* Transcriptome Dynamics of Developing Photoreceptors in Three-Dimensional Retina Cultures Recapitulates Temporal Sequence of Human Cone and Rod Differentiation Revealing Cell Surface Markers and Gene Networks. *Stem cells (Dayton, Ohio)* **33**, 3504–18 (2015).

17. Phillips, M. J. *et al.* A Novel Approach to Single Cell RNA-Sequence Analysis Facilitates In Silico Gene Reporting of Human Pluripotent Stem Cell-Derived Retinal Cell Types. *Stem Cells* **36**, 313–324 (2018).

18. Kim, S. *et al.* Generation, transcriptome profiling, and functional validation of cone-rich human retinal organoids. *Proceedings of the National Academy of Sciences of the United States of America* **116**, 10824–10833 (2019).

19. Phillips, M. J. *et al.* Blood-Derived Human iPS Cells Generate Optic Vesicle–Like Structures with the Capacity to Form Retinal Laminae and Develop SynapsesProduction of Retina from Human Blood iPS Cells. *Investigative Ophthalmology & Visual Science* **53**, 2007–2019 (2012).

20. Wahlin, K. J. *et al.* Photoreceptor Outer Segment-like Structures in Long-Term 3D Retinas from Human Pluripotent Stem Cells. *Scientific Reports* **7**, 766 (2017).

21. Gonzalez-Cordero, A. *et al.* Recapitulation of Human Retinal Development from Human Pluripotent Stem Cells Generates Transplantable Populations of Cone Photoreceptors. *Stem Cell Reports* **9**, 820–837 (2017).

22. Lowe, A., Harris, R., Bhansali, P., Cvekl, A. & Liu, W. Intercellular Adhesion-Dependent Cell Survival and ROCK-Regulated Actomyosin-Driven Forces Mediate Self-Formation of a Retinal Organoid. *Stem Cell Reports* **6**, 743–756 (2016).

23. O'Hara-Wright, M. & Gonzalez-Cordero, A. Retinal organoids: a window into human retinal development. *Development* **147**, dev189746 (2020).

24. Cora, V. *et al.* A Cleared View on Retinal Organoids. *Cells* **8**, 391 (2019).

25. Mellough, C. B. *et al.* IGF-1 Signaling Plays an Important Role in the Formation of Three-Dimensional Laminated Neural Retina and Other Ocular Structures From Human Embryonic Stem Cells. *Stem Cells* **33**, 2416–2430 (2015).

26. Ovando-Roche, P. *et al.* Use of bioreactors for culturing human retinal organoids improves photoreceptor yields. *Stem Cell Res Ther* **9**, 156 (2018).

27. Hallam, D. *et al.* Human-Induced Pluripotent Stem Cells Generate Light Responsive Retinal Organoids with Variable and Nutrient-Dependent Efficiency. *Stem cells (Dayton, Ohio)* **36**, 1535–1551 (2018).

28. Dorgau, B. *et al.* Decellularised extracellular matrix-derived peptides from neural retina and retinal pigment epithelium enhance the expression of synaptic markers and light responsiveness of human pluripotent stem cell derived retinal organoids. *Biomaterials* **199**, 63–75 (2019).

29. Sridhar, A. *et al.* Single-Cell Transcriptomic Comparison of Human Fetal Retina, hPSC-Derived Retinal Organoids, and Long-Term Retinal Cultures. *Cell Rep* **30**, 1644-1659.e4 (2020).

30. Gagliardi, G. *et al.* Characterization and Transplantation of CD73-Positive Photoreceptors Isolated from Human iPSC-Derived Retinal Organoids. *Stem cell reports* **11**, 665–680 (2018).

31. Reichman, S. *et al.* Generation of Storable Retinal Organoids and Retinal Pigmented Epithelium from Adherent Human iPS Cells in Xeno-Free and Feeder-Free Conditions. *Stem cells (Dayton, Ohio)* **35**, 1176–1188 (2017).

32. Zhong, X. *et al.* Generation of three-dimensional retinal tissue with functional photoreceptors from human iPSCs. *Nat Commun* **5**, 4047 (2014).

33. Ribeiro, J. *et al.* Restoration of visual function in advanced disease after transplantation of purified human pluripotent stem cell-derived cone photoreceptors. *Cell Reports* **35**, (2021).

34. Liu, Y. *et al.* The application of hyaluronic acid hydrogels to retinal progenitor cell transplantation. *Tissue Eng Part A* **19**, 135–142 (2013).

35. Ballios, B. G. *et al.* A Hyaluronan-Based Injectable Hydrogel Improves the Survival and Integration of Stem Cell Progeny following Transplantation. *Stem Cell Reports* **4**, 1031–1045 (2015).

36. Ballios, B. G., Cooke, M. J., van der Kooy, D. & Shoichet, M. S. A hydrogel-based stem cell delivery system to treat retinal degenerative diseases. *Biomaterials* **31**, 2555–2564 (2010).

37. Mitrousis, N. *et al.* Hydrogel-mediated co-transplantation of retinal pigmented epithelium and photoreceptors restores vision in an animal model of advanced retinal degeneration. *Biomaterials* **257**, 120233 (2020).

38. Tucker, B. A. *et al.* The use of progenitor cell/biodegradable MMP2-PLGA polymer constructs to enhance cellular integration and retinal repopulation. *Biomaterials* **31**, 9–19 (2010).

39. Thompson, J. R. *et al.* Two-photon polymerized poly(caprolactone) retinal cell delivery scaffolds and their systemic and retinal biocompatibility. *Acta biomaterialia* (2019) doi:10.1016/j.actbio.2019.04.057.

40. Yao, J. *et al.* Enhanced differentiation and delivery of mouse retinal progenitor cells using a micropatterned biodegradable thin-film polycaprolactone scaffold. *Tissue Eng Part A* **21**, 1247–1260 (2015).

41. Lavik, E. B., Klassen, H., Warfvinge, K., Langer, R. & Young, M. J. Fabrication of degradable polymer scaffolds to direct the integration and differentiation of retinal progenitors. *Biomaterials* **26**, 3187–3196 (2005).

42. Humayun, M. S. *et al.* Human neural retinal transplantation. *Invest Ophthalmol Vis Sci* **41**, 3100–3106 (2000).

43. Gouras, P., Du, J., Kjeldbye, H., Yamamoto, S. & Zack, D. J. Long-term photoreceptor transplants in dystrophic and normal mouse retina. *Invest Ophthalmol Vis Sci* **35**, 3145–3153 (1994).

44. Mandai, M. *et al.* iPSC-Derived Retina Transplants Improve Vision in rd1 End-Stage Retinal-Degeneration Mice. *Stem Cell Reports* **8**, 69–83 (2017).

45. McLelland, B. T. *et al.* Transplanted hESC-Derived Retina Organoid Sheets Differentiate, Integrate, and Improve Visual Function in Retinal Degenerate Rats. *Invest. Ophthalmol. Vis. Sci.* **59**, 2586–2603 (2018).

46. Tu, H.-Y. *et al.* Medium- to long-term survival and functional examination of human iPSC-derived retinas in rat and primate models of retinal degeneration. *EBioMedicine* **39**, 562–574 (2019).

47. Iraha, S. *et al.* Establishment of Immunodeficient Retinal Degeneration Model Mice and Functional Maturation of Human ESC-Derived Retinal Sheets after Transplantation. *Stem Cell Reports* **10**, 1059–1074 (2018).

48. Lin, B. *et al.* Retina Organoid Transplants Develop Photoreceptors and Improve Visual Function in RCS Rats With RPE Dysfunction. *Invest. Ophthalmol. Vis. Sci.* **61**, 34–34 (2020).

49. Zerti, D. *et al.* Transplanted pluripotent stem cell-derived photoreceptor precursors elicit conventional and unusual light responses in mice with advanced retinal degeneration. *Stem Cells* (2021) doi:10.1002/stem.3365.

50. Aboualizadeh, E. *et al.* Imaging Transplanted Photoreceptors in Living Nonhuman Primates with Single-Cell Resolution. *Stem Cell Reports* **15**, 482–497 (2020).

51. Worthington, K. S. *et al.* Two-photon polymerization for production of human iPSC-derived retinal cell grafts. *Acta Biomater* **55**, 385–395 (2017).

52. Grossmann, J. Molecular mechanisms of “detachment-induced apoptosis—Anoikis”. *Apoptosis* **7**, 247–260 (2002).

53. Sharma, R., Bose, D., Maminishkis, A. & Bharti, K. Retinal Pigment Epithelium Replacement Therapy for Age-Related Macular Degeneration: Are We There Yet? *Annual Review of Pharmacology and Toxicology* **60**, 553–572 (2020).

54. Baldassarre, J. S., Joseph, A., Keane, M. & Heier, J. S. Subretinal Delivery of Cells via the Suprachoroidal Space: Janssen Trial. in *Cellular Therapies for Retinal Disease: A Strategic Approach* (eds. Schwartz, S. D., Nagiel, A. & Lanza, R.) 95–104 (Springer International Publishing, 2017). doi:10.1007/978-3-319-49479-1_8.

55. Tao, S. *et al.* Survival, migration and differentiation of retinal progenitor cells transplanted on micro-machined poly(methyl methacrylate) scaffolds to the subretinal space. *Lab Chip* **7**, 695–701 (2007).

56. Nickerson, P. E. B., Ortin-Martinez, A. & Wallace, V. A. Material Exchange in Photoreceptor Transplantation: Updating Our Understanding of Donor/Host

Communication and the Future of Cell Engraftment Science. *Front Neural Circuits* **12**, 17 (2018).

57. Laver, C. R. J. & Matsubara, J. A. Structural divergence of essential triad ribbon synapse proteins among placental mammals – Implications for preclinical trials in photoreceptor transplantation therapy. *Experimental Eye Research* **159**, 156–167 (2017).

58. Seiler, M. J. & Aramant, R. B. Cell replacement and visual restoration by retinal sheet transplants. *Prog Retin Eye Res* **31**, 661–687 (2012).

59. Pearson, R. A. *et al.* Restoration of vision after transplantation of photoreceptors. *Nature* **485**, 99–103 (2012).

Chapter 4 -

Ultrathin micromolded scaffolds for high-density photoreceptor layer reconstruction

Lee, I.-K.†, Ludwig, A.L. †, Phillips M. J. †, Lee, J. †, Xie, R., Gong, S.*, Gamm, D.M.*, Ma, Z.* (2021). *Science Advances.* PMID: 10.1126/sciadv.abf0344

†These authors contributed equally to this work.

*Corresponding authors.

Author contributions: I.-K.L., J.L., and R.X. performed the scaffold fabrication and finite element analysis. A.L.L. and M.J.P. performed scaffold seeding and rodent experiments, immunostaining, confocal imaging, and analysis. B.S.S. performed in vitro spectral domain OCT imaging and analysis. L.D.J. assisted with rodent scaffold implantation. Figures were prepared by I.-K.L., A.L.L., J.L., M.J.P., and B.S.S. All authors contributed to the critical discussion of the experimental design, results, and interpretation. I.-K.L. and A.L.L. cowrote the original manuscript draft with input from all the authors. Z.M., S.G., and D.M.G. conceived the project and acquired funding.

Acknowledgements: The authors are indebted to the following individuals who assisted with cryosectioning: Ashley Willes, Uchenna Nlebedum, Maya Bhadkhamkar, Kelsy Nilles, Sara Stuedemann, Megan Piraino, Jamie Mustful, Karina Schmidt, and Alex Pitts.

Introduction

Photoreceptors (PRs) are light-sensitive cells that capture photons to initiate electrochemical impulses that traverse a complex neural network and ultimately confer visual function. Outer retinal degenerative diseases and injuries are characterized by primary or secondary PR loss with resulting severe vision loss. These conditions are common (affecting tens of millions worldwide)[1,2], devastating, and irreversible, since the human retina is incapable of intrinsic self-repair. While gene therapies hold promise for some affected patients[3], they are limited in scope to a small number of individuals with specific inherited retinal diseases (IRDs) who are early enough in their course to retain a sufficient amount of functional native PRs. Patients with acquired PR disorders and those in later stages of IRDs are unlikely to benefit from such approaches[4,5]. Furthermore, IRDs can be caused by mutations in more than 200 different genes[6], underscoring the difficulty of treating patients using gene- or mutation-specific strategies alone. As such, widely applicable approaches for restoring vision—and in particular cell replacement strategies—are highly attractive as they have the potential to reach a broad patient population even at later stages of degeneration[7].

Advances in stem cell biology and scale-up of differentiation protocols have rapidly moved cell replacement therapies toward the clinic. Diseases of the eye and outer retina have led the way[8], due in part to ease of surgical access, relative immune privilege, availability of noninvasive monitoring techniques, potential for high acuity vision replacement with a relatively low cellular dose, and relative safety of ocular surgical interventions compared to other organs and tissues[9]. Twelve years have passed since the first three-dimensional culture protocol for generating outer retinal cells from human pluripotent stem cells (hPSCs) was described[10], but the field has already reached a significant milestone with the initiation of more than 15 clinical trials that utilize hPSC-derived retinal cells[9]. All major retinal cell types can be produced from hPSCs with protocols mirroring human retinal development[11]; however, particular weight has been placed on the

generation of PRs owing to their position at the apex of visual function and their susceptibility to degenerative processes.

The first clinical trials for outer retinal cell replacement began with hPSC-retinal pigment epithelium (RPE) cells injected as a dissociated cell suspension bolus. These phase I/II trials revealed shortcomings of this approach including cell reflux at the time of delivery and disorganization of the donor RPE in the subretinal space (SRS), leading to poor long-term survival and integration[12]. Of note, cell reflux from the SRS (a potential space between the PR and RPE layers of the outer retina) into the vitreous cavity via the surgical retinotomy site can also lead to adverse patient outcomes such as epiretinal membrane formation, proliferative retinopathy, and retinal detachment[12,13]. In an effort to address these challenges and to promote more precise cell placement, multiple scaffold designs have been developed and studied to date. Three hPSC-RPE planar scaffolds—including a non-biodegradable parylene membrane, a slowly biodegradable polyethylene terephthalate (PET) scaffold, and a biodegradable poly(lactic-*co*-glycolic acid) (PLGA) electrospun scaffold—are currently being tested in clinical trials for hPSC-RPE monolayer delivery in patients with age-related macular degeneration (AMD)[12]. Early reports from these studies support in principle the safety and feasibility of delivering scaffolds into the SRS, but such scaffolds are restricted in application to patients with salvageable native PRs. Preclinical studies aimed at hPSC-derived PR replacement have largely been limited to subretinal transplantation of dissociated mixed cell suspensions or retinal organoid sheets[14]. A growing body of evidence from these animal studies suggests that similar to dissociated hPSC-RPE cell transplantation, bolus injections of hPSC-PRs often suffer from reflux during transplantation, poor cell survival, structural disorganization, and low integration rates[5,14]. Organoid-derived cellular aggregates and/or sheets have improved survival but rosettes are common; proportion of off-target cell types is rarely reported but likely substantial.

Solid and porous polymeric thin film scaffolds supporting hPSC-derived neural retina cell growth have been developed in recent years to overcome problems inherent to bolus cell suspension injections[15-26]. Despite these advances, two of the core engineering challenges these scaffolds are intended to address—cell disorganization and low or unpredictable cell payloads—have remained largely unsolved. We recently developed a 'wineglass' design scaffold that succeeded in orienting a single layer of individually spaced hPSC-PRs[26]. However, this design did not support the close association of multiple layers of hPSC-PRs, and overall demonstrated a high burden of synthetic biomaterial relative to the cell payload. A need therefore exists for strategies to deliver dense populations of PRs to a discrete region of the retina, particularly for macular diseases that affect high-acuity central vision like AMD. With these primary engineering goals in mind, we developed an ultrathin biodegradable scaffold patterned with micron-level precision, constructed specifically to improve cell payload and reduce biomaterial burden (i.e., the volume of biomaterial used to generate a single 5 mm diameter scaffold with a thickness of 30 μm), while maintaining optimal mechanical properties for subretinal applications. Herein we describe 1) the development and optimization of the 3D microstructure shape and size (i.e., scaffold design), 2) the scaffold fabrication processes (i.e., scale-up manufacturing), 3) the formulation and curing of the elastomeric stamp (i.e., material optimization), and 4) the cell seeding method leading to the production of an hPSC-PR patch aimed at reconstructing the outer neural retina.

Results and Discussion

Second-generation PR scaffold design

We sought to engineer a biocompatible and biodegradable scaffold capable of capturing a high density of PRs. In the retina of humans and other vertebrates, PRs are exclusively found in the outer nuclear layer (ONL), which is approximately 8-10 cell nuclei thick and 30 μm in height, with PR cell densities ranging from tens of thousands to hundreds of thousands per mm^2 in the macular

region of healthy human retinas[27-31]. In designing the scaffold, we drew upon our previous experience with the first-generation scaffold possessing wineglass-shaped cell capture wells[26]. While the wineglass PR scaffold introduced key advancements in biomaterial scaffold engineering, including the potential to promote PR polarization, its cell carrying capacity was low (1-2 cells/well) in comparison to the relatively high volume of synthetic biomaterial (**Table 1**). Therefore, an "ice-cube tray"-shaped scaffold was designed as a second-generation scaffold to maximize cell payload while also reducing overall biomaterial burden (**Table 1** and **Fig. S1**). Specifically, our second generation scaffold was comprised of two layers: 1) a reservoir layer (i.e., cell capture well layer) in which PRs are seeded, and 2) a base layer with regularly placed through-holes to facilitate fluid and nutrient transport (**Fig. 1A**)[32]. Reservoirs were designed to have sufficient volume and height (i.e., length/width/height 29/29/25 μm) to enable capture of multiple PRs in an individual reservoir. Furthermore, to promote cell seeding inside the wells as opposed to along the top of the walls, the reservoir wall width was designed as thin as possible (~3 μm) while retaining structural integrity. Similarly, to prevent cells (whose nuclei average 6 μm in diameter) from escaping through the perforated base layer, the through-hole diameter was also minimized (~5 μm). The desired scaffold thickness was near that of the native macular ONL (~30 μm), which is also consistent with recent arguments that scaffolds with a thickness less than 50 μm can enable interactions between seeded neuroretinal cells and the host RPE[30,33,34].

Biomaterial selection for scaffold fabrication

Desirable retinal scaffold characteristics include the use of fully biodegradable materials possessing mechanical properties compatible with those of the human retina, both of which are important for clinical translation. The retina has a Young's modulus of just 0.02 MPa[35], making this tissue extremely flexible as well as fragile. A higher modulus (>1 MPa) has been shown to enhance surgical handling of RPE scaffolds[36] without sacrificing safety or performance following implantation in the SRS. We thus sought to develop a scaffold with a Young's modulus slightly

above 1.0 MPa, balancing the need for rigidity during transplantation with flexibility to conform to the curvature of the eye upon delivery. The ideal biomaterial and its degradation products should also have proven compatibility with retinal tissue so as not to induce damage to surrounding host cells in vivo. Furthermore, the scaffold material must form thin (ideally <50 μm to facilitate interactions with RPE)[33], stable films and be amenable to the formation of precise, three-dimensional PR capture well geometries during the micromolding process. Poly(glycerol-sebacate) (PGS) was selected as the biomaterial of choice due to its retinal biocompatibility[37,38], known degradation behavior in the subretinal space (<30-60 days)[38,39], and suitable Young's modulus (1.18-1.66 MPa)[26,39]. Furthermore, PGS undergoes gradual hydrolytic and enzymatic degradation to generate sebacic acid and glycerol, both of which are natural mammalian metabolites that are fully eliminated via physiologic mechanisms[39,56]. Lastly, PGS provides the ideal combination of relatively rapid degradation in vivo with slow degradation in vitro[39]. We did not observe scaffold degradation after hPSC-PR seeding for up to 30 days in culture[26], which offers a wide time window to seed and maintain scaffolds while making arrangements for transplantation.

PGS ice cube tray PR scaffold fabrication

With the aforementioned desirable scaffold characteristics in mind, the second-generation outer retinal scaffold with an ice cube tray structure was fabricated using microfabrication and micromolding techniques, which are among the most promising approaches currently used in drug and cell delivery systems[40,41]. **Fig. 1, B to G** depicts the process workflow for fabricating PGS ice cube tray PR scaffolds. First, to fabricate a reusable silicon (Si) master mold with two distinctly patterned layers, a dense array of Si microstructures (through-holes and reservoirs) was created using photolithography and deep reactive ion etching (DRIE), a highly anisotropic etch process optimal for creating steep-sided holes or trenches in Si wafers (**Fig. 1, B and C**)[42]. Here, during the DRIE process, RIE-lag effect and microloading effect were manipulated to

achieve desired structure dimensions. RIE-lag effect refers to the dependency of etch rate on feature size (e.g., smaller features result in slower etch rates), while the microloading effect describes the relationship between local etch rate and pattern density (i.e., features in areas of high pattern density experience more competition for reactants, leading to a gradient in reactant flux and slower etch rate)[43]. While generating the Si master mold, through-holes underwent two etching steps: a primary etching step and a secondary etching step (**Fig. S2**). The etch rates of the through-holes in each step differed due to the microloading effect, with the primary etch rate and the secondary etch rate set at 2.148 μm/min and 1.746 μm/min, respectively. On the other hand, reservoirs only went through the secondary etching step and the etch rate of the reservoirs was 2.448 μm/min, which was higher than the primary etch rate of the through-holes (i.e., 2.148 μm/min) due to the RIE-lag effect caused by the difference in feature size. By considering these effects and precisely calculating the etch rates, the desired target depths—approximately 5 μm for the through-hole layer and 25 μm for the reservoir layer—were successfully achieved (**Fig. 2A**). The final Si master mold included a base layer of through-holes with a diameter of 5.1 μm and a depth of 4.8 μm, and a secondary layer of cuboidal (i.e., ice cube tray) reservoirs with a dimension of 29 μm × 29 μm × 24.5 μm. The width of the reservoir walls and the distance between adjacent through-holes were 2.8 μm and 5 μm, respectively, meeting the target dimensions. To facilitate smooth molding and demolding in the next fabrication step (**Fig. 1D**), the fabricated Si master mold was coated with a chemically inert passivation layer. Plasma-polymerization was conducted with octafluorocyclobutane (C_4F_8) as a precursor by DRIE, generating a Teflon-like polymer film with long linear $(CF_2)_n$ chains[44].

Next, to create a reusable elastomeric stamp (i.e., a negative master mold for the fabrication of the final scaffold) that would not deform, bend, or buckle during the molding process (**Fig. 1E**), polydimethylsiloxane (PDMS) was selected as the ideal material. Soft-PDMS stamps were initially tested, but these were frequently deformed during the demounting process

due to the adherent nature of soft-PDMS (**Fig. S3**). Hard-PDMS (h-PDMS) proved sufficiently strong to serve as the optimal stamp material. To create the stamp, liquid h-PDMS was poured over the fabricated Si master mold and left to cure for 12 hours at room temperature followed by 2 hours at 60°C. After curing, the stamp was carefully demolded from the Si master mold without large surface defects, producing a high yield (>95%) of the desired ice cube tray microstructures (**Fig. 2D**). The stamp surface was coated with a monolayer of hydrophobic silane (an anti-adhesive layer) under vacuum to facilitate demounting from the final PGS scaffold. The microfabrication processes for the Si master mold and h-PDMS stamp are described in greater detail in the Materials and Methods section.

Fig. 1, E and F depict the final steps in the micromolding process for fabricating the ice cube tray PR scaffold from a PGS prepolymer with the h-PDMS stamp. First, PGS prepolymer was placed on a clean Si wafer and melted on a hotplate at 120°C. The micropatterned surface of the h-PDMS stamp was then immersed into the liquid PGS. A glass slide with an overlying weight of 380 g was placed atop the stamp, pressing the liquid PGS between the h-PDMS stamp and the Si wafer (**Fig. 1E**) to control the scaffold thickness (**Fig. S4**). The scaffold microfabrication apparatus was subsequently placed into a vacuum oven and cured under high vacuum (<1 mbar) at 120°C for 3 days. **Fig. 3A** shows a cured PGS scaffold between the h-PDMS stamp and the Si wafer prior to demounting. After curing was complete, the h-PDMS stamp was demounted from the Si wafer, taking care to avoid fractures of the h-PDMS ice cube tray microstructures due to the rigid nature of h-PDMS. Fabricated PGS scaffolds were evaluated via scanning electron microscopy (SEM) to screen for surface defects attributable to the demounting process.

Despite careful handling, early microfabrication experiments often resulted in retention of fractured h-PDMS microstructures in the final scaffold product, rendering the h-PDMS stamp inoperable for further use (**Fig. S5**). To address this challenge, isopropyl alcohol (IPA) soaking

was employed, as it allows polymers to swell and can facilitate release from secondary mold structures[45]. The h-PDMS stamp, cured PGS, and Si wafer were incubated in isopropyl alcohol (IPA) at room temperature for 12 hours, allowing IPA to permeate the PGS scaffold. Using this approach, the PGS scaffold on a Si wafer could be reliably demounted from the h-PDMS stamp without surface defects or retained h-PDMS stamp microstructures (**Fig. 3B**), maintaining the h-PDMS stamp surface integrity for reuse (**Fig. S6**). Thereafter, the PGS scaffold was carefully delaminated from the Si wafer using a single razor blade (**Fig. 1F**) and unrolled with sonication treatment in IPA. The microfabrication process was subsequently optimized to produce a scaffold with minimal biomaterial burden and sufficient structural integrity for successful delamination (**Fig. S7**). The final micro-patterned ice cube tray scaffold is shown via a schematic (**Fig. 1G**) and low magnification photography (**Fig. 3C**). To assess microstructure quality and uniformity in the final product, the scaffolds were imaged with SEM; top, bottom, and cross-sectional views of the fabricated scaffold revealed precise, neat, and uniform ice cube tray reservoirs with the desired through-hole structures in the base of the scaffold (**Fig. 3, D to F**). In particular, the microstructure surfaces were smooth with no irregular or elevated edges and minimal structural defects. Furthermore, the final scaffold product had a high microstructure yield (>98%) over a large area (**Fig. 3G**). A detailed description of the fabrication process for ice cube tray PGS scaffolds can be found in the Materials and Methods section. Taken together, the optimized fabrication process for the ice cube tray design achieves a finely tuned balance between three critical and interrelated design criteria: target dimension, minimized biomaterial burden, and structural integrity.

Mechanical compliance of PGS ice cube tray PR scaffolds

Since the eye is spherical in shape and outer retinal scaffolds necessarily experience internal and external stresses during delivery to the SRS, an ideal PR scaffold must be not only flexible enough to conform to curved surfaces, but durable enough to withstand local stresses without

structural deformation. In addition, the scaffold should return to its original form when local stresses are removed to protect and maintain proper organization of captured cells. To model this, the mechanical properties of the PGS ice cube tray PR scaffold were assessed via finite element analysis and compared to those of our original wineglass PR scaffold[26] to elucidate mechanical benefits and tradeoffs of each design (**Fig. 4**).

To determine how the scaffolds with two different designs (wineglass vs. ice cube tray) behave under external stresses, a fixed constraint was set to a square area in the center of each design that incorporated 9 through-holes. Thereafter, 5 N of tensile force per unit area was applied to the four sides of each scaffold in the x- and y-directions. As presented in **Fig. 4A**, the wineglass design had high stress concentrations along the boundary of the fixed constraint, leading to a change in the shape of the scaffold. In contrast, the resulting stress was uniformly and efficiently distributed throughout the ice cube tray scaffold, without causing any appreciable deformation of the scaffold (**Fig. 4B**), although the ice cube tray design had a higher stress than the wineglass design due to its thinner through-hole layer (i.e., 5 vs. 10 μm), which largely determines the mechanical properties of the scaffolds because the reservoir layer only consists of very thin reservoir walls (i.e., ≤ 3 μm). Tensile strength and elastic modulus were also measured to assess the ice cube tray scaffold's mechanical properties. The modulus of the ice cube tray scaffold was 1.3 MPa, and all microstructures recovered to their original shapes after the tensile stress was removed (**Fig. S8**), indicating favorable pliability for any surgical handling associated with transplantation. These results convincingly demonstrated that the ice cube tray design has superior mechanical properties compared to the wineglass design, both in terms of uniformity of stress distribution and extent of scaffold deformation under a defined tensile stress, two factors that are key for safe and consistent scaffold delivery in vivo.

Scaffold sterilization, stability, and degradation

To facilitate cell seeding, scaffolds were incorporated into a commercially available 12 mm polyester transwell cell culture insert (Corning® Costar® Snapwell, Sigma) prior to sterilization (**Fig. 5, A to C**). To mount scaffolds into the insert, a 5 mm biopsy punch was used to create a round hole in the center of the polyester transwell membrane, which is the approximate diameter of the human macula[27]. Scaffolds were then mounted in the center of the transwell membrane and secured with soft-PDMS as an adhesive (**Fig. 5A**). Transwell inserts were snapped into holders (**Fig. 5B**) and placed in a 6 well plate (**Fig. 5C**). Scaffolds were treated with O_2 plasma to enhance the surface hydrophilicity and thus microstructure wettability, preventing microbubbles from forming within each capture well (**Fig. S9**) and promoting uniform cell seeding in the capture wells[26,46,47].

Scaffolds were subsequently gas sterilized with ethylene oxide (**Fig. S10**), a process widely used to sterilize delicate medical devices due to its compatibility with a variety of heat or pressure-sensitive materials[48]. In addition, gas sterilization does not melt the tissue culture plastic housing the scaffolds, as occurs during autoclaving. Sterilized scaffolds were pre-treated with an extracellular matrix protein substrate (human recombinant Laminin 521, BioLamina) previously shown to optimally facilitate hPSC-PR adhesion in similar culture systems[26].

To assess in vitro stability, scaffolds were monitored over 6 weeks in culture via optical coherence tomography (OCT) imaging. During this time, scaffolds did not appreciably degrade, remaining at 100 ± 5.4% of baseline thickness at the 6-week time point. Scaffold degradation within the subretinal space of nude rats was also examined. Comparable to previously published PGS studies[38,39], scaffold thickness steadily decreased to 12.6 ± 3.5% of starting scaffold thickness by 2 months post-implantation (**Fig. S11**).

PR cell seeding in ice cube tray scaffolds

To assess the performance of the PGS ice cube tray PR scaffold in vitro, an established protocol was used to generate retinal organoids from a previously characterized human ESC reporter line (WA09-CRX$^{+/tdTomato}$) that fluorescently labels PRs throughout differentiation and maturation[49]. WA09-CRX$^{+/tdTomato}$ retinal organoids were differentiated to late stage 2 (approximately D120 of differentiation)[11] to achieve peak PR differentiation prior to seeding[11,49]. Retinal organoids were then dissociated to produce a cell suspension containing a high percentage (60-80%) of fluorescent CRX$^{+/tdTomato}$-PRs. Laminin-coated scaffolds were seeded with cell suspensions at several concentrations (1, 3, 5 or 7 million cells/transwell) and cultured for 5 days to assess biocompatibility and determine the minimum number of cells necessary to achieve maximal scaffold carrying capacity (**Fig. 5, D and E**). Confocal imaging of fixed, immunostained scaffolds confirmed successful seeding and survival of multiple CRX$^{+/tdTomato}$-expressing PRs in individual wells of laminin-coated PGS ice cube tray scaffolds (**Fig. 5D**). As shown in **Fig. 5E**, maximal scaffold carrying capacity (17.8 ± 2.4 CRX$^{+/tdTomato}$-PRs/well, or 1.74 ± 0.24 x10^5 CRX+/tdTomato-PRs/mm^2) could be achieved by seeding at a concentration of 5 million cells per transwell (total area of transwell = 467 mm^2) (**Table 2**). An optimized seeding concentration of 5 million cells/transwell was thus used for all subsequent experiments. Importantly, these experiments revealed that the ice cube tray design enabled a 3.4-fold increase in cell carrying capacity (calculated with **equations S1 and S2**) compared to the original wineglass shaped PR scaffold design (**Table 2**). The ice cube tray scaffold also facilitated capture of a multi-cellular layer of PRs up to 3 cell layers thick (average = 2.6 ± 0.7 nuclei layers/well).

The differentiated PRs expressed cone- (cone arrestin; ARR3) and rod-specific (NR2E3) proteins as expected for hPSC-PRs derived from stage 2 retinal organoids[11] (**Fig. 5F**). The substantial increase in the cell payload capacity of the ice cube tray design, combined with its

decreased overall biomaterial burden, which was 50% less for the ice cube tray design than the wineglass design (calculated with **equation S3**), further underscores its relative superiority (**Tables 1 and 2**). These results represent the highest-density capture of hPSC-PRs for any retinal scaffold described to date. Furthermore, this construct provides a means of exceeding the often-cited threshold of 150,000 photoreceptors within a single scaffold (**Table 2**), which is the threshold theoretically needed to achieve an electroretinographic (ERG) response[14,50].

PR organization within PGS ice cube tray scaffold constructs

Given the importance of cell packing, organization, and polarization within the retina, particularly with regard to cones (the Stiles-Crawford effect[51] and the Nyquist limit[52] are tied to outer segment orientation and cone density, respectively), we sought to determine whether the ice cube tray scaffold design facilitated pre-organization of hPSC-PRs within scaffold constructs. To assess PR polarity and scaffold construct organization, whole mounts of PGS ice cube tray scaffolds seeded with 5 million cells per transwell were screened for the presence of 1) outer segments (specialized light-detecting structures situated apically within PRs) and 2) presynaptic vesicles, which localize to the basal PR axon terminal (**Fig. 6**). 3D reconstructions of scaffold flat mounts were analyzed to determine the primary location of outer segments and presynaptic terminals. $CRX^{+/tdTomato}$-PRs in scaffolds expressed Peripherin 2 (PRPH2) (**Fig. 6, A and C**), a protein crucial to the development of rod and cone outer segments[53] that contain photosensitive opsins. PRPH2-positive PR outer segments oriented perpendicularly to the base of the scaffold (**Fig. 6C, inset**). $CRX^{+/tdTomato}$-PRs also expressed VGLUT1, a presynaptic marker expressed within PR axon terminals (**Fig. 6, B and D**), which was primarily localized to the top half of the scaffold in 3D reconstructions (**Fig. 6D**).

Interestingly, in the wineglass design, PR axons tended to extend into the through-holes, with presynaptic markers localized at the base of the scaffold. The reversal in PR polarity seen

with the ice cube tray design could be due to its substantially shorter through-hole length compared to the wineglass design (5 μm vs. 10 μm). Alternatively, the clustering of multiple PRs within a single well may provide local cell-cell interactions that are not present in the wineglass scaffold design. Regardless of the mechanism, a significant benefit of the PR polarity within the ice cube tray scaffold is the greater exposure area of donor PR axon terminals at the top of the scaffold, immediately adjacent to the dendritic terminals of host interneurons (i.e., bipolar cells). Such an orientation not only minimizes barriers at the donor-host synaptic interface (prior to degradation of the biomaterial), it also positions the through-holes in the scaffold base to allow fluid and material exchange between the donor PRs and the host RPE and choroid as the scaffold degrades over time. Lastly, it concentrates the bulk of the biomaterial volume adjacent to the host RPE, the cell layer that plays a role in scaffold degradation within the SRS[54], possibly due to secretion of extracellular matrix-remodeling matrix metalloproteases (MMPs)[55].

Conclusion

In conclusion, we have described state-of-the-art microfabrication and micromolding processes for generating biodegradable, micro-structured, ultrathin scaffolds that support formation of a dense layer of hPSC-derived PRs. Analysis of the scaffold's mechanical properties reveal favorable advances in the uniformity of stress distribution and the extent of deformation for optimal scaffold handling in downstream surgical applications. Furthermore, in vitro experiments underscored the potential of ice cube tray scaffolds to serve as an organized delivery system for more than 300,000 hPSC-PRs in a single 5 mm diameter (19.63 mm^2) scaffold (approximately the area of the human macula, **see equation 2**). PGS ice cube tray PR scaffolds exhibited not only a higher cell payload capacity and decreased biomaterial burden, but also optimal donor PR orientation for integration in transplantation studies. We expect that hPSC-PRs delivered on PGS scaffolds will be better poised to survive and function post-transplantation and will prevent or eliminate cell reflux and disorganization. Future studies will be aimed at assessing scaffold-

mediated delivery in small and large animal models of outer retinal disease and damage, exploring minimally invasive surgical approaches, and optimizing manufacturing strategies for scale-up and Good Manufacturing Practice (GMP) production of PR-seeded scaffolds. In addition, the scaffold micromolding and microfabrication strategies developed here may prove useful for high-density, layered, and oriented cell replacement in other tissues throughout the body.

Materials and Methods

Materials

(7.0-8.0% Vinylmethylsiloxane)-dimethylsiloxane copolymer (VDT-731), platinum-divinyltetramethyl-disiloxane complex (Pt catalyst, SIP6831.2LC), (25-35% Methylhydrosiloxane)-dimethylsiloxane copolymer (HMS-301), and (Tridecafluoro-1,1,2,2-tetrahydrooctyl)trichlorosilane (SIT8174.0) were purchased from Gelest, Inc. (USA). 2,4,6,8-Tetramethyl-2,4,6,8-tetravinylcyclotetrasiloxane, glycerol, sebacic acid, acetone, and isopropanol (IPA) were obtained from Sigma-Aldrich, Inc. (USA). All reagents were used as received without further purification.

Fabrication of silicon master mold

An undoped Si wafer was used as a starting material. After a standard RCA cleaning process an array of through-hole patterns was formed by photolithography using an AZ2020 photoresist and etched with deep reactive-ion etching (DRIE). During the DRIE process, etch/passivation cycles, etch/passivation time per cycle, plasma power, ICP power, and $SF_6/O_2/C_4F_8$ gas flows were 33/33 cycles, 10/5 sec, 11.7 W, 600 W, and 102/12/100 sccm, respectively. The diameter and depth of the etched through-holes were 5.1 μm and 11.8 μm, respectively (**Fig. S12**). After removing the photoresist with organic solvents (acetone and IPA), the reservoir was formed by the same procedure used for the through-hole patterning and etching, except that the DRIE etch/passivation

cycles were 60/60 cycles, respectively. For the fabricated Si master mold, the diameter and depth of through-holes were 5.1 μm and 4.8 μm, respectively, and the length, width, and depth of reservoirs were 29 μm, 29 μm, and 24.5 μm, respectively. The width of reservoir wall and the distance between adjacent through-holes were 2.8 μm and 5 μm, respectively. After the master mold was cleaned with organic solvents and piranha solution, it was treated with oxygen plasma (Unaxis 790 RIE) for 20 sec at a plasma power of 40 W, pressure of 120 mTorr, and oxygen gas flow rate of 20 sccm to remove the remaining organic contaminants. Finally, to coat a chemically inert passivation layer on the Si master mold, plasma-polymerization was conducted with octafluorocyclobutane (C_4F_8) as a precursor by DRIE (C_4F_8 = 97 sccm, time = 1 min), generating a Teflon-like polymer film with long linear $(CF_2)_n$ chains[44].

Fabrication of h-PDMS stamp

The h-PDMS was prepared by mixing and degassing 17 g of vinyl PDMS pre-polymer (VDT-731), 90 μL of a Pt catalyst (SIP6831.2LC), 250 μL of 2,4,6,8-Tetramethyl-2,4,6,8-tetravinylcyclotetra-siloxane, and 5 g of a hydrosilane pre-polymer (HMS-301). Then, the h-PDMS mixture was poured onto the fabricated Si master mold and cured at room temperature for 12 hours, followed by 2 hours inside an oven at 60°C. Thereafter, the stamp was gently demolded from the master mold and cut with a single edge razor blade to obtain nine sets of 1×1×1 cm^3 cubes. After the stamp was cleaned with IPA, it was treated with O_2 plasma using RIE at a plasma power of 40 W, a working pressure of 120 mTorr, and a flow rate of 30 sccm for 20 sec to facilitate subsequent hydrophobic silane coating (anti-stick coating). Then, the stamp was placed in a desiccator with a beaker containing 400 μL of (Tridecafluoro-1,1,2,2-tetrahydrooctyl)trichlorosilane (SIT8174.0) and pumped down for 12 hours at room temperature to allow the stamp's surface to be fully functionalized by the evaporated silane. Finally, the stamp was rinsed with IPA again and gently blow-dried using nitrogen.

Poly(glycerol-sebacate) (PGS) prepolymer synthesis

The PGS prepolymer was synthesized according to previously published protocols[26,39,56]. Briefly, equimolar glycerol (4.60 g, 50 mmol) and sebacic acid (10.11 g, 50 mmol) were homogenously mixed under nitrogen atmosphere for 24 hours at 120°C. Thereafter, the reaction pressure was reduced to <1 mbar while keeping the temperature at 120°C for another 24 hours to allow further condensation polymerization. The PGS prepolymer was a white wax-like solid after it was cooled down to 20°C.

Fabrication of PGS scaffold

Approximately 10 mg of PGS pre-polymer solid was placed on a clean and pre-heated Si wafer and melted. Then, the patterned side of the h-PDMS stamp was placed against the liquid PGS on the Si wafer. This apparatus was placed in the vacuum oven (120°C and <1 mbar) for 15 min to remove bubbles between the Si wafer and the stamp. Thereafter, a glass slide plus a 380-gram weight were placed on the stamp to press it against the Si wafer to control the scaffold thickness at room temperature and the apparatus was placed back into the vacuum oven and kept at 120°C for 72 hours under <1 mbar for complete curing of PGS. After that, the Si wafer and the stamp were soaked together in IPA for 12 hours to gently demount the stamp from the Si wafer. Once the stamp was removed, the PGS scaffold on the Si wafer was blow-dried with nitrogen gas and carefully delaminated using a single razor blade. In order to unroll the scaffold tangled during the delamination process and remove any residues on its surface, it was soaked in an IPA solution, followed by a sonication treatment for 20 min. Finally, the PGS scaffold was transferred onto a Teflon plate using a transfer pipet and three drops of water were added on its

surface to restore the swollen PGS scaffold to its original morphology. Lastly, it was carefully blow-dried with the cell reservoirs facing upward.

Mounting PGS scaffolds on transwell inserts

A 12 mm polyester transwell membrane with a central 5 mm hole was secured to the scaffold with PDMS. The scaffold was degassed in a desiccator for 5 min and cured at 60°C for 4 hours to adhere the scaffold to the transwell membrane. Then, the PGS scaffold and transwell membrane were carefully detached from the Teflon plate and mounted in a transwell insert for cell culture. Lastly, for better cell capture, brief (20 sec) oxygen plasma treatment was carried out on the top and bottom surfaces of PGS scaffold using RIE (Unaxis 790; O2 = 30 sccm, pressure = 120 mTorr, plasma power = 40 W).

Finite element analysis

To predict the mechanical properties of the PGS wineglass and ice cube tray scaffolds, the equivalent von Mises stress distributions were numerically solved using a finite element simulation software (Comsol Multiphysics 4.2, Comsol Ltd). A nonlinear elastic Neo–Hookean model was used to characterize the mechanical properties and the relevant material parameters used for the PGS polymer were E = 1.3 MPa, Density = 1060 kg/m^3, v = 0.49. Here, E is Young's modulus and v is Poisson's ratio.

Retinal organoid differentiation and culture

WA09-CRX+/tdTomato hPSCs were differentiated to stage 2 retinal organoids (~D120) using an established protocol for retinal differentiation[11,50]. Briefly, pluripotent colonies were maintained in mTeSR Plus medium on Matrigel (Thermo Fisher Scientific) and lifted with ReLeSR (STEMCELL Technologies) to generate free-floating embryoid bodies (EBs). EBs were transitioned to neural induction medium [NIM; 1:1 Dulbecco's modified Eagle's medium

(DMEM):F12 (Thermo Fisher Scientific), 1× minimal essential medium (MEM) nonessential amino acids (Thermo Fisher Scientific), 1× GlutaMAX (Thermo Fisher Scientific), heparin (2 mg/ml; Sigma-Aldrich), and 1% N2 supplement (Thermo Fisher Scientific)] over 4 days before receiving NIM with a pulse of bone morphogenetic protein 4 (BMP4) (R&D Systems) on day 6. EBs were plated onto Matrigel-coated plates on day 7 and gradually transitioned to retinal differentiation medium [RDM; 3:1 DMEM:F12 (Thermo Fisher Scientific), 1× MEM nonessential amino acids, 1× GlutaMAX, 1× antibiotic-antimycotic (Thermo Fisher Scientific), and 2% B27 supplement (Thermo Fisher Scientific)] after a series of half media changes in NIM to gradually reduce the BMP4 concentration over time. At approximately day 30 of differentiation, retinal organoids were manually dissected and maintained in free-floating cultures in RDM with 2% fetal bovine serum (FBS; WiCell). Retinal organoids were maintained in polyhydroxyethylmethacrylate (MilliporeSigma)–treated tissue culture flasks and fed twice weekly with RDM and 2% FBS until scaffold seeding. Organoids were monitored via epifluorescence microscopy to ensure that PR differentiation had peaked (as indicated by tdTomato fluorescence) as organoids reached stage 2 (~D120). Cultures were routinely screened for the presence of mycoplasma by polymerase chain reaction (WiCell).

Scaffold seeding and maintenance in culture

For cell seeding and scaffold organization experiments, stage 2 organoids (approximately D120 of differentiation) were dissociated enzymatically with papain (Worthington Biochemical) and seeded onto gas sterilized scaffolds pre-coated with 0.05 mg/mL laminin 521 (human recombinant Laminin 521, BioLamina) in Hanks' Balanced Salt Solution (HBSS) with calcium and magnesium (Thermo Fisher) and subsequently incubated for a minimum of 4 hours at 25 °C to enable sufficient laminin polymerization. Cells were plated onto scaffolds in RDM + 10% FBS at a volume ≤ 300 µL. Scaffolds were left undisturbed for the first 24 hours post-seeding to facilitate cell adhesion, then gradually transitioned back to RDM + 2% FBS medium for scaffold

maintenance. Scaffolds were maintained in culture for up to 5 days and fed daily with RDM + 2% FBS.

Optical coherence tomography imaging and analysis

To assess in vitro biodegradability of the PGS scaffolds, optical coherence tomography (OCT) was performed on 3 scaffolds—1 seeded with hPSC-PRs and 2 without cells—for 6 weeks. Scaffolds were incorporated into glass-bottomed 6 well plates (MatTek Life Sciences) and maintained as previously described, with the exception of brief transitions to imaging media [Hibernate E Flow Fluorescence (BrainBits), 1× antibiotic-antimycotic, 2% B27 supplement, 2% FBS] for ≤2 hours each week during OCT imaging. At 24 hours post-seeding and weekly thereafter, the cell-seeded scaffold and 2 unseeded controls were imaged within glass-bottomed 6 well plates using a Ganymede spectral domain OCT (SD-OCT) (ThorLabs). Central scaffold height was measured using calipers within the ThorImage OCT software (version 5.2.1).

Animals

4 male and female SD-Foxn1 Tg(S334ter)3Lav rats[57] (age: 1-4 months) were used. Animal studies were reviewed and approved by the UW-Madison Institutional Animal Care and Use Committee. All animals were handled in accordance with the Association for Research in Vision and Ophthalmology (ARVO) statement for the use of animals in Ophthalmic and Vision Research, the National Institute of Health Guide for the Care and Use of Laboratory Animals, and the laws of the United States and regulations of the Department of Agriculture.

Scaffold Implantation in Rodents

One-mm round PGS scaffolds were obtained using a sterile trephine punch (Electron Microscopy Sciences) and implanted into nude rats using a previously published approach for subretinal scaffold delivery in rodents[36]. Briefly, rats were anesthetized with intraperitoneal

ketamine (80 mg/kg) and xylazine (10 mg/kg) and eyes were treated with mydriatic (1% tropicamide and 2.5% phenylephrine HCl) and topical anesthetic (0.5% tetracaine HCl) ophthalmic solutions prior to scaffold delivery. Eyes were proptosed, coated with Goniovisc (Dynamic Diagnostics International), and covered with a coverslip to visualize scaffold entry. A scleral incision was made with a 23G MVR knife and a subretinal bleb was raised with sodium hyaluronate viscoelastic (Abbott Medical Optics). Internal limiting membrane forceps were used to gently guide a 1-mm scaffold punch into the subretinal space.

Histology

Rats were humanely euthanized at 1 week, 2 weeks, 1 month, or 2 months post-implant and eyes were fixed in 4% paraformaldehyde for 1 hour to prepare tissue for histology. Eyes were placed in 30% sucrose overnight and frozen in blocks of OCT for cryosectioning at 25µm. Single plane ×20 magnification images of cryosections with degrading subretinal scaffolds were acquired via differential interference contrast microscopy and analyzed in ImageJ. 15 evenly spaced individual measurements of scaffold thickness (measured perpendicular to the scaffold base) were obtained from 1-3 cryosections per eye. Thickness was reported as the mean percentage of starting scaffold thickness (± standard deviation) and graphed using GraphPad Prism.

Immunocytochemistry and confocal imaging

Scaffolds seeded with hPSC-PRs were fixed in 4% paraformaldehyde for 30 minutes, washed in 1× Phosphate Buffered Saline (PBS; Thermo Fisher) and processed for immunocytochemistry as previously described to assess expression and localization of PR-specific proteins[26]. Briefly, scaffold whole mounts were incubated in blocking solution [10% normal donkey serum (Abcam), 5% bovine serum albumin (Millipore Sigma), and 0.5% Triton-X (Millipore Sigma) in 1× PBS] for 1 hour at room temperature followed by overnight incubation at 4 °C in primary antibodies.

Scaffolds were washed with 1× PBS to remove residual primary antibody solution before incubating for 30 minutes at room temperature in secondary antibodies at 1:500 (Alexa Fluor 488, 545, and 633, Thermo Fisher). After an additional round of washes in 1× PBS, scaffolds were carefully removed from transwells and mounted in Prolong Gold Antifade with DAPI mounting medium (Thermo Fisher) prior to coverslipping. Confocal z-stacks of immunostained scaffolds were captured at ×20 magnification with a Nikon A1R confocal microscope. 3D z-stack reconstruction, maximum intensity projection image generation, and cell capture quantification were performed with Nikon Elements software. Descriptive statistics for quantitative analyses were performed with and visualized in GraphPad Prism. Averages reported herein are identified as the mean ± standard deviation.

Figures and Tables

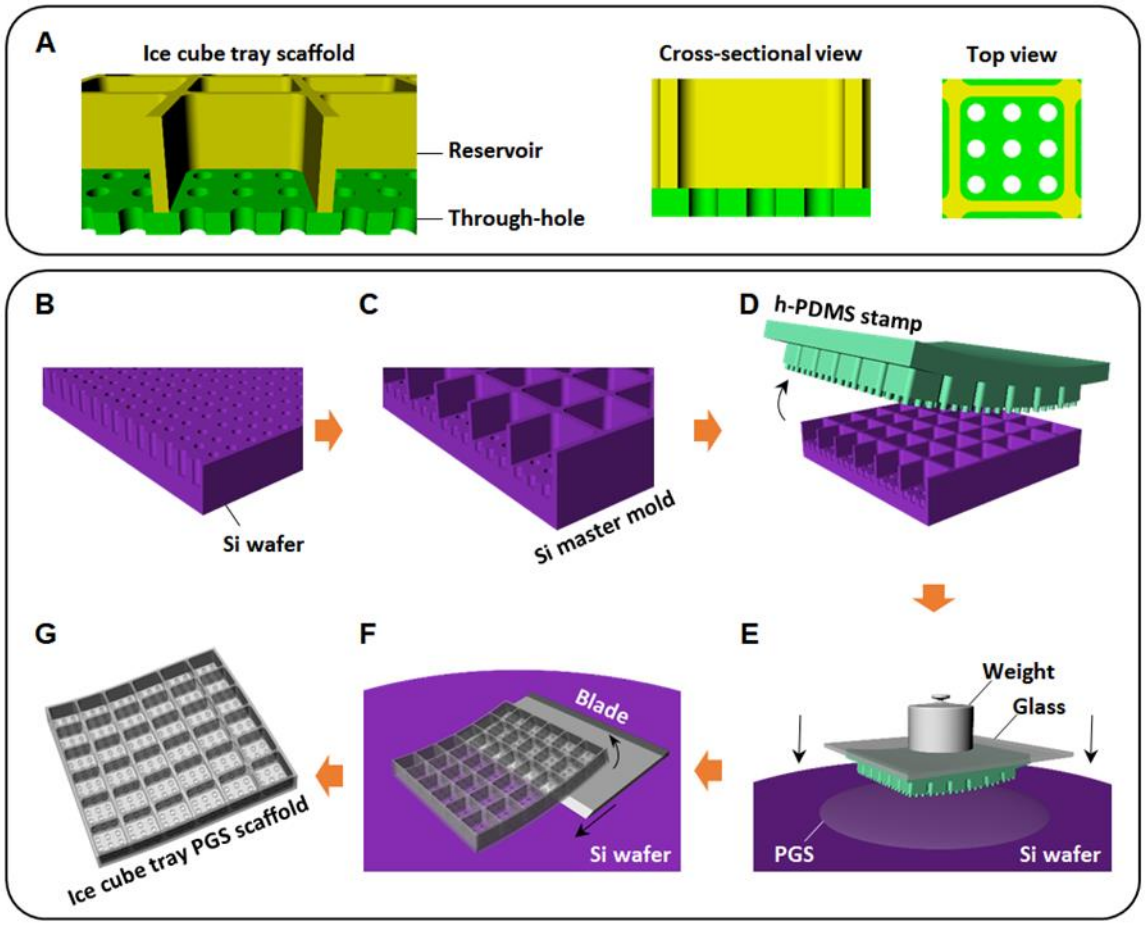

Fig. 1. PGS ice cube tray scaffold manufacturing process. (**A**) Schematic illustration of the ice cube tray PR scaffolds designed to have a reservoir layer for cell capture and retention and a through-hole layer for exchange of fluid, waste products, and nutrients both in vitro and during scaffold degradation in vivo. (**B to G**) Schematic illustration of the procedure to fabricate the ice cube tray PR scaffolds using a PGS prepolymer. (**B**) Through-hole and (**C**) reservoir etching processes of a Si master mold. (**D**) Molding and demolding processes of a h-PDMS stamp from the Si master mold. (**E**) Mounting and demounting processes of the h-PDMS stamp for fabricating a PGS ice cube tray PR scaffold. (**F**) Delamination process of the scaffold using a razor blade. (**G**) Final PGS ice cube tray PR scaffold.

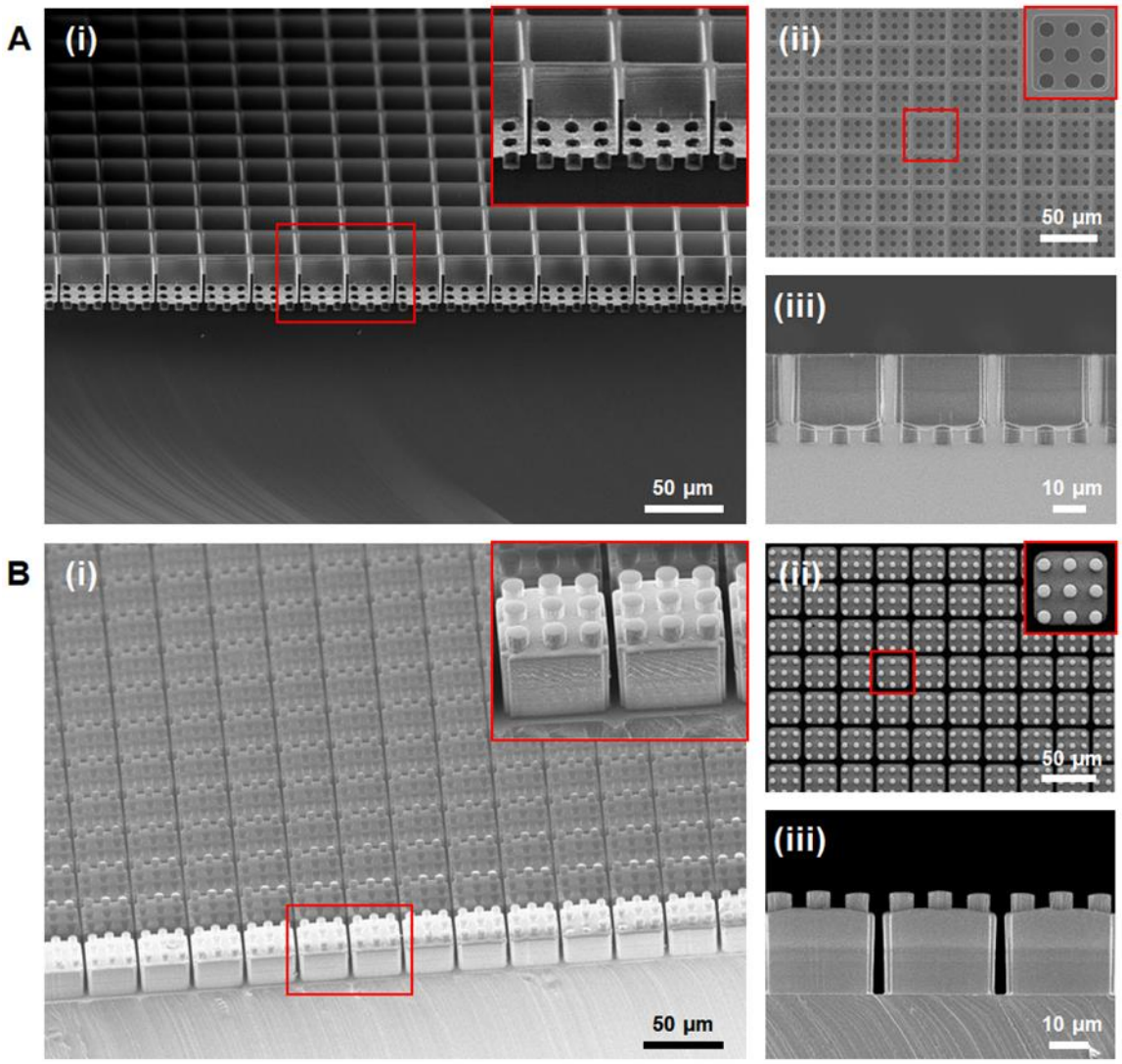

Fig. 2. Fabrication of Si master mold and h-PDMS stamp. SEM images of the ice cube tray-shaped (**A**) Si master mold, and (**B**) h-PDMS stamp showing (**i**) a tilted view, (**ii**) a top view, and (**iii**) a cross-sectional view, respectively. The inset images show a magnified view of the microstructures of the fabricated Si master mold and h-PDMS stamp.

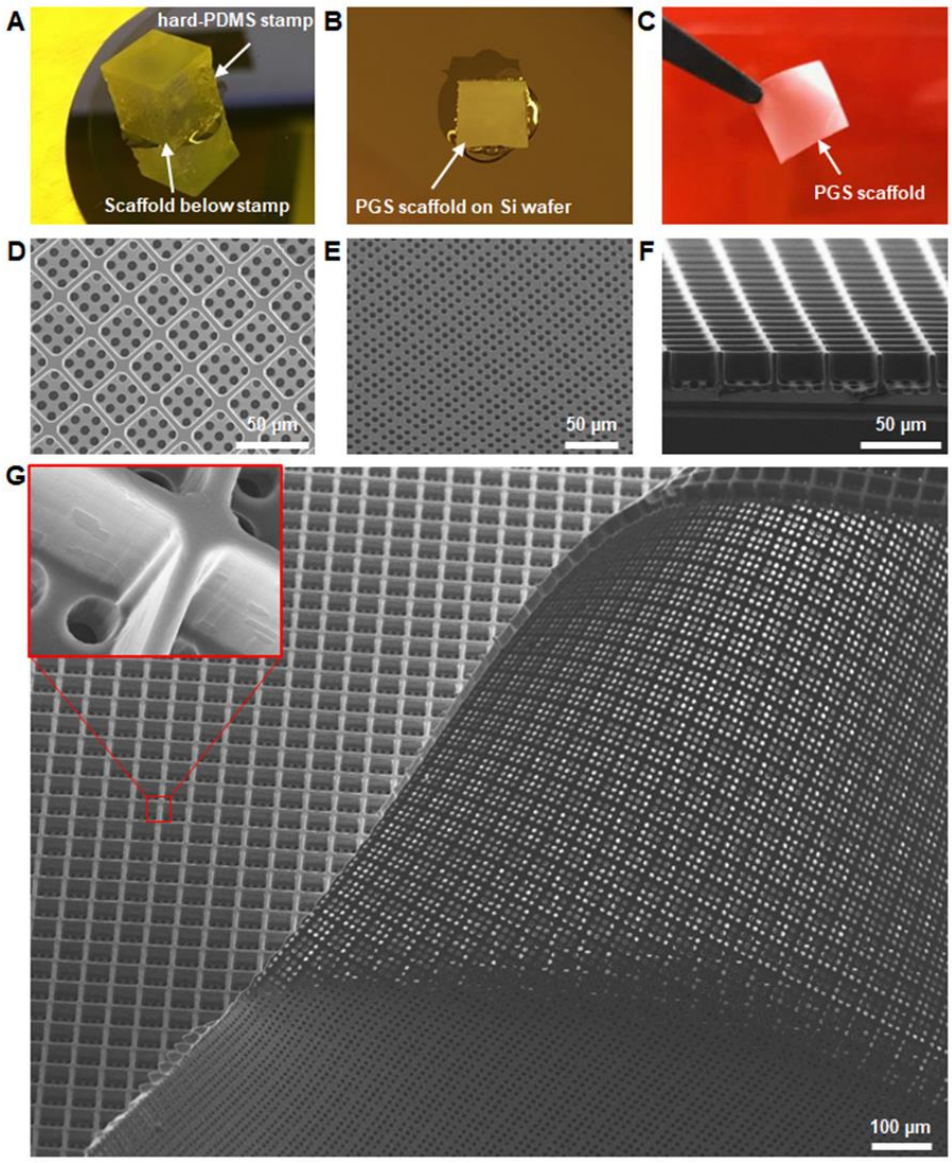

Fig. 3. Fabrication of the PGS ice cube tray PR scaffold. (**A to C**) Low magnification photographic images depicting the fabrication process of the PGS ice cube tray PR scaffold. (**A**) h-PDMS stamp ready to be demounted from the scaffold on a Si wafer after complete PGS curing. (**B**) A PGS scaffold on the Si wafer after stamp removal. After removing scaffold edges, the scaffold was delaminated from the Si wafer using a single edge razor blade. (**C**) Fabricated PGS ice cube tray scaffold held with fine forceps. (**D to G**) SEM images of the fabricated ice cube tray retinal scaffold showing (**D**) a top view, (**E**) a bottom view, and (**F**) a cross-sectional view. (**G**) Large area SEM image of the fabricated scaffold and a magnified view of a scaffold reservoir wall (inset).

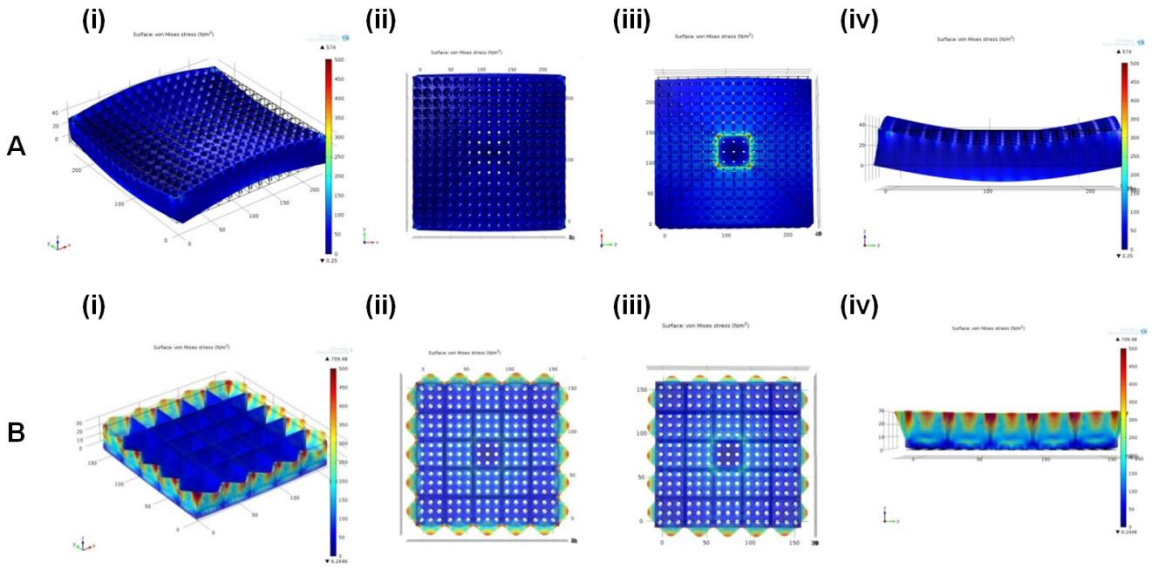

Fig. 4. Finite element analysis showing equivalent von Mises stress distribution in the PGS scaffolds. (**A**) Wineglass and (**B**) ice cube tray design under 5 N of tensile force in the x- and y-directions: (**i**) isometric view, (**ii**) top view, (**iii**) bottom view, and (**iv**) orthogonal view. The color bar shows the von Mises stress (in N/m^2) for an applied tensile force.

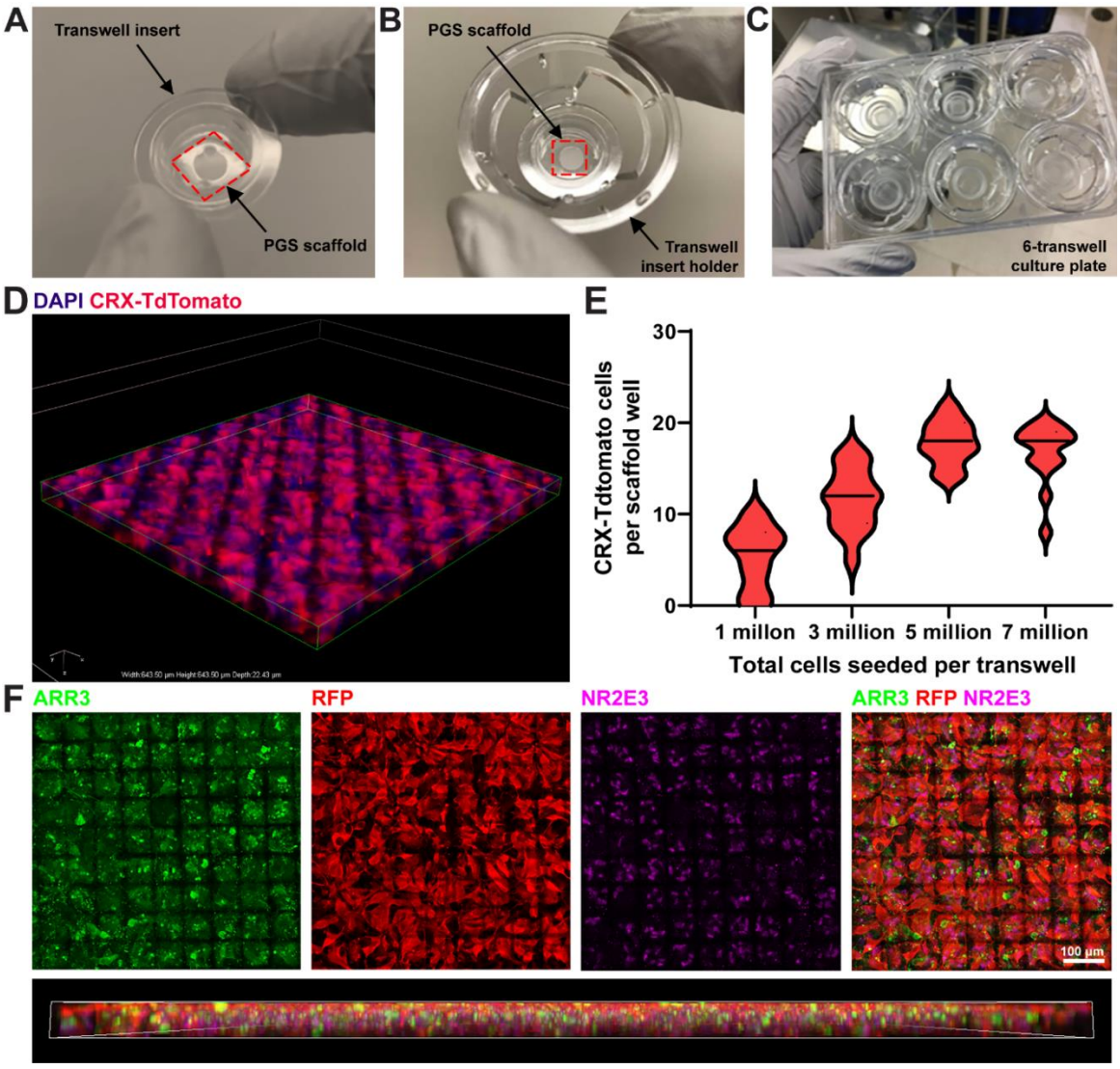

Fig. 5. Generation of PGS ice cube tray PR scaffold constructs. (**A to C**) Low magnification photographic images depicting scaffold mounting into the transwell insert. (**A**) Transwell insert with PGS scaffold below. The outer edge of the scaffold was glued to the transwell insert with soft PDMS. The area of the transwell insert removed to mount scaffolds was 19.6 mm^2 (internal diameter: 5 mm). (**B**) Transwell insert holder with a PGS ice cube tray scaffold mounted into a transwell insert. (**C**) 6-transwell scaffold cell culture system. (**D to F**) Laminin-coated ice cube tray scaffolds are readily filled with hPSC-derived $CRX^{+/tdTomato}$-expressing PRs (**D**) 3D rendering of a scaffold (176 µm × 185 µm × 22 µm) confirms successful capture of multiple PRs (labeled in red) in individual capture wells. Cell nuclei are labeled with DAPI (blue). (**E**) Cells were seeded onto scaffolds at varying densities to determine the minimum number required to achieve the maximum carrying capacity of $CRX^{+/tdTomato}$-PRs per well. Median (bold dashes)

and quartiles (fine dashes) are shown within individual violin plots. (**F**) Scaffolds seeded with CRX$^{+/tdTomato}$ PRs (RFP+, red) contain both ARR3-expressing cone PRs (green) and NR2E3-expressing rod PRs (pink). A 3D lateral view of the scaffold demonstrates relatively even distribution of ARR3+ cones and NR2E3+ rods. 3D rendering is 644 µm × 644 µm × 20 µm.

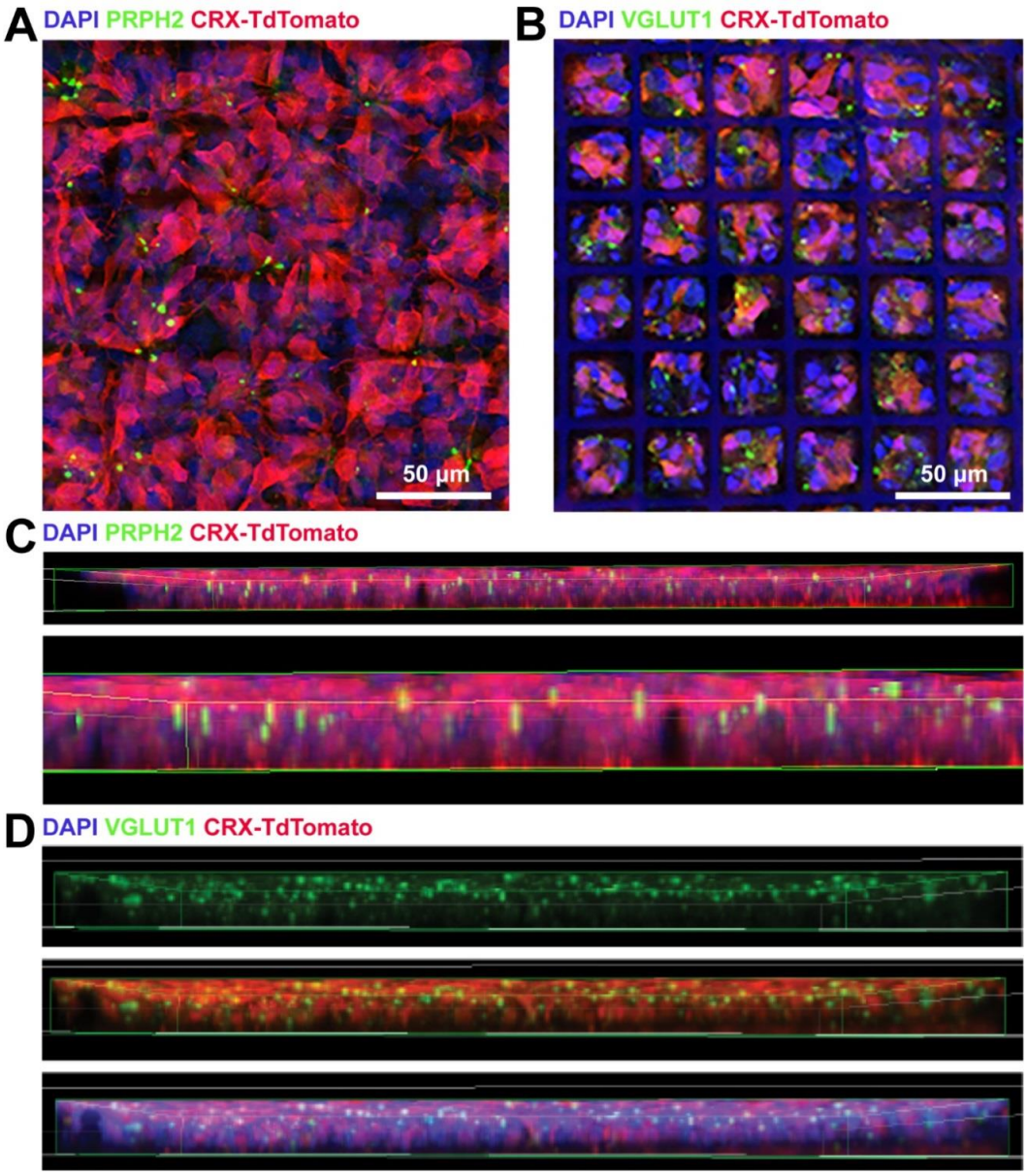

Fig. 6. Micro-patterned ice cube tray scaffolds support prearranged orientation of seeded PRs. (**A and B**) Maximum intensity projections of scaffold whole mounts seeded with $CRX^{+/tdTomato}$-PRs (red) revealed that PRs plated on scaffolds express PRPH2 (**3A**, green) and VGLUT1 (**3B**, green). DAPI-labeled cell nuclei and PGS autofluorescence are shown in blue. (**C**) PRPH2-positive outer segments were often oriented perpendicular to the base of the scaffold (inset magnified in underlying image). (**D**) Expression of presynaptic marker VGLUT1 (green) primarily localizes to the top portion of the scaffold. 3D renderings (**C** and **D**) are 644 µm × 644 µm × 20 µm.

Table 1. Structural and mechanical specifications for wineglass and ice cube tray scaffolds.

	Wineglass scaffold design (Jung and Phillips et al., 2018)	**Ice cube tray scaffold design**
Overall thickness [µm]	25	30
Space between through-holes [µm]	16	10
Through-holes [µm]	5 diameter, 10 depth (1 hole per capture well)	5 diameter, 5 depth (9 holes per capture well)
Capture well reservoir volume [mm^3]	0.177×10^{-5}	2.103×10^{-5}
Scaffold biomaterial volume (based on a 5 mm diameter scaffold) [mm^3]	0.34	0.169 **(50% less biomaterial)**
Young's modulus	1.18 MPa	1.3 MPa

Table 2. Cell payload advantages of ice cube tray versus wineglass scaffold designs.

	Wineglass scaffold design (Jung and Phillips et al., 2018)	**Ice cube tray scaffold design**
Average number of photoreceptors per capture well	1.3 ± 0.5	17.8 ± 2.4
Photoreceptors within a single scaffold [5 mm diameter or 19.63 mm^2]	1.005×10^5	3.412×10^5
Scaffold photoreceptor density [cells/mm^2] [$6.0 – 20.0 \times 10^4$ cells/mm^2 within the macula in healthy retina]	0.512×10^4	1.74×10^4

Supplemental Information

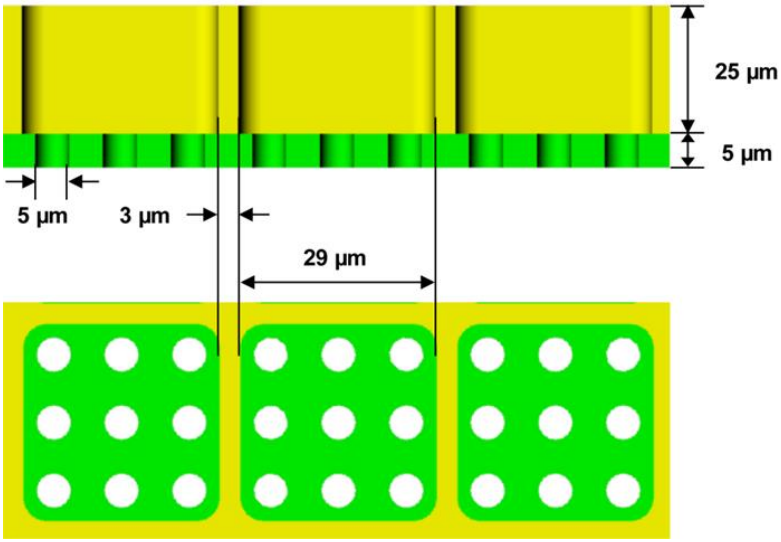

Fig. S1. Schematic illustration of the ice cube tray Si master mold. Detailed dimensions of the through-hole layer (green) and the reservoir layer (yellow) are as shown.

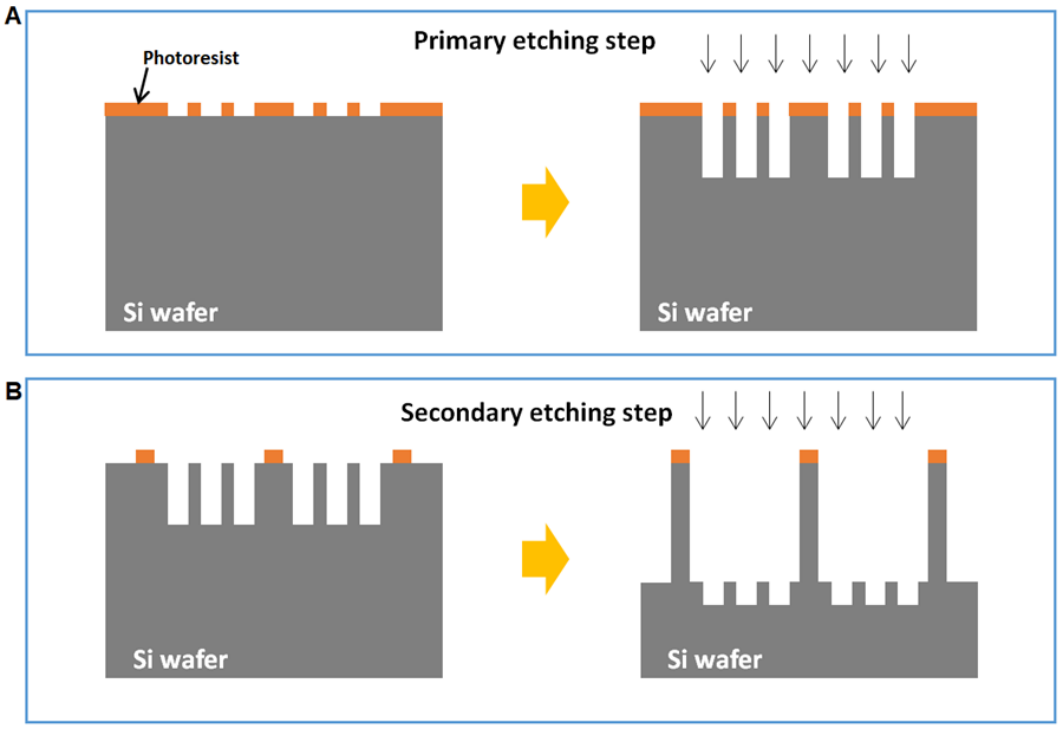

Fig. S2. Two-step Si master mold fabrication. Both microloading and RIE-lag effects influence the etch rate during (**A**) the primary etching step and (**B**) the secondary etching step.

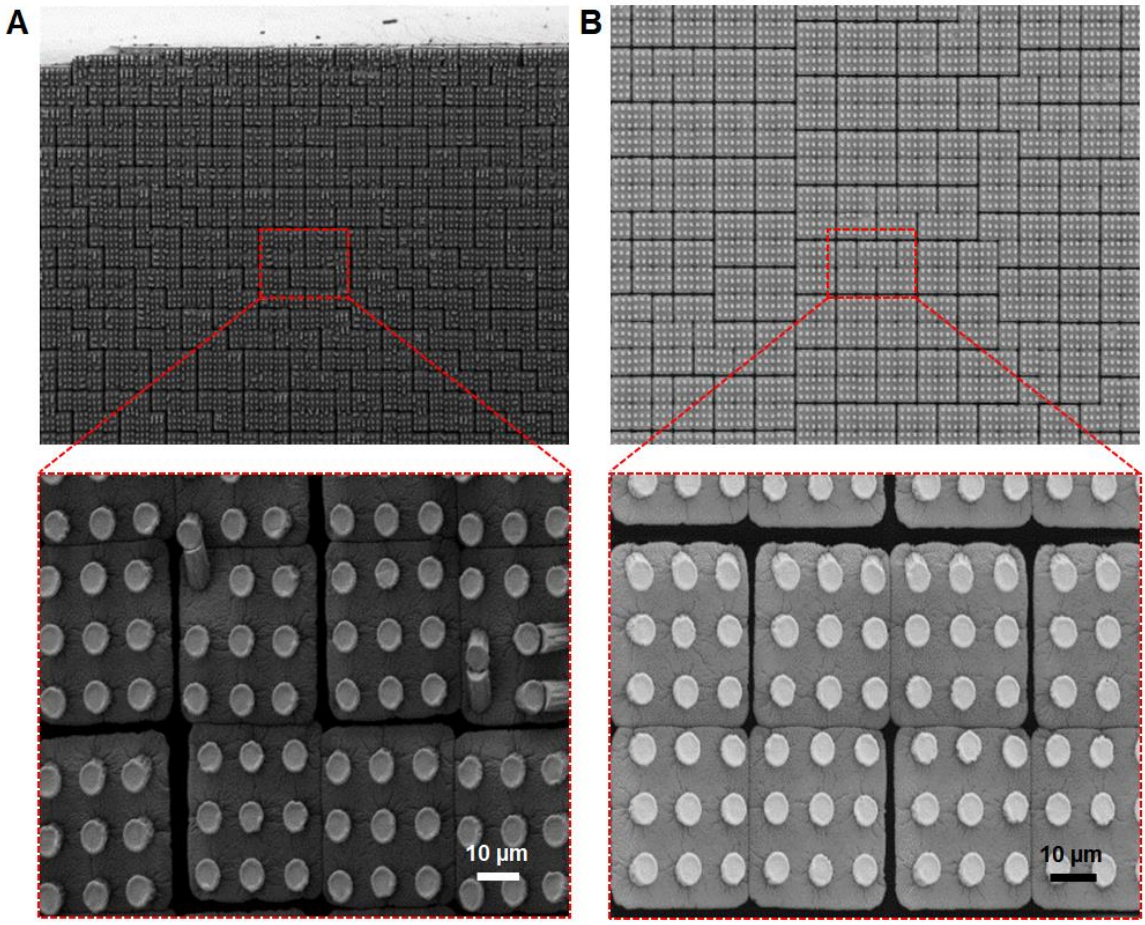

Fig. S3. SEM images of soft-PDMS stamp microstructures with differing ratios of silicone elastomer base and curing agent. (**A**) A soft-PDMS 10:1 (base: curing agent) stamp. (**B**) A soft-PDMS 4:1 stamp. Microstructures made from soft-PDMS were frequently deformed or adherent; as such, hard-PDMS was used for the final fabrication process.

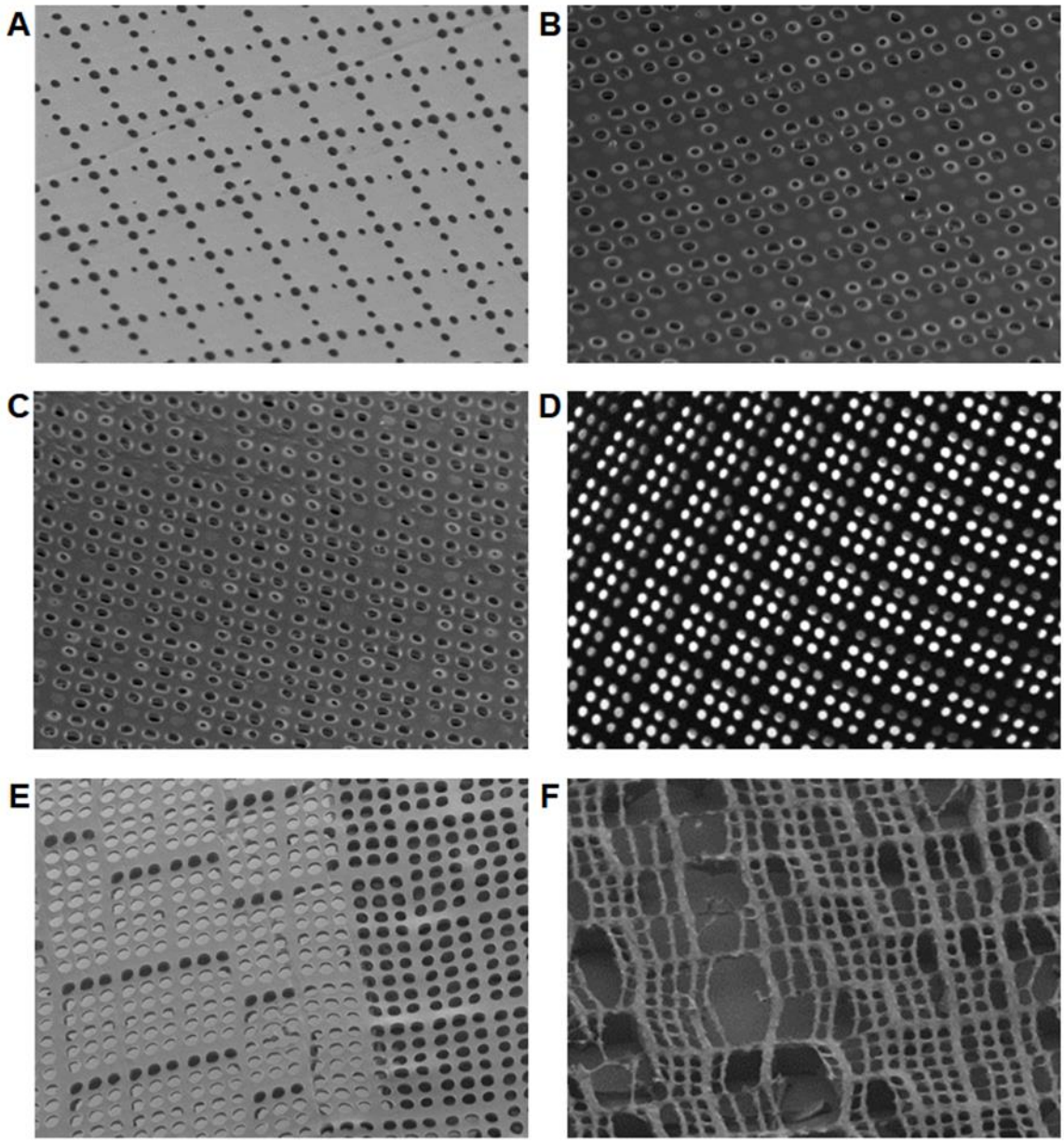

Fig. S4. SEM images (bottom view) of the PGS ice cube tray PR scaffolds fabricated with different molding weights. (**A**) 120 g. (**B**) 240 g. (**C**) 300 g. (**D**) 380 g. (**E**) 580 g. and (**F**) 780 g.

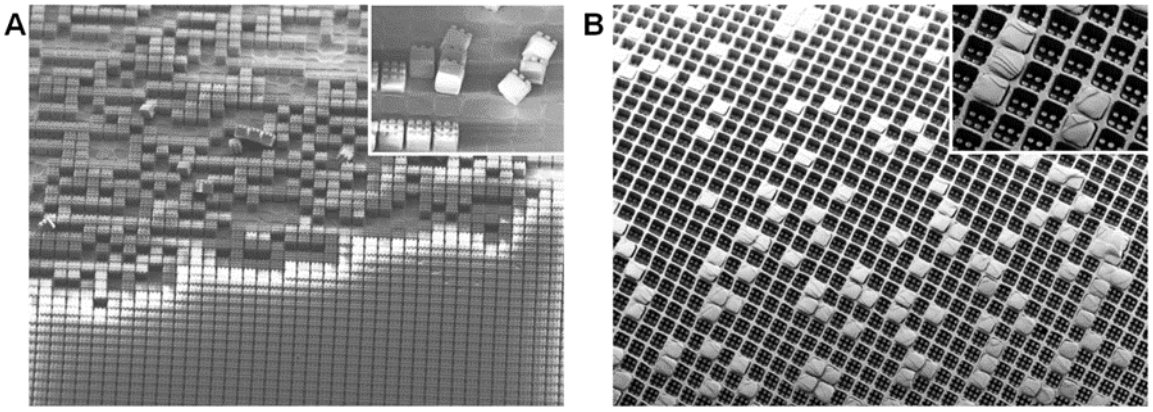

Fig. S5. SEM images of a h-PDMS stamp and a PGS ice cube tray PR scaffold after stamp demounting without isopropyl alcohol (IPA) soaking. (**A**) A h-PDMS stamp with microstructures broken or damaged during the demounting process. (**B**) A PGS ice cube tray PR scaffold with broken h-PDMS microstructures after stamp demounting.

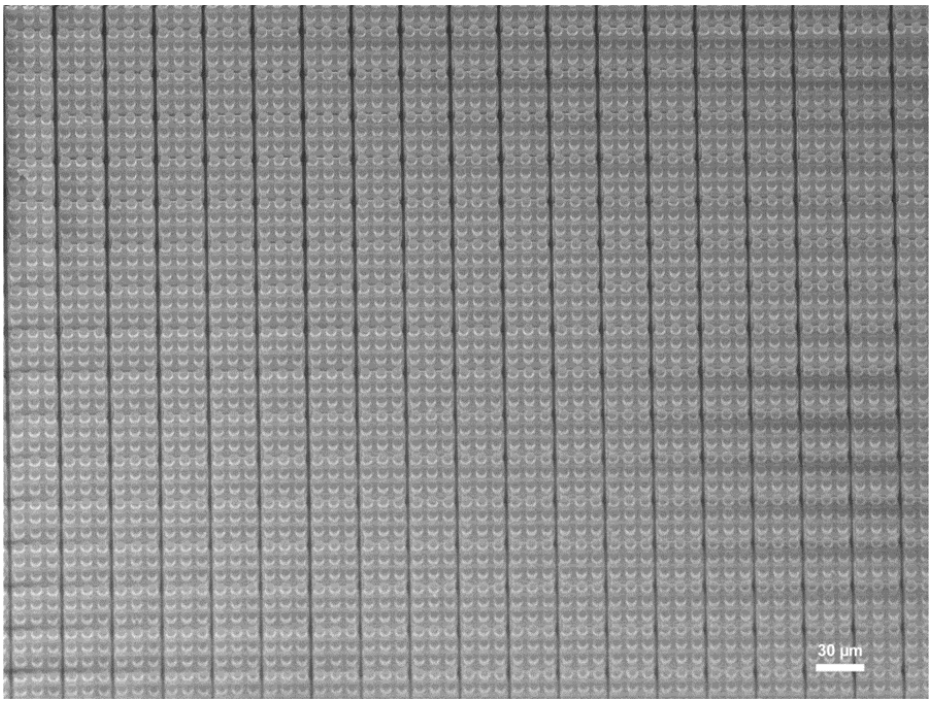

Fig. S6. SEM image of a h-PDMS stamp (top view) after demounting from a Si master mold in an IPA solution. Immersion in the IPA solution resulted in smooth demounting of the stamp.

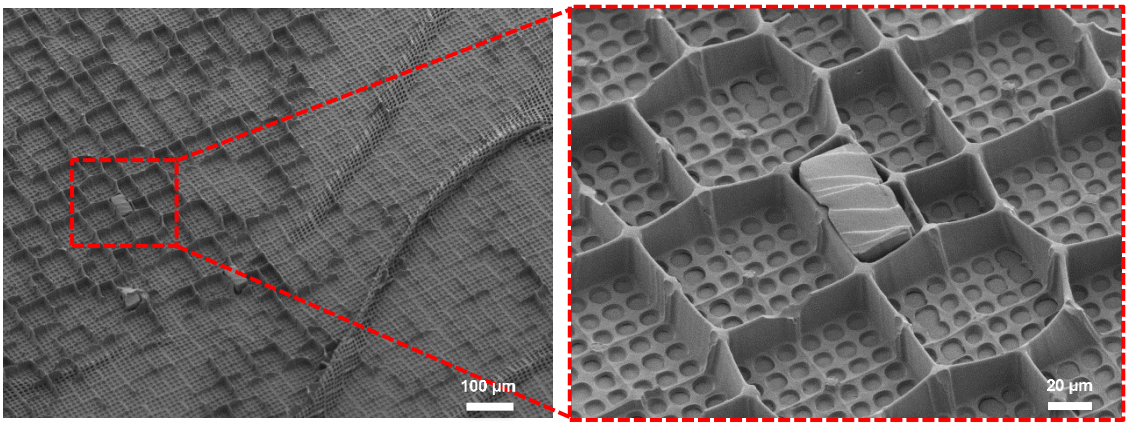

Fig. S7. SEM images of torn PGS scaffold reservoir walls. The PGS scaffold reservoir walls were damaged during the demounting process when spacing between wells was reduced (i.e., walls were <3 µm).

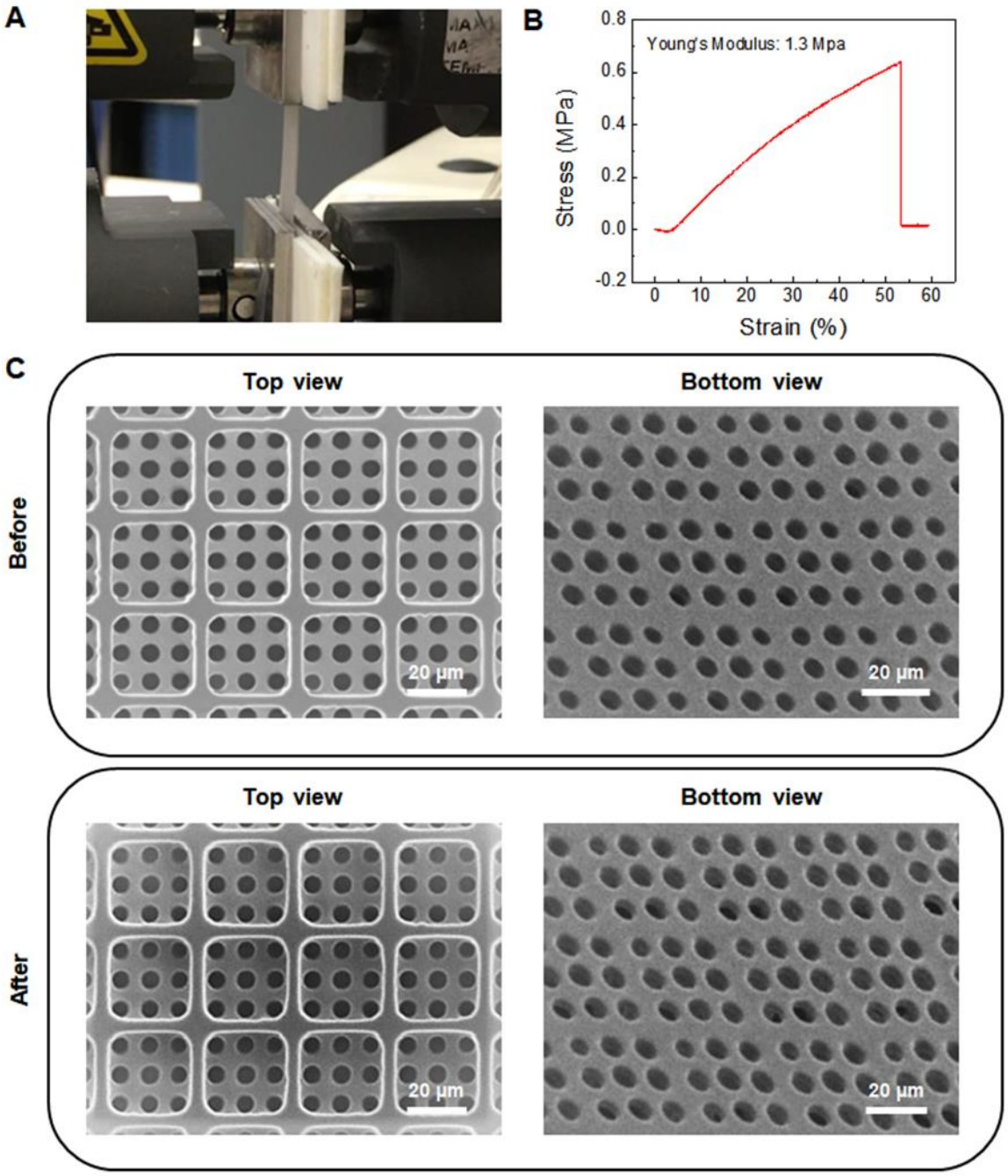

Fig. S8. Tensile stress test for the fabricated PGS ice cube tray PR scaffold. (**A**) Low magnification photographic image of the PGS scaffold during a tensile stress. (**B**) Tensile stress-strain curve of the PGS scaffold. (C) SEM images comparing PGS scaffold surfaces before and after the tensile strain.

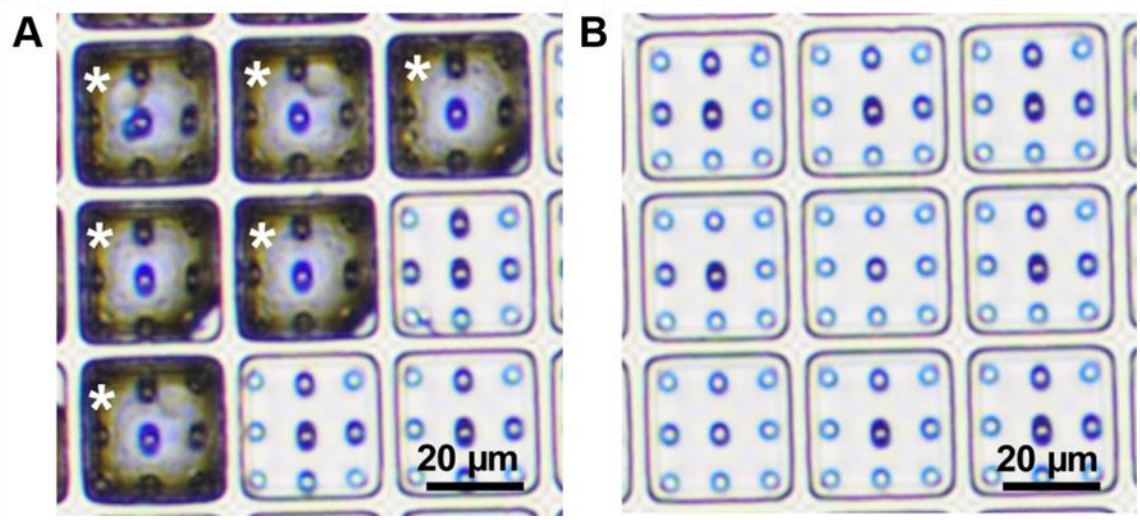

Fig. S9. Light microscopic images of laminin-coated PGS ice cube tray scaffolds. (**A**) Scaffold surfaces with poor water wettability often result in formation of microbubbles within scaffold capture wells (asterisks), which prevent laminin from effectively polymerizing on scaffold surfaces, and thus decreasing PR capture. (**B**) Proper treatment with O_2 plasma prevents the formation of microbubbles within scaffold capture wells, facilitating uniform surface coating with laminin prior to PR capture.

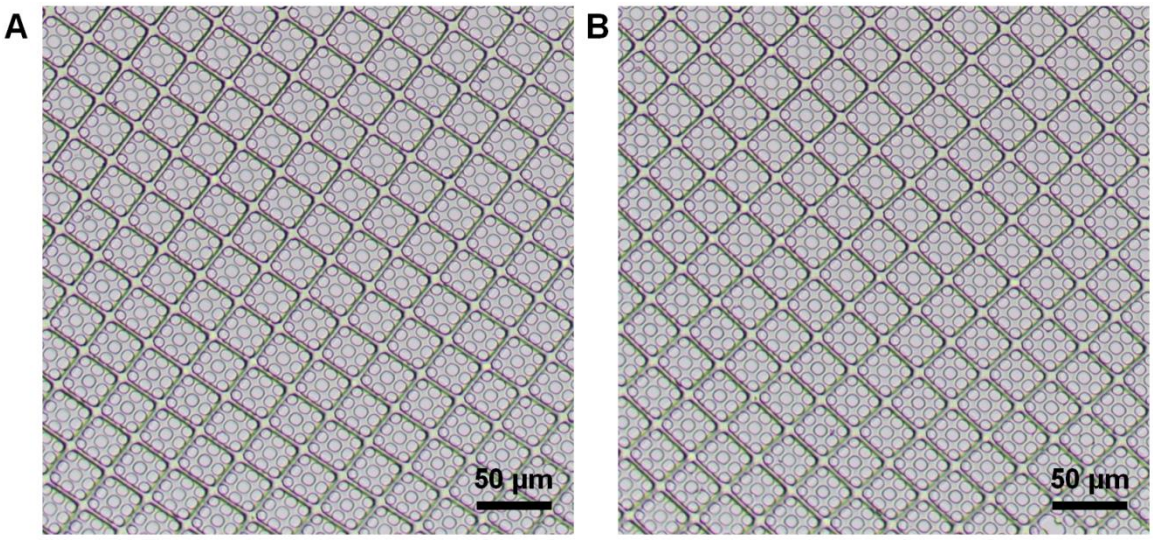

Fig. S10. Light microscopic images of empty PGS ice cube tray scaffolds. Images were taken (**A**) before and (**B**) after ethylene oxide gas sterilization, revealing no alterations to scaffold microstructures.

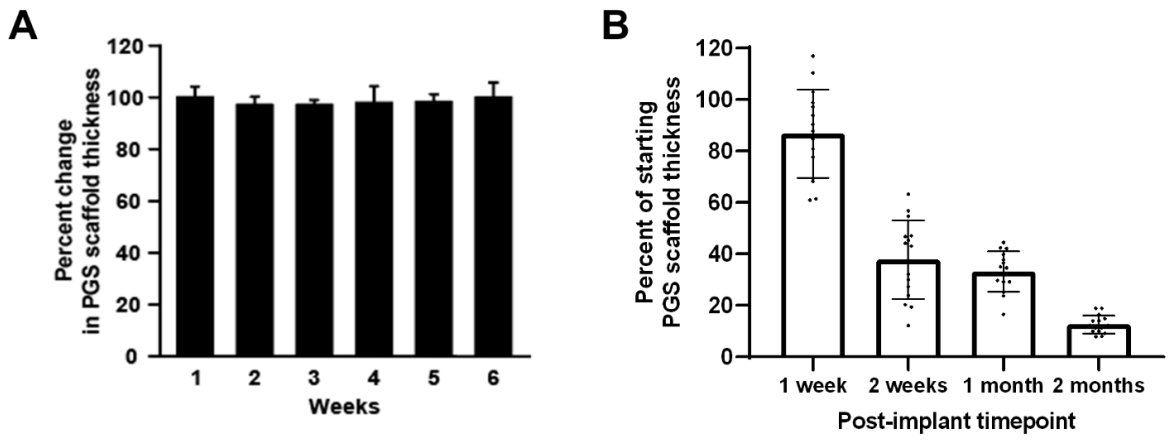

Fig. S11. In vitro stability and in vivo biodegradation of PGS ice cube tray scaffolds. (**A**) Longitudinal in vitro spectral domain optical coherence tomography (SD-OCT) imaging of PGS ice cube tray scaffolds. No significant change in scaffold thickness from baseline was detected over 6 weeks in culture. Bars represent the average percentage of baseline scaffold thickness for 3 scaffolds (1 seeded with hPSC-PRs and 2 unseeded controls) at each timepoint; error bars represent the standard deviation. (**B**) In vivo biodegradation of the PGS ice cube tray scaffold in nude rats. Each point represents an individual scaffold thickness measurement (n=15/scaffold); bars represent the average scaffold thickness in one eye at each timepoint after subretinal implantation.

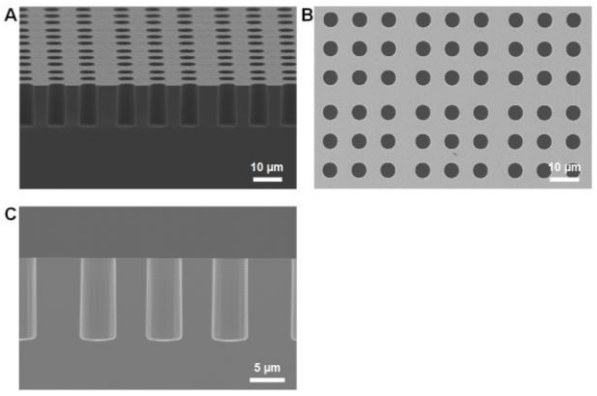

Fig. S12. SEM images of through-hole trenches on a Si wafer. (**A**) An orthogonal view. (**B**) A top view. (**C**) A cross sectional view.

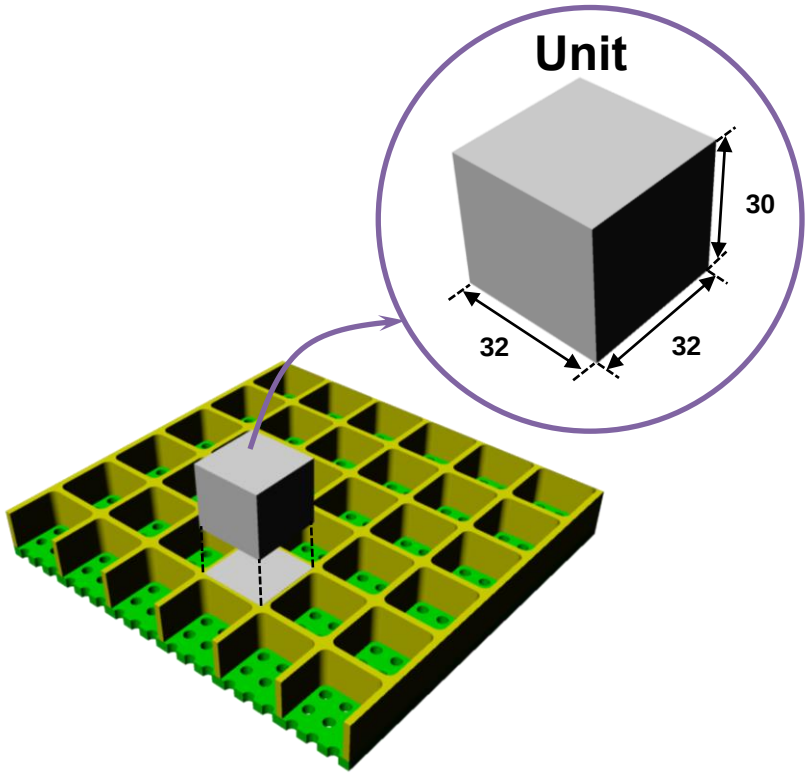

Fig. S13. Schematic illustration of a single reservoir unit of the ice cube tray scaffold showing its detailed dimensions. It measures 32 μm in length/width and 30 μm in depth.

Equation S1. Mathematical calculation of the number of reservoirs (n_{res}) contained within the area of the single 5 mm diameter round scaffold. A_{scaf} is the area of a single scaffold (19.63 mm^2, or the area of a 5 mm diameter circular scaffold) and A_{ru} is the area of a single reservoir unit, which is defined as a square area centered in the middle of one reservoir and extending in all four orthogonal directions to a point mid-way to the center of each adjacent reservoir as shown in fig. S13.

$$\mathbf{n_{res} = A_{scaf} / A_{ru}} \quad (1)$$

Equation S2. Estimated cell carrying capacity of a single scaffold, defined as the estimated number of PRs present within a single 5 mm diameter round scaffold. n_{PR} is defined as the average number of PRs counted in a single reservoir.

$$\textbf{Cell carrying capacity = nPR × nres} \quad (2)$$

Equation S3. Mathematical calculation of the scaffold biomaterials volume (V_{scaf}) used for generating a PGS scaffold (based on a single 5 mm diameter scaffold). V_{ru} is the volume of a single reservoir unit (fig. S13). V_{th} and V_{res} are defined as the volume of through-hole(s) within a single reservoir unit and the volume of a reservoir within a single reservoir unit, respectively.

$$\textbf{Vscaf = \{Vru – (Vth + Vres)\} × nres} \quad (3)$$

Table S1. Primary antibodies used for scaffold whole mount immunostaining.

Antibody	Source	Catalog number	Host	Dilution
Cone arrestin (ARR3)	Novus	NBP1-37003	Goat	1:300
NR2E3	Abcam	ab172542	Mouse	1:300
Peripherin (PRPH2)	Proteintech	18109-1-AP	Rabbit	1:500
RFP	Rockland	600-401-379	Rabbit	1:300
TdTomato	SICGEN	AB8181-200	Goat	1:300
VGLUT1	Millipore	AB5905	Guinea Pig	1:1000

References

1. Flaxman, S. R. *et al.* Global causes of blindness and distance vision impairment 1990-2020: a systematic review and meta-analysis. *The Lancet. Global health* **5**, e1221–e1234 (2017).
2. Cockerham, G. C. *et al.* Closed-Eye Ocular Injuries in the Iraq and Afghanistan Wars. *New England Journal of Medicine* **364**, 2172–2173 (2011).
3. Garafalo, A. V. *et al.* Progress in treating inherited retinal diseases: Early subretinal gene therapy clinical trials and candidates for future initiatives. *Progress in Retinal and Eye Research* 100827 (2019) doi:10.1016/j.preteyeres.2019.100827.
4. Singh, M. S. *et al.* Retinal stem cell transplantation: Balancing safety and potential. *Progress in Retinal and Eye Research* **75**, 100779 (2020).
5. Gamm, D. M., Wong, R. & Panelists, and the A. W. Report on the National Eye Institute Audacious Goals Initiative: Photoreceptor Regeneration and Integration Workshop. *Trans. Vis. Sci. Tech.* **4**, 2–2 (2015).
6. Verbakel, S. K. *et al.* Non-syndromic retinitis pigmentosa. *Progress in Retinal and Eye Research* **66**, 157–186 (2018).
7. Thompson, D. A. *et al.* Advancing Therapeutic Strategies for Inherited Retinal Degeneration: Recommendations From the Monaciano Symposium. *Invest. Ophthalmol. Vis. Sci.* **56**, 918–931 (2015).
8. Stern, J. H. *et al.* Regenerating Eye Tissues to Preserve and Restore Vision. *Cell Stem Cell* **22**, 834–849 (2018).
9. Zarbin, M. Cell-Based Therapy for Retinal Disease: The New Frontier. *Methods Mol. Biol.* **1834**, 367–381 (2019).

10. Meyer, J. S. *et al.* Modeling early retinal development with human embryonic and induced pluripotent stem cells. *Proceedings of the National Academy of Sciences of the United States of America* **106**, 16698–703 (2009).
11. Capowski, E. E. *et al.* Reproducibility and staging of 3D human retinal organoids across multiple pluripotent stem cell lines. *Development* **146**, dev171686 (2019).
12. Sharma, R., Bose, D., Maminishkis, A. & Bharti, K. Retinal Pigment Epithelium Replacement Therapy for Age-Related Macular Degeneration: Are We There Yet? *Annual Review of Pharmacology and Toxicology* **60**, 553–572 (2020).
13. Baldassarre, J. S., Joseph, A., Keane, M. & Heier, J. S. Subretinal Delivery of Cells via the Suprachoroidal Space: Janssen Trial. in *Cellular Therapies for Retinal Disease: A Strategic Approach* (eds. Schwartz, S. D., Nagiel, A. & Lanza, R.) 95–104 (Springer International Publishing, 2017). doi:10.1007/978-3-319-49479-1_8.
14. Gasparini, S. J., Llonch, S., Borsch, O. & Ader, M. Transplantation of photoreceptors into the degenerative retina: Current state and future perspectives. *Progress in retinal and eye research* (2018) doi:10.1016/j.preteyeres.2018.11.001.
15. Singh, D. *et al.* A biodegradable scaffold enhances differentiation of embryonic stem cells into a thick sheet of retinal cells. *Biomaterials* **154**, 158–168 (2018).
16. Neeley, W. L. *et al.* A microfabricated scaffold for retinal progenitor cell grafting. *Biomaterials* **29**, 418–26 (2008).
17. Ahmed, T. A. E., Ringuette, R., Wallace, V. A. & Griffith, M. Autologous fibrin glue as an encapsulating scaffold for delivery of retinal progenitor cells. *Front Bioeng Biotechnol* **2**, 85 (2014).
18. Tomita, M. *et al.* Biodegradable polymer composite grafts promote the survival and differentiation of retinal progenitor cells. *Stem cells (Dayton, Ohio)* **23**, 1579–88 (2009).

19. Shrestha, A., Allen, B. N., Wiley, L. A., Tucker, B. A. & Worthington, K. S. Development of High-Resolution Three-Dimensional-Printed Extracellular Matrix Scaffolds and Their Compatibility with Pluripotent Stem Cells and Early Retinal Cells. *J Ocul Pharmacol Ther* (2019) doi:10.1089/jop.2018.0146.
20. Yao, J. *et al.* Enhanced differentiation and delivery of mouse retinal progenitor cells using a micropatterned biodegradable thin-film polycaprolactone scaffold. *Tissue Eng Part A* **21**, 1247–1260 (2015).
21. McUsic, A. C., Lamba, D. A. & Reh, T. A. Guiding the morphogenesis of dissociated newborn mouse retinal cells and hES cell-derived retinal cells by soft lithography-patterned microchannel PLGA scaffolds. *Biomaterials* **33**, 1396–405 (2012).
22. Baranov, P., Michaelson, A., Kundu, J., Carrier, R. L. & Young, M. Interphotoreceptor matrix-poly(ϵ-caprolactone) composite scaffolds for human photoreceptor differentiation. *J Tissue Eng* **5**, 2041731414554139 (2014).
23. Tucker, B. A. *et al.* The use of progenitor cell/biodegradable MMP2-PLGA polymer constructs to enhance cellular integration and retinal repopulation. *Biomaterials* **31**, 9–19 (2010).
24. Worthington, K. S. *et al.* Two-photon polymerization for production of human iPSC-derived retinal cell grafts. *Acta Biomater* **55**, 385–395 (2017).
25. Thompson, J. R. *et al.* Two-photon polymerized poly(caprolactone) retinal cell delivery scaffolds and their systemic and retinal biocompatibility. *Acta biomaterialia* (2019) doi:10.1016/j.actbio.2019.04.057.
26. Jung, Y. H. *et al.* 3D Microstructured Scaffolds to Support Photoreceptor Polarization and Maturation. *Advanced materials (Deerfield Beach, Fla.)* **30**, e1803550 (2018).
27. Polyak, S. *The retina*. (University of Chicago Press, 1941).

28. Curcio, C. A. & Allen, K. A. Topography of ganglion cells in human retina. *J. Comp. Neurol.* **300**, 5–25 (1990).

29. Lujan, B. J. *et al.* Directional Optical Coherence Tomography Provides Accurate Outer Nuclear Layer and Henle Fiber Layer Measurements. *Retina* **35**, 1511–1520 (2015).

30. Yu, Y. *et al.* Developing a potential retinal OCT biomarker for local growth of geographic atrophy. *Biomed Opt Express* **11**, 5181–5196 (2020).

31. Jonas, J. B., Schneider, U. & Naumann, G. O. H. Count and density of human retinal photoreceptors. *Graefe's Arch Clin Exp Ophthalmol* **230**, 505–510 (1992).

32. Prévot, P.-H. *et al.* Behavioural responses to a photovoltaic subretinal prosthesis implanted in non-human primates. *Nat Biomed Eng* (2019) doi:10.1038/s41551-019-0484-2.

33. Kador, K. E. & Goldberg, J. L. Scaffolds and stem cells: delivery of cell transplants for retinal degenerations. *Expert Rev Ophthalmol* **7**, 459–470 (2012).

34. Trese, M., Regatieri, C. V. & Young, M. J. Advances in Retinal Tissue Engineering. *Materials (Basel)* **5**, 108–120 (2012).

35. Jones, I. L., Warner, M. & Stevens, J. D. Mathematical modelling of the elastic properties of retina: A determination of Young's modulus. *Eye* **6**, 556–559 (1992).

36. Sharma, R. *et al.* Clinical-grade stem cell-derived retinal pigment epithelium patch rescues retinal degeneration in rodents and pigs. *Sci Transl Med* **11**, (2019).

37. Ghosh, F., Neeley, W. L., Arnér, K. & Langer, R. Selective Removal of Photoreceptor Cells In Vivo Using the Biodegradable Elastomer Poly(Glycerol Sebacate). *Tissue Engineering Part A* **17**, 1675–1682 (2009).

38. Redenti, S. *et al.* Engineering retinal progenitor cell and scrollable poly(glycerol-sebacate) composites for expansion and subretinal transplantation. *Biomaterials* **30**, 3405–3414 (2009).

39. Rai, R., Tallawi, M., Grigore, A. & Boccaccini, A. R. Synthesis, properties and biomedical applications of poly(glycerol sebacate) (PGS): A review. *Progress in Polymer Science* **37**, 1051–1078 (2012).

40. Hynes, S. R. & Lavik, E. B. A tissue-engineered approach towards retinal repair: Scaffolds for cell transplantation to the subretinal space. *Graefes Arch Clin Exp Ophthalmol* **248**, 763–778 (2010).

41. Zhang, H., Jackson, J. K. & Chiao, M. Microfabricated Drug Delivery Devices: Design, Fabrication, and Applications. *Advanced Functional Materials* **27**, 1703606 (2017).

42. Karttunen, J., Kiihamaki, J. & Franssila, S. Loading effects in deep silicon etching. in *Micromachining and Microfabrication Process Technology VI* vol. 4174 90–97 (International Society for Optics and Photonics, 2000).

43. Wu, B., Kumar, A. & Pamarthy, S. High aspect ratio silicon etch: A review. *Journal of Applied Physics* **108**, 051101 (2010).

44. Laermer, F., Franssila, S., Sainiemi, L. & Kolari, K. Chapter 21 - Deep Reactive Ion Etching. in *Handbook of Silicon Based MEMS Materials and Technologies (Second Edition)* (eds. Tilli, M. et al.) 444–469 (William Andrew Publishing, 2015). doi:10.1016/B978-0-323-29965-7.00021-X.

45. Kim, M. J., Hwang, M. Y., Kim, J. & Chung, D. J. Biodegradable and Elastomeric Poly(glycerol sebacate) as a Coating Material for Nitinol Bare Stent. *Biomed Res Int* **2014**, (2014).

46. Liu, M., Wang, S. & Jiang, L. Nature-inspired superwettability systems. *Nature Reviews Materials* **2**, 1–17 (2017).

47. Jo, H., Park, H. S. & Kim, M. H. Single bubble dynamics on hydrophobic–hydrophilic mixed surfaces. *International Journal of Heat and Mass Transfer* **93**, 554–565 (2016).

48. Shintani, H. Ethylene Oxide Gas Sterilization of Medical Devices. *Biocontrol Sci* **22**, 1–16 (2017).

49. Phillips, M. J. *et al.* A Novel Approach to Single Cell RNA-Sequence Analysis Facilitates In Silico Gene Reporting of Human Pluripotent Stem Cell-Derived Retinal Cell Types. *Stem Cells* **36**, 313–324 (2018).

50. Pearson, R. A. *et al.* Restoration of vision after transplantation of photoreceptors. *Nature* **485**, 99–103 (2012).

51. Westheimer, G. Directional sensitivity of the retina: 75 years of Stiles–Crawford effect. *Proc Biol Sci* **275**, 2777–2786 (2008).

52. Yellott, J. I. *The Photoreceptor Mosaic as an Image Sampling Device*. (National Academies Press (US), 1990).

53. Stuck, M. W., Conley, S. M. & Naash, M. I. PRPH2/RDS and ROM-1: Historical context, current views and future considerations. *Prog Retin Eye Res* **52**, 47–63 (2016).

54. Liu, Z., Yu, N., Holz, F. G., Yang, F. & Stanzel, B. V. Enhancement of retinal pigment epithelial culture characteristics and subretinal space tolerance of scaffolds with 200 nm fiber topography. *Biomaterials* **35**, 2837–2850 (2014).

55. Alexander, J. P., Bradley, J. M., Gabourel, J. D. & Acott, T. S. Expression of matrix metalloproteinases and inhibitor by human retinal pigment epithelium. *Invest. Ophthalmol. Vis. Sci.* **31**, 2520–2528 (1990).

56. Wang, Y., Ameer, G. A., Sheppard, B. J. & Langer, R. A tough biodegradable elastomer. *Nat. Biotechnol.* **20**, 602–606 (2002).

57. Seiler, M. J. *et al.* A new immunodeficient pigmented retinal degenerate rat strain to study transplantation of human cells without immunosuppression. *Graefes Arch. Clin. Exp. Ophthalmol.* **252**, 1079–1092 (2014).

Chapter 5 -

Re-formation of synaptic connectivity in dissociated human stem cell-derived retinal organoid cultures

Ludwig, A. L. †, Mayerl, S. J. †, Gao, Y., Banghart, M., Bacig, C., Fernandez, A., Zhao, X., Gamm, D. M.

†These authors contributed equally to this work.

A revised version of this chapter has been accepted for publication:

Ludwig, A.L., Mayerl, S.J., Gao, Y., Banghart, M., Bacig, C., Fernandez Zepeda, M.A., Zhao, X., Gamm, D.M. (2023). Proceedings of the National Academy of Sciences USA. PMID: 36598946

Author contributions: D.M.G. and X.Z. established experimental aims and acquired funding. Y. G. designed and constructed the lentiviral vectors, produced lentivirus, and generated pseudotyped rabies virus for tracing experiments. A.L.L. and S.J.M. designed experiments with input from D.M.G, X.Z., and Y.G. A.L.L. and S.J.M. conducted experiments, collected data, analyzed data, and co-wrote the manuscript with input from all authors. C. Bacig and A. Fernandez produced and maintained retinal organoids. All authors contributed to critical discussion of experimental design, results, and interpretation.

Acknowledgements: The authors thank Dr. Rick Chappell (UW-Madison Dept. of Statistics) for statistical consultation , Dr. Karla Knobel (Waisman Center Cellular Imaging and Analysis Core) for high content imaging consultation, Dr. Edward Callaway (Salk Institute) for providing pseudotyped rabies virus stock, H. Adam Steinberg (Artforscience.com) for graphical consultation, and members of the Gamm lab for thoughtful discussion and critique of these experiments.

Introduction

Cajal's first observation of microscopic gaps between neurons more than a century ago[1] led to our current understanding of synaptic connections, which are required to establish the circuity of the CNS, including the neural retina. Within the retina, two plexiform layers of synapses sequentially relay neurosensory signals from photoreceptors (PRs) to retinal interneurons to retinal ganglion cells (RGCs). The first—the outer plexiform layer (OPL)—contains glutamatergic synapses between light-sensitive PRs (rods and cones) and interneurons (bipolar and horizontal cells, BPCs and HCs). The inner plexiform layer (IPL) comprises a network of synaptic connections between interneurons (BPCs, HCs, and amacrine cells, ACs) and retinal output RGCs.

Changes in the OPL are an early indicator of retinal degenerative diseases (RDDs)[2] and synaptic disassembly precedes the widespread neuronal death that defines end stages of RDDs like retinitis pigmentosa[3] and glaucoma[4], which target PRs and RGCs, respectively. Periods of cellular and synaptic remodeling exist during PR[5] and RGC[6] degenerations, suggesting the potential for tissue plasticity, but mammalian retinas are incapable of regenerating neurons once they have been lost in the course of disease or injury. As such, much effort has been directed toward strategies to restore vision in late-stage disease, either by exogenous introduction of new PRs[7] and RGCs[8] or endogenous re-purposing of surviving cell types[9,10]. Indeed, PR and RGC regeneration is the focal point of the multi-year Audacious Goals Initiative of the National Eye Institute[11] and similarly-focused research activities. The success of these programs and all PR and RGC cell replacement therapies hinges upon the ability of new retinal neurons to form synaptic contacts.

In preclinical animal model studies, human donor cells are most frequently delivered to the subretinal space as dissociated cell suspensions[12–17] or as sheets[18–22]. Both delivery approaches require transplanted retinal neurons to establish new synaptic connections in an

evolutionarily mismatched environment, which limits their potential to predict results in human patients. One way to begin to address this important limitation is to create a culture system capable of assessing whether singularized human retinal neurons can form *de novo* connections with each other. Ideally, the testing platform would utilize authentic retinal cell types and facilitate high through-put analysis with rigorous controls and rapid readouts.

From a cell source perspective, human pluripotent stem cell (hPSC)-derived retinal organoids (ROs) fulfill many of the aforementioned system criteria. ROs can be produced in virtually unlimited supply, and multiple studies have confirmed the authenticity of their retinal cell progeny. More specifically, extensive evidence indicates that PRs, RGCs, and other retinal neurons differentiated within ROs exhibit hallmark histologic, physiologic, and functional characteristics of developing retinal neurons[23–30]. Transcriptomic studies of RO-derived neurons have revealed synaptic marker transcripts to be among the most highly expressed in both RO-derived PRs[30–32] and RGCs[33,34]. Likewise, protein expression studies have shown robust, developmentally-appropriate localization of synaptic proteins within the putative plexiform layer(s) of ROs[23,24,35–38], and along processes of cultured retinal neurons extracted from dissociated ROs[26,39]. Importantly, the synapses and circuits that develop within intact ROs were recently confirmed to be functional using GCaMP6s imaging[24]. Thus, a growing body of in vitro evidence suggests that hPSC-derived retinal neurons are capable of forming *bona fide* functional synapses, at least within an unperturbed 3D organoid environment.

Despite xenograft limitations, modest alterations to light-evoked responses also have been reported after transplantation of hPSC-RO-derived PRs as single cells[12,13,15,40,41] or sectioned tissue sheets[19–22,42] in animal models *in vivo* or *in vitro*[12,41]. suggesting that some degree of *de novo* hPSC-RN synaptogenesis is possible. However, it can be difficult to determine whether such function is attributable to cell replacement with synaptic reconstruction or indirect effects on

host neurons via neuroprotective factors or biomaterial transfer[7,20,43,44]. Furthermore, nearly all existing electrophysiologic and behavioral tests used to assess outcomes of retinal neuron replacement in preclinical animal models rely on the assumption that synaptic connections with donor cells have occurred[12,12,13,15,19,21,22,40–42]. Direct demonstration of the innate capacity for cultured PRs and RGCs to form such connections would therefore increase confidence in their use a donor material for future clinical trials.

Synaptic tracing is a widely used approach for studying connections between neurons within the CNS[45,46]. Monosynaptic tracing with G-glycoprotein-deleted rabies virus (RVdG)—which travels retrograde across a single synapse—is the current gold standard for synaptic tracing studies[45] due to its relatively low neurotoxicity in short term culture and greater versatility relative to historically used viral tracers[47]. Combined with appropriate controls[46], monosynaptic RVdG tracing can serve as a powerful tool for studying existing and reconstructed neural circuits[48–50]. In the present study, we used monosynaptic RVdG tracing to ask a simple but as yet unanswered question: do hPSC-derived retinal neurons possess intrinsic potential to form new synapses after dissociation from organoids? We dissociated ROs and plated the resulting mixed population of retinal cell types in 96-well plates to permit subsequent analysis using automated high content imaging. After 10 days in culture, the retinal cell cultures were subjected to an established *in vitro* monosynaptic RVdG tracing assay, which revealed robust tracing of multiple types of retinal neurons, including PRs and RGCs. With appropriate titration of viral transduction levels and incorporation of rigorous controls, this system enables qualitative and quantitative assessment of RVdG transmission between retinal neurons. In addition, our results lend credence to the employment of RO-derived PRs and RGCs for cell replacement efforts.

Results

Dissociated hPSC-RO cultures contain multiple neuron classes and express synaptic proteins

Prior to investigating whether RO-derived neurons can reconnect following dissociation, we first needed to convert 3D ROs to a 2D culture system and determine the proportion of different cell classes that remained after plating. Stage 2 (day 80, or D80) wild type WA09[51] hPSC-ROs were produced as previously described[23], dissociated to a single cell suspension using papain, mixed, and plated onto individual wells of 96-well plates (200,000 cells/well) (**Fig. 1A**). D80 of differentiation was selected because ROs contain a cross-section of retinal neuron subpopulations at this timepoint, including including RGCs, interneurons, and PRs[23,52] (**Fig. 1B**), but do not yet contain many Müller glia. In addition, some neural retinal types, particularly RGCs, degenerate within ROs at later timepoints. Last, photoreceptors in older ROs are less tolerant of dissociation and more expensive to manufacture clinically, all of which favors the use of earlier stages for cell replacement therapies[7,8].

After dissociation and plating on day 80, cells were allowed to recover and extend neuronal processes for 20 days, whereupon they were fixed in paraformaldehyde and screened with a battery of previously-validated antibodies against neuroretinal cell fate markers (**Table 1**). Markers with consistent, reliable expression in the 2D cultures included CRX, RCVN, SNCG, and CALB. Other cell type-selective markers known to be expressed in intact ROs at this stage were not detected post-dissociation (**Table 1**), either due to selective cell loss or marker downregulation. With the limited battery of markers available, we were able to confidently distinguish the following broad classes of retinal cells: PRs (CRX, RCVN), RGCs (SNCG), and some retinal interneurons (CALB). Of note, none of these markers are wholly specific individually. For example, CRX is present in all PRs but is also found in some immature retinal pigment epithelial (RPE) cells[31]. However, unlike PRs, RPE cells do not express RCVN. In addition to marker expression, cell morphology and proliferative status were also used to delineate cell classes. RPE are large, flat, and do not have processes, whereas RGCs display long axons and PRs possess 1-2 short processes. Lastly, both retinal progenitor cells (RPCs) and RPE cells are

highly proliferative (Ki67+), whereas all neural retina cell classes of interest are post-mitotic. Based on these collective criteria, we were confident in assigning retinal neurons as either PRs, RGCs, or retinal interneurons, but we were not able to reliably distinguish between subclasses of retinal interneurons (ACs, HCs, BPCs).

After validating antibodies in the 2D system, we quantified cell populations via unbiased high content image analysis (HCIA) (**Fig. 1C**) in accordance with previously described methods[31,53]. A substantial population of Ki67-positive proliferative cells (20.8 ± 1.1% of DAPI-positive cells, *n* = 24 replicate wells) were observed (**Fig. S1A** and **1C**) in re-associated hPSC-RO cultures; at this stage of RO development, representing presumptive retinal pigment epithelium (RPE) and retinal progenitor cells (RPCs) [23,52]. SNCG+ RGCs (5.3 ± 1.3% of DAPI-positive cells, *n* = 12 replicate wells) and CALB+ cells (6.7 ± 0.9% of DAPI-positive cells, *n* = 16 replicate wells) were also detected (**Fig. 1C**). CRX+ cells—representing all PRs and some RPE[31]—predominated within dissociated 2D cultures (49.6 ± 2.0% of DAPI-positive cells, *n* = 32 replicate wells) (**Fig. S1B and 1C**). RCVN, expressed in PRs (and a subset of later-born BPCs[21]), was detected in 15.2 ± 0.4% of all DAPI-positive cells (*n* = 26 replicate wells) (**Fig. 1B and 1C**). Overall, the relative proportions of broad cell classes found in 2D cultures of dissociated ROs at 20 days post-plating approximated that of intact ROs at the time of dissociation[21,31].

We next examined the potential for plated retinal neurons to express synaptic markers 20 days after RO dissociation. Consistent with a recent study using developmentally-matched dissociated retinal neurons[56], expression of synaptic proteins was observed in RCVN+ PRs by day 20. More specifically, the presynaptic proteins vesicular glutamate transporter 1 (VGLUT1) and synaptophysin (SYP) frequently colocalized, forming puncta (**Fig. 1D**). To assure that any preexisting synaptic connections were abolished during dissociation, we also examined VGLUT1 localization at 1, 2, 5, and 20 d postplating. On day 1, rare photoreceptor processes were present,

none of which contained VGLUT1+ puncta. This finding is in accordance with Rempel et al.[56], who showed that synaptic proteins redistribute to the cytoplasm of photoreceptor cell bodies following dissociation of ROs with papain. Thereafter, the percentage of RCVN+ photoreceptors possessing processes with VGLUT1+ puncta increased substantially ($P < 0.05$, Kruskal–Wallis with pairwise Mann–Whitney U analyses, n = 3-4 20X images quantified per time point), reaching 29.5 ± 7.1% of RCVN+ cells by day 20 (**Fig. 1E**). Last, we immunostained for an additional synaptic marker, excitatory amino acid transporter 3 (EAAT3)[58], and observed EAAT3-positive puncta within SNCG-positive RGC neurites (**Fig. S1C**). Taken together, these results demonstrate the presence of three broad classes of retinal neurons in 2D plated cultures of dissociated ROs, with concurrent expression of synaptic proteins in RGCs and PRs.

Monosynaptic tracing assay design and validation

To determine whether RO-derived neurons could re-form synaptic connections following dissociation, we designed a monosynaptic tracing assay for validation in retinal neurons (**Fig. 2**). A replication-deficient rabies virus that includes an mCherry transgene (RaV-mCherry) was pseudotyped by replacing the *Rgp* gene (R), which encodes the rabies envelope glycoprotein and allows RaV to enter mammalian cells, with *EnvA*, an envelope glycoprotein-encoding gene specific to the avian sarcoma leukosis virus. EnvA-pseudotyping alters RaV tropism, eliminating its ability to infect mammalian cells and limiting its entry exclusively to cells expressing the avian sarcoma leukosis virus receptor, subgroup A (abbreviated TVA).

To facilitate controlled introduction of pseudotyped RaV-mCherry into retinal cells, we transduced a subset of dissociated “starter” cells with three transgenes: green fluorescent protein (nuclear GFP, to label the “starter” cells), TVA (to enable RaV-ΔR-mCherry cell entry) and Rgp (to facilitate retrograde RaV transmission across synaptic connections from “starter” cells to “traced” presynaptic cells) via lentivirus (lenti-GTR). Since efficient monosynaptic tracing requires

titration of TVA delivery to avoid excessive labeling of “traced” presynaptic cells[59,60], lentivirus transduction was optimized in re-associated hPSC-RO cultures to achieve sufficient identification of individually transduced cells (**Fig. S2**) in 2D cultures. Lentiviral transduction efficiencies between 1-5% were determined to be optimal for efficient tracing in re-associated hPSC-RO cultures.

For monosynaptic tracing experiments, re-associated hPSC-RO cultures were treated with lentivirus and RaV-ΔR-mCherry to label “starter” cells (i.e., those with a green nucleus and red cytoplasm) and “traced” presynaptic cells (i.e., those with a red cytoplasm alone) (**Fig. 2A**) for quantification with unbiased HCIA. As above, cultures were fixed on D100 for confocal (Nikon A1R) and high-content widefield imaging (Perkin-Elmer Operetta), enabling qualitative and quantitative analysis of synaptic tracing, respectively. A negative control (no lentivirus) was included to confirm that RaV uptake was exclusive to “starter” cells transduced with lentivirus; no lentivirus controls were treated with vehicle (1X phosphate buffered saline) ten days after dissociation (D90) and RaV-ΔR-mCherry on D95. In the absence of lentiviral delivery of TVA, no “starter” cells or “traced” presynaptic cells were observed (0.02%, [95% CI: 0.01, 0.04], n = 34 replicate wells) (**Fig. 2B**).

Recent studies have highlighted non-synaptic transfer of fluorescent reporter proteins—termed biomaterial transfer—as a potentially confounding variable in retinal cell replacement[44,61–65]. Similar concerns have been raised regarding the potential for non-synaptic spread of RVdG in monosynaptic tracing[46]. To control for biomaterial transfer (*i.e.*, non-synaptic spread of RaV-mCherry) a previously-validated Rgp-null control construct[60] was delivered via lentivirus (Lenti-GTΔR) (**Fig. 2C**). Lenti-GTΔR control cultures were transduced on D90 and infected with RaV-ΔR-mCherry on D95 as above, labeling a population of “starter” cells with a green nucleus and red cytoplasm. The median detection rate of artefactually “traced” presynaptic cells in lenti-GTΔR

controls was low in the absence of lentiviral Rgp delivery to “starter” cells (1.4% [95% CI: 1.1, 1.9] of DAPI-positive cells, *n* = 37 replicate wells), which is in line with prior reports[60,66] and consistent with only rare instances of nonsynaptic transfer of mCherry protein.

In dissociated hPSC-RO cultures containing “starter” cells treated with lenti-GTR (**Fig. 2D**), we observed a 5-fold increase in the detection of “traced” presynaptic cells relative to lenti-GTΔR controls (and a >200-fold increase relative to RaV only controls). The median proportion of “traced” cells was significantly higher ($p < 0.001$, Mood’s test of equal medians) within lenti-GTR + RaV cultures (6.2% [95% CI: 5.6, 6.9] of all DAPI-positive cells, *n* = 45 replicate wells $P < 0.00001$ for both comparisons using Mood’s test of equal medians) relative to lenti-GTΔR and RaV only controls (see **Fig. S3** for reproducibility across five independent differentiations). Synaptic contacts, as demonstrated by successful RaV-mCherry transmission, were thus readily identifiable within post-dissociation retinal neuron cultures.

Photoreceptors, retinal ganglion cells and interneurons contribute to “traced” cell populations

Finally, we sought to determine whether specific groups of retinal neurons—PRs, interneurons, and RGCs—were also among “traced” cell populations (**Fig. 3A**). Lenti-GTR + RaV treated cultures were co-labeled with the set of five cell type-specific markers validated in untraced cultures to determine the identity of “starter” and “traced” presynaptic cells (due to limitations of antibody cross-reactivity, only one cell type marker could be used per well). Qualitative examples of traced neuronal classes were followed with unbiased HCIA to assess which retinal neurons, if any, were consistently identifiable among “traced” cells. All three major classes of hPSC-RNs (**Fig. 3A**) were detected among “traced” presynaptic cells. “Starter” cells within lenti-GTR cultures were almost exclusively neural (**Fig. 3B**); CRX- or RCVN-positive PRs were the most prevalent (43.3 ± 4.5% and 44.8 ± 5.3% of all “starter” cells; *n* = 8 and 6 replicate wells, respectively) and were detected at a similar rate, suggesting that this population is

predominantly of PR origin. SNCG-positive RGCs (32.2 ± 5.7%, *n* = 8 replicate wells) and CALB-positive interneurons (12.0 ± 3.2%, *n* = 3 replicate wells) were the next most prevalent among "starter" neurons, while a smaller proportion (3.2 ± 0.9%, *n* = 6 replicate wells) were Ki67-positive.

As in "starter" cells, CRX- or RCVN-positive PRs were most frequently traced and were observed at similar rates (39.7 ± 4.1% and 41.1 ± 4.2% of "traced" presynaptic neurons, respectively; *n* = 8, *n* = 10 replicate wells, respectively) (**Fig. 3C and S4**), consistent with predominant labeling of PRs in both populations. RGCs were the second-most abundant, with SNCG-positive cells representing 19.0 ± 2.8% of all "traced" presynaptic neurons (*n* = 8 wells, *n* = 23 technical replicates per well). "Traced" presynaptic CALB-positive cells with interneuron-like morphology (larger soma and multiple dendrites) comprised 12.2 ± 0.6% of "traced" cells (*n* = 4). As an internal control, Ki67-positive cells (presumptive RPE, RPCs, and MG)—deemed unlikely to form synaptic contacts—were also quantified. Relative to neuronal cells, "traced" Ki67-positive cells were rarely detected (3.1 ± 1.1%). The synapse formation index (SFI)—a ratio of "traced" to "starter" cells—reflects the population-level average of "traced" presynaptic cells per "starter" cell. In lenti-GTR + RaV cultures the SFI was 1.3, consistent with connectivity slightly greater than 1-to-1 between "starter" and "traced" cells.

Discussion

These results demonstrate that hPSC-derived retinal neurons—predominantly PRs and RGCs—are capable of synaptogenesis after retinal organoid dissociation, forming synaptic puncta and traceable synaptic connections. Our characterization of post-dissociation hPSC-RN synapses extends the work of several elegant studies describing synaptic structure and function of hPSC-PRs and other organoid-derived retinal neurons[23,24,35,39]. A study led by Cowan *et al.* recently used two-photon imaging and the calcium indicator GCaMP6s to visualize—for the first time—evidence of functional synapses within retinal organoids. The origin of detected synaptic signals was

assumed by cells' relative intra-organoid location rather than marker colocalization, leaving the exact identity of contributing cells ambiguous, but Cowan *et al.* provided the strongest evidence to date that hPSC-RNs can in at least some cases form functional synapses in live organoids. Our work complements and builds upon these findings, suggesting that hPSC-RNs (especially those of interest for cell replacement) retain the capacity to form new synaptic contacts following dissociation. Monosynaptic RVdG tracing as used in the present study facilitates a systematic, quantitative approach to studying *de novo* synaptogenesis among hPSC-RNs during the optimal developmental window for retinal cell replacement. Though the strength of correlation between synaptic tracing and general synaptic function remains to be determined [46], our results demonstrate plasticity of hPSC-RN synaptic connections and highlight remarkable synaptogenic capacity in re-associated stage 2 organoid-derived retinal neurons.

This study specifically highlights the utility of monosynaptic RVdG tracing for identifying PR contributions to synaptic connections, which were a predominant feature among "traced" presynaptic neurons in our dataset. Despite wide adoption in CNS development and transplantation research (see Saleeba *et al.,* 2019[45] and Adler *et al.,* 2020[48]) as well as precedent for its use in the retina[67,68], monosynaptic RVdG tracing has not previously been applied to hPSC-RNs[7]. A recent review of PR transplantation by Gasparini et al. highlights prior ambiguity surrounding hPSC-PRs and monosynaptic tracing[7]: "…it must first be determined whether rabies or attenuated rabies viruses can actually spread to photoreceptors. While rabies viruses have been utilized in synaptic tracing to retinal ganglion cells…little has been demonstrated in terms of photoreceptor uptake." Work by Camelo et al. in the early 2000s suggested that retrograde transmission of wild type RaV halted at the level of the ganglion cell layer (potentially due to the presence of specialized ribbon synapses within the inner and outer plexiform layers) in RaV-induced ocular disease[69], raising the possibility that monosynaptic RVdG tracing would not effectively spread to interneurons or PRs and would thus be unusable for studying these

populations[7]. Our results suggest that this phenomenon is limited to wild type RaV, and that the pseudotyped RaV utilized here is in fact capable of spreading to hPSC-PRs via synaptic connections.

With rapid advancement toward human clinical trials for neuroretinal cell replacement[70–72], there is a growing need for hypothesis-driven research aimed at testing and understanding synaptic connectivity of hPSC-derived donor RNs. To date, there is a preponderance of indirect evidence consistent with low-to-modest rates of functional synaptogenesis following hPSC-PR transplantation in rodents and non-human primates [12–14,18,20,22,73], but the field still lacks direct and definitive evidence of afferent donor cell synaptic connections. Far less is known about the degree of synaptogenesis occurring after hPSC-RGC delivery [8]. The paradigm-shifting discovery of biomaterial transfer as a predominant mechanism in previous studies of PR transplantation [44,61–65] has underscored a growing need for direct investigation of mechanistic underpinnings in neuroretinal cell therapies [7,43,70]. Functional integration of donor hPSC-RNs requires afferent donor-to-host connections, and recent studies suggest that the degree to which these connections are formed may be lower than previously estimated [7,70,74,75]. Our approach provides a means of testing this and other hypotheses; beyond determining baseline rates of connectivity, it also affords opportunities to assess endogenous and exogenous factors which may modulate hPSC-RN synaptogenesis.

While identification of *de novo* synaptogenesis between hPSC-RNs is a critical first step, there are several aspects of this phenomenon that remain to be explored. Detection for interneurons in “starter” and “traced” presynaptic neurons was challenging in the present study. Their relative rarity at this developmental stage[23], downregulation of interneuron specific markers, and lower rates of monosynaptic RVdG tracing efficiency in neuromodulatory synapses[76] likely contributed to this observation. While our results are consistent with synaptic transmission

between connected hPSC-RNs, given the low rate of detection for interneurons, many of the "traced" presynaptic cells have presumably not formed typical PR-to-interneuron or interneuron-to-RGC synaptic connections. Nonetheless, these data suggest that hPSC-RNs retain a remarkable capacity for re-forming synaptic connections following singularization.

Conclusion

Collectively, we have developed a simple approach for identifying and quantifying synaptic contacts formed by hPSC-derived retinal neurons. Given a lack of robust anterograde synaptic labeling strategies, monosynaptic RVdG tracing as used in the present study represents one of few available strategies for definitively identifying hPSC-RN synaptic connections. A logical next step would be to utilize this approach for studying enriched populations of hPSC-RNs, though a current lack of specific cell surface markers for interneurons may limit its utility in studying specific patterns of connectivity. Although this system cannot currently be used in combination with fluorescent reporter lines, increasingly sophisticated methods for multiplex imaging may one day facilitate such approaches[77]. Ex vivo (*i.e*., retinal explant co-culture) and in vivo tracing could provide a translational workaround to this limitation; they also hold promise for addressing questions of synaptic efficiency in conspecific and xenogeneic transplantation [75]. With the inclusion of appropriate controls (i.e., lenti-GTΔR), this assay also serves as a powerful tool for distinguishing *bona fide* synapse formation from material transfer at the level of the synapse of interest, potentially providing a means for directly studying the mechanism behind vision recovery observed following hPSC-RN transplantation.

Materials and Methods

Retinal organoid differentiation

Stage 2 (day 80 of differentiation, D80) retinal organoids were differentiated from WA09 hPSCs (WiCell) according to a retinal differentiation protocol recently described by Capowski *et al*.[23].

Reagents and plasticware were obtained from Thermo Fisher unless otherwise indicated. hPSC colonies were maintained on Matrigel (WiCell) in MTesR Plus pluripotency media (STEMCELL Technologies) prior to initiating retinal differentiation (see **Table S2** for all media formulations). Colonies were lifted with ReLeSR passaging reagent (STEMCELL Technologies) and grown in suspension to form 3D embryoid bodies (EBs) on D0. EBs were gradually transitioned from pluripotency medium to neural induction medium (NIM) on D6. EBs were plated onto Matrigel on D7 and maintained with periodic NIM half media changes to reduce the BMP4 concentration through D15. On D16 cultures were transitioned to retinal differentiation medium (RDM) and maintained with thrice-weekly media changes until dissection. Near D30 of differentiation, retinal organoids were dissected and maintained in polyhydroxyethylmethacrylate (poly-HEMA, MilliporeSigma)-coated T25 flasks with twice weekly 3D RDM changes.

Virus production

Lenti-GFP-TVA-Rgp (lenti-GTR) and Lenti-GFP-TVA (lenti-GTΔR) were cloned using lenti-CMV-GFP vector as a backbone[78] and the CMV-GFP cassette was replaced with EF1-GFP-TVA-Rgp and EF1-GFP-TVA. The GFP-TVA-Rgp and GFP-TVA were cloned from yugao-1 (addgene plasmid #158208) and yugao-2 (addgene plasmid #158209) The sequence of the inserted cassette was confirmed by sequencing. Lentivirus production was performed as described previously[78] with modifications. Briefly, lentiviral DNA was co-transfected with packaging plasmids pMDL, REV and pCMV-Vsvg into HEK293T cells using the polyethylenimine (PEI) method. The viral transfer vector DNA and packaging plasmid DNA were transfected into one 15-cm dish of cultured HEK293T cells with PEI. The medium containing lentivirus was collected at 36, 60 and 84 hours post-transfection, pooled, filtered through a 0.2-μm filter, and concentrated using an ultracentrifuge at 19,000 rpm for 2 h at 4°C using a SW32Ti rotor (Beckman). The virus was washed once and then resuspended in 50 μL 1X phosphate buffered saline (PBS). We routinely

obtained 5 × 10^8 infectious viral particles/mL for lentivirus. Lentivirus stock solutions were diluted with sterile 1X PBS to prepare a 1:10 working solution for use.

Pseudotyped rabies virus (RaV-ΔR-MCherry): Pseudotyped rabies viral vector was produced as previously described[66,79]. Briefly, envelope protein EnvA-pseudotyped (i.e., Rgp-null) rabies virus carrying an mCherry reporter gene was generated in a helper cell line (BHK-EnvARGCD). RaV-ΔR-mCherry stock was produced by collecting, filtering, and concentrating the supernatant. Stock titers of 10^8 viral particles/ml were routinely obtained. Rabies virus stock was diluted in a 1:5 working solution with 1X PBS prior to use.

Monosynaptic RVdG retrograde tracing

Stage 2 (D80) retinal organoids were dissociated with papain (Worthington Biochemical) and plated onto 96-well plates coated with poly-D-lysine (MilliporeSigma) at a density of 200,000 cells/well (6,250 cells/mm^2). Cultures were transfected with viral vectors according to methods described by Sun *et al.* with slight modifications[60]. On D90, cultures were transfected with lentiviral vectors (Lenti-GTR working solution 1:16 in 3D RDM; Lenti-GTΔR working solution 1:80 in 3D RDM) to sparsely label a population of “starter” neurons, avoiding oversaturation of cultures with “traced” presynaptic neurons. RaV only controls were concurrently treated with 1X PBS. On D95, cultures were treated with 1:40 RaV-ΔR-MCherry working solution in 3D RDM. A full media change with fresh 3D RDM was performed 24 hours after each transfection.

Immunocytochemistry (ICC)

Samples were fixed on D100 in 4% paraformaldehyde for 10 minutes at room temperature and washed three times with 1X PBS. Fixed samples were incubated in donkey blocking solution [10% normal donkey serum (MilliporeSigma), 5% bovine serum albumin (MilliporeSigma), and 0.5% Triton-X (MilliporeSigma) in 1X PBS] for 1 hour and incubated in primary antibodies overnight at 4°C. Following primary antibody incubation, samples were washed with 1X PBS and incubated

for 35 minutes in the dark at room temperature in secondary antibody solution with 4',6-Diamidino-2-Phenylindole, Dihydrochloride (DAPI) and species-specific secondary antibodies (Alexa Fluor 488, 546, and 647) diluted at 1:500. Samples were washed with 1X PBS and stored in light-protective containment at 4°C until imaging. Antibodies used for ICC are summarized in **Table S3**.

High content image analysis

Immunostained 96 well plate samples from 5 independent hPSC-RO differentiations were imaged for high content analysis as previously described by Phillips *et al.* with minor modifications[31]. Briefly, 23 fields were captured per well (**Fig. S5A**) at 20X magnification with a high content widefield imaging system (Operetta, PerkinElmer). Segmentation and analysis were performed on unprocessed images using Columbus software (PerkinElmer). Border objects and pyknotic nuclei (determined by size and DAPI intensity) were excluded from quantitative analyses (**Fig S5C**). Cells positive for each marker were identified by scatter plot gating of fluorescence intensity for standardized segmentation and analysis workflows. For consistency in gating and marker analysis, data from all 5 replicates were used to develop each HCIA workflow. Cell counts from all 23 image fields for a single well were summed for a single biological replicate (on average, approximately 25,000 cells/well) for quantitative analyses; reported *n* values throughout the text are equivalent to the number of wells included in each experiment.

Statistics

Descriptive statistics were initially produced with and visualized in GraphPad Prism. Central tendency was reported as the mean ± standard error unless otherwise specified in the text. Statistical analyses for assay validation were performed in R version 4.0.0 (R Core Team, 2020) using packages described in Table S2. A median-based test (Mood's test of equal medians) was used in lieu of mean-based tests to compare the proportion of "traced" presynaptic cells between

treatment groups due to heteroscedastic error in generalized linear binomial models and no lentivirus control values being near zero. R packages used for this analysis are listed in **Table S3**. Where referenced, median values and a 95% confidence interval (CI) were determined using the exact method.

Figures

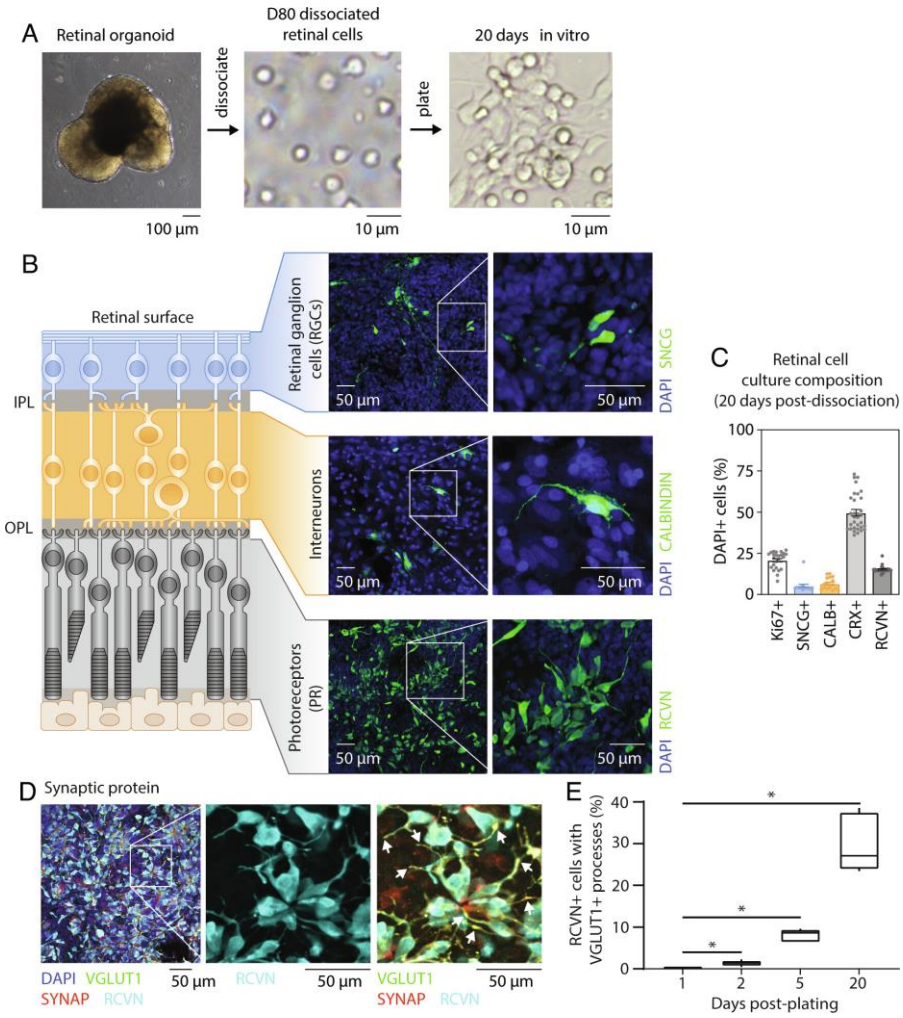

Figure 1. Retinal neuron diversity in re-associated hPSC-RN cultures. (**A**) Experimental overview showing the appearance of (Left) an intact stage 2 RO (D89 shown), (Middle) retinal cells immediately following dissociation of a D80 RO, and (Right) dissociated retinal cells 20 d after plating. (**B**) ICC showing the relative appearance and qualitative abundance of SNCG+ (RGCs), CALB+ (retinal interneurons), and RCVN+ (maturing photoreceptors) cells in dissociated D80 RO cultures 20 d after plating, alongside a schematic depicting their location in intact retinal tissue. (**C**) Quantification of retinal cell populations expressing SNCG, CALB, RCVN, Ki67 (dividing cells, including retinal progenitors and RPE cells), and/or CRX (newborn and maturing photoreceptors) in dissociated D80 RO cultures 20 d after plating. (**D**) RCVN+ photoreceptors express the synaptic proteins VGLUT1 and SYNAP 20 d after

D80 RO dissociation and plating, which colocalize with each other along photoreceptor axons (arrows). Scale bars: 100 µm, 50 µm, or 10 µm as indicated on their respective panels. (**E**) Quantification of RCVN+ cells possessing processes with VGLUT1+ puncta at day 1, 2, 5, and 20 d postplating. At day 1, RCVN+ cells (n = 467) displayed rare processes, none of which contained VGLUT1+ puncta. Thereafter, the percentage of RCVN+ cells having processes with VGLUT1+ puncta increased substantially (day 2: 1.4 ± 0.6%, n = 559 cells; day 5: 8.4 ± 1.4%, n = 633 cells; day 20: 29.5 ± 7.1%, n = 749 cells) (*$P < 0.05$, Kruskal–Wallis with pairwise Mann–Whitney U analyses).

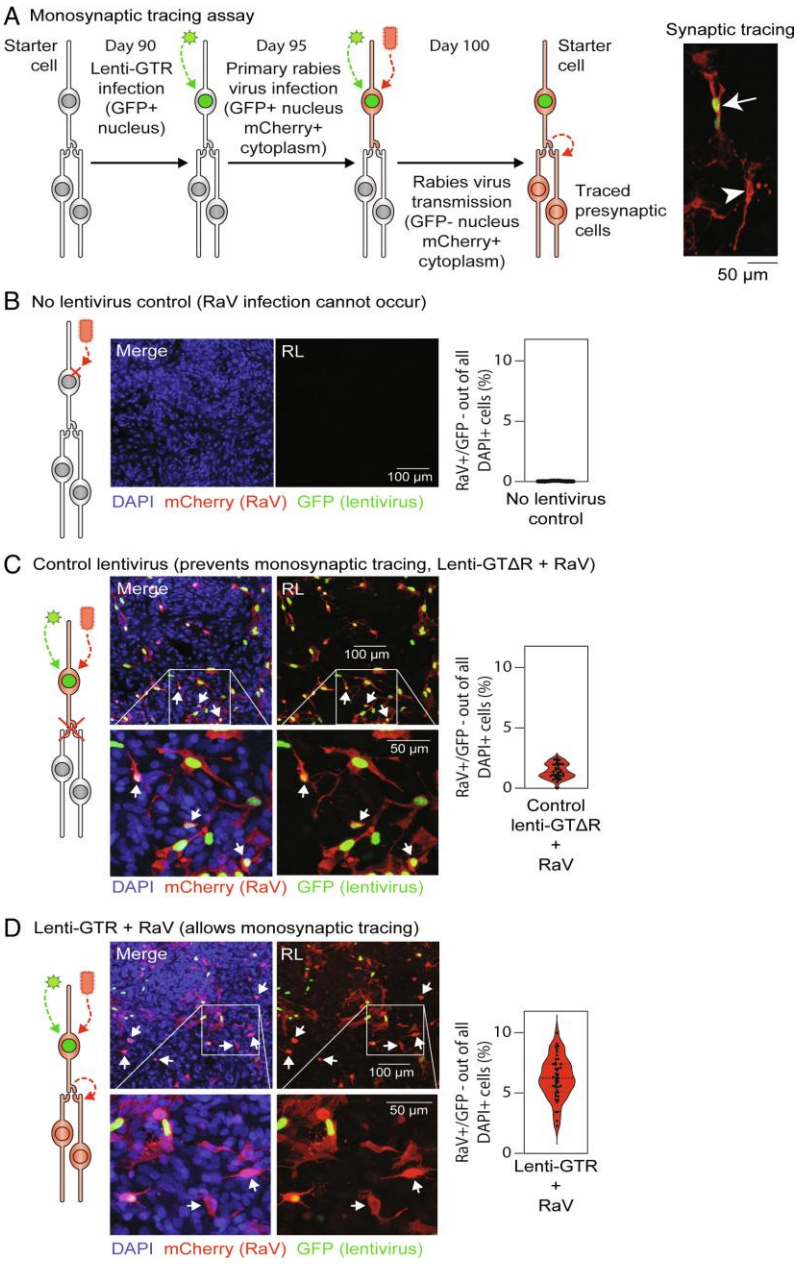

Fig. 2. Monosynaptic retrograde rabies virus tracing assay design and validation. (**A**) Schematic depicting the two-step RaV synaptic tracing assay utilized for this study, alongside a fluorescence image from one of the experiments (Far Right) showing an example of a starter retinal cell (arrow) and a traced presynaptic retinal cell (arrowhead). ROs were dissociated and plated on day 80 of differentiation. Resulting 2D cultures were infected with lentivirus 10 d later (day 90), followed by RaV infection at day 95 and examination for the presence of starter and traced presynaptic cells at day 100. (**B**) In the absence of primary transduction with lenti-GTR (i.e., no lentivirus control), secondary RaV infection cannot occur,

resulting in negligibly detectable fluorescent cells. (**C**) Primary transduction with lenti-GTΔR followed by secondary RaV infection permits labeling of starter retinal cells (GFP+ nuclei and mCherry+ cytoplasm) (arrows) but does not allow true monosynaptic tracing. Therefore, the small fraction of cells that have GFP-negative nuclei and mCherry+ cytoplasm in these control experiments represent nonspecific biomaterial transfer (i.e., false traced presynaptic cell detection rate). (**D**) In experimental cultures, primary transduction with lenti-GTR followed by secondary RaV infection leads to labeling of both starter retinal cells and traced presynaptic retinal cells (arrows). The median percentage of traced presynaptic cells was significantly greater in lenti-GTR + RaV cultures [6.2% (95% CI: 5.6, 6.9) of DAPI+ cells, n = 45 replicate wells] (**D**) relative to lenti-GTΔR + RaV controls [1.4% (95% CI: 1.1, 1.9) of DAPI+ cells, n = 37 replicate wells] (**C**) or RaV-only controls [0.02% (95% CI: 0.01, 0.04) of DAPI+ cells, n = 34 replicate wells]; $P < 0.00001$ using Mood's test of equal medians. Scale bars: 100 μm, 50 μm as indicated on respective panels.

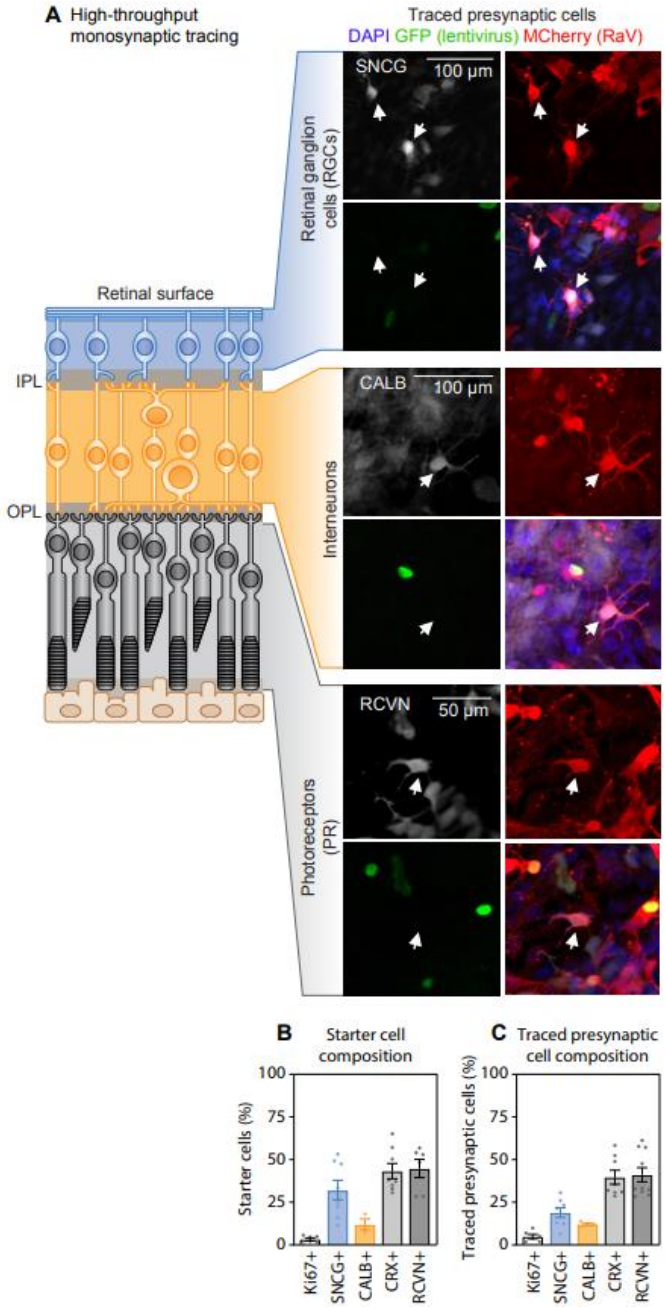

Figure 3. Monosynaptic RVdG tracing reveals new synaptic contacts formed by photoreceptors, interneurons, and retinal ganglion cells after re-association in vitro. (**A**) Representative "traced" presynaptic SNCG+ retinal ganglion cells, a rare CALB+ "traced" presynaptic interneuron, and RCVN+ "traced" presynaptic (RaV+/GFP-) photoreceptor (each labeled with arrows). (**B**) Quantification of "starter" cells. (**C**) Quantification of "traced" presynaptic cell populations within D100 re-associated hPSC-RO cultures. Each dot represents a single well and error bars represent standard error of the mean.

Supplemental Information

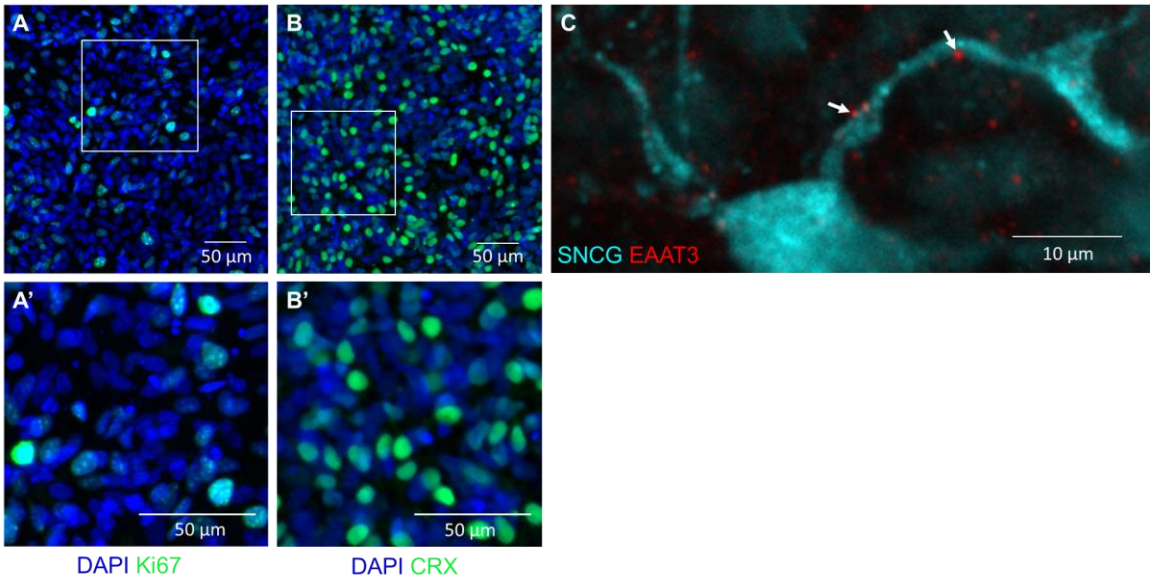

Fig. S1. Further characterization of dissociated hPSC-RO culture composition. (**A**) Ki67-positive cells within re-associated hPSC-RN cultures (inset magnified in A'). (**B**) CRX-positive cells predominated in plated cultures (inset magnified in B'). (**C**) EAAT3-positive puncta (arrows) within an SNCG-positive hPSC-RGC dendrite. Scale bars = 50 µm (A, B) and 10 µm (C).

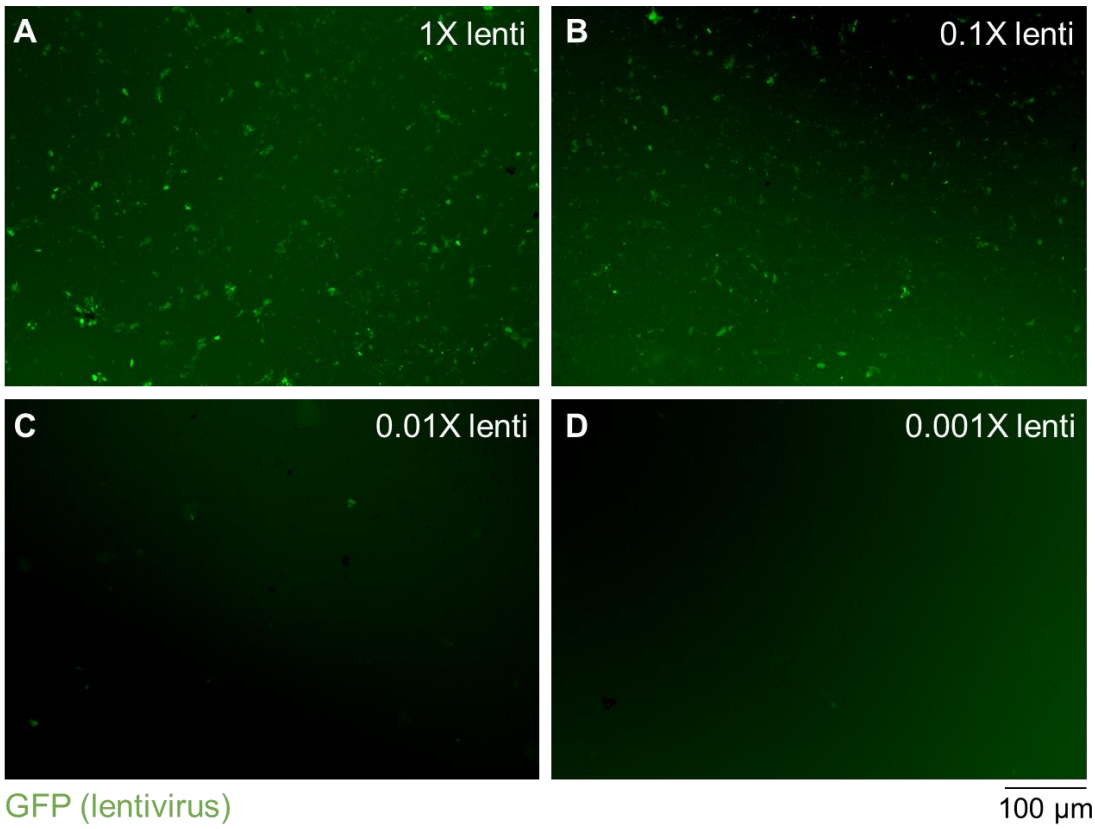

Fig. S2. Optimization of lentiviral transduction in re-associated hPSC-RO cultures. (**A**) Lenti-GTR stock (1X) was titrated to achieve relatively uniform labeling of "starter" cells. (**B**) 0.1X lentivirus (i.e., a 1:10 dilution) was sufficient for optimal distribution of "starter" cells (**C, D**) 0.01X and 0.001X lenti-GTR stock dilutions both produced insufficient levels of "starter" cell transduction. Scale bar = 100 µm.

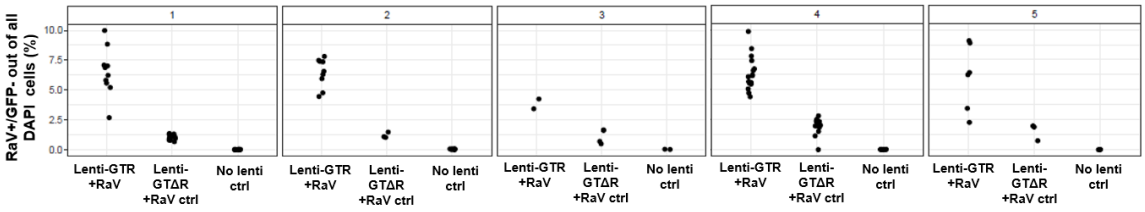

Fig. S3. Monosynaptic tracing across 5 independent differentiations. Quantification of "traced" presynaptic cells (RaV+/GFP-) consistently resulted in high rates of detection among Lenti-GTR + RaV cultures and few if any "traced" presynaptic cells among lenti-GTΔR and no lenti control cultures. Each dot represents the proportion of "traced" presynaptic cells within 23 20X images taken within a single well.

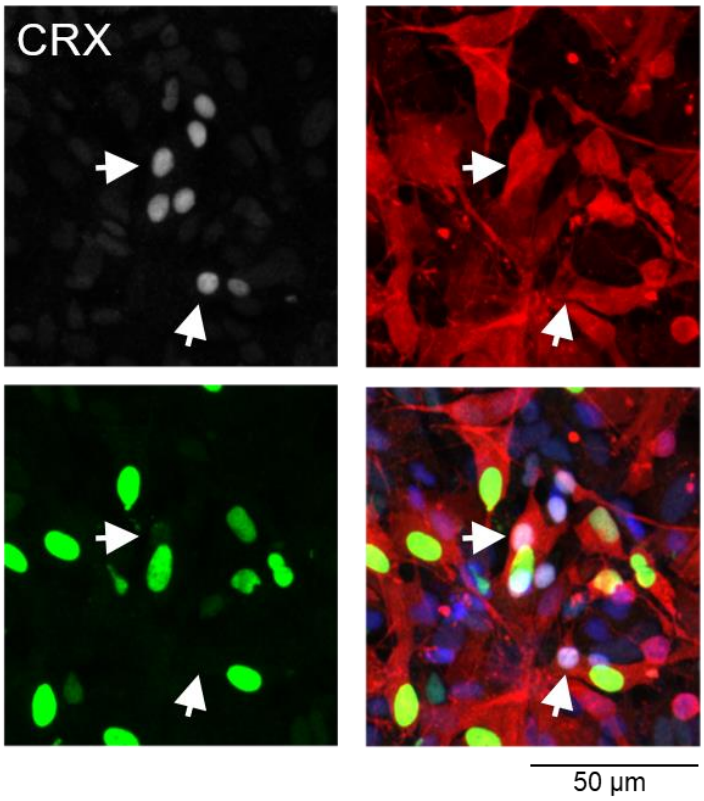

Fig. S4. "Traced" presynaptic CRX+ cells. Representative image of "traced" presynaptic CRX+ cells in re-associated hPSC-RO cultures.

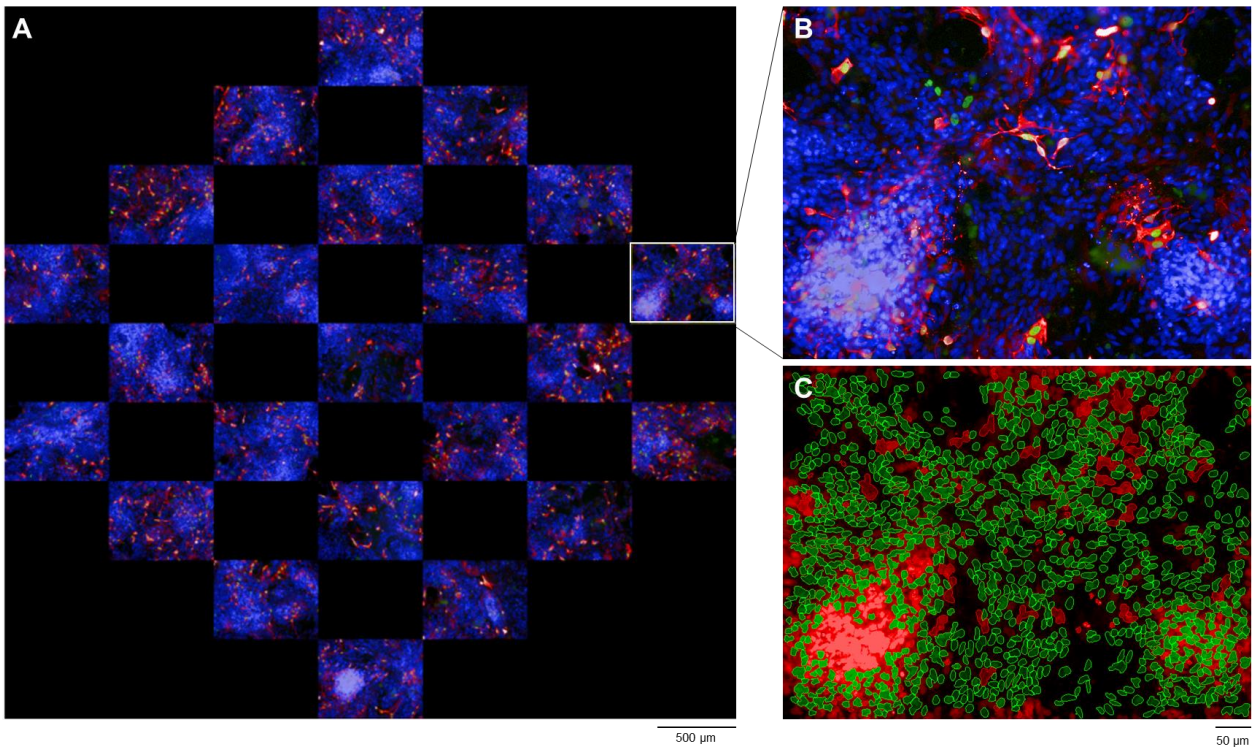

Fig. S5. Representative high content imaging and analysis. (**A**) Twenty three individual 20X magnification widefield images were captured within a single well of a 96 well plate. (**B**) Representative image depicting cell nuclei (blue), lentivirus (green) and RaV (red)-labeled cells within re-associated hPSC-RO cultures. (**C**) Example of image segmentation in which border objects, pyknotic nuclei, and mounded/out-of-focus nuclei are excluded (labeled in red) from DAPI cell counts (labeled in green). Scale bars = 500 µm (A) and 50 µm (B, C).

Table 1. Summary of immunohistochemical findings in 2D re-associated RO cultures.

Antibody	Cell type(s)	Detected in 2D (+/-)
CALB1	Interneurons (HCs, ACs, ON cone BPCS), RGCs [80]	+
CALR	Interneurons (ACs), RGCs[25]	-
CRX	PRs, RPE[25,33]	+
CRALBP	Müller glia[25]	-
GFAP	Müller glia	+/-
Goα	Interneurons (ON BPCs)[25]	-
HNF6 (ONECUT1)	RPCs, HCs, immature RGCs and cone PRs[25]	+/-
Ki67	Proliferative cells (RPCs, RPE, glia) [25,33]	+
MITF	RPE[81]	-
PKCα	Interneurons (rod BPCs) [25]	-
RCVN	PRs, subset of interneurons (BPCs)[25,33]	+
SNCG	RGCs[25]	+
VSX2	RPCs, interneurons (BPCs), glia[25,33]	-

Table 2. Media formulation for each stage of hPSC-RO differentiation (~500 mL total volume)

Medium	Formulation	Vendor/Catalog Number
Pluripotency maintenance	mTeSR Plus Basal Medium – 400 mL mTeSR Plus Supplement (5X) – 100 mL	STEMCELL Technologies / 100-0276
Neural induction	Dulbecco's Modified Eagle Medium (DMEM): Nutrient Mixture F12 – 500 mL	Thermo Fisher Scientific / 11330057
	Minimum Essential Medium (MEM) Non-Essential Amino Acids (NEAA) (100X) – 5 mL	Thermo Fisher Scientific / 11140-076
	GlutaMAX Supplement (100X) – 5 mL	Thermo Fisher Scientific / 350500079
	Heparin (2 mg/mL) – 0.5 mL	Sigma-Aldrich / H-3149
	N-2 Supplement (100X) – 5 mL	Thermo Fisher Scientific / 17502048
Retinal differentiation	DMEM – 350 mL	Thermo Fisher Scientific / 11965-118
	F12 – 150 mL	Thermo Fisher Scientific / 11765070
	Antibiotic-antimycotic (100X) – 5 mL	Thermo Fisher Scientific / 15240096
	MEM NEAA (100X) – 5 mL	Thermo Fisher Scientific / 11140-076
	GlutaMAX (100X) – 5 mL	Thermo Fisher Scientific / 35050079
	B-27 Supplement (50X) – 5 mL	Thermo Fisher Scientific / 17504044
3D retinal differentiation	DMEM – 350 mL	Thermo Fisher Scientific / 11965-118
	F12 – 150	Thermo Fisher Scientific / 11765070
	Antibiotic-antimycotic (100X) – 5 mL	Thermo Fisher Scientific / 15240096
	MEM NEAA (100X) – 5 mL	Thermo Fisher Scientific / 11140-076
	GlutaMAX (100X) – 5 mL	Thermo Fisher Scientific / 35050079
	Taurine (0.2M) – 0.5 mL	Sigma-Aldrich / T0625-10G
	Fetal Bovine Serum (FBS) – 25 mL	WiCell
	Chemically Defined Lipid Concentrate – 5 mL	Thermo Fisher Scientific / 11905031
	B-27 Supplement (50X) – 5 mL	Thermo Fisher Scientific / 17504044

Table 3. Primary antibodies for immunocytochemistry.

Antibody	Source	Catalog number	Host	Dilution
TdTomato (Mcherry)	SICGEN	AB8181-200	Goat	1:300
Green fluorescent protein (GFP)	ThermoFisher	A10262	Chicken	1:250
Synuclein gamma (SNCG)	Abnova	H00006623-M01	Mouse	1:500
Calbindin (CALB)	SWANT	CB38	Rabbit	1:100
Ki67	BD Pharmagen	556003	Mouse	1:300
Recoverin (RCVN)	MilliporeSigma	5585	Rabbit	1:2000
Cone-rod homeobox (CRX)	Abnova	H0001406-M02	Mouse	1:1000
Synaptophysin (SYP)	ThermoFisher	14-6525-80	Mouse	1:100
Vesicular glutamate transporter 1 (VGLUT1)	MilliporeSigma	AB5905	Guinea Pig	1:1000
Excitatory amino acid transporter 3 (EAAT3)	Cell Signaling Technology	14501S	Rabbit	1:500

Table 4. R packages used to analyze traced presynaptic cells for assay validation.

Package name	**Version**
DescTools	0.99.40
coin	1.4-1
survival	3.1-12
xtable	1.8-4
readxl	1.3.1
forcats	0.5.0
stringr	1.4.0
dplyr	1.0.2
purrr	0.3.4
readr	1.3.1
tidyr	1.0.3
tibble	3.0.1
ggplot2	3.3.0
tidyverse	1.3.0

References

1. López-Muñoz, F., Boya, J. & Alamo, C. Neuron theory, the cornerstone of neuroscience, on the centenary of the Nobel Prize award to Santiago Ramón y Cajal. *Brain Research Bulletin* **70**, 391–405 (2006).

2. Pfeiffer, R. L., Marc, R. E. & Jones, B. W. Persistent remodeling and neurodegeneration in late-stage retinal degeneration. *Progress in Retinal and Eye Research* **74**, 100771 (2020).

3. Verbakel, S. K. *et al.* Non-syndromic retinitis pigmentosa. *Progress in Retinal and Eye Research* **66**, 157–186 (2018).

4. Quigley, H. A. Glaucoma. *The Lancet* **377**, 1367–1377 (2011).

5. Soto, F., Zhao, L. & Kerschensteiner, D. Synapse maintenance and restoration in the retina by NGL2. *eLife* **7**, e30388 (2018).

6. Agostinone, J. *et al.* Insulin signalling promotes dendrite and synapse regeneration and restores circuit function after axonal injury. *Brain* **141**, 1963–1980 (2018).

7. Gasparini, S. J., Llonch, S., Borsch, O. & Ader, M. Transplantation of photoreceptors into the degenerative retina: Current state and future perspectives. *Progress in retinal and eye research* (2018) doi:10.1016/j.preteyeres.2018.11.001.

8. Zhang, K. Y., Aguzzi, E. A. & Johnson, T. V. Retinal Ganglion Cell Transplantation: Approaches for Overcoming Challenges to Functional Integration. *Cells* **10**, 1426 (2021).

9. Zhao, C., Wang, Q. & Temple, S. Stem cell therapies for retinal diseases: recapitulating development to replace degenerated cells. *Development* **144**, 1368–1381 (2017).

10. Duebel, J., Marazova, K. & Sahel, J.-A. Optogenetics. *Curr Opin Ophthalmol* **26**, 226–232 (2015).

11. Becker, S. M. & Wright, C. B. Update on the Status and Impact of the National Eye Institute Audacious Goals Initiative for Regenerative Medicine. *Journal of Ocular Pharmacology and Therapeutics* **37**, 144–146 (2021).

12. Ribeiro, J. *et al.* Restoration of visual function in advanced disease after transplantation of purified human pluripotent stem cell-derived cone photoreceptors. *Cell Reports* **35**, (2021).

13. Garita-Hernandez, M. *et al.* Restoration of visual function by transplantation of optogenetically engineered photoreceptors. *Nature Communications* **10**, 4524 (2019).

14. Aboualizadeh, E. *et al.* Imaging Transplanted Photoreceptors in Living Nonhuman Primates with Single-Cell Resolution. *Stem Cell Reports* **15**, 482–497 (2020).

15. Barnea-Cramer, A. O. *et al.* Function of human pluripotent stem cell-derived photoreceptor progenitors in blind mice. *Sci Rep* **6**, 29784 (2016).

16. Gagliardi, G. *et al.* Characterization and Transplantation of CD73-Positive Photoreceptors Isolated from Human iPSC-Derived Retinal Organoids. *Stem cell reports* **11**, 665–680 (2018).

17. Chao, J. R. *et al.* Transplantation of Human Embryonic Stem Cell-Derived Retinal Cells into the Subretinal Space of a Non-Human Primate. *Transl Vis Sci Technol* **6**, 4 (2017).

18. Shirai, H. *et al.* Transplantation of human embryonic stem cell-derived retinal tissue in two primate models of retinal degeneration. *Proceedings of the National Academy of Sciences of the United States of America* **113**, E81-90 (2016).

19. Iraha, S. *et al.* Establishment of Immunodeficient Retinal Degeneration Model Mice and Functional Maturation of Human ESC-Derived Retinal Sheets after Transplantation. *Stem Cell Reports* **10**, 1059–1074 (2018).

20. Tu, H.-Y. *et al.* Medium- to long-term survival and functional examination of human iPSC-derived retinas in rat and primate models of retinal degeneration. *EBioMedicine* **39**, 562–574 (2019).

21. McLelland, B. T. *et al.* Transplanted hESC-Derived Retina Organoid Sheets Differentiate, Integrate, and Improve Visual Function in Retinal Degenerate Rats. *Invest. Ophthalmol. Vis. Sci.* **59**, 2586–2603 (2018).

22. Lin, B. *et al.* Retina Organoid Transplants Develop Photoreceptors and Improve Visual Function in RCS Rats With RPE Dysfunction. *Invest. Ophthalmol. Vis. Sci.* **61**, 34–34 (2020).

23. Capowski, E. E. *et al.* Reproducibility and staging of 3D human retinal organoids across multiple pluripotent stem cell lines. *Development* **146**, dev171686 (2019).

24. Cowan, C. S. *et al.* Cell Types of the Human Retina and Its Organoids at Single-Cell Resolution. *Cell* **182**, 1623-1640.e34 (2020).

25. Bell, C. M., Zack, D. J. & Berlinicke, C. A. Human Organoids for the Study of Retinal Development and Disease. *Annu Rev Vis Sci* **6**, 91–114 (2020).

26. Phillips, M. J. *et al.* Blood-Derived Human iPS Cells Generate Optic Vesicle–Like Structures with the Capacity to Form Retinal Laminae and Develop SynapsesProduction of Retina from Human Blood iPS Cells. *Investigative Ophthalmology & Visual Science* **53**, 2007–2019 (2012).

27. Zhong, X. *et al.* Generation of three-dimensional retinal tissue with functional photoreceptors from human iPSCs. *Nat Commun* **5**, 4047 (2014).

28. Ohlemacher, S. K. *et al.* Advances in the Differentiation of Retinal Ganglion Cells from Human Pluripotent Stem Cells. in *Pluripotent Stem Cells in Eye Disease Therapy* (ed. Bharti, K.) 121–140 (Springer International Publishing, 2019). doi:10.1007/978-3-030-28471-8_5.

29. Hallam, D. *et al.* Human-Induced Pluripotent Stem Cells Generate Light Responsive Retinal Organoids with Variable and Nutrient-Dependent Efficiency. *Stem cells (Dayton, Ohio)* **36**, 1535–1551 (2018).

30. Kim, S. *et al.* Generation, transcriptome profiling, and functional validation of cone-rich human retinal organoids. *Proceedings of the National Academy of Sciences of the United States of America* **116**, 10824–10833 (2019).

31. Phillips, M. J. *et al.* A Novel Approach to Single Cell RNA-Sequence Analysis Facilitates In Silico Gene Reporting of Human Pluripotent Stem Cell-Derived Retinal Cell Types. *Stem Cells* **36**, 313–324 (2018).

32. Kallman, A. *et al.* Investigating cone photoreceptor development using patient-derived NRL null retinal organoids. *Commun Biol* **3**, 82 (2020).

33. Yang, Y.-P. *et al.* Glutamate Stimulation Dysregulates AMPA Receptors-Induced Signal Transduction Pathway in Leber's Inherited Optic Neuropathy Patient-Specific hiPSC-Derived Retinal Ganglion Cells. *Cells* **8**, (2019).

34. Langer, K. B. *et al.* Retinal Ganglion Cell Diversity and Subtype Specification from Human Pluripotent Stem Cells. *Stem Cell Reports* **10**, 1282–1293 (2018).

35. Cora, V. *et al.* A Cleared View on Retinal Organoids. *Cells* **8**, 391 (2019).

36. Gonzalez-Cordero, A. *et al.* Recapitulation of Human Retinal Development from Human Pluripotent Stem Cells Generates Transplantable Populations of Cone Photoreceptors. *Stem Cell Reports* **9**, 820–837 (2017).

37. Wahlin, K. J. *et al.* Photoreceptor Outer Segment-like Structures in Long-Term 3D Retinas from Human Pluripotent Stem Cells. *Scientific Reports* **7**, 766 (2017).

38. Singh, R. K. *et al.* Characterization of Three-Dimensional Retinal Tissue Derived from Human Embryonic Stem Cells in Adherent Monolayer Cultures. *Stem Cells Dev.* **24**, 2778–2795 (2015).

39. VanderWall, K. B. *et al.* Astrocytes Regulate the Development and Maturation of Retinal Ganglion Cells Derived from Human Pluripotent Stem Cells. *Stem Cell Reports* **12**, 201–212 (2019).

40. Barnea-Cramer, A. O. *et al.* Repair of Retinal Degeneration following Ex Vivo Minicircle DNA Gene Therapy and Transplantation of Corrected Photoreceptor Progenitors. *Molecular Therapy* **28**, 830–844 (2020).

41. Zerti, D. *et al.* Transplanted pluripotent stem cell-derived photoreceptor precursors elicit conventional and unusual light responses in mice with advanced retinal degeneration. *Stem Cells* (2021) doi:10.1002/stem.3365.

42. Mandai, M. *et al.* iPSC-Derived Retina Transplants Improve Vision in rd1 End-Stage Retinal-Degeneration Mice. *Stem Cell Reports* **8**, 69–83 (2017).

43. Léveillard, T. & Klipfel, L. Mechanisms Underlying the Visual Benefit of Cell Transplantation for the Treatment of Retinal Degenerations. *Int J Mol Sci* **20**, (2019).

44. Nickerson, P. E. B., Ortin-Martinez, A. & Wallace, V. A. Material Exchange in Photoreceptor Transplantation: Updating Our Understanding of Donor/Host Communication and the Future of Cell Engraftment Science. *Front Neural Circuits* **12**, 17 (2018).

45. Saleeba, C., Dempsey, B., Le, S., Goodchild, A. & McMullan, S. A Student's Guide to Neural Circuit Tracing. *Front. Neurosci.* **13**, (2019).

46. Rogers, A. & Beier, K. T. Can transsynaptic viral strategies be used to reveal functional aspects of neural circuitry? *Journal of Neuroscience Methods* **348**, 109005 (2021).

47. Callaway, E. M. & Luo, L. Monosynaptic Circuit Tracing with Glycoprotein-Deleted Rabies Viruses. *J Neurosci* **35**, 8979–8985 (2015).

48. Adler, A. F., Björklund, A. & Parmar, M. Transsynaptic tracing and its emerging use to assess graft-reconstructed neural circuits. *STEM CELLS* **38**, 716–726 (2020).

49. Grønning Hansen, M. *et al.* Grafted human pluripotent stem cell-derived cortical neurons integrate into adult human cortical neural circuitry. *Stem Cells Transl Med* **9**, 1365–1377 (2020).

50. Palma-Tortosa, S., Coll-San Martin, B., Kokaia, Z. & Tornero, D. Neuronal Replacement in Stem Cell Therapy for Stroke: Filling the Gap. *Front. Cell Dev. Biol.* **0**, (2021).

51. Thomson, J. A. *et al.* Embryonic stem cell lines derived from human blastocysts. *Science* **282**, 1145–1147 (1998).

52. Kruczek, K. & Swaroop, A. Pluripotent stem cell-derived retinal organoids for disease modeling and development of therapies. *STEM CELLS* **n/a**,.

53. Phillips, M. J. *et al.* Generation of a rod-specific NRL reporter line in human pluripotent stem cells. *Scientific Reports* **8**, 2370 (2018).

54. Jensen, C. & Teng, Y. Is It Time to Start Transitioning From 2D to 3D Cell Culture? *Front. Mol. Biosci.* **0**, (2020).

55. Scuderi, S., Altobelli, G. G., Cimini, V., Coppola, G. & Vaccarino, F. M. Cell-to-Cell Adhesion and Neurogenesis in Human Cortical Development: A Study Comparing 2D Monolayers with 3D Organoid Cultures. *Stem Cell Reports* **16**, 264–280 (2021).

56. Lee, I.-K. *et al.* Ultrathin micromolded 3D scaffolds for high-density photoreceptor layer reconstruction. *Science Advances* **7**, eabf0344 (2021).

57. Lamba, D. A., Karl, M. O., Ware, C. B. & Reh, T. A. Efficient generation of retinal progenitor cells from human embryonic stem cells. *PNAS* **103**, 12769–12774 (2006).

58. Schniepp, R. *et al.* Retinal Colocalization and In Vitro Interaction of the Glutamate Receptor EAAT3 and the Serum- and Glucocorticoid-Inducible Kinase SGK1. *Invest. Ophthalmol. Vis. Sci.* **45**, 1442–1449 (2004).

59. Lavin, T. K., Jin, L., Lea, N. E. & Wickersham, I. R. Monosynaptic Tracing Success Depends Critically on Helper Virus Concentrations. *Front. Synaptic Neurosci.* **12**, (2020).

60. Sun, Y. *et al.* Loss of MeCP2 in immature neurons leads to impaired network integration. *Human molecular genetics* **28**, 245–257 (2019).

61. Ortin-Martinez, A. *et al.* A Reinterpretation of Cell Transplantation: GFP Transfer From Donor to Host Photoreceptors. *Stem Cells* **35**, 932–939 (2017).

62. Pearson, R. A. *et al.* Donor and host photoreceptors engage in material transfer following transplantation of post-mitotic photoreceptor precursors. *Nat Commun* **7**, 13029 (2016).

63. Santos-Ferreira, T. *et al.* Retinal transplantation of photoreceptors results in donor-host cytoplasmic exchange. *Nat Commun* **7**, 13028 (2016).

64. Singh, M. S. *et al.* Transplanted photoreceptor precursors transfer proteins to host photoreceptors by a mechanism of cytoplasmic fusion. *Nat Commun* **7**, 13537 (2016).

65. Decembrini, S. *et al.* Cone Genesis Tracing by the Chrnb4-EGFP Mouse Line: Evidences of Cellular Material Fusion after Cone Precursor Transplantation. *Mol. Ther.* **25**, 634–653 (2017).

66. Guo, W. *et al.* Fragile X Proteins FMRP and FXR2P Control Synaptic GluA1 Expression and Neuronal Maturation via Distinct Mechanisms. *Cell Rep* **11**, 1651–1666 (2015).

67. Foik, A. T. *et al.* Detailed Visual Cortical Responses Generated by Retinal Sheet Transplants in Rats with Severe Retinal Degeneration. *J. Neurosci.* **38**, 10709–10724 (2018).

68. Rompani, S. B. *et al.* Different Modes of Visual Integration in the Lateral Geniculate Nucleus Revealed by Single-Cell-Initiated Transsynaptic Tracing. *Neuron* **93**, 767-776.e6 (2017).

69. Camelo, S., Castellanos, J., Lafage, M. & Lafon, M. Rabies virus ocular disease: T-cell-dependent protection is under the control of signaling by the p55 tumor necrosis factor alpha receptor, p55TNFR. *J Virol* **75**, 3427–3434 (2001).

70. Singh, M. S. *et al.* Retinal stem cell transplantation: Balancing safety and potential. *Progress in Retinal and Eye Research* 100779 (2019) doi:10.1016/j.preteyeres.2019.100779.

71. Wang, Y., Zhang, D., Shen, B., Zhang, Y. & Gu, P. Stem/Progenitor Cells and Biodegradable Scaffolds in the Treatment of Retinal Degenerative Diseases. *Curr Stem Cell Res Ther* **13**, 160–173 (2018).

72. Maeda, T., Sugita, S., Kurimoto, Y. & Takahashi, M. Trends of Stem Cell Therapies in Age-Related Macular Degeneration. *Journal of Clinical Medicine* **10**, 1785 (2021).

73. Assawachananont, J. *et al.* Transplantation of embryonic and induced pluripotent stem cell-derived 3D retinal sheets into retinal degenerative mice. *Stem Cell Reports* **2**, 662–674 (2014).

74. Zarbin, M. Cell-Based Therapy for Retinal Disease: The New Frontier. *Methods Mol. Biol.* **1834**, 367–381 (2019).

75. Laver, C. R. J. & Matsubara, J. A. Structural divergence of essential triad ribbon synapse proteins among placental mammals – Implications for preclinical trials in photoreceptor transplantation therapy. *Experimental Eye Research* **159**, 156–167 (2017).

76. Wall, N. R., De La Parra, M., Callaway, E. M. & Kreitzer, A. C. Differential innervation of direct- and indirect-pathway striatal projection neurons. *Neuron* **79**, 347–360 (2013).

77. Kishi, J. Y. *et al.* SABER amplifies FISH: enhanced multiplexed imaging of RNA and DNA in cells and tissues. *Nat Methods* **16**, 533–544 (2019).

78. Gao, Y. *et al.* RGS6 Mediates Effects of Voluntary Running on Adult Hippocampal Neurogenesis. *Cell Reports* **32**, 107997 (2020).

79. Vivar, C. *et al.* Monosynaptic inputs to new neurons in the dentate gyrus. *Nat Commun* **3**, 1107 (2012).

Chapter 6 -

Conclusions

Optimizing form for function: Current status and future perspectives

Numerous studies of human pluripotent stem cell (hPSC)-derived retinal organoid and adjacent research reviewed in the first two chapters of this dissertation convincingly demonstrate that hPSC-ROs can efficiently and reproducibly generate *bona fide* photoreceptors (PRs) with tremendous potential for use in cell replacement strategies. The ability of these lab-grown retinal neurons to survive, mature, self-organize, and establish new connections after dissociation from ROs are all key to building confidence in their capacity to restore visual function in human patients. In this dissertation, I have explored the capacity for hPSC-PRP survival, maturation, organization, and connectivity with *in vivo* and *in vitro* model systems, aiming to bridge the gap between bench and bedside for retinal regenerative therapies.

We initially determined that clustered delivery of hPSC-RO-derived photoreceptor precursors (PRP) as aggregates markedly improved donor cell survival and engraftment relative to dissociated cell transplants in a rat model of severe PR degeneration. Despite survival and maturation of donor PRP in the degenerative retinal environment, including synaptic protein expression, grafts remained relatively disorganized, and we did not observe meaningful improvement in visual acuity or electroretinographic function, raising two subsequent questions. First, how might we improve organization within hPSC-PRP grafts? And second, does synaptic protein expression in hPSC-PRP necessarily mean that they retain the capacity to form new synapses after being dissociated from ROs?

To address the former, we developed a micro-patterned biodegradable scaffold to bias orientation of a high-density layer of hPSC-PRP for transplantation[1]. To address the latter, we employed a high-throughput *in vitro* monosynaptic tracing assay to identify *de novo* synapse formation within hPSC-PRP following dissociation. Equipped with these tools, we can now address key remaining challenges: methods for organizing grafts and identifying *bona fide* donor

cell synapses *in vivo*. In this final chapter, I outline potential applications of these findings in further preclinical studies and identify future directions for this line of research.

Subretinal scaffold delivery for organized PRP replacement in translational model systems

In chapter 4, we demonstrated that many hPSC-PRP could be pre-organized on biodegradable grafts prior to transplantation. A logical next step in this line of research is determining whether such scaffolds can improve retention and survival in a manner similar to aggregate transplants while also maintaining orientation. Scaffold delivery requires a more complex surgical approach than subretinal injections; careful selection of appropriate animal models thus is important in the context of studying cell replacement with scaffolds. Intraocular anatomy dictates the degree to which surgical delivery faithfully models a similar approach in humans. Large animals like the dog, pig, and non-human primate (NHP) have eyes that are in many ways similar to humans, with a proportionate lens and fairly large globe. These models are thus highly attractive for testing scaffold delivery. In contrast, the relatively large lens in the rat (**Fig. 1**) complicates scaffold delivery and requires substantial modification to the surgical approach to avoid damaging the retina, limiting translation of such studies to humans. Thus, large animal models are likely best suited for quantitative assessment of survival and orientation of PRP delivered on scaffolds.

Initial studies of PRP transplantation on micro-patterned scaffolds in nude retinal degenerative (Foxn1-S334ter-3) rats have nonetheless been promising to date. $CRX^{+/tdTomato}$-PRP can be delivered on biodegradable scaffolds (**Fig. 2**), surviving in the SRS for at least two weeks post-transplant (n = 8 rats to date). Expression of presynaptic protein VGLUT1 between donor PRP and the host INL appears to mimic the intended orientation on scaffolds, whereby seeded PRP primarily express synaptic proteins in the upper half of the scaffold[1]. $CRX^{+/tdTomato}$-PRP delivered on scaffolds co-labeled with human nuclear antigen (HNA), and evidence of biomaterial transfer was not observed. For future preclinical studies, exploration of outer segment orientation (PRPH2), ribbon synapse (RIBEYE, CtBP2, PIKACHURIN) and human-specific synaptic protein

expression (Synaptophysin, etc.) with high-resolution imaging can facilitate quantitative assessment of the degree of *in vivo* polarization achievable with PRP scaffold delivery.

Imaging modalities to study engraftment in real-time

In vivo imaging techniques to monitor survival and integration in real time has potential to fast-track development of scaffold approaches. Optical coherence tomography (OCT) and other conventionally used imaging modalities often cannot distinguish regions of retinal disruption (more common in scaffold surgeries) from engrafted host cells or scaffolds. The scaffold described in Chapter 4 was intentionally designed to be optically clear, thereby enabling light to reach transplanted PRP upon entering the eye. In combination with the relatively colorless appearance of donor PRP, however, optical clarity complicates visibility for the surgical team during subretinal delivery and for locating the scaffold post-operatively to monitor scaffold degradation or cell integration. Retinal pigment epithelium (RPE) have been successfully delivered and monitored on scaffolds in multiple species[2] and are far more easily visualized due to their inherent pigmentation. To this end, approaches for temporarily enhancing visibility of PRP scaffolds—via conjugation of commonly used intraocular dyes like fluorescein or indocyanine green—may enhance surgical delivery and post-operative monitoring.

In preclinical studies, fluorescent PRP reporter lines like the $CRX^{+/tdTomato}$ reporter[3] used throughout this dissertation should also be effective for tracking engraftment of cells delivered on scaffolds. 2-photon imaging of transplanted PRP can be achieved in live animals with limited resolution[4], while more sophisticated methods like fluorescence adaptive optics scanning light ophthalmoscopy (FAOSLO) enable *in vivo* monitoring at the level of individual cells. Until methods for enhancing basic visibility of PRP scaffolds become reality, high-resolution fluorescence imaging is likely to be the best option for monitoring survival and engraftment of scaffold-delivered cells in real-time.

Functional integration and synaptogenesis

For PR replacement therapy to be successful in patients, it is critical to definitively show that donor hPSC-PRs can establish functional synapses with host second order retinal interneurons, including BPCs and HCs. There is strong evidence to suggest that they form functional synapses with co-differentiating second order BPCs in ROs[5–7], and we now know that hPSC-PRP and other RO-derived retinal neurons possess intrinsic potential to form new synapses after dissociation from organoids (Chapter 5). What we do not know, however, is whether they form similar synapses with mature retinal neurons. Moreover, evolutionary divergence in key synaptic proteins has likely limited the efficiency of hPSC-PR synapse formation with second order neurons across model species, particularly in human-to-rodent xenografts. This synaptic discordance is one possible explanation for the lack of vision rescue observed in aggregate transplant studies in Chapter 3—synapses, if present, may be incapable of properly relaying information between neurons of different species. The monosynaptic tracing assay developed in Chapter 5 is, to our knowledge, one of the only systems currently available for directly studying synaptic contacts at the level of the donor cell synapse. In order of clinical relevance, the following instances of donor PRP-to-host synaptic connectivity are of high interest for further investigation with synaptic tracing:

1) Human PRP to mature interneurons in adult human degenerative retinal tissue

2) Human PRP to mature interneurons in healthy adult human degenerative retinal tissue

3) Human PRP to animal hosts with minimal synaptic discordance (NHP, cat)

4) Allogeneic PSC-derived PRP to same-species animal hosts (pig, dog, NHP, rodent)

5) Human PRP to animal hosts with moderate synaptic discordance (dog, pig, rodent)

The limited availability of sufficiently viable human cadaveric retinal tissue has limited pursuit of the first two instances, though such evidence would greatly increase confidence in PSC-derived PRP ahead of clinical trials. Testing synaptic efficiency between human PRP and animal hosts with minimal synaptic discordance is likely a more achievable near-term goal. Allogeneic synaptic tracing studies with PSC-derived PRP also have potential to effectively model the likelihood of synaptic connectivity achievable in human clinical trials. Optimization of retinal differentiation from a variety of laboratory animal species is thus currently an area of high priority. For the animal studies listed (items 3-5), *ex vivo* tracing and *in vivo* tracing are both theoretically possible, though there are benefits and drawbacks to each approach. *Ex vivo* tracing in retinal explants is the simplest approach between the two, but management of contamination, viability, and selective removal of host PRs to access the inner nuclear layer remain challenging. Dissociation of mature retinal tissues may provide greater access to inner retinal neurons for tracing, although mature retinal interneurons thus far appear to respond poorly to deafferentation and singularization. Moreover, although a handful of methods for enriching PRP exist (see below), there are far fewer options for purification of inner retinal neurons to study interactions between enriched donor and host cell populations.

In vivo tracing is increasingly employed in the context of transplantation[8–10] and is of high interest for retinal regenerative therapies[11]. With evidence of its utility for tracing hPSC-PRP synaptic contacts, *in vivo* applications of this approach are all the more promising. However, in its present form the assay requires multiple subretinal injections at the exact same site, which increases inflammation and creates a challenging environment for promoting (and subsequently tracing) synaptic connections. Intriguingly, a genetically engineered hESC line has recently been developed to facilitate monosynaptic retrograde tracing in xenografts[9]; retinal differentiation and subsequent transplantation of PRP from such a line may provide more robust labeling than dual subretinal viral injections with unmodified hPSC-PRP. Further customization of synaptic tracing

reagents may also be useful in overcoming some of the challenges faced in further assay development. As outlined in Chapter 5, titration of tumor virus receptor A (TVA) delivery via a helper virus is critical to successful use of any synaptic tracing assay. Modification of TVA delivery to selectively infect interneurons would be a highly attractive option, particularly for *in vivo* studies. An ON-bipolar cell-specific promoter for targeting rod and cone ON-BCs *in vivo* has recently been described[12]; modifications to the TVA delivery method incorporating this promoter have the potential to substantially increase the likelihood of successful tracing *in vivo*.

Donor cell enrichment

Studies of PRP replacement, including those described in this dissertation, still remain somewhat limited by the tools available for obtaining enriched PRP populations from retinal organoids. Published methods for magnetic activated cell sorting (MACS)[13] and fluorescence activated cell sorting (FACS)[14] have primarily been modeled after approaches used in rod-dominant rodent models and are variably successful in enriching for PRP between various RO differentiation protocols. We initially tried replicating existing MACS protocols (including positive selection for CD-73, the most common cell surface marker for hPSC-PRP sorting[11,13]) but were unable to obtain a sufficient yield of donor cells for transplantation, often resulting in fewer than 200,000 total cells after sorting.

With a lack of viable sorting methods initially available, unsorted dissociated stage 2 organoids were employed in studies throughout this dissertation due to the relatively high proportion of PRP in fully dissociated RO cultures (40-80%), with PRP purity comparable to that obtained in recent studies using FACS enrichment (~70%[4,15]). As observed in Chapter 3, PRP are still the predominate cell type in aggregate grafts, but a considerable number of proliferating retinal progenitor cells (RPCs) remain. The rosettes observed within aggregate and retinal sheet transplants exhibit striking similarly to those observed in chick retinal reaggregates, with columnar organization reminiscent of clonal differentiation from RPCs. The presence of residual RPCs is

suspected to have contributed to the rosettes observed in this study and similar studies with retinal sheet transplantation. Studies in mice[16,17], rats[18,19], nonhuman primates[17], and cats[20] suggest that rosettes are not inherently unsafe and often survive perfectly well within the subretinal space, but the lack of organization and failure to interact with host retina leave much to be desired. Regardless of delivery approach—as dissociated cells, aggregates, or on scaffolds—a PRP enriched donor cell population still remains the most desirable type of donor cell for replacement.

Thus, a reproducible method for removing residual proliferating and off-target cells from the donor cell population is highly desirable. The ideal approach should also yield a high number of cells (millions to billions) and be gentle enough to maintain high viability. To this end, several methods for PRP enrichment were tested over the course of this dissertation, including traditional FACS, low-pressure microfluidic sorting, and MACS with novel cell surface markers. Consistent with recent reports[4,14,15,21], enrichment of PRP from fluorescently labeled reported lines was possible but was ultimately deemed not feasible for isolating millions to billions of cells while also maintaining cell viability. We have recently developed a novel protocol for successfully enriching a high yield of PRP (millions of cells) via positive MACS selection for CD133/1 (**Fig. 3**). We have also identified a cell cycle inhibitor targeting the gamma secretase pathway (PD0332991) previously untested in hPSC-derived retinal organoid cell derivatives that is sufficient for arresting proliferation in dissociated, unsorted cells (**Fig. 4**). Combining these strategies in a two-pronged approach has the potential to provide the greatest yield of enriched hPSC-PRs of any published strategy to date, accelerating efforts to study cell replacement therapy for blinding retinal diseases. Further characterization of this enrichment protocol will ideally include a dose-titration assay for PD0332991, since cell cycle inhibitors are often cytotoxic at high enough doses. Moreover, a time course of the efficiency of CD133/1 sorting at various stages of organoid development would provide greater insight regarding the window for achieving maximal PRP yield. Further characterization of PR subtypes that result from CD133/1 sorting and cell cycle

inhibitor treatment is particularly intriguing; cones are considered more attractive from a cell replacement perspective as they provide high-acuity daylight vision, and current approaches for cone enrichment from organoids are limited. Regardless of the exact rod-to-cone ratio of enriched cells, virtually all studies conducted in this dissertation would be greatly enhanced by the use of a PRP-enriched donor cell product as described in this section, and replication of *in vivo* studies using PRP-enriched donor cells would be of particular utility for investigating a potential dose response.

Stereologic quantification of donor cell survival and engraftment

A critical point of convergence for all proposed studies mentioned here lies in testing the safety and efficacy of hPSC-PRP therapies in translational model systems. Establishing diverse animal model platforms for investigating photoreceptor replacement is essential for understanding disease-specific applications of regenerative medicine in the retina, and these models advance distinct but interconnected translational platforms to accelerate progress towards human trials. Key parameters to be investigated in large animal studies picking up where this dissertation leaves off include:

1) donor cell differentiation and survival (including orientation and polarization)

2) donor cell distribution within the retina

3) donor cell connectivity with host retinal neurons

4) host immune response to transplanted donor cells

While in-life analyses of visual function are crucial, some of the richest data obtained in pending preclinical studies lies in quantitative analyses of transplanted donor cells to determine cell survival and optimize dosing protocols. Investigational New Drug (IND) application-enabling studies are explicitly intended to inform the design of early phase human clinical trials for photoreceptor replacement, and as such will rely heavily upon accurate and unbiased

characterization of engrafted cells to determine the necessary dose for achieving anatomic and/or functional rescue.

The quantitative approaches to studying engraftment outlined in Chapter 3 are a first step toward understanding donor-host interactions and exceeded current field standards but are ultimately an imperfect method for estimating cell survival and engraftment relative to the starting dose. Unbiased quantification of donor cell survival and engraftment will be essential to achieving the most reliable estimates of cell survival and integration from these experiments. Stereology, which relies upon systematic random sampling through histologic sections, is the current gold standard for quantitative histologic analysis[22]. Although time-consuming to initially validate, design-based stereology provides the exact type of quantitative data necessary to advance the field from academically-relevant observations to clinically-meaningful outcomes in preclinical research. Future preclinical studies should use design-based stereology whenever possible to gain the most accurate picture of PRP survival, safety, and maturation.

The role of the immune system in subretinal cell therapy

In particular, the role of cytotoxic T cell-mediated immune response in long-term transplant integration will be of critical importance since the nude, immunocompromised rat model employed in pursuit of this dissertation lacks T cells. In controlling the immune response as a variable, we were able to study the relationship between key parameters of interest—survival, engraftment, and maturation—and delivery method without complicating factors of transplant rejection. There are conflicting views on the degree of immune suppression necessary for successful subretinal transplantation, but most agree that at a minimum, local immune suppression will be necessary in allotransplantation[23–26]. Parallel allogeneic studies in immune competent animal models will be paramount to understanding the degree of immunosuppression that will be most appropriate for human clinical trials.

PRP are just the beginning: the other end of the synapse

While we are beginning to gain a better understanding of the PRP side of the donor-host synapse, very little is known about factors contributing to axonal targeting, dendritic sprouting, and INL-driven responses to donor-host interactions. We now know that hPSC-PRP can reliably be delivered to the subretinal space and survive with varying degrees of synaptic protein expression adjacent to host inner neurons and mild effects on vision[11]. The window of opportunity for transplantation in which host inner retinal neurons remain receptive to forming putative connections with donor cells is far from established[11,27,28]. Once the efficiency of synapse formation between donor and host neurons is better characterized, strategies for increasing the efficiency of synapse formation may potentially include modulation of inner retinal neuron plasticity[29,30]. Descriptive and discovery-driven basic science research into mechanisms of inner retinal neuron synaptogenesis—particularly for bipolar cells—has the potential to greatly augment retinal regenerative therapies from the host end of the synapse.

Overall conclusions

For patients suffering from vision loss due to PR death, new cells generated from hPSC-derived retinal organoids clearly have the potential to unlock new treatment options via cell replacement therapy. The field of PSC-derived PR replacement therapy is still relatively young, and preclinical studies have been limited by the tools available for organizing donor cells and studying their connections. The studies described in this dissertation have laid crucial groundwork for future retinal cell therapies, providing the necessary tools to advance next-generation cell therapies and outlining the best path to successful translation of such approaches. The new methodologies described in this dissertation set the stage for directly addressing two of the greatest challenges that lie ahead in PR replacement: organization of donor cells and functional synaptogenesis between donor and host cells. While the ultimate success of such approaches remains to be fully

realized, this dissertation adds to a growing body of preclinical research suggesting that the future of PSC-derived photoreceptor cell replacement therapies for degenerative retinal diseases remains promising.

Figures

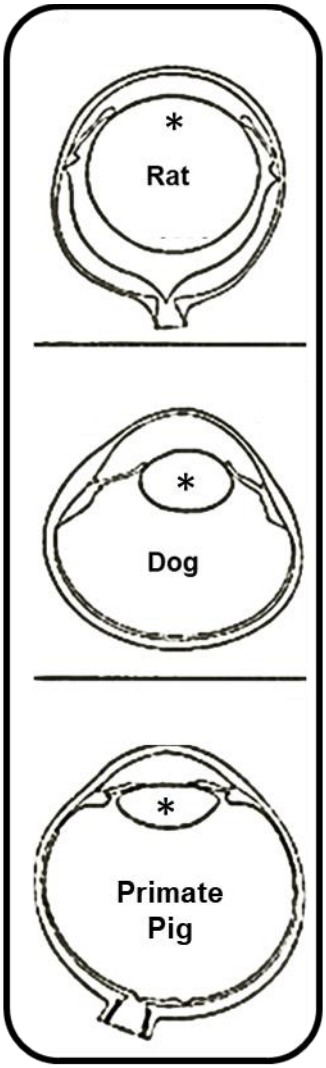

Adapted from Walls, 1942

Fig. 1. Comparative ocular anatomy of select preclinical animal models. Large animal models, including the dog, pig, and primate, have ocular anatomy that more closely mimics the human eye. Rodent species, including the rat, have a comparatively large lens (*) relative to the overall volume of the globe that renders scaffold delivery in these models less clinically translational.

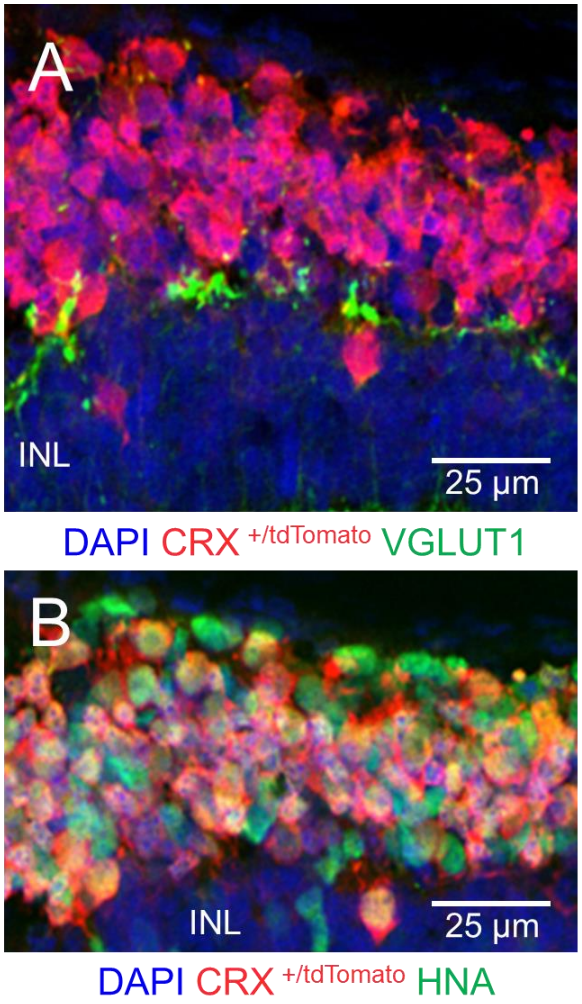

Fig. 2. Immunolabeling of anatomic CRX$^{+/tdTomato}$-PRP engraftment in a rat model of retinal degeneration two weeks after scaffold transplantation. (**A**) CRX$^{+/tdTomato}$-PRP aggregates express presynaptic protein VGLUT1 in regions adjacent to the host inner nuclear layer (INL). (**B**) All CRX$^{+/tdTomato}$-PRP delivered via scaffold also co-labeled with human nuclear antigen (HNA).

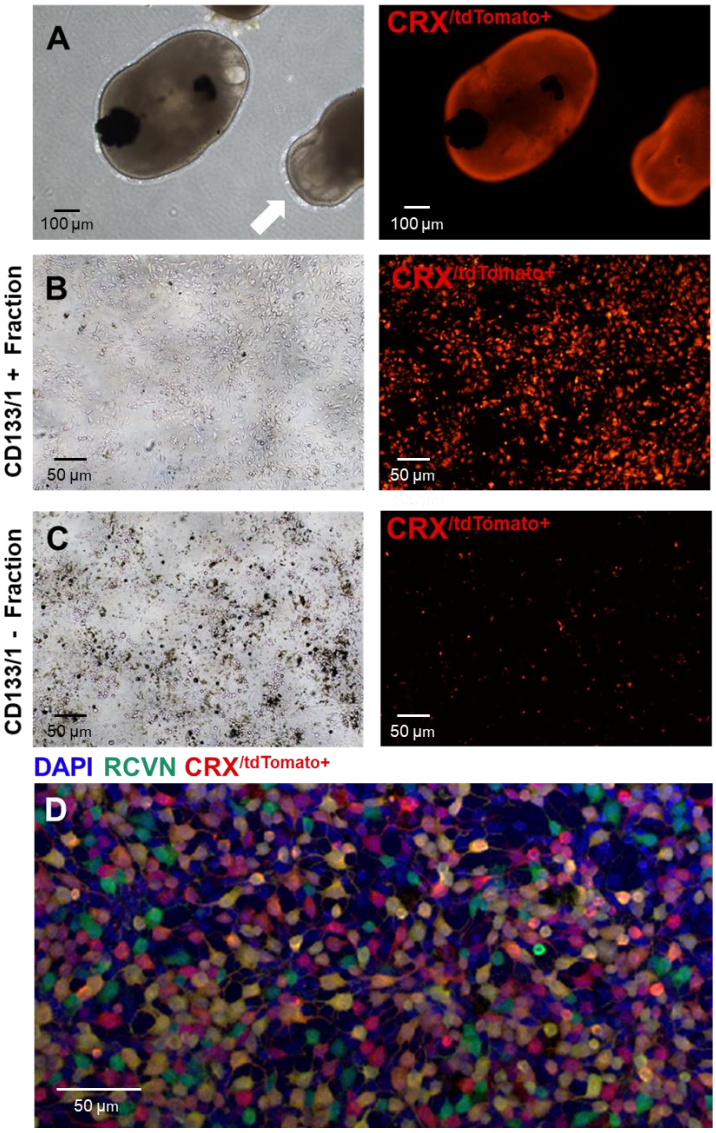

Fig. 3. Photoreceptor enrichment from CRX$^{+/tdTomato}$ retinal organoids via CD133/1 MACS. (**A**) Brightfield (*left*) and red epifluorescent (*right*) images of stage 3 (>D200) WA09 hESC CRX$^{+/tdTomato}$ reporter retinal organoids. The white arrow indicates outer segments of photoreceptors lining the outer rim of the retinal organoids. (**B, C**) Dissociated, sorted, and plated retinal organoids. (**B**) CD133/1 positive fraction, enriched for CRX$^{+/tdTomato}$ positive cells. (**D**) 24 hours after CD133/1 sorting, cells in the positive fraction are enriched (>85%) for recoverin (RCVN) and/or CRX$^{+/tdTomato}$.

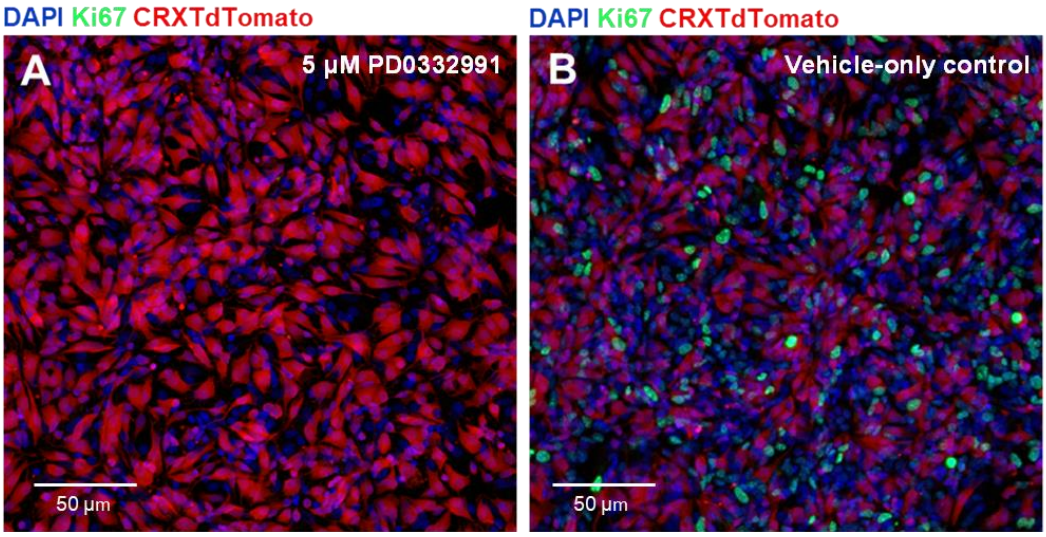

Fig. 4. Continuous treatment with cell cycle inhibitor reduces proliferation in unsorted CRX$^{+/tdTomato}$ hPSC-PRs over 1 week in culture. (**A**) Treatment with 5 µM PD0332991 substantially limits the presence of proliferating Ki67+ cells among CRX$^{+/tdTomato}$ positive cells relative to (**B**) vehicle-only control-treated cells.

References

1. Lee, I.-K. *et al.* Ultrathin micromolded 3D scaffolds for high-density photoreceptor layer reconstruction. *Science Advances* **7**, eabf0344 (2021).

2. Sharma, R., Bose, D., Maminishkis, A. & Bharti, K. Retinal Pigment Epithelium Replacement Therapy for Age-Related Macular Degeneration: Are We There Yet? *Annual Review of Pharmacology and Toxicology* **60**, 553–572 (2020).

3. Phillips, M. J. *et al.* A Novel Approach to Single Cell RNA-Sequence Analysis Facilitates In Silico Gene Reporting of Human Pluripotent Stem Cell-Derived Retinal Cell Types. *Stem Cells* **36**, 313–324 (2018).

4. Garita-Hernandez, M. *et al.* Control of Microbial Opsin Expression in Stem Cell Derived Cones for Improved Outcomes in Cell Therapy. *Front Cell Neurosci* **15**, 648210 (2021).

5. Capowski, E. E. *et al.* Reproducibility and staging of 3D human retinal organoids across multiple pluripotent stem cell lines. *Development* **146**, dev171686 (2019).

6. Cowan, C. S. *et al.* Cell Types of the Human Retina and Its Organoids at Single-Cell Resolution. *Cell* **182**, 1623-1640.e34 (2020).

7. Cora, V. *et al.* A Cleared View on Retinal Organoids. *Cells* **8**, 391 (2019).

8. Linaro, D. *et al.* Xenotransplanted Human Cortical Neurons Reveal Species-Specific Development and Functional Integration into Mouse Visual Circuits. *Neuron* **104**, 972-986.e6 (2019).

9. Xing, Q. *et al.* Retrograde monosynaptic tracing through an engineered human embryonic stem cell line reveals synaptic inputs from host neurons to grafted cells. *Cell Regen (Lond)* **8**, 1–8 (2019).

10. Adler, A. F., Björklund, A. & Parmar, M. Transsynaptic tracing and its emerging use to assess graft-reconstructed neural circuits. *STEM CELLS* **38**, 716–726 (2020).

11. Gasparini, S. J., Llonch, S., Borsch, O. & Ader, M. Transplantation of photoreceptors into the degenerative retina: Current state and future perspectives. *Progress in retinal and eye research* (2018) doi:10.1016/j.preteyeres.2018.11.001.

12. Hulliger, E. C., Hostettler, S. M. & Kleinlogel, S. Empowering Retinal Gene Therapy with a Specific Promoter for Human Rod and Cone ON-Bipolar Cells. *Mol Ther Methods Clin Dev* **17**, 505–519 (2020).

13. Gagliardi, G. *et al.* Characterization and Transplantation of CD73-Positive Photoreceptors Isolated from Human iPSC-Derived Retinal Organoids. *Stem cell reports* **11**, 665–680 (2018).

14. Gonzalez-Cordero, A. *et al.* Recapitulation of Human Retinal Development from Human Pluripotent Stem Cells Generates Transplantable Populations of Cone Photoreceptors. *Stem Cell Reports* **9**, 820–837 (2017).

15. Garita-Hernandez, M. *et al.* Restoration of visual function by transplantation of optogenetically engineered photoreceptors. *Nature Communications* **10**, 4524 (2019).

16. Iraha, S. *et al.* Establishment of Immunodeficient Retinal Degeneration Model Mice and Functional Maturation of Human ESC-Derived Retinal Sheets after Transplantation. *Stem Cell Reports* **10**, 1059–1074 (2018).

17. Tu, H.-Y. *et al.* Medium- to long-term survival and functional examination of human iPSC-derived retinas in rat and primate models of retinal degeneration. *EBioMedicine* **39**, 562–574 (2019).

18. McLelland, B. T. *et al.* Transplanted hESC-Derived Retina Organoid Sheets Differentiate, Integrate, and Improve Visual Function in Retinal Degenerate Rats. *Invest. Ophthalmol. Vis. Sci.* **59**, 2586–2603 (2018).

19. Lin, B. *et al.* Retina Organoid Transplants Develop Photoreceptors and Improve Visual Function in RCS Rats With RPE Dysfunction. *Invest. Ophthalmol. Vis. Sci.* **61**, 34–34 (2020).

20. Singh, R. K., Occelli, L. M., Binette, F., Petersen-Jones, S. M. & Nasonkin, I. O. Transplantation of Human Embryonic Stem Cell-Derived Retinal Tissue in the Subretinal Space of the Cat Eye. *Stem Cells and Development* **28**, 1151–1166 (2019).

21. Ribeiro, J. *et al.* Restoration of visual function in advanced disease after transplantation of purified human pluripotent stem cell-derived cone photoreceptors. *Cell Reports* **35**, (2021).

22. Kubínová, L. & Janáček, J. Confocal stereology: an efficient tool for measurement of microscopic structures. *Cell Tissue Res* **360**, 13–28 (2015).

23. Singh, M. S. *et al.* Retinal stem cell transplantation: Balancing safety and potential. *Progress in Retinal and Eye Research* 100779 (2019) doi:10.1016/j.preteyeres.2019.100779.

24. Fujii, S. *et al.* A Strategy for Personalized Treatment of iPS-Retinal Immune Rejections Assessed in Cynomolgus Monkey Models. *International Journal of Molecular Sciences* **21**, 3077 (2020).

25. Petrash, C. C., Palestine, A. G. & Canto-Soler, M. V. Immunologic Rejection of Transplanted Retinal Pigmented Epithelium: Mechanisms and Strategies for Prevention. *Front. Immunol.* **12**, (2021).

26. Yamasaki, S. *et al.* Low Immunogenicity and Immunosuppressive Properties of Human ESC- and iPSC-Derived Retinas. *Stem Cell Reports* **16**, 851–867 (2021).

27. Aboualizadeh, E. *et al.* Imaging Transplanted Photoreceptors in Living Nonhuman Primates with Single-Cell Resolution. *Stem Cell Reports* **15**, 482–497 (2020).

28. Reh, T. A. Photoreceptor Transplantation in Late Stage Retinal Degeneration. *Invest. Ophthalmol. Vis. Sci.* **57**, ORSFg1-7 (2016).

29. Chan, K. *et al.* Vigabatrin-Induced Retinal Functional Alterations and Second-Order Neuron Plasticity in C57BL/6J Mice. *Invest Ophthalmol Vis Sci* **61**, 17 (2020).

30. Telias, M., Nawy, S. & Kramer, R. H. Degeneration-Dependent Retinal Remodeling: Looking for the Molecular Trigger. *Front Neurosci* **14**, 618019 (2020).